



The  
University  
Of  
Sheffield.

# **Investigation of the novel retargeted botulinum toxin ChoBot for the treatment of neuropathic pain**

**Eve Corrie**

A thesis submitted in partial fulfilment of the requirements for the degree of  
Doctor of Philosophy

The University of Sheffield  
Faculty of Science  
Department of Biomedical Sciences

**December 2021**

## Abstract

Botulinum toxins (BoNTs) have shown efficacy as analgesics for chronic pain conditions such as peripheral neuropathic pain. This is thought to be due to the disruption of soluble N-ethylmaleimide-Sensitive Factor attachment protein receptor (SNARE)-mediated neuronal activity. However, the use of native BoNTs for pain treatment is limited by their potent paralytic effects and incomplete targeting of peripheral sensory neurons. To address these issues, ChoBot, a novel chimeric botulinum toxin, was created. ChoBot consists of the receptor binding domain of cholera toxin conjugated to the translocation-light chain domains of BoNT/A using a self-assembling protein staple.

Initial experiments of this thesis focused on the development of an *in vitro* model of chemotherapy-induced peripheral neuropathy to test novel BoNTs, but failed to produce a robust read-out of a pain related phenomenon. *In vitro*, ChoBot was shown to target a higher proportion of rat primary dorsal root ganglion neurons than the most commonly used analgesic BoNT, BoNT/A. This included increased targeting of calcitonin gene-related peptide (CGRP)-expressing putative nociceptors, leading to successful inhibition of depolarisation-evoked CGRP release. While showing increased potency of sensory neuron intoxication *in vitro*, ChoBot proved the least paralytic of four botulinum toxins tested *in vivo*, never inducing any more than 40% neuromuscular blockade. ChoBot was also shown to be active in sensory neurons after peripheral injection into the plantar surface of the paw. Despite proteolytic activity, ChoBot failed to induce a reversal of behavioural pain thresholds in rat models of neuropathy. However, the creation of this novel toxin provides further evidence for the potential utility of retargeted botulinum toxins for the treatment of chronic pain. ChoBot is the first toxin to retain, or potentially improve, SNARE cleavage in sensory neurons without significant muscle paralysis, even at doses 1000-fold higher than paralysis-causing doses of native BoNTs.

## *Author's declaration*

I, the author, confirm that the Thesis is my own work. I am aware of the University's Guidance on the Use of Unfair Means ([www.sheffield.ac.uk/ssid/unfair-means](http://www.sheffield.ac.uk/ssid/unfair-means)). This work has not been previously been presented for an award at this, or any other, university.

## *Acknowledgements*

First of all I'd like to thank those that helped this project come to life, my supervisors Liz Seward, Bazbek Davletov and Many Sher. This project never would have got to this stage without all of your guidance and expertise. I'd also like to give particular thanks to my advisor Mohammed Nassar, who has been a source of endless knowledge and infectious enthusiasm, and always genuinely willing to help when things weren't going to plan! Thanks also to Freek van Eeden for being a fantastically altruistic advisor, involving himself in my project despite having little personal involvement in the field. Thank you to all the lab members who've assisted me in becoming a halfway decent scientist along the way: Ciara Doran for her mastery of the sensory neuron field (among many others); Charlotte Leese for her protein wizardry; Claire Christmas for her command of seemingly all *in vivo* techniques; James Alix for teaching me to become a neurophysiologist in a very small way; Rebecca Bresnahan for taking the time to teach a newly fledged PhD student practically everything she knew whilst also rushing to complete her own experiments! Thank you also to Judit Meszaros for her endless support. You always knew exactly what I was going through, as you'd gone through it just a year before. Thank you to everyone at the BSU for managing and caring for all the animals, and to the animals themselves – I hope I did the best I could for all of you. Thank you to everybody who made my time at Eli Lilly so enjoyable, Helen Sanger, Luis Coy and Adrian Mogg in particular. Thank you also to all the other Lilly students who made my brief life in Reading a little less grey. I also want to give a massive thank you to the entire Sheffield biomedical student community. A new start in a new city could have been a lonely experience but I felt part of a society as soon as I arrived. Here's to all the Friday pub trips and regrettable late nights at the Leadmill. Thank you to my mum, my dad, and the rest of my family and friends for never doubting, even for a second, that I would get through even the toughest parts of this experience. And thank you to Luna for always being ready to jump all over my keyboard for headbutts when she's decided I've been working for too long. Finally, thank you to every single person who has helped me get to the submission of my thesis in any way, big or small! I've had the pleasure of working with so many delightful people and I'm sure I'm forgetting many of you in the acknowledgements, but I'll never forget what you've all helped me achieve.

## *Table of contents*

<b>Abstract</b> .....	<b>2</b>
<b>Author's declaration</b> .....	<b>3</b>
<b>Acknowledgements</b> .....	<b>4</b>
<b>Table of contents</b> .....	<b>5</b>
<b>List of figures</b> .....	<b>10</b>
<b>List of tables</b> .....	<b>13</b>
<b>List of abbreviations</b> .....	<b>14</b>
<b>1. Introduction</b> .....	<b>17</b>
<b>1.1 The peripheral pain signalling pathway</b> .....	<b>17</b>
1.1.1 Primary afferent nerve fibres .....	18
1.1.2 The dorsal root ganglia.....	20
1.1.2.1 Cell types of the dorsal root ganglia .....	21
1.1.2.2 Ion channels of the dorsal root ganglia.....	23
1.1.2.3 Transient receptor potential vanilloid 1.....	24
1.1.2.4 Regulation of ion channels at the membrane of sensory neurons .....	26
1.1.3 Dorsal horn of the spinal cord .....	30
<b>1.2 Acute and chronic pain</b> .....	<b>32</b>
1.2.1 Pathophysiology of chronic pain.....	33
1.2.1.1 Peripheral sensitisation.....	33
1.2.1.2 Central sensitisation.....	36
1.2.1.3 Glial activation .....	37
1.2.2 Neuropathic pain .....	38
<b>1.3 Chemotherapy-induced peripheral neuropathy</b> .....	<b>38</b>
1.3.1 Paclitaxel .....	40
1.3.2 Paclitaxel-induced peripheral neuropathy .....	40
1.3.2.1 Susceptible populations of sensory neurons.....	40
1.3.2.2 Axonal toxicity, microtubule disruption, and intraepidermal nerve fibre loss .....	42
1.3.2.3 Ion channel changes .....	43
1.3.2.4 Calcitonin gene-related peptide and substance P .....	45
1.3.2.5 Neuroinflammation and glial activation.....	46
1.3.2.6 Mitochondrial damage and oxidative stress.....	47
1.3.2.7 Calcium homeostasis dysregulation.....	48
1.3.2.8 Cremophor EL.....	49

<b>1.4</b>	<b>Botulinum neurotoxins.....</b>	<b>49</b>
1.4.1	Structure and function .....	51
1.4.2	Effect on muscle.....	52
1.4.3	Botulinum neurotoxins in chronic pain .....	53
1.4.3.1	Mechanisms of analgesia .....	53
1.4.3.2	Prevention of ion channel trafficking to the membrane of sensory neurons.....	55
1.4.4	Re-engineering botulinum neurotoxins .....	57
1.4.4.1	Retargeting to different cell types .....	57
1.4.4.2	Retargeting to different substrates.....	60
1.4.5	SNARE-stapling.....	60
1.4.5.1	ChoBot .....	63
<b>1.5</b>	<b>Hypothesis and aims.....</b>	<b>66</b>
<b>2.</b>	<b>Materials and methods .....</b>	<b>68</b>
<b>2.1</b>	<b>Frequently used reagents .....</b>	<b>68</b>
2.1.1	Solutions and buffers .....	68
2.1.2	Antibodies and fluorescent molecules.....	70
<b>2.2</b>	<b>Primary culture of dorsal root ganglion neurons .....</b>	<b>72</b>
2.2.1	Animals.....	72
2.2.2	Coating of 96-well plates and coverslips.....	72
2.2.3	Dissociation of dorsal root ganglion neurons.....	73
<b>2.3</b>	<b>Stapled botulinum toxin production.....</b>	<b>75</b>
<b>2.4</b>	<b>Treatment of cultured dorsal root ganglion neurons.....</b>	<b>80</b>
2.4.1	Paclitaxel treatment.....	80
2.4.2	Toxin treatment .....	81
<b>2.5</b>	<b>Immunocytochemistry and imaging of dorsal root ganglion neurons.....</b>	<b>82</b>
2.5.1	Fixation and immunocytochemistry .....	82
2.5.2	Epifluorescent microscopy of cell cultures.....	84
2.5.3	Image analysis for ChoBot, cholera toxin subunit B and GM1 ganglioside subtyping.....	84
2.5.4	Image analysis for ATF3 expression and area covered by neuronal processes.....	85
2.5.5	Extracellular TRPV1 immunocytochemistry .....	86
2.5.6	Confocal microscopy .....	86
2.5.7	Extracellular TRPV1 image analysis.....	88
<b>2.6</b>	<b>Live cell assays.....</b>	<b>89</b>
2.6.1	Calcitonin gene-related peptide release assay .....	89
2.6.2	Fura2-AM single cell calcium imaging .....	89
2.6.3	Fluorescent Imaging Plate Reader calcium imaging .....	91

2.6.4	Incucyte .....	92
<b>2.7</b>	<b>In vivo experiments .....</b>	<b>93</b>
2.7.1	Paclitaxel injections.....	93
2.7.2	Spared nerve injury.....	93
2.7.3	Intraplantar injection of botulinum toxin.....	93
2.7.4	Von Frey testing .....	94
2.7.5	Dry ice cold allodynia testing.....	95
2.7.6	Compound muscle action potential recordings.....	95
<b>2.8</b>	<b>Immunohistochemistry and imaging of sections .....</b>	<b>96</b>
2.8.1	Tissue preparation, fixation and sectioning .....	96
2.8.2	Immunohistochemistry .....	97
2.8.3	Epifluorescent microscopy of tissue sections.....	97
2.8.4	Image analysis of tissue sections .....	98
2.8.5	Statistical analysis .....	98
<b>3.</b>	<b>Characterisation of an in vitro model of chemotherapy-induced peripheral neuropathy....</b>	<b>99</b>
<b>3.1</b>	<b>Introduction.....</b>	<b>99</b>
<b>3.2</b>	<b>Summary and objectives .....</b>	<b>101</b>
<b>3.3</b>	<b>Results .....</b>	<b>101</b>
3.3.1	Paclitaxel induces expression of a stress-response transcription factor in a subset of sensory neurons.....	101
3.3.2	Paclitaxel induces the retraction of neurites in dorsal root ganglion cultures.....	109
3.3.3	Paclitaxel exposure has no effect on whole population calcium responses to certain nociceptive agonists .....	113
3.3.4	Veratridine responses are not a valid assay of nociceptive populations in rat dorsal root ganglion cultures .....	115
3.3.5	Paclitaxel increases the amplitude of calcium response to capsaicin, but not other nociceptive agonists.....	117
3.3.6	Capsaicin-induced release of calcitonin gene-related peptide from DRG cultures is potentiated by in vitro paclitaxel exposure .....	119
3.3.7	The density of TRPV1 at the membrane of dorsal root ganglion neurons is not affected by in vitro paclitaxel exposure.....	121
3.3.8	Cadmium block of voltage-gated calcium channels alters the time-course of capsaicin responses but has no effect on the amplitude in the presence or absence of paclitaxel .....	125
<b>3.4</b>	<b>Discussion .....</b>	<b>127</b>
<b>4.</b>	<b>In vitro characterisation of a novel chimeric botulinum toxin, ChoBot .....</b>	<b>131</b>

<b>4.1</b>	<b>Introduction.....</b>	<b>131</b>
<b>4.2</b>	<b>Summary and objectives .....</b>	<b>133</b>
<b>4.3</b>	<b>Results .....</b>	<b>133</b>
4.3.1	The botulinum A light chain-translocation domain that has not undergone stapling to a receptor binding domain is not internalised into sensory neurons .....	133
4.3.2	A subpopulation of sensory neurons express the ganglioside target of ChoBot and bind fluorescent cholera toxin subunit B.....	135
4.3.3	ChoBot cleaves SNAP25 in a subpopulation of dorsal root ganglion neurons over a 1000-fold concentration range .....	138
4.3.4	Myelinated and peptidergic neurons are more susceptible to SNAP25-cleavage by ChoBot than other subpopulations .....	140
4.3.5	Comparison of ChoBot selectivity to cholera toxin subunit B binding and GM1 expression in neuronal subpopulations.....	143
4.3.6	ChoBot has a higher targeting efficacy of sensory neurons in vitro than BoNT/A .....	148
4.3.7	Comparison of BoNT/A and ChoBot subpopulation selectivity.....	150
4.3.8	Paclitaxel co-applied with ChoBot does not widen the susceptible subpopulation.....	152
4.3.9	Exposure to paclitaxel prior to ChoBot increases the proportion of neurons that are susceptible to cleavage of SNAP25.....	154
<b>4.4</b>	<b>Discussion.....</b>	<b>158</b>
<b>5.</b>	<b>Comparison of the paralytic properties of native and engineered botulinum toxins.....</b>	<b>162</b>
<b>5.1</b>	<b>Introduction.....</b>	<b>162</b>
<b>5.2</b>	<b>Summary and objectives .....</b>	<b>164</b>
<b>5.3</b>	<b>Results .....</b>	<b>164</b>
5.3.1	Effect of BoNT/A injection on compound muscle action potential amplitude.....	164
5.3.2	Effect of Bitox/AA injection on compound muscle action potential amplitude.....	166
5.3.3	Effect of BoNT/C injection on compound muscle action potential amplitude.....	167
5.3.4	Effect of ChoBot injection on compound muscle action potential .....	169
5.3.5	Comparison of the effect of native and engineered botulinum toxins on the compound muscle action potential .....	170
<b>5.4</b>	<b>Discussion.....</b>	<b>172</b>
<b>6.</b>	<b>In vivo testing of ChoBot as an analgesic agent.....</b>	<b>174</b>
<b>6.1</b>	<b>Introduction.....</b>	<b>174</b>
<b>6.2</b>	<b>Summary and objectives .....</b>	<b>177</b>
<b>6.3</b>	<b>Results .....</b>	<b>178</b>
6.3.1	ChoBot cleaves SNAP25 in nerve fibres innervating the skin at the site of injection .....	178

6.3.2	ChoBot cleaves SNAP25 in a subpopulation of NF200- and CGRP-expressing fibres in the dermis	180
6.3.3	SNAP25 cleavage can be detected at the level of the dorsal root ganglia after ChoBot injection	182
6.3.4	ChoBot has no effect on mechanical or cold allodynia in a model of chemotherapy-induced peripheral neuropathy.....	184
6.3.5	ChoBot has no effect on mechanical allodynia in the spared nerve injury model of neuropathy	187
<b>6.4</b>	<b>Discussion.....</b>	<b>189</b>
<b>7.</b>	<b>General discussion.....</b>	<b>192</b>
7.1	General findings .....	192
7.2	Limitations of the study.....	193
7.3	Future directions .....	195
<b>Appendix.....</b>		<b>198</b>
<b>8.</b>	<b>Bibliography .....</b>	<b>199</b>

## List of figures

Figure 1.1. The sensory pathway.....	18
Figure 1.2. Sensory innervation of the skin .....	19
Figure 1.3. Sensory neuron classification based on single cell transcriptomics as defined by Usoskin et al., 2014 .....	22
Figure 1.4. Termination of primary sensory afferents onto the dorsal horn of the spinal cord ...	31
Figure 1.5. Release of calcitonin gene-related peptide (CGRP) from primary afferent neurons ..	35
Figure 1.6. Structure and function of synaptic vesicle SNARE proteins .....	50
Figure 1.7. Structure of botulinum neurotoxin A (BoNT/A) .....	51
Figure 1.8. Structure of a protein stapled botulinum neurotoxin .....	61
Figure 2.1. Western blot demonstrating specificity of the in-house rabbit cleaved SNAP25 antibody to BoNT/A light chain cleavage .....	72
Figure 2.2. Production of ChoBot .....	77
Figure 2.3. Production of BiTox/AA.....	79
Figure 2.4. Effect of octyl glucoside (OG) on the speed of SNARE complex formation.....	80
Figure 2.5. Effect of Kolliphor/ethanol vehicle on calcium responses of neuronally differentiated IMR32 cells assayed by FLIPR .....	81
Figure 2.6. Effect of cell permeabilisation with triton on immunocytochemistry of the GM1 ganglioside .....	83
Figure 2.7. Imaging of TRPV1 extracellular antibody immunocytochemistry of dorsal root ganglion cultures.....	87
Figure 2.8. Analysis of TRPV1 extracellular antibody immunocytochemistry .....	88
Figure 2.9. CMAP recording using AcqKnowledge software.....	96
Figure 3.1. $\beta$ -III-tubulin and Activating Transcription Factor 3 (ATF3) expression in 3 day-old dorsal root ganglion cultures exposed to paclitaxel.....	103
Figure 3.2. $\beta$ -III-tubulin and Activating Transcription Factor 3 (ATF3) expression in 7 day-old dorsal root ganglion cultures exposed to paclitaxel.....	104
Figure 3.3. Size frequency distributions of dorsal root ganglion (DRG) neurons exposed to paclitaxel in vitro.....	105
Figure 3.4. Proportion and size distribution of dorsal root ganglion (DRG) neurons expressing the neuronal damage marker Activating Transcription Factor 3 (ATF3) after in vitro paclitaxel exposure .....	108

<b>Figure 3.5. Incucyte Neurotrack imaging of dorsal root ganglion (DRG) cultures exposed to paclitaxel in vitro.....</b>	<b>110</b>
<b>Figure 3.6. Neuronal processes of dorsal root ganglion neurons marked with <math>\beta</math>-III-tubulin following exposure to paclitaxel in vitro .....</b>	<b>112</b>
<b>Figure 3.7. FLIPR calcium imaging of dorsal root ganglion (DRG) neurons exposed to paclitaxel in vitro or in vivo .....</b>	<b>114</b>
<b>Figure 3.8. Single cell calcium imaging veratridine response profiles of rat dorsal root ganglion (DRG) neurons compared to published veratridine response profiles of mouse DRG neurons..</b>	<b>116</b>
<b>Figure 3.9. Effect of in vitro paclitaxel exposure on the proportion of rat dorsal root ganglion (DRG) neurons responding to nociceptive agonists and the amplitude of responses .....</b>	<b>118</b>
<b>Figure 3.10. The effect of paclitaxel on the release of calcitonin gene-related peptide.....</b>	<b>120</b>
<b>Figure 3.11. Validation of TRPV1 extracellular antibody and effect of capsaicin-induced TRPV1 internalisation .....</b>	<b>122</b>
<b>Figure 3.12. Effect of in vitro paclitaxel exposure on extracellular TRPV1 membrane intensity immunolabelling of dorsal root ganglion (DRG) cultures .....</b>	<b>124</b>
<b>Figure 3.13. Effect of voltage gated calcium channel (VGCC) block with cadmium chloride on calcium responses to capsaicin .....</b>	<b>126</b>
<b>Figure 4.1. The effect of light chain-translocation domain-SNAP25 (LC-TD-SNAP25) on SNAP25 cleavage .....</b>	<b>134</b>
<b>Figure 4.2. Subtypes of sensory neurons that bind fluorescent cholera toxin subunit B .....</b>	<b>136</b>
<b>Figure 4.3. Subtypes of sensory neurons that express extracellular GM1 ganglioside.....</b>	<b>137</b>
<b>Figure 4.4. ChoBot cleaves SNAP25 in dorsal root ganglion cultures at concentrations from 10pM to 10nM.....</b>	<b>139</b>
<b>Figure 4.5. Subtypes of sensory neurons susceptible to SNAP25 cleavage by Chobot .....</b>	<b>141</b>
<b>Figure 4.6. ChoBot inhibits depolarisation-induced calcitonin gene-related peptide release ....</b>	<b>142</b>
<b>Figure 4.7. Subtyping of neurons susceptible to SNAP25 cleavage by ChoBot, CTB binding and GM1 expression .....</b>	<b>144</b>
<b>Figure 4.8. Expression of full-length SNAP25 in dorsal root ganglion neurons.....</b>	<b>146</b>
<b>Figure 4.9. SNAP25 immunofluorescence is decreased in peripherin-expressing neurons compared to the total population.....</b>	<b>147</b>
<b>Figure 4.10. ChoBot cleaves SNAP25 in a larger proportion of dorsal root ganglion neurons than BoNT/A.....</b>	<b>149</b>
<b>Figure 4.11. Subtypes of sensory neurons susceptible to SNAP25 cleavage by BoNT/A .....</b>	<b>151</b>

<b>Figure 4.12. The effect of paclitaxel co-application on SNAP25 cleavage by ChoBot .....</b>	<b>153</b>
<b>Figure 4.13. Effect of paclitaxel pre-treatment on SNAP25 cleavage by ChoBot.....</b>	<b>155</b>
<b>Figure 4.14. Effect of paclitaxel pre-treatment on SNAP25 cleavage by BitoxAA.....</b>	<b>157</b>
<b>Figure 4.15. Distribution of SNARE RNA expression in dorsal root ganglion subpopulations ....</b>	<b>160</b>
<b>Figure 5.1. Compound muscle action potential recordings following a subcutaneous injection of BoNT/A over the gastrocnemius muscle .....</b>	<b>165</b>
<b>Figure 5.2. Compound muscle action potential recordings following a subcutaneous injection of Bitox/AA over the gastrocnemius muscle .....</b>	<b>167</b>
<b>Figure 5.3. Compound muscle action potential recordings following a subcutaneous injection of BoNT/C over the gastrocnemius muscle .....</b>	<b>168</b>
<b>Figure 5.4. Compound muscle action potential recordings following a subcutaneous injection of ChoBot over the gastrocnemius muscle .....</b>	<b>170</b>
<b>Figure 5.5. Dose response of native and retargeted botulinum toxins on compound muscle action potential amplitude.....</b>	<b>171</b>
<b>Figure 6.1. ChoBot cleaves SNAP25 in dermal sensory fibres, fibres innervating blood vessels, and motor neurons .....</b>	<b>179</b>
<b>Figure 6.2. SNAP25 cleavage in the dermis of ChoBot injected footpad .....</b>	<b>181</b>
<b>Figure 6.3. SNAP25 cleavage in the dorsal root ganglia (DRG) ipsilateral to the ChoBot injected footpad.....</b>	<b>183</b>
<b>Figure 6.4. Effect of paclitaxel injections on mechanical and cold withdrawal thresholds .....</b>	<b>185</b>
<b>Figure 6.5. Effect of ChoBot injection on mechanical allodynia induced by paclitaxel.....</b>	<b>186</b>
<b>Figure 6.6. Effect of ChoBot injection on cold allodynia induced by paclitaxel .....</b>	<b>187</b>
<b>Figure 6.7. Effect of spared nerve injury on mechanical withdrawal thresholds.....</b>	<b>188</b>
<b>Figure 6.8. Effect of ChoBot injection on mechanical allodynia induced by spared nerve injury</b>	<b>189</b>
<b>Figure 0.1. Effect of in vitro paclitaxel exposure on veratridine response profiles in rat dorsal root ganglion (DRG) neurons.....</b>	<b>198</b>

*List of tables*

**Table 1.1. Fibre classes of the primary afferent sensory neurons ..... 20**

**Table 1.2. Classification of chronic pain types of the International Classification of Diseases (ICD)-11 ..... 33**

**Table 1.3. Categories of antineoplastic that cause chemotherapy-induced peripheral neuropathy (CIPN). ..... 39**

**Table 1.4. Targeting and SNARE cleavage of different BoNT serotypes ..... 52**

**Table 5.1. BoNT/A doses used in published compound muscle action potential studies..... 163**

**Table 5.2. BoNT/A doses used in this chapter in Units and picograms..... 164**

**Table 5.3. Regression expressions and doses required to reduce the compound muscle action potential (CMAP) amplitude by 50% ..... 171**

**Table 6.1. Published effects of intraplantar botulinum toxin A injection in rat models of neuropathy..... 177**

## List of abbreviations

$\alpha,\beta$ -methylene-ATP	$\alpha,\beta$ -Methyleneadenosine 5'-triphosphate lithium salt
AITC	Allyl isothiocyanate
AMPA	$\alpha$ -amino-3-hydroxy-5-methyl-4-isoxazolepropionic acid
ANOVA	Analysis of variance
ATF3	Activating transcription factor 3
ATP	Adenosine triphosphate
BoNT	Botulinum neurotoxin
BSA	Bovine serum albumin
CaMKII	Ca <sup>2+</sup> /calmodulin-dependent protein kinase 2
Cdk5	Cyclin dependent kinase 5
CFA	Complete Freund's adjuvant
CGRP	Calcitonin gene-related peptide
CIPN	Chemotherapy-induced peripheral neuropathy
CLR	Calcitonin receptor-like receptor
CMAP	Compound muscle action potential
CNS	Central nervous system
CTB	Cholera toxin binding domain
DAPI	4',6-diamidino-2-phenylindole
DAS	Digit abduction score
DIV	Days <i>in vitro</i>
DMSO	Dimethyl sulfoxide
DREADD	Designer receptor exclusively activated by designer drugs
DRG	Dorsal root ganglia
EGF	Epidermal growth factor
ELISA	Enzyme-linked immunosorbent assay
EPSC	Excitatory postsynaptic current
FLIPR	Fluorescent Imaging Plate Reader
GPCR	G-protein coupled receptor
GTP	Guanosine-5'-triphosphate
HEPES	4-(2-hydroxyethyl)-1-piperazineethanesulfonic acid
HRP	Horseradish peroxidase

IB4	Isolectin B4
IENF	Intraepidermal nerve fibre
IGF1	Insulin-like growth factor 1
IgG	Immunoglobulin G
IL1 $\beta$	Interleukin 1 beta
iPSC	Induced pluripotent stem cell
KIF5B	Kinesin Family Member 5B
KIF17	Kinesin Family Member 17
LcTd	Light chain-translocation domain
LTD	Long-term depression
LTP	Long-term potentiation
mEPSC	Miniature excitatory postsynaptic current
mPTP	Mitochondrial permeability transition pore
NF200	200-kDa neurofilament protein
NGF	Nerve growth factor
NK1R	Neurokinin 1 receptor
NMDA	N-methyl-D-aspartate
OG	Octyl glucoside
PAR2	Protease-activated receptor 2
PBS	Phosphate buffered saline
PGE2	Prostaglandin E2
PIP2	Phosphatidylinositol 4,5-bisphosphate
PKA	Protein kinase A
PKC	Protein kinase C
PLC	Phospholipase C
PDL	Poly-D-lysine
RAMP1	Receptor activity modifying protein 1
ROI	Region of interest
ROS	Reactive oxygen species
RT-PCR	Real-time polymerase chain reaction
SNAP23	Synaptosomal-associated protein, 23kDa
SNAP25	Synaptosomal-associated protein, 25kDa
SNARE	Soluble NSF attachment protein receptor

SNI	Spared nerve injury
Src	Proto-oncogene tyrosine-protein kinase Src
TNF $\alpha$	Tumour necrosis factor alpha
TrkA	Tropomyosin receptor kinase A
TrkB	Tropomyosin receptor kinase B
TrkC	Tropomyosin receptor kinase C
TRP	Transient receptor potential
TRPA1	Transient receptor potential ankyrin receptor 1
TRPV1	Transient receptor potential vanilloid receptor 1
TRPV4	Transient receptor potential vanilloid receptor 4
U	Botulinum toxin activity units
USP5	Ubiquitin carboxyl-terminal hydrolase 5
VAMP1	Vesicle-associated membrane protein 1
VAMP2	Vesicle-associated membrane protein 2
VGCCs	Voltage gated calcium channels
VGKC	Voltage gated potassium channels
VGSC	Voltage gated sodium channel
VIP	Vasoactive intestinal peptide

# 1. Introduction

## 1.1 The peripheral pain signalling pathway

Pain is a feeling which every single human is familiar with, but can be difficult to describe or define. The International Association for the Study of Pain defines this sensory phenomenon as “an unpleasant sensory and emotional experience associated with, or resembling that associated with, actual or potential tissue damage” (Raja et al., 2020). This encompasses a wide variety of bodily sensations arising from an equally diverse number of different situations. In broad brushstrokes, this aversive sensation is designed to arise in response to, or in preclusion of, bodily damage. This elicits a reaction to prevent further damage and also to protect the tissue as it heals.

The peripheral mammalian pain-sensing system is made up of a network of sensory fibres which innervate the body, and these are attuned to fire in response to different modalities of potentially damaging stimuli, such as thermal, chemical and mechanical (Dubin & Patapoutian, 2010). Sensory neurons which transmit painful, or nociceptive, information to the central nervous system (CNS) are called nociceptors. All sensory fibres, including nociceptive fibres, arise from neuronal cell bodies which reside in peripheral ganglia. Much of the face and head is innervated by neurons from the trigeminal ganglia but the focus of this thesis will be on the neurons of the dorsal root ganglia (DRG), which innervate the majority of the body. The DRG are clusters of sensory neuron cell bodies and glia (such as Schwann cells and satellite cells) that are located within the dorsal root of the spinal nerves, which lie just outside the spinal cord on either side (Figure 1.1). The first order neurons of the DRG synapse onto neurons in the dorsal horn of the spinal cord. Processing of the nociceptive inputs from the sensory neurons takes place in the spinal cord and is projected up the ascending pain pathways to the brain, which leads to the bodily and aversive feelings of pain.

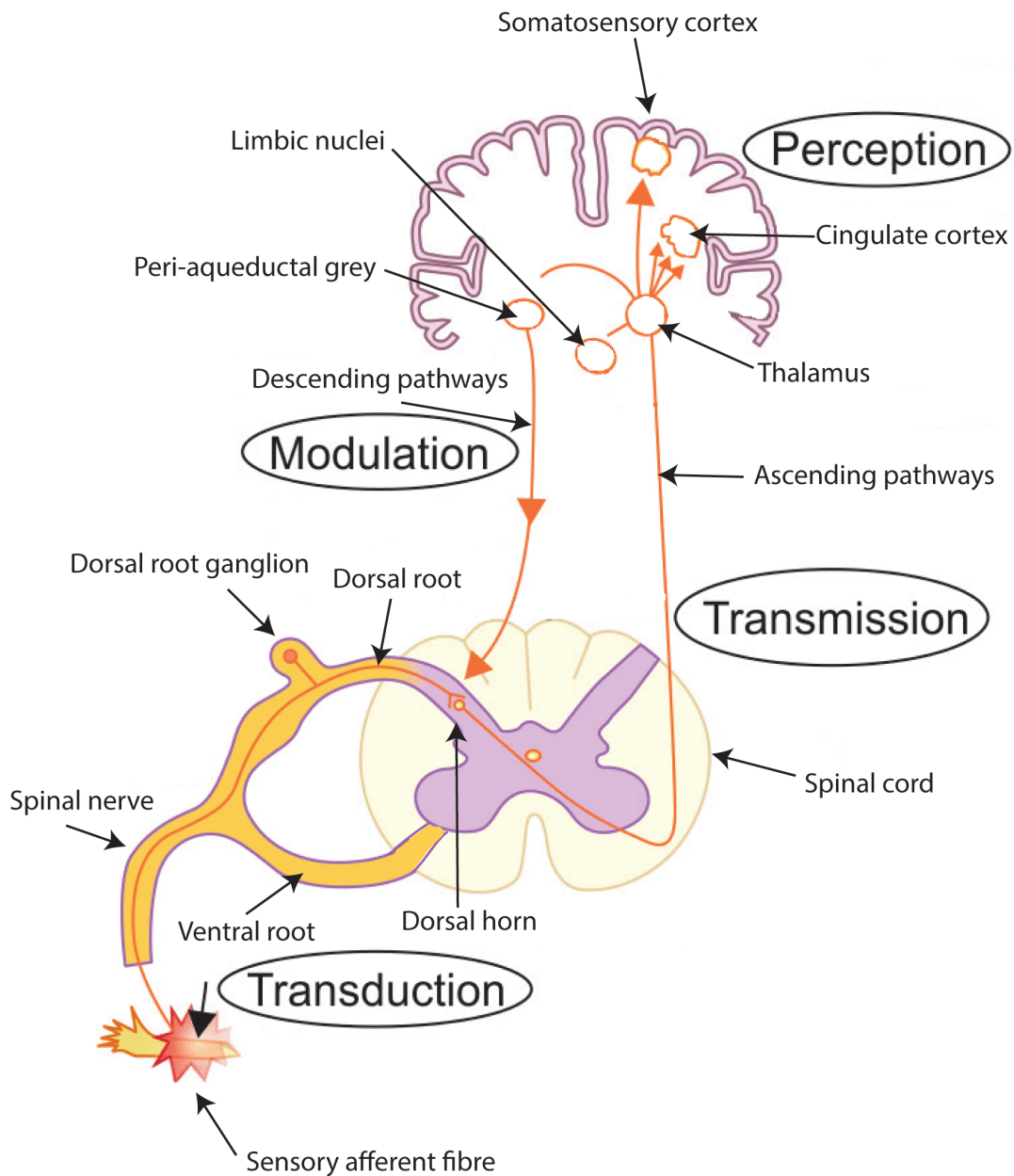


**Figure 1.1. The sensory pathway.** Transduction takes place via specialised ion channels and receptors expressed by peripheral afferent fibres. These fibres are provided by sensory neurons with their cell bodies found in the dorsal root ganglia (DRG), and they transmit information to the spinal cord via the dorsal root of the spinal nerve. DRG neurons synapse onto second order neurons in the dorsal horn of the spinal cord, where inputs can be modulated by descending pathways from the brain. This input is transmitted via ascending pathways to various areas of the brain which leads to the perception of the physical and affective feelings of sensation. Modified from Das, 2017.

### 1.1.1 Primary afferent nerve fibres

The skin and the viscera are innervated by a range of primary afferent nerve fibres which are either associated with specialised sensory receptors or terminate as free nerve endings. This array

of innervation is responsible for all sensation, encoding the full range of temperatures from noxious cold through to noxious heat, all intensities of mechanical stimuli as well as responding to many chemical stimuli including acid, irritants and inflammatory mediators.

Low threshold mechanical stimuli such as light touch and vibration are transduced by specialised low threshold mechanoreceptors such as Merkel's disks, Meissner's and Pacinian corpuscles and Ruffini's endings in the dermis of the skin (Figure 1.2a). However, noxious stimuli are transduced into electrical stimuli in free unencapsulated nerve endings that terminate more superficially in the skin, in the epidermis (Figure 1.2b) (Zimmerman et al., 2014).

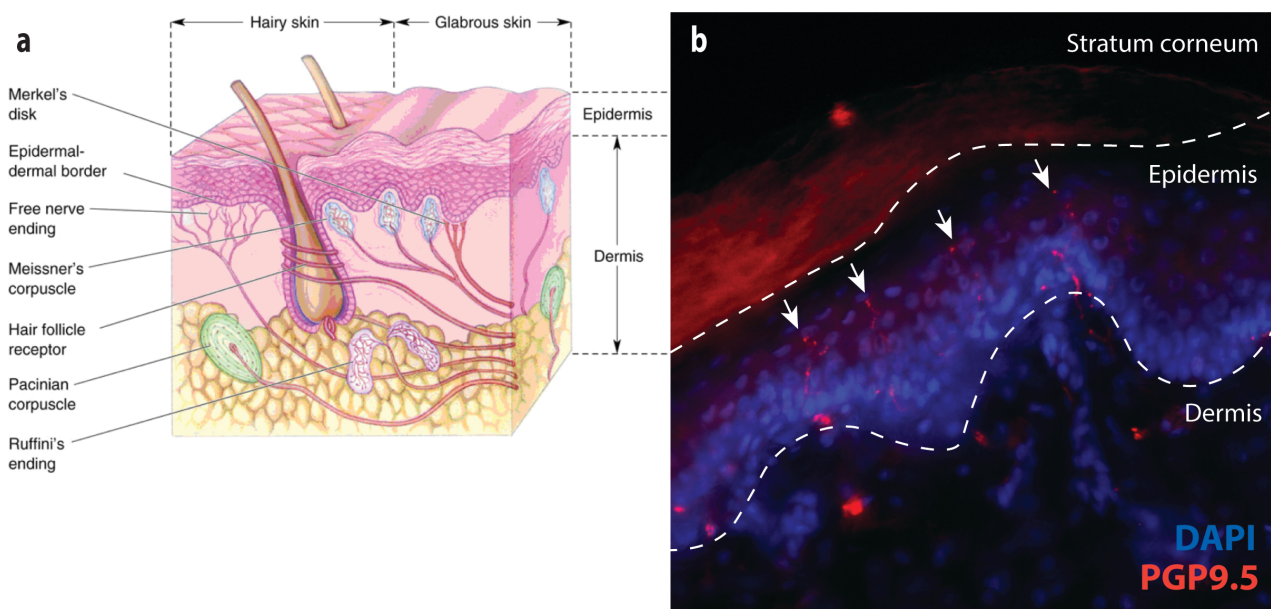


**Figure 1.2. Sensory innervation of the skin. a)** Diagram of the various receptors and sensory neurons residing in the hairy (left) and glabrous (right) types of skin. Figure adapted from Bear et al., 2006. **b)** Photomicrograph showing the glabrous skin of the plantar surface of a rat hind paw, with the nuclear marker DAPI in blue and the pan-neuronal marker protein gene product 9.5 (PGP9.5) in red. Dashed lines delineate the dermal-epidermal border and the beginning of the outermost layer of keratinised cells of the epidermis, known as the stratum corneum. Arrows mark epidermal free nerve endings. **Original image and figure.**

The sensory fibres that innervate the body can be classed into three main classes depending on their speed of conduction, governed by their diameter and degree of myelination (Table 1.1) (Pocock et al., 2013). The fastest conducting are the A $\beta$  fibres, followed by the A $\delta$  fibres and the slowest, smallest fibres are classified as C fibres. It is generally accepted that noxious stimuli are transduced by A $\delta$  and C nociceptors, whereas the A $\beta$  fibres mostly transmit the signals from low

threshold mechanoreceptors (such as Merkel’s disks, Meissner’s corpuscles and Pacinian corpuscles). The majority of C fibre nociceptors are polymodal which respond to heat, cold, mechanical and chemical stimuli and the majority of A $\delta$  nociceptors are predominately heat sensitive, mechanosensitive, or respond to both (Dubin & Patapoutian, 2010). The A $\delta$  fibres conduct fastest and mediate the quickly felt, pricking “first pain” and the C fibres slower conduction mediates the second, burning “slow pain” following a noxious insult.

<b>Fibre class</b>	<b>Conduction velocity (m/s)</b>	<b>Axon diameter (<math>\mu\text{m}</math>)</b>	<b>Degree of myelination</b>	<b>Modality</b>
A $\beta$	33-75	6-12	Heavily myelinated	Innocuous mechanical, vibration, proprioception
A $\delta$	5-30	1-5	Lightly myelinated	Noxious mechanical, noxious and innocuous thermal
C	0.5–2	0.2-1.5	Unmyelinated	Noxious mechanical, noxious and innocuous thermal, chemical

**Table 1.1. Fibre classes of the primary afferent sensory neurons.**

### 1.1.2 The dorsal root ganglia

The DRG encompass all the cell bodies of sensory neurons that innervate the body. In humans there are 31 pairs of ganglia associated with the spinal nerves that run down the left and right hand sides of the spinal cord. These run through cervical, thoracic, lumbar, sacral and coccygeal regions of the spine, and are named C1-8, T1-12, L1-5, S1-5 and the coccygeal. This is not absolutely conserved in rats, which instead run through C1-8, T1-13, L1-6 and S1-4, and don’t possess coccygeal spinal nerves (Krames, 2014). In rats, the large DRG of L4-6 innervate the hind leg and paw via the sciatic nerve (Swett et al., 1991). Many rodent pain models focus on the sciatic nerve and these particular lumbar DRG (Decosterd et al., 2000).

The morphology of all sensory neurons is described as pseudounipolar, a form of bipolarity. The cell bodies found in the DRG have an axon which projects from the cell body then branches into two directions, one branching distally from the cell body to the periphery and the other branching proximally to the spinal cord (Krames, 2014). The distal branch of the axon therefore functions as the “dendrites” of the DRG neuron. As the DRG lie outside the CNS, the sensory neurons within them are not protected by the blood brain barrier. The DRG also have high density vascularisation

which does not possess a functional nerve-blood barrier, leaving them exposed to small and large molecules in the plasma (Jimenez-Andrade et al., 2008). Sensory neurons are therefore particularly vulnerable to neurotoxic agents in the circulation and these can accumulate in the DRG leading to toxicity and neuropathy, such as chemotherapy-induced peripheral neuropathy (CIPN) (Section 1.3).

#### *1.1.2.1 Cell types of the dorsal root ganglia*

The sensory neurons of the DRG are notoriously heterogeneous. They vary greatly in terms of cell body diameter, the sensory modalities they respond to, sensory thresholds, and the proteins they express. In rat, DRG neurons with large cell bodies (average area  $1150\mu\text{m}^2$ ) are associated with the fast conduction  $\text{A}\beta$  fibres, medium sized neurons (average area  $600\mu\text{m}^2$ ) give rise to the finely myelinated  $\text{A}\delta$  fibres and the smallest diameter neurons (average area  $350\mu\text{m}^2$ ) are associated with C fibres (Lawson et al., 2019). The myelinated A fibres can be distinguished from C fibres by their immunoreactivity of certain neurofilaments such as neurofilament heavy chain (NF200) (Lawson & Waddell, 1991). The smaller, nociceptive C fibre neurons can be classed into two main subtypes, peptidergic and non-peptidergic. This nomenclature arises from the peptidergic class expressing signalling neuropeptides such as calcitonin gene-related peptide (CGRP) and substance P which are important in the transmission of pain stimuli (Wiesenfeld-Hallin et al. 1984; Hökfelt et al., 1975). The non-peptidergic class of C fibres is traditionally identified by the ability of the plant isolectin B4 (IB4) to bind to carbohydrate residues on the cell surface, and also highly overlaps with the expression of P2X3 receptors (Stucky & Lewin, 1999; Bradbury et al., 1998). However, this basic classification of nociceptors is based on a handful of markers that tell us little about the functionality of the neurons as classes.

With the advent of genomics and single cell RNA sequencing, classification of DRG neurons is no longer limited to histology or immunoreactivity and can instead be directly linked to their expression of functional markers such as ion channels, receptors and neuropeptides. Usoskin et al. (2014) published a seminal piece of work that used single cell RNA sequencing to sample and classify mouse DRG neurons, without using any pre-existing knowledge of the traditional subtypes and their markers. 799 cells were analysed and their transcriptomes were used to cluster and propose an unbiased classification of sensory neurons (Figure 1.3). This approach flagged up many of the traditional markers of A and C fibres, with neurofilament heavy chain (NEFH/NF200)

positive classes (NF group), CGRP-expressing classes (PEP group) and P2X3 expressing classes (NP group). These correspond relatively well to the myelinated A fibres, peptidergic C fibres and non-peptidergic C fibres respectively. There was also a tyrosine hydroxylase-expressing group described. However, these classes were further subdivided and with additional complexity compared to the traditional classes.

NF1	NF2	NF3	NF4	NF5	NP1	NP2	NP3	PEP1	PEP2	TH
LDHB CACNA1H TRKB <sup>high</sup> NECAB2	LDHB CACNA1H TRKB <sup>low</sup> CALB1 RET	LDHB TRKC <sup>high</sup> FAM19A1 RET	LDHB TRKC <sup>low</sup> PV SPP1 CNTNAP2	LDHB TRKC <sup>low</sup> PV SPP1 CNTNAP2	PLXNC1 <sup>high</sup> P2X3 GFRA2 MRGPRD	PLXNC1 <sup>high</sup> P2X3 TRKA CGRP MRGPR3	PLXNC1 <sup>high</sup> P2X3 SST	TRKA CGRP KIT TAC1 PLXNC1 <sup>low</sup>	TRKA CGRP KIT CNTNAP2 FAM19A1	PIEZO2 <sup>high</sup> VGLUT3 GFRA2
LTMRs		Proprioceptors			Nonpeptidergic			Peptidergic		C-LTMRs
NEFH		Myelinated			Unmyelinated			Myel.		Unmyel.
NEFH RET		NEFH RET			RET TRPV1 TRPA1 TRPC3 NAV1.8/9			TRPV1 TRPA1 TRPC3 NAV1.8/9		RET TRPA1 TRPC3 NAV1.8/9

**Figure 1.3. Sensory neuron classification based on single cell transcriptomics as defined by Usoskin et al., 2014.** NF = neurofilament positive groups corresponding to Aβ low threshold mechanoreceptors. NP = non-peptidergic C nociceptors. PEP = peptidergic C and Aδ nociceptors. TH = tyrosine hydroxylase positive C-type low threshold mechanoreceptors. Reprinted with permission from Springer Nature.

For example, the NF200-expressing NF group was split into 5; 3 classes of low threshold mechanoreceptors and 2 classes of proprioceptors. These subdivisions were based on their expression of, among other markers, tropomyosin receptor kinase B (TrkB), tropomyosin receptor kinase C (TrkC) and parvalbumin. However, the NF group is not the only one expressing NF200, with the PEP2 group also expressing this key marker, yet has been classified as peptidergic due to its expression of CGRP. The PEP2 class is therefore likely a lightly myelinated Aδ nociceptor. The PEP1 class is identified by its expression of substance P (TAC1). The NP group is characterised by their expression of P2X3, but it is interesting to note that one of these “non-peptidergic” classes, NP2, actually expresses the peptide CGRP. All of the nociceptive classes express NaV1.8 which is thought to be nociceptor specific (Stirling et al., 2005). Some of the nociceptor classes also express the transient receptor potential channel ankyrin 1 (TRPA1), the transient receptor potential channel vanilloid 1 (TRPV1), or both. Finally, the TH group is suggested to be a type of C low

threshold mechanoreceptor, involved in mechanical pain and also pleasant touch due to its high expression of the low threshold mechanosensitive ion channel Piezo2.

Since the Usoskin paper, other groups have also performed their own transcriptome analysis of rodent somatosensory neurons. For example, one group performed a deeper, high-coverage single-cell RNA-seq analysis of lumbar mouse DRG, as opposed to the low-coverage but high neuron number approach taken by Usoskin et al. (Li et al., 2016). This resulted in the classification of 10 distinct clusters named C1-C10, which could be further separated into 14 subclusters. The authors then went on to functionally classify neurons with electrophysiology prior to performing transcriptomic analysis. Clusters C1-6 were found to include small neurons that were mechano- and heat-sensitive nociceptors, mechanoreceptors, and itch-sensitive neurons. One cluster was shown to be a C-fibre low threshold mechanoreceptor, corresponding to the TH group in Usoskin et al. Clusters C7-C10 were large neurons which largely consisted of mechanoreceptors, but also included some heat-sensitive TRPV1-expressing neurons. A more recent study performed single-cell RNA-seq of the whole mouse nervous system and identified the main subdivisions of DRG neurons as non-peptidergic, peptidergic and neurofilament-expressing (Zeisel et al., 2018). They further subdivided these into 6 non-peptidergic, 8 peptidergic and 3 neurofilament-expressing subgroups, many of which matched to classifications originally elucidated by Usoskin et al.

Studies such as these are essential for relating the physiology of sensory neurons to their function, and are also important as they show that the traditional markers are not an exact classification system. For example, Usoskin et al. showed that CGRP is expressed at high levels in a subgroup of neurons which are classified as non-peptidergic.

#### *1.1.2.2 Ion channels of the dorsal root ganglia*

The electrical properties of any neuron are dictated by the distribution of ion channels at its membrane. This is true for sensory neurons as well but with added complexity, as the transduction of sensory inputs is also regulated by specialised ion channels. Transduction ion channels can be opened by mechanical deformation, certain temperatures, or the binding of chemicals, protons, or inflammatory mediators (Dubin & Patapoutian, 2010). These channels are cation selective and their opening leads to depolarisation of the membrane. An action potential is then initiated if this depolarisation reaches threshold. Sensory neurons express a wide range of voltage gated ion

channels, including voltage gated sodium channels (VGSCs), voltage gated calcium channels (VGCCs) and voltage gated potassium channels (VGKCs), which govern the action potential characteristics and transduce the receptor potential into one, or a set of, action potentials that encode the stimulus (Stenkowski & Smith, 2012). This travels to the CNS where the opening of VGCCs leads to the exocytosis of glutamate onto second order neurons. This ion channel-mediated process is vital for sensory neurons as it determines their modality, threshold, firing frequency, refractory period and also maintains intensity coding. Dysregulation of the ion channels governing these characteristics is a key factor in the development and maintenance of chronic pain and the focus of many current analgesics (Wood, 2007).

### *1.1.2.3 Transient receptor potential vanilloid 1*

The transient receptor potential (TRP) channels are differentially expressed by subpopulations of DRG neurons and play a key role in sensory transduction (Samanta et al., 2018). The TRPV1 channel is highly expressed by a subpopulation of small diameter, nociceptive fibres (Caterina & Julius, 2001). This multisensor channel is activated by a range of modalities including noxious heat above 42°C, acidic pH and capsaicin (Caterina et al., 1997). This channel is directly involved in the transduction of nociceptive sensation. Homozygous knockout mice show reduced capsaicin- and noxious heat-induced pain behaviours and show reduced thermal hypersensitivity following inflammation with mustard oil or complete Freund's adjuvant (CFA), demonstrating this channel's importance for noxious heat sensation and inflammatory pain (Caterina et al., 2000). Ablation of the TRPV1-expressing neurons during development using diphtheria toxin leads to a complete loss of heat sensation (Mishra et al., 2011). However, adult knockout of TRPV1 causes only minor deficits of acute noxious heat sensation. It has been shown that knockout of multiple TRP channels, specifically TRPV1, TRPM3 and TRPA1, is required to cause an absolute lack of behavioural response to noxious, burning heat (Vandewauw et al., 2018). These TRP channels have highly overlapping expression in particular subpopulations of DRG neurons, and it is hypothesised that this evolved as a fail-safe mechanism to maintain heat sensation even if the function of one of these channels is compromised.

Repeated or prolonged stimulation of TRPV1 leads to desensitisation of the nociceptor to subsequent TRPV1 activation. This is thought to be mediated by multiple mechanisms, but commonly triggered by calcium influx through the activated TRPV1 channel, as substitution of

barium ions for calcium ions prevents desensitisation in patch clamp experiments (Vyklícký et al., 2008). These proposed calcium-dependent mechanisms include a) protein kinase A-dependent phosphorylation of the channel leading to internalisation and lysosomal degradation, b) phosphatidylinositol 4,5-bisphosphate (PIP<sub>2</sub>) depletion in the membrane leading to modulation of the channel, and c) calmodulin-mediated gating of the channel (Sanz-Salvador et al., 2012; Yao & Qin, 2009; Numazaki et al., 2003). Tian et al. (2019) visualised the removal and insertion of a TRPV1-pHluorin construct at the membrane of HEK cells and DRG neurons in response to different concentrations of capsaicin. This showed that capsaicin induces a rapid decrease of membrane fluorescence over approximately 2 minutes, indicating an internalisation of the TRPV1-pHluorin from the membrane. The higher the concentration of capsaicin, the longer it took for the pHluorin to be re-inserted at the membrane, corresponding with the desensitisation of the cell to capsaicin. The propensity of TRPV1 channels to undergo rapid desensitisation is exploited for analgesic reasons by the use of high capsaicin doses to treat chronic pain such as neuropathy and musculoskeletal pain (Anand & Bley, 2011). However, morphological changes to the nociceptors also take place following capsaicin application, whereby it induces the degeneration of nerve fibres innervating the epidermis, lasting for a number of weeks (Simone et al., 1998). The gradual restoration of these epidermal nerve fibres coincide with the restoration of heat and pinprick pain sensation in skin biopsy patients injected with capsaicin.

The individual channel activity of TRPV1 can also be sensitised. This is due to the phosphorylation of various residues by protein kinase A (PKA), protein kinase C (PKC), calmodulin-dependant kinase 2 (CaMKII), proto-oncogene tyrosine-protein kinase Src (Src) and Cyclin dependent kinase 5 (Cdk5), which enhance the channel's responsiveness to agonists, heat and acid, as well as changing the open/closed kinetics of the channel to promote opening (Joseph et al., 2019; Studer & McNaughton, 2010). This has been shown to be an important factor of hyperalgesia development by inflammatory substances (phorbol myristate acetate and capsaicin) by the removal of a particular PKC phosphorylation site in mice (Joseph et al., 2019).

Sensitisation of TRPV1 is an important component of the thermal hypersensitivity associated with inflammatory pain. Inflammatory mediators such as bradykinin, prostaglandin E<sub>2</sub> (PGE<sub>2</sub>), adenosine triphosphate (ATP) and nerve growth factor (NGF) are able to upregulate the expression of TRPV1 at the RNA and protein levels, sensitise the TRPV1 channel, as well as enhance its trafficking to the membrane (Huang et al., 2006). NGF increases the percentage of

DRG neurons that express TRPV1 mRNA and protein shown by in situ hybridisation and immunocytochemistry (Amaya et al., 2004). Anti-NGF subsequently prevented this upregulation and reversed the behavioural thermal allodynia associated with CFA injection. The amount of receptor inserted in the membrane is also modulated by NGF, which may contribute to pain in inflammatory states. NGF binding to its receptor tropomyosin receptor kinase A (TrkA) leads to a signalling cascade involving phosphoinositide 3-kinase and Src which phosphorylates TRPV1 at a single tyrosine residue (Zhang et al., 2005). This leads to the rapid insertion of new TRPV1 channels into the membrane and therefore increased membrane current through the channels.

#### *1.1.2.4 Regulation of ion channels at the membrane of sensory neurons*

As with all proteins, ion channels are synthesised in the endoplasmic reticulum, undergo posttranslational modifications and folding and are then sorted into vesicles via the Golgi apparatus (Planells-Cases & Ferrer-Montie, 2007). The density of ion channels at the membrane is based on a balance of the synthesis of new protein, the transport of that protein to its functional location, the insertion of readily-available protein near the membrane via exocytosis, and the removal and recycling or degradation of protein already at the membrane via endocytosis.

Intracellular transport of proteins is performed by three families of molecular motors; myosin, kinesin, and dynein, which associate with microfilaments and microtubules (Stenoien & Brady, 1999). These motor proteins are responsible for the transport of ion channels from the soma to their functional location in the neuron, which may be over a metre away in the human body. The role of kinesins in ion channel localisation and trafficking is the most studied of the motor proteins. As an example, kinesin-1 has been shown to transport the voltage gated potassium channel Kv3.1 via direct binding to a Kinesin Family Member 5B (KIF5B) domain on the kinesin (Xu et al., 2010). This is essential for transport of fully assembled and functioning Kv3.1 channels to the axonal membrane. Other ion channels, such as  $\alpha$ -amino-3-hydroxy-5-methyl-4-isoxazolepropionic acid (AMPA) and N-methyl-D-aspartate (NMDA) receptors, require specialised adaptor proteins to interact with and be transported by kinesins. Glutamate receptor interacting protein-1 is one such adaptor protein which associates the GluR2 AMPA subunit with kinesin-1, actively transporting AMPA channels to its functional location at the dendrites (Setou et al., 2002). Kinesin Family Member 17 (KIF17), a member of the kinesin 2 family, has similarly been implicated in the trafficking of the NR2B NMDA receptor subunit within the dendrites of cortical,

hippocampal and olfactory neurons (Setou et al., 2000). This trafficking requires the adaptor molecule mLin-10.

In DRG neurons, kinesins have also been shown to transport the sensory neuron specific VGSC NaV1.8, and that this process may be one mechanism behind inflammatory sensitisation (Su et al., 2013). This publication demonstrated an interaction of the kinesin-1 protein KIF5B with NaV1.8. This interaction promoted NaV1.8 surface expression and maintained NaV1.8 currents, although this was demonstrated by cell surface biotinylation and patch clamping of transfected cell lines rather than sensory neurons. They then showed that this was taking place by KIF5B promoting forward transport of the channel. In DRG neurons they then used immunocytochemistry and western blotting to demonstrate NaV1.8 accumulation in the dendrites after transfection with KIF5B. They also demonstrated that KIF5 was upregulated in the sciatic nerve following CFA injection, which was correlated with accumulation of NaV1.8. Together, they take these experiments to mean that KIF5B is playing an active role in pain following peripheral inflammation, although most of the experiments were not performed in sensory neurons, or were performed with sensory neurons artificially overexpressing KIF5B.

As well as being trafficked via microtubules, ion channels must then be inserted into the membrane via exocytosis. There are two pathways of exocytosis, constitutive and regulated. Constitutive exocytosis occurs in all eukaryotic cells and provides a steady fusion of vesicles with the membrane. Regulated exocytosis is only present in certain cell types such as neurons or endocrine cells and delivers vesicles (for example those containing neurotransmitters) to the membrane in response to a stimulus, most often a rise in intracellular calcium concentration (Gerber & Südhof, 2002). Changes in the rate of these processes theoretically could lead to either a build-up of neuron-exciting ion channels such as VGSCs or TRP channels, or the deficit of channels that depress activity such as VGKCs.

A proposed general mechanism for the regulation of different types of protein at the membrane is known as constitutive cycling (Royle & Murrell-Lagnado, 2002). This model states that proteins undergo regular internalisation and reinsertion at the membrane, and the levels of protein are controlled by a balance of this endo- and exocytosis. All it takes to rapidly increase or decrease membrane levels of a protein like this is to modify the rates at which these two opposing processes happen. It has been suggested that this is the case with AMPA receptors at the post-

synapse (Burrone & Murthy, 2001). Changing the density and number of AMPA receptors at the membrane has physiological relevance as this would determine the strength of the synapse via long term potentiation and depression (LTP/LTD) and have the ability to unmask silent synapses containing NMDA receptors. This is evidenced by blockade of exocytosis leading to reductions in AMPA receptor excitatory postsynaptic currents (EPSCs), whereas inhibiting endocytosis caused an opposing increase in EPSCs, demonstrated in hippocampal CA1 pyramidal cells (Lüscher et al., 1999). As chronic pain is known to be associated with LTP at the synapse from the sensory neurons to the spinal cord then an imbalance of constitutive cycling could theoretically play a role.

Rather than regulation purely by constitutive exocytosis, there is significant literature suggesting that ion channel membrane expression may be actively controlled by regulated exocytosis.

Members of the TRP family of ion channels utilise regulated exocytosis to acutely increase their expression in the membrane of sensory neurons following exposure to inflammatory sensitisers, which may play a role in the mechanism of inflammatory pain. Camprubí-Robles et al. (2009) demonstrated that certain inflammatory mediators upregulated both the amplitude of calcium responses of capsaicin-stimulated DRG, as well as immunoreactivity of TRPV1 at the membrane with an extracellular antibody. NGF, ATP, and insulin-like growth factor 1 (IGF1) all potentiated TRPV1 surface expression. Potentiation of TRPV1 expression was blocked by a synaptosomal-associated protein, 25kDa (SNAP25) blocking peptide, demonstrating that certain inflammatory mediators induce regulated exocytosis that is dependent on soluble NSF attachment protein receptor (SNARE) proteins to deliver TRPV1 to the membrane of sensory neurons.

Another publication showed multiple interactions and involvements of TRPV1 with vesicular proteins involved in regulated exocytosis (Morenilla-Palao et al., 2004). TRPV1 was demonstrated to be associated with multiple vesicle proteins in a yeast two-hybrid screen, pull-downs in HEK293 cells, and immunofluorescence of primary DRG neurons. The yeast two-hybrid screen and pull-down assay showed an interaction with snapin and Syt9, and immunofluorescence showed TRPV1 colocalisation with vesicle-associated membrane protein 2 (VAMP2). The publication also showed PKC-mediated potentiation of TRPV1 currents in oocytes treated with 12-O-tetradecanoylphorbol-13-acetate, a PKC activator. The interaction with snapin was shown to be functionally relevant as overexpression blocked the PKC-mediated translocation of the channel. Treatment with BoNT/A also abolished this upregulation, demonstrating an action of SNAP25, a SNARE protein directly involved in regulated exocytosis. These experiments lead to the conclusion that TRPV1 currents

are potentiated by rapid insertion in the membrane via a regulated, SNARE-dependent mechanism. However, the finding that TRPV1 colocalises with VAMP2-containing vesicles is directly in conflict with another report that claims that TRPV1 (and TRPA1) do not colocalise with VAMP2 but instead with vesicle-associated membrane protein 1 (VAMP1) (Meng et al., 2016). Whichever the particular VAMP isoform, it is evident that TRPV1 is carried by vesicles containing proteins involved in regulated exocytosis.

In a similar manner to TRPV1, TRPA1 translocation to the membrane of transfected HEK cells has been associated with exposure to the inflammatory mediator mustard oil, which has direct relevance to sensitisation leading to inflammatory pain (Schmidt et al., 2009). Mustard oil significantly increased surface labelling of TRPA1 in these cells, which was dependent on calcium influx and PKA and PKC signalling. This study demonstrated that mustard oil also increased TRPA1 membrane labelling of cultured DRG neurons as well as the HEK cells. Calcium imaging was used to determine the number of neurons that had potentiated TRPA1 responses following mustard oil application. This number was significantly decreased when neurons were intoxicated with tetanus, which inhibits vesicle fusion by cleavage of the SNARE protein VAMP2. Using patch clamping to measure membrane capacitance of TRPA1-expressing neurons, mustard oil was shown to increase the surface area of the membrane, suggesting fusion of vesicles by exocytosis. Taken together, these experiments suggest that mustard oil induces the translocation of TRPA1 channels to the membrane requiring a SNARE-dependent mechanism.

Perhaps the most well documented effect on pain that involves ion channel trafficking within DRG neurons is the prevention of VGCC trafficking by gabapentinoids. Gabapentinoids are ligands of the auxiliary  $\alpha_2\delta$  subunits of VGCCs, and binding prevents these subunits from enhancing VGCC trafficking to the membrane (Hendrich et al., 2008). This takes place in DRG neurons and reduces calcium currents, and subsequently synaptic transmission, to the spinal cord over time.

Gabapentinoids are first line treatments for various neuropathic pains, clearly showing that pain can be reduced by regulating the distribution of ion channels at the membrane of sensory neurons via trafficking mechanisms.

As well as the expression and insertion of various ion channels at the DRG membrane, altered degradation of certain channels have also been demonstrated to affect membrane excitability in pain conditions (Cheng et al., 2021). Proteins such as ion channels are degraded by the ubiquitin-

proteasome pathway. Proteins are targeted for degradation via ubiquitination by ubiquitin ligases, and removed from this pathway by deubiquitinating enzymes. An example of this pathway's involvement in pain regulation was demonstrated by identification of an interaction of the deubiquitinating enzyme ubiquitin carboxyl-terminal hydrolase 5 (USP5) with the calcium channel CaV3.2 in mouse DRG neurons (García-Caballero et al., 2014). This publication showed an upregulation of USP5 in DRG and spinal cord following CFA injection or chronic constriction injury, as well as higher association of CaV3.2 with USP5 after chronic constriction injury. Knockdown of USP5 by short hairpin RNA was able to reverse mechanical hyperalgesia associated with CFA injection and chronic constriction injury, and this was associated with reduced CaV3.2 protein levels and CaV3.2 currents. Uncoupling the association between USP5 and CaV3.2 channels also causes analgesia.

Conversely to deubiquitination, altered activity of ubiquitin ligases has also been associated with pain. The ubiquitin ligase NEDD4-2 is involved in the ubiquitination of NaV1.7 and NaV1.8 in mouse DRG (Laedermann et al., 2013). After spared nerve injury (SNI), a neuropathic injury model, NEDD4-2 expression was reduced, leading to an increased NaV current amplitudes in freshly dissociated DRG neurons. Knockout of NEDD4-2 led to increased expression of NaV1.7 and increased NaV1.7 and NaV1.8 currents. These studies provide evidence that inflammation or neuropathic injury can affect the expression of ubiquitin ligases and deubiquitinating enzymes, altering degradation and leading to increased expression of excitatory ion channels at the membrane, leading to hyperexcitability.

### *1.1.3 Dorsal horn of the spinal cord*

The primary afferent neurons of the DRG travel to the CNS and synapse onto interneurons or projection neurons in the dorsal horn of the spinal cord. All sensory neurons release glutamate as their primary neurotransmitter but may also signal with a range of other transmitters such as neuropeptides like substance P and CGRP (Dubin & Patapoutian, 2010).

The spinal cord is divided dorsally to ventrally into distinct layers, or laminae. The sensory neurons entering the dorsal horn terminate in distinct laminae based on fibre diameter and function. The nociceptive C-fibres terminate in the superficial dorsal horn in laminae I and II, and nociceptive A $\delta$ -fibres terminate in laminae I with some branching to lamina V (Figure 1.4). The low threshold A $\beta$

fibres generally terminate in deeper layers of the spinal cord in laminae III to V with some extension to laminae II (Todd, 2010).

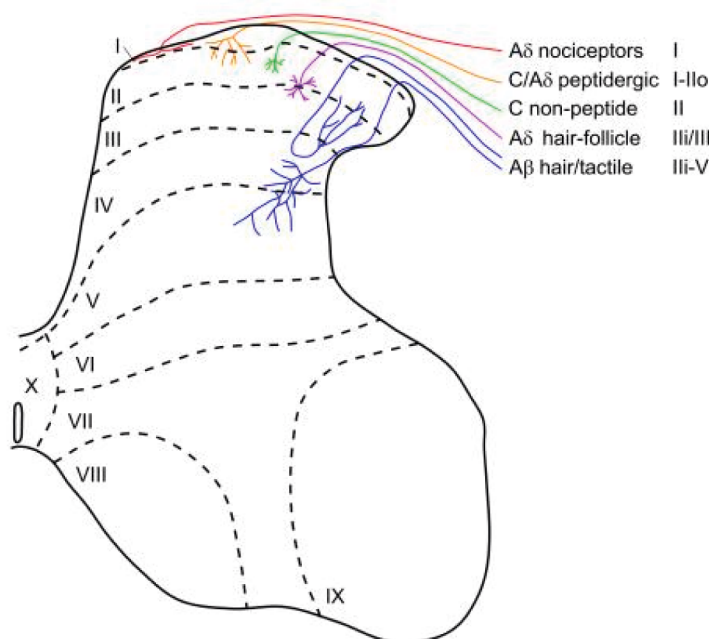


**Figure 1.4. Termination of primary sensory afferents onto the dorsal horn of the spinal cord.** Different classes of sensory neuron fibres terminate in different laminae within the dorsal horn of the spinal cord. Nociceptive C- and A $\delta$ -fibres generally terminate more superficially in laminae I and II, and non-nociceptive A $\beta$ -fibres generally terminate in deeper layers III to V. Figure adapted from Todd, 2010, reprinted with permission from Springer Nature.

There is processing of sensory signals within the spinal cord, and inputs are subject to top-down modulation from higher brain areas. These processed signals then travel to the brain via ascending spinal cord tracts and the thalamus. The discriminative and affective aspects of touch and pain are then “felt” due to activity of cortical areas such as the somatosensory cortex, anterior cingulate cortex and insula (Treede et al., 1999).

It is thought that circuits of the spinal cord must play a major role in the development of allodynia in pain states, as under normal conditions the perceptions of non-painful sensory modalities and painful stimuli are segregated (Sandkühler, 2009). However, after injury this segregation is disrupted and A $\beta$ -mediated sensations that ought to be below the threshold for eliciting nociception can become painful. Allodynia can develop very quickly, suggesting that the structural pathways linking touch and pain already exist in non-pathological states. Genetic modulation has led to the understanding that distinct populations of spinal interneurons gate the circuit

connecting touch and pain pathways, leading to mechanical allodynia when these gating neurons are disinhibited. A recent publication published in *Neuron* used chemogenetic manipulation and designer receptor exclusively activated by designer drug (DREADD)-based inhibition or activation to probe the involvement of interneurons in more superficial laminae II-III (calretinin or PKC gamma expressing) and those in deeper laminae III-IV (cholecystokinin and transient vesicular glutamate transporter 3-expressing) in bringing about allodynia following different types of injury (Peirs et al., 2021). They found that these different types of neurons are required for the induction of mechanical allodynia after different types of injury. Specifically, calretinin interneurons are important for allodynia after inflammatory insults (CFA injection and surgical incision) but not neuropathic insults. The opposite was true of the PKC gamma interneurons, as inhibition with DREADDs blocked neuropathic SNI allodynia but not allodynia after inflammation. The deeper cholecystokinin interneurons were required for allodynia following either neuropathic or inflammatory pain models. This publication highlights the complexity of the circuits that mediate allodynia and is the first to suggest that these circuits are likely different following different types of injury.

## ***1.2 Acute and chronic pain***

Acute pain in response to potential or actual tissue damage serves an evolutionary purpose to protect the body. However, chronic pain is defined as pain which lasts or recurs for 3 months or more, and this type of pain differs from acute pain in that it can occur in the absence of damage, persist after tissue damage has been resolved, and/or spread beyond the site of injury (Treede et al., 2015). This type of pain therefore becomes pathophysiological and is no longer directly coupled to **the protective function of** nociception. There are different classifications of chronic pain based on their nature of origin (Table 1.2).

<b>Chronic pain classification</b>	<b>Definition of classification</b>	<b>Examples</b>
Cancer-related	Pain caused by cancer or its treatment	Tumour pain Chemotherapy-induced peripheral neuropathy
Post-surgical and post-traumatic	Pain that persists beyond healing after surgery or other tissue injury	Post-surgical pain
Neuropathic	Pain caused by lesion or disease of the somatosensory nervous system	Post-stroke pain Diabetic neuropathy
Headache and orofacial	Primary idiopathic headache and orofacial pain, rather than secondary to another disorder	Migraine Temporomandibular disorders Trigeminal neuralgia
Visceral	Pain that originates from the internal organs	Ischemia Thrombosis Obstruction and distension
Musculoskeletal	Pain that arises as disease of the bones, joints, muscles or related tissues	Rheumatoid arthritis Osteoarthritis
Primary	Pain that cannot be better explained by another chronic pain condition	Fibromyalgia Irritable bowel syndrome

**Table 1.2. Classification of chronic pain types of the International Classification of Diseases (ICD)-11.** Chronic pains have been subdivided into 7 groups based on the perceived location of pain, its etiology or the primarily affected anatomical system. Pain diagnoses which defy these classification principles are defined as chronic primary pains. Certain types of pain may have aspects of multiple classifications (Treede et al., 2015).

### 1.2.1 Pathophysiology of chronic pain

The maintenance of chronic pain that outlasts acute injury is a complex phenomenon, but can be linked to sensitisation and electrical hyperexcitability of neurons within the pain pathway. This can occur at many levels of the nervous system; the nociceptors, the synapses onto the spinal cord, within the spinal cord, or from top down modulation by higher brain areas. This leads to symptoms such as spontaneous pain (pain in the absence of sensory stimulation), hyperalgesia (an abnormally increased feeling of pain to nociceptive stimuli) and allodynia (pain caused by a stimulus that normally would not elicit pain).

#### 1.2.1.1 Peripheral sensitisation

Peripheral sensitisation is a mechanism which reduces nociceptor thresholds for firing and/or increases their responsiveness to stimulation (Schaible et al., 2011). This is as a result of chemical mediator release from injured cells, mast cells or leukocytes which can occur as a result of tissue damage, disease or inflammation. The chemical mediators acting on the peripheral nociceptors include ATP, bradykinins, prostaglandins, histamine and NGF (Iyengar et al., 2017). These mediators can bind to receptors on nociceptors and directly activate them. However, the activity of ion channels on the membrane of the primary afferents can also be modulated by the action of inflammatory mediators, either at the transcriptional or post-translational level. For example, phosphorylation of ion channels is affected via kinase activation, but kinases can also enhance the expression of certain ion channels via the recruitment of transcription factors (Gangadharan & Kuner, 2013).

As the DRG are pseudounipolar and project both proximally and distally, stimulation of the primary afferents themselves can lead to peripheral sensitisation as a result of an axon reflex (Iyengar et al., 2017). When nociceptors are stimulated, neuropeptides such as CGRP and substance P can be released from peripheral terminals of the same axon (Figure 1.5). These neuropeptides activate receptors which induce the release of inflammatory mediators from non-neuronal cells and also sensitise peripheral primary afferents, in a process called neurogenic inflammation. Over time this causes further increased release of neuropeptides and also changes the distribution of ion channels on the nociceptors. This lowers thresholds for activation of the nociceptors, leading to a self-maintaining mechanism whereby pain can outlast tissue healing and become chronic.

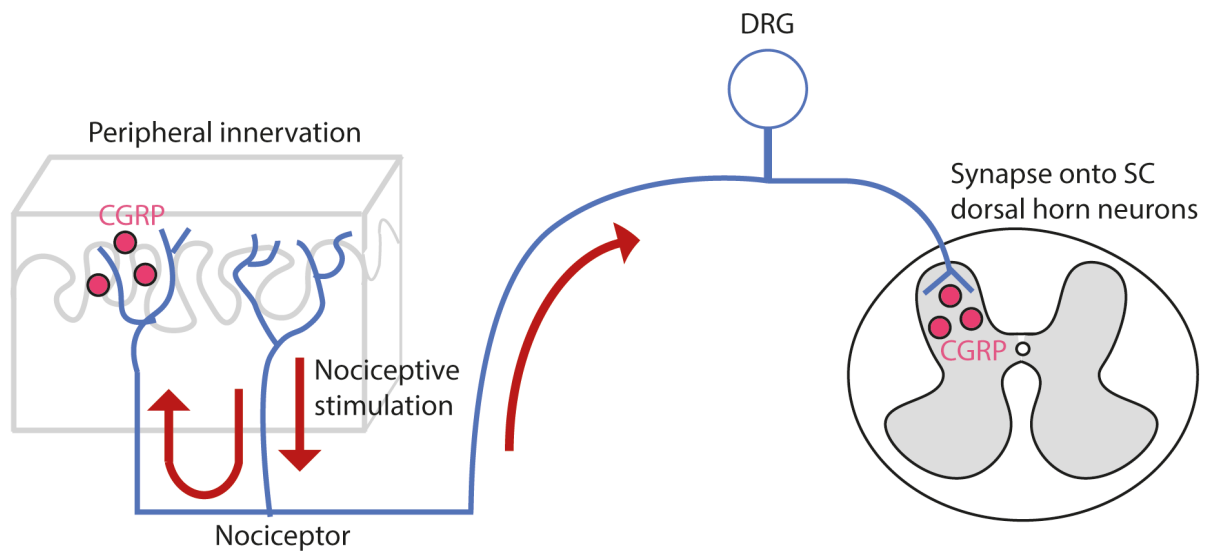


**Figure 1.5. Release of calcitonin gene-related peptide (CGRP) from primary afferent neurons.** Stimulation of nociceptors can lead to the release of CGRP from both central and peripheral terminals. CGRP is released as a co-transmitter onto the spinal cord, or in the periphery leading to neurogenic inflammation and peripheral sensitisation.

The neuropeptide CGRP is expressed in a subpopulation of sensory neurons and is fundamentally important to the mechanism of peripheral sensitisation. This 37 amino acid peptide acts via a G-protein coupled receptor (GPCR) formed by the dimerisation of the calcitonin receptor-like receptor (CLR) and receptor activity modifying protein-1 (RAMP1) (Choksi et al., 2002). Repeated injections of low concentration CGRP (5 injections of 0.1 fmol) into the rat paw induces mechanical hypersensitivity as assessed by response latency to the Randall-Selitto test (Nakamura-Craig et al., 1991). However, a single injection of CGRP at a much higher dose (100 fmol) was not sufficient to induce any hypersensitivity, suggesting that CGRP sensitises the nociceptors over time. This effect is long lasting, as after waiting 3 hours for the hypersensitivity induced by repeated CGRP injections to return to baseline, just one more injection of CGRP was enough to return to the peak of hypersensitivity. Stimulation of the primary afferents, for example using capsaicin, is also sufficient to induce CGRP release in the periphery (Kilo et al., 1997). This leads to the characteristic increased blood flow “flare response” due to neurogenic inflammation, which can be successfully blocked with a CGRP antagonist (Sinclair et al., 2010).

### *1.2.1.2 Central sensitisation*

Another area of the pain-sensing pathway that can be modulated by persistent nociceptive stimulation is the synapse from the primary afferent to the secondary neuron in the dorsal horn of the spinal cord. Persistent firing can result in maladaptive neuroplasticity in a mechanism called central sensitisation (Latremoliere & Woolf, 2009). The NMDA receptor plays a key role in this process (Woolf & Thompson, 1991). The sustained release of glutamate and neuropeptides from the primary afferent depolarises the postsynaptic membrane enough to overcome the magnesium block of the NMDA receptor pore. This allows calcium in through the pore, leading to the activation of intracellular pathways which strengthen the synapse and sensitise the dorsal horn neuron. Calcium ions activate kinases such as PKC and CaMKII (Latremoliere & Woolf, 2009). This has multiple effects, including the phosphorylation of NMDA and AMPA receptors, changing their kinetics. The trafficking of AMPA receptors to the membrane is also increased in an LTP-type mechanism, strengthening the synapse. Transcription factors are also activated by intracellular calcium, driving the expression of genes to produce a long-lasting strengthening of the synapse. These changes can therefore lead to hyperexcitability of the pain pathway at the synapse from the primary afferent to the dorsal horn, leading to the perception of pain in response to low intensity sensory input.

As well as its role in peripheral sensitisation, CGRP also plays a role in central sensitisation, as shown by the application of CGRP antagonists to the dorsal horn via microdialysis (Sun et al., 2003; Sun et al., 2004a). Antagonists applied to the dorsal horn prevent the sensitisation of second order neurons by an injection of capsaicin into the hindpaw, and subsequently prevent the secondary mechanical hyperalgesia and allodynia that capsaicin induces. CGRP is thought to facilitate nociceptive synaptic transmission by inducing plasticity changes that are the driving feature of central sensitisation. These changes are dependent on the activation of PKA and PKC, and modulate the properties of the synapse from the DRG neuron to the spinal cord (Sun et al., 2004b). For example, the electrical stimulation of the dorsal root afferents evoked larger amplitude monosynaptic EPSCs from rats following an injection of kaolin/carrageenan into the knee compared to control, and dorsal horn neurons showed increased firing rates (Bird et al., 2006). The application of a CGRP antagonist to the spinal cord brought this facilitated synaptic transmission back down to baseline in the inflammatory injection model but had no effect on

naïve spinal cord, suggesting that CGRP is playing a role in the potentiation of the synapse from primary afferent to dorsal horn.

Top-down modulation from the brain can also affect spinal pain signalling via descending pathways. These projections originate in midbrain and brainstem areas such as the periaqueductal grey, amygdala, rostroventral medulla, dorsal reticular nucleus, and nucleus of the solitary tract (Millan et al., 2002). These descending pathways act on spinal cord interneurons to either inhibit or facilitate pain transmission. These pathways can result in the release of endogenous opioids (also known as endorphins) in the dorsal horn of the spinal cord, resulting in the inhibition of excitability and neuropeptide release (Heinke et al., 2011). Descending monoaminergic pathways also have the ability to inhibit or excite neuronal responses of the dorsal horn. Specifically, noradrenaline release is anti-nociceptive via activation of adrenoceptors on GABA-ergic and glycinergic inhibitory interneurons, leading to inhibition of pain pathway spinal cord projection neurons (Bannister & Dickenson, 2016). On the other hand, descending 5-HT pathways can be facilitatory or inhibitory to pain transmission in the spinal cord. Evidence points to maladaptive responses of these descending projections in chronic pain conditions such as neuropathy, and action in the spinal cord is likely a significant mechanism of analgesia for opiates and anti-depressants.

### 1.2.1.3 Glial activation

Another change that occurs in the spinal cord that is thought to be a key mechanism of chronic pain is the activation of glial cells in response to nerve injury, tissue damage, inflammation, or activation of the nociceptive pathways. Microglia and astrocytes are non-neuronal cell types that are present in the CNS that react to changes which are interpreted as a potential threat. Their morphology and motility changes in response to conditions such as damage, ischemia or pathogenic invasion and they become “activated” and proliferate. It is now known that there is complex neuron-glia signalling occurring in the CNS, and there is increasing evidence that glia directly affect spinal neurotransmission with implications for the development and maintenance of chronic pain (Bradesi et al., 2010). Inhibition of glial activation using minocycline (an antibiotic targeting microglia) or fluorocitrate (which disrupts both microglial and astrocytic metabolism) reduces inflammatory pain, neuropathic pain and post-operative pains (Suter et al., 2007)

Following damage, glia are thought to be activated by circulating mediators such as ATP, chemokines or glucocorticoids, or neurotransmitters that are released by the primary afferent following stimulation, such as substance P, CGRP or glutamate (Bradesi et al., 2010). Repetitive firing of the DRG neuron is also sufficient to induce microglia activation. The activation of microglia following SNI can be blocked by bupivacaine, a local anaesthetic, showing that microglia respond directly to peripheral neuronal activity (Wen et al., 2007). In turn, the activated microglia and astrocytes then secrete pro-inflammatory mediators such as cytokines, chemokines, ATP and nitric oxide which act to sensitise the spinal cord neurons but also feed back onto the glia themselves, leading to an amplification loop (Bradesi et al., 2010). It is therefore important to recognise that the neurons of the pain-sensing pathway do not function in isolation, and the impact of non-neuronal cells on chronic pain must be taken into account.

### ***1.2.2 Neuropathic pain***

One form of chronic pain with poorly understood pathophysiology is neuropathic pain. This form of pain is estimated to affect 6.9-10% of the UK population and can have many diverse causes (van Hecke et al., 2013). Neuropathic pain is caused by damage or disease of the somatosensory nervous system, including the peripheral nerves, spinal cord, or brain. Central neuropathic pains are caused by lesions of the CNS, for example following a stroke or as a result of autoimmune disorders such as multiple sclerosis. Traumatic damage can also induce neuropathic pain either centrally or peripherally, but the most common cause of peripheral neuropathy is peripheral diabetic neuropathy. Viral infections can also damage the peripheral nerves, as in post-herpetic neuralgia. Chemotherapy drugs are toxic to the peripheral sensory neurons, inducing neuropathic pain. CIPN fits into both the chronic neuropathic and the chronic cancer-related categories of chronic pain set out in the International Classification of Diseases (ICD)-11 (Treede et al., 2015).

### ***1.3 Chemotherapy-induced peripheral neuropathy***

CIPN is a form of neuropathy that arises from common cancer treatment drugs. Primarily it is a sensory axonal neuropathy but in severe cases the motor neurons can be affected, leading to muscle weakness. Sensory symptoms include tingling, numbness, spontaneous shooting pains or burning, mechanical hyperalgesia, hot and cold hypersensitivity. These sensations particularly

affect the distal extremities of the hands and feet in a “stocking and glove” distribution, as longer axons are affected first (Zajączkowska et al., 2019). Considering that the incidence of CIPN is estimated to be as high as 60% three months after the cessation of chemotherapy, this is a major clinical problem which can considerably affect quality of life (Seretny et al., 2014). It is also the most common reason for dose-reduction or cessation of chemotherapy, so also has a direct impact on cancer survival rates. With the exception of paclitaxel and oxaliplatin which can occasionally cause acute neuropathy immediately after exposure, the majority of CIPN develops weeks or months after treatment, and can continue or worsen after the succession of treatment in a phenomenon known as “coasting”. As CIPN can persist for many years after treatment, this is commonly becoming a problem for the increasing number of cancer survivors in the population as cancer treatment improves (Polomano et al., 2006).

Category of antineoplastic	Antineoplastic mechanism	Drug name
Platinum-based	Crosslinking of DNA, subsequent inhibition of DNA repair and/or DNA synthesis (Mehmood, 2014)	Cisplatin Carboplatin Oxaliplatin
Protease inhibitor	Binds the 26S proteasome, preventing degeneration of pro-apoptotic factors, promoting apoptosis (Chen et al., 2011)	Bortezomib
Immunomodulatory	Complex, inhibits angiogenesis, inhibits cell adhesion and cytokine circuit, enhances immune cell response, induces oxidative stress and apoptosis (Zhou et al., 2013)	Thalidomide
Vinca alkaloid	Binds tubulin and prevents microtubule polymerisation, preventing segregation of chromosomes, preventing mitosis and inducing apoptosis (Moudi et al., 2013)	Vincristine
Taxane	Stabilises tubulin in the microtubule, preventing depolymerisation and causing cell cycle arrest and subsequent apoptosis (Weaver et al., 2017)	Paclitaxel (Taxol) Docetaxel

**Table 1.3. Categories of antineoplastic that cause chemotherapy-induced peripheral neuropathy (CIPN).** Many antineoplastic agents with different mechanisms can cause CIPN. This table lists the drugs with the highest incidence of CIPN with the mechanism of their antineoplastic activity.

Interestingly, CIPN is a shared feature of many neoplastic agents, including those with disparate mechanisms (Table 1.3). It can occur with either a single high dose or cumulative doses over time and can vary in intensity from mild to dose-limiting, and in duration up to years following exposure (Zajączkowska et al., 2019). The mechanisms by which chemotherapy agents damage sensory axons and induce CIPN are complex and multifactorial, involving microtubule disruption, oxidative

stress, mitochondrial damage, neuro-inflammatory mechanisms, structural axonal changes including demyelination, and the dysregulation of ion channels, ultimately leading to alterations of sensory neuron excitability and subsequent pain. The focus of this thesis is on the taxane based chemotherapy drug paclitaxel, and the specific mechanisms by which this drug induces neuropathy will be discussed further below.

### *1.3.1 Paclitaxel*

Paclitaxel (also referred to by its brand name Taxol) was originally derived from the bark of the Pacific yew tree, *Taxus brevifolia*, and is a member of the taxane family of antineoplastics. It is prescribed to treat many types of cancer, including ovarian, breast, non-small cell lung, and pancreatic cancers (National Institute for Health and Care Excellence, 2020). The taxanes target and bind to  $\beta$ -tubulin subunits of microtubules, stabilising the microtubule polymer by blocking the effects of guanosine-5'-triphosphate (GTP) hydrolysis and preventing microtubule depolymerisation (Löwe et al., 2001; Amos & Löwe, 1999). In tumour cells this is desirable as it arrests the cell cycle at mitosis, inducing cytotoxicity and apoptosis (Wang et al., 2000). How this action of paclitaxel also leads to toxicity of long axons of the peripheral sensory neurons, however, is complex and far from fully understood.

### *1.3.2 Paclitaxel-induced peripheral neuropathy*

Paclitaxel is one of the most neurotoxic chemotherapy drugs widely used. One study reported neuropathic symptoms in 50%, 79% and 100% of patients with starting dose levels of 135, 175, and 250mg/m<sup>2</sup> respectively, and this incidence increased even further with repeated cumulative dosing (Postma et al., 1995). The symptoms occur in the stocking and glove distribution typical of CIPN, and can include mechanical allodynia, cold allodynia, burning pains, shooting pains, numbness and tingling (Toftthagen et al., 2013).

#### *1.3.2.1 Susceptible populations of sensory neurons*

The particular sensory neurons affected by paclitaxel can be identified by immunohistochemistry of the stress responsive transcription factor Activating Transcription Factor 3 (ATF3). The number

of DRG nuclei that immunoreactive for ATF3 following paclitaxel treatment is variable within the published data. In some studies, the number of ATF3-expressing DRG nuclei remains relatively low, increasing from approximately 0.4% in the control condition to approximately 1% 13 days after the first injection (Makker et al., 2017). This increase was driven by damage of larger myelinated, NF200-expressing neurons and non-peptidergic IB4-binding neurons. There was no double labelling of ATF3 with CGRP, a marker of peptidergic DRG neurons. A similarly modest increase of ATF3 labelling, from 0.16% to 1.24% was also demonstrated by Jamieson et al. (2007), 7 days after the final injection of paclitaxel. The size distribution of the ATF3 positive neurons was investigated and showed this increase within only medium and large neurons. Some groups find virtually no induction of ATF3 expression after paclitaxel treatment whatsoever (Flatters & Bennett, 2006). One study reported a much more drastic increase in total ATF3 labelling in the DRG, peaking 6 days after treatment at over 20%, but still at between 5-10% at day 10 (Peters et al., 2007). Again, this was driven by increased co-labelling with large diameter sensory neurons.

Crucially, all these publications detected electrophysiological changes, physiological changes or behavioural hyperalgesia due to paclitaxel treatment, despite the disparity in the percentage of damaged DRG as identified by ATF3 expression. These differences may have arisen through the drastically different treatment regimens used. Peters et al. injected a relatively large cumulative dose of 36mg/kg over 2 days, whereas Makker et al. used a lower dose of 20mg/kg over 8 days and Jamieson used a much longer 9 week timescale to give a cumulative dose of 108mg/kg. The greatest ATF3 expression shown by Peters et al. was also the only study to use intravenous dosing of paclitaxel, rather than intraperitoneal.

It is striking that larger, myelinated populations of neurons appear to be those most damaged by paclitaxel, despite the common painful phenotype. This is a finding replicated using microscopy to directly visualise the degeneration of axons (Boehmerle et al., 2014). It is also notable that a higher incidence of spontaneous discharges and increased electrical excitability are only detected in large-medium diameter DRG when patch clamping is performed on DRG cultures from animals that underwent a paclitaxel injection protocol (Zhang & Dougherty, 2014). Numbness and paraesthesia can be present in patients with CIPN, which could be accounted for by the damage or axonal degeneration of these particular large diameter DRG neurons which are largely attributed to low threshold mechanoreceptors and proprioceptors (Toftagen et al., 2013). Why CIPN also

induces a painful phenotype, normally presumed to be mediated by smaller diameter nociceptive neurons, when this subpopulation doesn't appear particularly vulnerable to paclitaxel is not clear.

### 1.3.2.2 Axonal toxicity, microtubule disruption, and intraepidermal nerve fibre loss

Damage caused by paclitaxel seems to most dramatically affect axons of sensory neurons distally to proximally, leading to degeneration and demyelination as shown in rodent models (Tasnim et al., 2016; Gornstein & Schwarz, 2017). This effect can be measured *in vivo* as a reduction in the sensory nerve action potential amplitude and nerve conduction velocity of the caudal nerve (Gornstein & Schwarz, 2017). Both these electrophysiological measures have also been demonstrated in patients with CIPN, correlating with the severity of their symptoms (Matsuoka et al., 2016).

Another quantifiable manifestation of the axonal toxicity caused by paclitaxel (and other anti-neoplastics) in rodent models is the reduction of intraepidermal nerve fibre (IENF) density in the skin. The timecourse of this reduction is correlated with pain symptoms, developing over weeks (Boyette-Davis et al., 2011). It's also notable that chemotherapy drugs which are more likely to induce CIPN induce a greater reduction of IENF densities (Wozniak et al., 2018). This finding supports the idea that chemotherapy drugs induce degeneration of the most distal axons first, which are found in the epidermis. Structural and functional changes to the nociceptors which innervate the epidermis may well be a factor in the development of pain but, while there is a clear correlation of reduced IENFs with painful CIPN symptoms, a definitive causation is yet to be proven.

Structural changes to neurites in cultures of DRG neurons can be induced by paclitaxel and other chemotherapy drugs applied *in vitro*, suggesting that a similar type of axonal toxicity is also present in culture. A commonly observed feature is the retraction and degeneration of neurites in the culture, leading to reduced neurite length and branching (Yang et al., 2009; James et al., 2008). Paclitaxel's microtubule stabilising effects are likely the primary cause of this axonal toxicity, as other microtubule stabilising agents such as epitholone B also induce identical axonal structural changes to DRG neurons in culture (Gornstein & Schwarz, 2017). Exposure of the distal axon rather than the mid-axon using microfluidic chambers particularly disrupts axon outgrowth. Microtubule stabilisation also has significant effects on fast axonal transport within neurons. Vesicles were

observed by electron microscopy to accumulate at both ends of a chamber which bathed a portion of the sciatic nerve with paclitaxel, demonstrating an inhibition of both anterograde and retrograde axonal transport (Nakata & Yofifuji, 1999). This impairment of the transport of organelles, proteins and ion channels may be associated with the development of neurotoxicity and pain, though it is still not understood why.

### 1.3.2.3 Ion channel changes

Chemotherapy drugs are thought to induce pain by altering peripheral sensory neuron signalling, leading to hyperexcitability, lowered thresholds for nociception and spontaneous activity. This can be measured directly in sensory neurons, as DRG neurons taken from rats injected with paclitaxel have significantly more spontaneous activity and a decreased rheobase compared to control (Zhang & Dougherty, 2014). This is likely to be induced by the dysregulation of ion channels, as is the case in many other chronic pain states. Whether these ion channel changes are caused directly by disruption of the microtubules or via a secondary mechanism (such as oxidative stress) isn't clear. It has been established that after *in vivo* paclitaxel administration there is an upregulation of certain TRP channels, NaV1.7, CaV3.2, CaV2.3, and CaV2.2, and a downregulation of potassium channels K2P and Kv7 in DRG neurons (Staff et al., 2020). All these changes push the cell membrane to a hyperexcitable state, reducing the threshold for nociceptive firing.

There is a significant amount of literature providing evidence for changes in the function and expression of TRPV1 following paclitaxel exposure in rodents. Multiple studies have shown that paclitaxel injections increase the expression of TRPV1 mRNA in the DRG, as well as the number of DRG cell bodies and epidermal fibres expressing TRPV1 protein (Li et al., 2015; Hara et al., 2013). Conversely, TRPV1 antagonists or TRPV1 desensitisation protocols are able to reverse the allodynic effects of paclitaxel on mechanical and heat thresholds (Li et al., 2015; Chen et al, 2011; Rossato et al., 2018).

This upregulation of TRPV1 protein has also been shown to have functional implications on electrical excitability. One study published in the Journal of Neuroscience assessed the effects of paclitaxel on dissociated DRG neurons by calcium imaging as well as on dorsal horn neurons of *ex vivo* spinal cord slices using electrophysiology (Li et al., 2015). They looked at the effects of both *in vitro* and *in vivo* paclitaxel exposure. They showed that direct perfusion of paclitaxel onto DRG

neurons prevented the desensitisation of calcium responses due to multiple capsaicin stimulations. The frequency of spontaneous EPSCs recorded from neurons of the dorsal horn was increased after *in vivo* paclitaxel treatment, and application of a TRPV1 antagonist attenuated this increase. *In vitro* paclitaxel application was also shown to increase the frequency of miniature EPSCs (mEPSCs) in the dorsal horn, which was also prevented by the TRPV1 antagonist.

A further publication involving many of the same researchers also looked at the frequency of patch clamp recorded mEPSCs from mouse dorsal horn neurons *ex vivo* (Adamek et al., 2019).

Injections of paclitaxel *in vivo* significantly increased the frequency of basal mEPSCs in the dorsal horn, and mEPSCs in response to a single capsaicin application, observations that weren't detected after *ex vivo* paclitaxel application. However, paclitaxel applied to the spinal cord slices *ex vivo*, as well as slices taken from paclitaxel-treated mice, did show an increased response to a second application of capsaicin, rather than the smaller response shown in naïve conditions due to tachyphylaxis. This demonstrates that paclitaxel is able to prevent desensitisation of capsaicin responses whether exposure occurred *in vivo* or *in vitro*.

As well as upregulating the amount of TRPV1, paclitaxel also appears to sensitise behavioural pain responses via TRPV1-mediated processes, as well as transient receptor potential vanilloid receptor 4 (TRPV4) and TRPA1 (Chen et al., 2011). The proposed mechanism of this sensitisation begins by the release of mast cell tryptase in response to paclitaxel, shown by increased tryptase protein concentration in the DRG and spinal cord in a rat model. Antagonists of protease-activated receptor 2 (PAR2), the GPCR for tryptase, or its downstream signalling molecules phospholipase C (PLC), PKA or PKC successfully prevented the development of pain behaviours in the rats treated with paclitaxel. PAR2 is known to sensitise TRPV1, TRPV4 and TRPA1 via these kinases and Chen et al. indirectly provide evidence for this as a cause of paclitaxel-induced pain by reversing hyperalgesia with antagonists of these particular TRP channels.

The contribution of the highly pain-associated sodium channel NaV1.7 to paclitaxel-induced CIPN has also been hypothesised. Li et al. (2018) used a combination of immunofluorescence, patch clamping and Western blot to look at the expression of NaV1.7 in both rat and, importantly, human DRG. Rats that had received paclitaxel injections had a significantly increased NaV1.7 protein level in DRG between 7 and 14 days after the first injection, and dissociated cultures taken from these rats had increased NaV1.7 activation and current flow at more hyperpolarised

voltages. Immunohistochemistry then showed an increase in the proportion of NaV1.7 positive DRG neurons after paclitaxel administration, as well as increased NaV1.7 immunoreactivity in the dorsal horn of the spinal cord. The focus of this publication then shifts to human DRG.

Electrophysiology of dissociated human DRG cultures showed functional activity of NaV1.7 (demonstrated by block with ProTxII). One patient with neuropathic cancer pain had donated one ganglia from a painful dermatome and one control from a non-painful area. The DRG from the neuropathic area showed increased NaV1.7 immunofluorescence and, when cultured, significant spontaneous activity that was not measured in the control DRG, which could be blocked by ProTxII. These spontaneously active neurons also had a significantly more depolarised resting membrane potential.

Another publication that utilised human DRG looked at the expression of NaV1.8 as well as NaV1.7 in dissociated DRG cultures in the context of *in vitro* paclitaxel treatment (Chang et al., 2017). In naïve conditions, real-time polymerase chain reaction (RT-PCR) analysis showed the most highly expressed NaV channel was different between human and mouse, being NaV1.7 and NaV1.8 respectively. When paclitaxel was added to the human cultured neurons for 24 hours, the expression of NaV1.7 increased but there was no effect on NaV1.8 expression. This led to greater amplitude sodium currents and action potential firing frequency. The study did not replicate the paclitaxel experiments on the mouse cultures, but it is worth considering if the differential expression of NaV1.7 channels brings into doubt the applicability of mouse DRG research to humans. Whether these findings can be applied to the development of CIPN in patients is not yet known, but this research is an important step toward using human tissue to understand human disease and demonstrates the importance of the NaV channels in inducing spontaneous DRG activity associated with neuropathic pain states.

#### 1.3.2.4 Calcitonin gene-related peptide and substance P

*In vitro* paclitaxel has been shown to affect the release of the neuropeptides CGRP and substance P from DRG cultures. In the case of CGRP, the concentration of paclitaxel used and the time-course of exposure appears to determine whether the release is enhanced or attenuated. One study looked at the effect of acute exposure on mouse DRG neurons by measuring the release of CGRP within 10 minutes in the presence of different concentrations of paclitaxel (He & Wang 2015).

They found that paclitaxel enhanced the CGRP released by the neurons in a dose dependent manner and found that this effect became maximal by 10nM.

A similar effect of acute paclitaxel on substance P release from DRG cultures has also been shown (Miyano et al., 2009). This publication treated rat DRG neurons with concentrations of paclitaxel from 0.1 to 10 $\mu$ M for 60 minutes, which potentiated the substance P released in a dose- and time-dependent manner. These acute types of experiment may not be ideal for replicating the pathophysiology of CIPN however, because an exposure in the order of minutes is very dissimilar to the chronic exposure that leads to neuropathy over days or weeks in patients.

Longer paclitaxel treatment of DRG neurons does also have an effect on neuropeptide release, however. Pittman et al. (2014) exposed rat DRG cultures to paclitaxel for up to 5 days before stimulating the neurons with capsaicin, allyl isothiocyanate (AITC) or potassium depolarisation and assayed CGRP released. Whether this stimulated CGRP release was enhanced or attenuated by paclitaxel depended on the concentration applied and the type of stimulus. A lower concentration of 10nM increased both TRPV1 (capsaicin) and TRPA1 (AITC)-mediated CGRP release, but a higher 300nM concentration attenuated release instead. When the neurons were depolarised by potassium, both concentrations induced a small but statistically significant increase in CGRP release. CGRP release was assayed after 1 day, 3 days or 5 days of exposure and this potentiation was shown to develop over time. Importantly, neuronal viability assays demonstrated that paclitaxel was not causing this change by decreasing cell survival, as even higher concentrations of up to 1 $\mu$ M paclitaxel for 5 days had no effect on the proportion of viable neurons in the culture. Why this disconnect between different doses of paclitaxel occurs isn't clear, but the authors lead on to speculate about TRP desensitisation mechanisms occurring at higher concentrations of paclitaxel.

From these studies it can be concluded that neuropeptide secretion is altered in paclitaxel-exposed states, at least from dissociated, cultured sensory neurons. There is a distinct lack of evidence for altered neuropeptide signalling *in vivo*, however. Considering the ability to measure CGRP release *in vivo*, for example by microdialysis or even measurement of a flare response, it raises the question of whether this finding translates to the intact sensory system.

#### 1.3.2.5 Neuroinflammation and glial activation

The administration of paclitaxel induces changes associated with neuroinflammation and immune cell activation. This can be detected in the blood by an increase of CD4+ and CD8+ T-cell populations, in the DRG by an increase of the chemokines CCL2 and CCL3, and in the spinal cord by the activation of astrocytes and the upregulation of many inflammatory cytokines and chemokines (Makker et al., 2017). These inflammatory mediators are able to act on nociceptors and induce sensitisation and pain.

Macrophage and microglia may also play a role in paclitaxel pain. Peters et al. (2007) showed an increase in the number of activated macrophages in the DRG and sciatic nerve, and the number of activated microglia in the dorsal horn of the spinal cord after paclitaxel injection in rats. Minocycline, an inhibitor of macrophages and microglia, is able to prevent the development of paclitaxel-induced mechanical allodynia and the loss of IENFs in the paw skin (Liu et al., 2010). It also reduced the proportion of ATF3-positive DRG neurons. It is therefore possible that the prevention of immune activation involving macrophages and microglia is able to block CIPN development.

There is conflicting research that disputes that microglial activation is necessary for paclitaxel-induced neuropathy and suggests that astrocyte activation is involved instead (Zhang et al., 2012). This research showed activation of astrocytes in the spinal cord by assessing glial fibrillary acidic protein levels but not activation of microglia with OX42, ionized calcium binding adaptor molecule 1, or phosphorylated p38 levels. They showed that minocycline prevented the activation of astrocytes, suggesting that rather than microglial inhibition, minocycline instead prevents CIPN development by acting on astrocytes. Whatever particular glial cell plays the most important role in CIPN pathophysiology, there is plenty of evidence that glial activation and neuroinflammation is involved.

#### *1.3.2.6 Mitochondrial damage and oxidative stress*

Although paclitaxel doesn't directly cause cross-linking and damage of mitochondrial DNA like some other chemotherapeutics (oxaliplatin, cisplatin and carboplatin), it does still seem to induce mitochondrial stress and damage. This is evidenced by the presence of swollen and vacuolated axonal mitochondria in the peripheral sensory nerves in animal models of paclitaxel-induced

neuropathy (Flatters & Bennett, 2006). This is associated with increased levels of reactive oxygen species (ROS) in sensory neurons, which is highly correlated with the timecourse of hyperalgesia (Duggett et al., 2015). ROS such as peroxynitrite and superoxide are known to be important in the development and maintenance of some persistent pain phenotypes, acting by modulating ion channels such as TRPV1 and NMDARs either directly or via protein kinases, by modulating glutamatergic signalling via glutamate transporters and glutamine synthetase, or by leading to glial activation and neuroinflammation (Salvemini et al., 2011). Preventing peroxynitrite overproduction using decomposition catalysts successfully prevents or reverses paclitaxel-induced hyperalgesia in a rat model, demonstrating the importance of ROS signalling in CIPN (Doyle et al., 2012).

#### *1.3.2.7 Calcium homeostasis dysregulation*

Paclitaxel has been shown to affect intracellular calcium signalling in non-neuronal and neuronal cells *in vitro*. In mouse pancreatic acinar cells, 10 $\mu$ M paclitaxel leads to a rapid, transient increase in cytosolic calcium (Kidd et al., 2002). This is caused by the rapid release of calcium due to the opening of the mitochondrial permeability transition pore (mPTP). The activation of the mPTP by the same concentration of paclitaxel has also been shown in CNS neuronal cells, specifically in brainstem pre-Bötzing complex neurons (Mironov et al., 2005). The opening of the mPTP by paclitaxel in these cells has no effect on basal intracellular calcium concentration but does lead to the generation of intracellular calcium oscillations. The group hypothesise that mPTP opening leads to mitochondrial calcium efflux which stimulates calcium-induced calcium release from the endoplasmic reticulum, leading to the observed spontaneous calcium transients. Similar calcium oscillations were also induced by lower, sub-micromolar paclitaxel concentrations in a human neuroblastoma neuronal cell line (Boehmerle et al., 2006). Rather than being dependent on mitochondrial calcium, this research found that it depended on the activity of inositol trisphosphate receptors, most of which are found in the endoplasmic reticulum. They identified a paclitaxel binding protein, neuronal Ca<sup>2+</sup> sensor 1, which increased its interaction with the inositol triphosphate receptor in the presence of paclitaxel. Knockdown of this protein prevented the calcium response to paclitaxel.

Although there hasn't been any published research on whether these kinds of effects occur in sensory neurons damaged by paclitaxel, altered intracellular calcium levels by mechanisms like

these could plausibly play a role in the hyperexcitability of sensory neurons leading to painful neuropathic symptoms.

#### 1.3.2.8 Cremophor EL

Although there is plenty of evidence that paclitaxel itself is neurotoxic, experiments can be confounded by effects of the vehicle that the drug is dissolved in. The most common formulation of paclitaxel (Taxol®) is in a mixture of the solvent Cremophor EL (also known as Kolliphor EL) and ethanol. Injection of this vehicle only has been shown to induce **noxious mechanical hypersensitivity** in rat models (Authier et al., 2000). Cremophor EL formulations appear to have different pharmacokinetic profiles than Cremophor free formulations, and clearance of paclitaxel from the blood plasma is significantly reduced compared to Tween-ethanol and dimethylacetate formulations (Sparreboom et al., 1996). This change may lead to accumulation of paclitaxel in vulnerable areas like the DRG and enhance its neurotoxic effects. In primary DRG cultures, Cremophor EL alone has also been associated with many of the same effects as paclitaxel, namely axonal swelling, vesicular degeneration and demyelination (Scripture et al., 2006). Cremophor EL free formulations of paclitaxel have subsequently been developed and do seem to show more limited neurotoxicity and neuropathy (Scripture et al., 2006). It is therefore important to take into account the vehicle used in studies on paclitaxel-induced peripheral neuropathy and perform the appropriate vehicle controls.

### 1.4 *Botulinum neurotoxins*

Botulinum neurotoxins (BoNTs) are a diverse family of neurotoxins produced by strains of the *Clostridium* family of bacteria (Popoff & Bouvet, 2013). Intoxication with these toxins, either through ingestion, inhalation, or via a wound, leads to a potent flaccid paralysis of the muscles called botulism. If left untreated, botulism leads to death via paralysis of the respiratory system (Palma et al., 2019). Presently, the BoNTs are characterised into at least 9 different major serotype groups, BoNT/A to BoNT/G, with new BoNT/FA (previously BoNT/H) and BoNT/X serotypes recently described (Peck et al., 2017; Hackett et al., 2018; Zhang et al., 2017). The shared feature of these different BoNTs is that they are all proteases that cleave SNARE proteins at the presynaptic terminals of neurons (Schiavo et al., 1993). The SNARE proteins are core exocytosis

machinery found on the vesicle membrane and the cell membrane that form a tetra-helical complex that facilitates membrane fusion, leading to secretion of neurotransmitters into the synapse (Figure 1.6) (Poirier et al., 1998). BoNTs truncate specific SNARE proteins, impairing SNARE complex formation and thereby preventing vesicle fusion and exocytosis.

Different BoNT serotypes each cause cleavage at distinct amino acid sites on their targeted SNARE protein, or proteins. BoNT/A and /E cleave SNAP25, BoNT/B, D, /F and /G cleave either the VAMP1 isoform only, or both VAMP isoforms, and BoNT/C is unique in that it cleaves two separate SNAREs, SNAP25 and syntaxin (Table 1.4) (Welch et al., 2000).

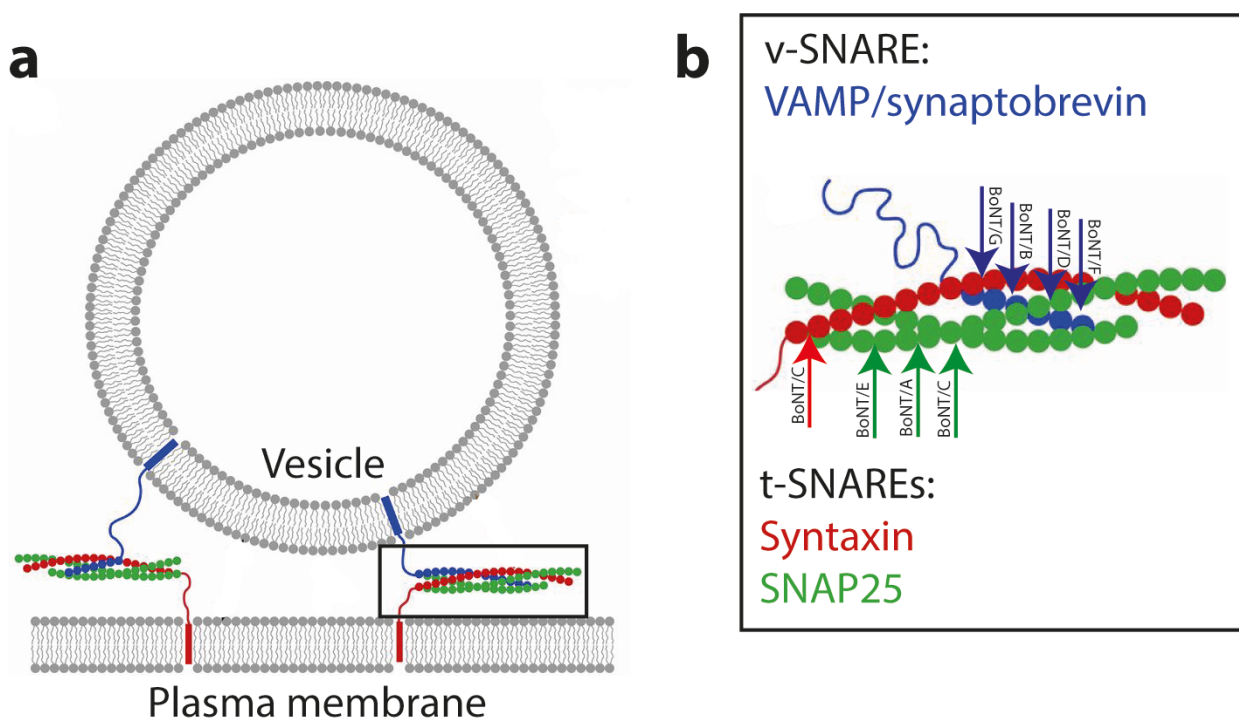


**Figure 1.6. Structure and function of synaptic vesicle SNARE proteins.** *a)* SNARE proteins are found on the vesicle membrane (v-SNAREs) and the plasma membrane (t-SNAREs) and these assemble to form a trans-SNARE complex which brings the vesicle into apposition with the membrane and facilitates fusion of the vesicle membrane with the plasma membrane. *b)* The structure of the SNARE complex is a tetra-helical coiled coil. The v-SNARE found on the synaptic vesicle is VAMP, also known as synaptobrevin (blue) which contributes one  $\alpha$ -helix to the coil. The t-SNAREs found on the plasma membrane are syntaxin (red), which also contributes one  $\alpha$ -helix and SNAP25 (green) which contributes two  $\alpha$ -helices. Syntaxin and VAMP/synaptobrevin are anchored in the membrane by their C-terminal domains, whereas SNAP25 is tethered to the plasma membrane via several cysteine-linked palmitoyl chains. **Coloured arrows represent SNARE protein cleavage sites for different BoNT serotypes.** Figure adapted from Mostafavi et al., 2017.

### 1.4.1 Structure and function

BoNTs are comprised of three domains: a ~50kDa light chain at the N terminal end, and a ~100kDa heavy chain at the C terminus (Figure 1.7). This heavy chain consists of a translocation domain and receptor binding domain (Lacy et al., 1998). The light and heavy chains are attached by a disulphide bond. The heavy chain allows the toxin to attach to the neuronal membrane and further facilitates endocytosis by binding luminal synaptic membrane proteins. The whole toxin is then endocytosed into the cell. The acidic environment of the vesicle reduces the disulphide bond between the two chains, activating the toxin (Wey et al., 2006). This allows the translocation domain to insert into the vesicular membrane, forming a pore which mediates translocation of the light chain into the cytosol (Lai et al., 2010). The light chain is a zinc endoprotease which proteolyse a specific peptide bond on a specific SNARE protein, which differs between BoNT serotypes (Schiavo et al., 1992).

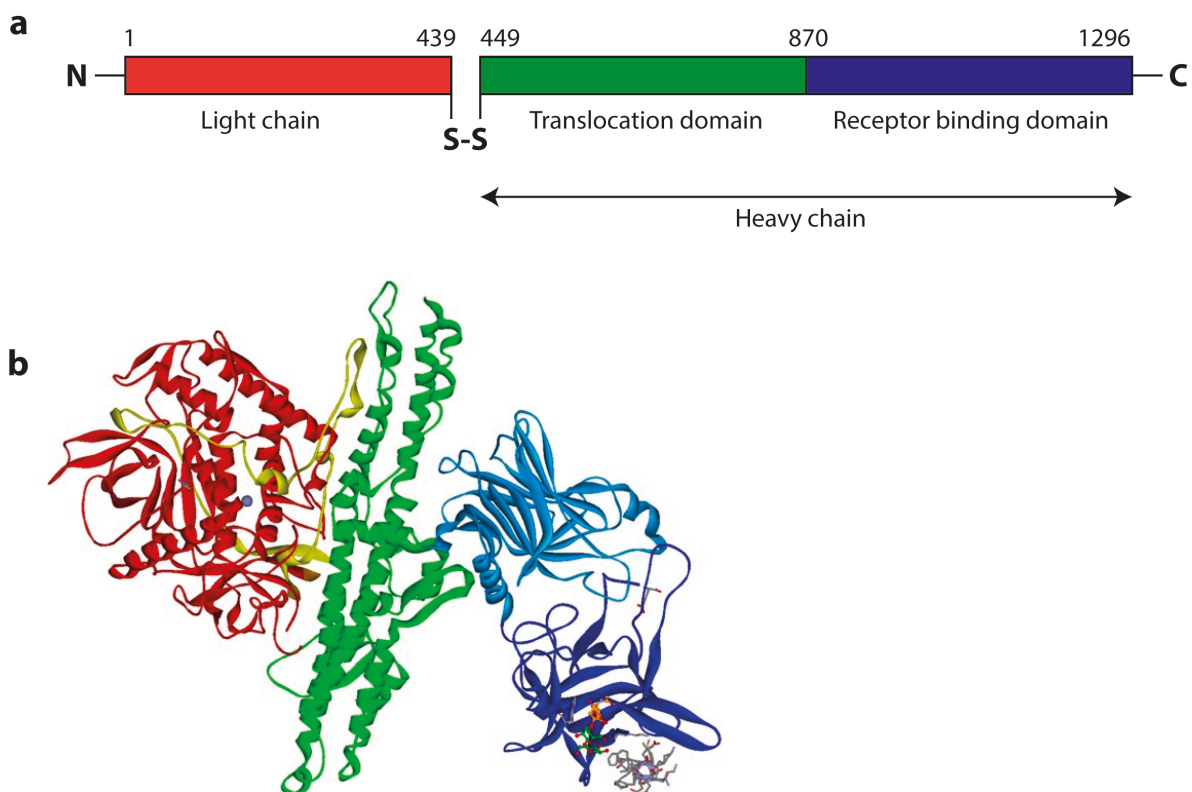


**Figure 1.7. Structure of botulinum neurotoxin A (BoNT/A).** **a)** All native BoNTs are formed of 3 domains, a light chain (red), translocation domain (green) and receptor binding domain (blue). The translocation and receptor binding domains comprise the heavy chain which binds the neuronal membrane and facilitates endocytosis and internalisation of the light chain into the cytosol. The light chain is the enzymatically active portion of the toxin which cleaves SNARE proteins. **b)** Crystallographic schematic structure of BoNT/A showing light chain (red), translocation domain (green/light blue) and receptor binding domain (dark blue). Figure from Binz & Rummel, 2009.

The majority of BoNTs are internalised via a double receptor binding mechanism (Rummel, 2013). First the receptor binding domain binds to polysialo-gangliosides on the surface of the neuron, then it binds to the intraluminal domains of synaptic vesicle proteins during the exocytosis of vesicles, allowing its subsequent endocytosis during vesicular recycling (Table 1.4).

BoNT serotype	Membrane binding	Vesicular protein	SNARE target
A	Ganglioside	Synaptic vesicle glycoprotein 2	SNAP25
B	Ganglioside	Synaptotagmin-I	VAMP1 & VAMP2
C	Ganglioside	2 <sup>nd</sup> ganglioside	SNAP25 & syntaxin
D	Ganglioside-independent	Synaptic vesicle glycoprotein 2 A and B	VAMP1
E	Ganglioside	Synaptic vesicle glycoprotein 2	SNAP25
F	Ganglioside	Synaptic vesicle glycoprotein 2	VAMP1 & VAMP2
G	Ganglioside	Synaptotagmin-II	VAMP1

**Table 1.4. Targeting and SNARE cleavage of different BoNT serotypes.** Table showing the membrane binding receptor and vesicular binding receptor for the various BoNT serotypes, as well as their targeted SNARE protein.

### 1.4.2 Effect on muscle

Native BoNTs have high potency for peripheral cholinergic nerve terminals at the neuromuscular junction due to expression of the relevant gangliosides and vesicular receptors, allowing the toxin to be taken up most efficiently into motor end plates by endocytosis (Binz & Rummel, 2009). This prevents acetylcholine release and silences the neuromuscular junction, leading to the flaccid paralysis which is the hallmark symptom of botulism (Burgen et al., 1949).

One way of quantifiably assessing the neuromuscular blockade of BoNTs is by recording the amplitude of the compound muscle action potential (CMAP) following an injection. The CMAP is a summation of the synchronous action potentials of muscle fibres in an area of muscle, and is an indication of the number of functional fibres (Feasby & Brown, 1974). In order to estimate the total number of functional muscle fibres, a supramaximal electrical stimulation is applied to the nerve or area of spinal cord innervating the muscle, then the resulting CMAP is recorded from the muscle using electromyography. BoNTs have been shown to decrease the amplitude of the CMAP of an injected muscle in a dose dependent manner, due to blockade of the neuromuscular

junction and a subsequent reduction in the number of functional muscle fibres (Cichon et al., 1995; Sakamoto et al., 2009; Torii et al., 2014). This is therefore a useful technique to quantitatively compare the time course and degree of paralysis of various BoNTs.

### *1.4.3 Botulinum neurotoxins in chronic pain*

Initially botulinum toxins were used to treat conditions where pain was as a result of overactive muscle activity such as dystonia or spasms. Initially it was assumed that the pain relief it provided was directly related to its muscle relaxant properties. However, more careful observation demonstrated a disconnect between muscle force and pain relief, with pain relief either continuing after muscle paralysis had worn off (Freund & Schwartz, 2003) or pain relief caused by BoNT concentrations too low to affect muscle activity (Relja & Klepac, 2002). It has become understood over the past few decades that botulinum toxins are useful as a pain treatment for many chronic pain conditions, independent of any direct effect on muscles.

A treatment involving multiple injections of BoNT/A over the head and neck has been approved by the FDA for the treatment of migraine and has also shown efficacy in treating various neuropathic pains such trigeminal neuralgia, post-herpetic neuralgia, post-surgical neuralgia, diabetic neuropathy, occipital neuralgia, spinal cord injury and post-stroke pain (Park & Park, 2017). Due to its long duration of action compared to other BoNT serotypes, BoNT/A is the serotype most frequently used and studied in clinical settings (Foran et al., 2002). However, BoNT/B formulations are also available and are starting to be investigated in randomised controlled trials (Breuer et al., 2006).

#### *1.4.3.1 Mechanisms of analgesia*

Just as BoNTs prevent the release of acetylcholine at the neuromuscular junction, it is also thought that the inhibition of neurotransmitter release within the sensory pathway is important for its analgesic effect. There is evidence that this occurs in the periphery, blocking the release of nociceptive transmitters and decreasing pain associated with the subsequent peripheral sensitisation. For example, BoNT/A injection reduced formalin-induced inflammatory pain in rats, which was associated with significantly attenuated glutamate release in the skin as measured by

microdialysis (Cui et al., 2004). A similar study also took place in humans, measuring glutamate release after capsaicin patch application in response to a mild heat stimulus. Pre-treatment with BoNT/A caused a reduction in glutamate release as well as pain intensity scores (da Silva et al., 2014).

Neuropeptides are also released from sensory neurons both in the periphery and in the spinal cord, which BoNT treatment is thought to prevent. CGRP release from trigeminal sensory neurons is a key factor in the pathophysiology of migraine (Iyengar et al., 2017). In trigeminal cultures, BoNT/A application decreases the amount of CGRP released when stimulated with potassium chloride or capsaicin (Durham et al., 2004). The blockade of neuropeptide release doesn't appear to be specific to trigeminal neurons in the case of migraine, and BoNTs are able to prevent release from other sensory neurons. Lucioni et al. (2008) used rat bladder preparations to demonstrate that *ex vivo* BoNT/A application blocks the release of both CGRP and substance P after inflammatory cyclophosphamide or hydrochloric acid insult.

As well as having peripheral effects local to the injection site, several high profile publications suggest that BoNT proteases are transported within neurons. Demonstration of BoNT trafficking was initially shown within central neurons of the brain (Antonucci et al., 2008). BoNT/A was injected unilaterally into the hippocampus. Over a timecourse of 3 days, the protein product of BoNT/A, cleaved SNAP25 (cS25) was detected in anatomically connected areas such as the contralateral hippocampus and the ipsilateral entorhinal cortex, shown by immunohistochemistry and immunoblotting. This had functional effects, as BoNT/A injection caused a nearly complete blockade of spontaneous spiking activity from ipsilateral hippocampal CA1 neurons, which also became evident on the contralateral side at the same time that cS25 became detectable. Similarly, in the visual system, BoNT/A injection into the superior colliculus led to SNAP25 cleavage in retinal and visual cortex neurons. This effect was blocked by colchicine, a microtubule inhibitor, demonstrating that direct neuronal transport is necessary, and ruling out passive systemic spread of the toxin from the injection site.

An elegant study utilising the different SNAP25 cleavage sites and duration of action of BoNT/A and /E proved that it was the active protease rather than the cleavage product that is transported (Restani et al., 2011). An injection of BoNT/A into the superior colliculus was allowed to induce SNAP25 cleavage in the retina. The optic nerve was then cut, and a BoNT/E injection given to the

eye. As expected, there was a decrease in the BoNT/A cleavage product and an increase in the BoNT/E cleavage product as BoNT/E cleaves more amino acids off SNAP25 than BoNT/A. However, the duration of action of BoNT/E is shorter than that of BoNT/A and as its effects wore off over 25 days the amount of BoNT/A-cleaved SNAP25 increased again. This shows that there was still active BoNT/A protease present in the retina which had been transported from the superior colliculus prior to the optic nerve transection.

Crucially for pain research, retrograde transport of BoNT/A has also been shown to occur within DRG neurons, having an effect in the spinal cord. Immunohistochemistry shows SNAP25 cleavage in both the dorsal and ventral horns of the spinal cord following BoNT/A injection into the gastrocnemius, an effect which is also blocked by colchicine (Matak et al., 2012). It has been hypothesised that this central effect is actually vital for the relief of pain following BoNT injections. Unilateral injection of BoNT/A has been shown to relieve mirror pain such as acidic saline injection or formalin-induced facial pain on both sides, not just unilateral to injection (Bach-Rojecky & Lacković, 2009; Matak et al., 2011). Injection of colchicine or sectioning of the nerve proximal to the injection blocks this pain relief, so these studies suggest that the transport of BoNT/A centrally is required for its analgesic effects. A similar bilateral reduction of mechanical hypersensitivity has also been demonstrated by a unilateral injection of BoNT/A following a paclitaxel-induced neuropathy model (Favre-Guilmond et al., 2009). Some speculated mechanisms for the relief of bilateral pain include translocation of the BoNT protease further than the spinal cord, for instance to the brain, or by an action (either directly or indirectly) on the activation of glia and neuroinflammation in the spinal cord.

#### *1.4.3.2 Prevention of ion channel trafficking to the membrane of sensory neurons*

The transport of certain ion channels to the membrane surface can be regulated by vesicular exocytosis, using the SNARE machinery that BoNTs so potently target (Section 1.1.2.4). It therefore stands to reason that BoNTs could be able to prevent the upregulation of surface ion channels of sensory neurons, an important feature in the mechanism of chronic pain. Although it is not clear whether the density of all ion channels at the membrane can be modulated by regulated, SNARE-mediated exocytosis, or whether turnover is via constitutive exocytosis in the majority of cases, there is clear evidence that BoNT action on SNARE proteins can change the membrane expression

of certain channels important for pain sensation. In the literature there is most evidence for this being true of the TRP channels.

Tumour necrosis factor alpha (TNF $\alpha$ ) is a pro-inflammatory cytokine which induces the insertion of TRPV1 and TRPA1 to the membrane, subsequently enhancing calcium influx when activated by their respective agonists (Meng et al., 2016). One study investigated the action of BoNTs on this process by performing live labelling using antibodies that recognise extracellular epitopes of TRPV1 or TRPA1, and therefore only label channels spanning the membrane. In cultured trigeminal neurons they showed that TRPV1 and TRPA1 appear to be transported together to the membrane in large dense core vesicles containing VAMP1. BoNT/A or BoNT/C1 treatment was demonstrated to block co-trafficking of TRPV1 and TRPA1 to the membrane in response to TNF $\alpha$  application. These botulinum toxins cleave the SNARE proteins SNAP25 and syntaxin1 on the plasma membrane, showing that these proteins are essential for the exocytosis of these vesicles. They then went on to show that these BoNTs prevent the enhanced calcium influx caused by TNF $\alpha$  treatment and proposed this as a mechanism of the ability of BoNTs to treat inflammatory and neurogenic pain disorders. The group later showed the same phenomenon using a SNAP25-cleaving chimera of full length BoNT/A and the light chain of BoNT/E in DRG neurons treated with TNF $\alpha$  (Nugent et al., 2018).

Evidence for this being relevant in the intact nociceptive system comes from a publication showing that TRPV1 protein (but not mRNA) levels are upregulated in the DRG of rats undergoing a CFA-induced arthritis model, as shown by Western blot and immunohistochemistry (Fan et al., 2017). The authors attribute this to enhanced trafficking and expression of TRPV1 at the membrane, though they do not directly assay this, for example using a membrane biotinylation assay. BoNT/A injection into the knee joint was able to prevent this protein upregulation, which they attribute to interference of TRPV1 trafficking. TRPV1 membrane expression has also been shown to decrease in rat trigeminal neurons following injections of BoNT/A (Shimizu et al., 2012). However, this was in naïve animals and may therefore not be applicable to preventing or reversing the increased TRPV1 expression that is a major factor in chronic pain conditions.

BoNT/A has also been shown to modulate the expression of TRPA1, TRPV1, TRPV2 and TRPM8 in trigeminal neurons (Wu et al., 2016). After a chronic constriction injury of the infraorbital nerve as a model of trigeminal neuralgia, the expression of all these channels increased in the spinal

trigeminal nucleus as shown by Western blotting. An injection of BoNT/A into the whisker pad subsequently reduced TRPA1, TRPV1 and TRPV2 protein expression in a dose dependent manner, but had no effect on TRPM8. However, again, this was total protein expression, rather than functional expression of these channels at the membrane.

The P2X receptors have also been shown in the literature to be affected by BoNT treatment in chronic pain models. The number of DRG neurons immunoreactive for the P2X3 receptor was shown to increase following a ventral root transection model of neuropathic pain in rats (Xiao et al., 2011). A subsequent injection of BoNT/A into the plantar surface of the paw was shown to reverse this change compared to control, as well as the mechanical hypersensitivity induced by the surgery.

#### *1.4.4 Re-engineering botulinum neurotoxins*

As BoNTs are such effective and specific pieces of proteolytic machinery, there is great interest in exploiting this function for biotechnological or therapeutic uses by modifying the native structure. This has many potential uses such as reducing paralysis while maintaining analgesia, enhancing SNARE cleavage specifically in sensory neurons, enhancing specificity to human proteins, cleavage of pain-specific proteins, cleavage of non-neuronal SNAREs such as synaptosomal-associated protein, 23kDa (SNAP23), use as a protein cargo delivery system into the cytosol, and cleaving proteins unrelated to the exocytotic machinery in non-neuronal cell types. Most of the current BoNT re-engineering research broadly fall into the categories of: 1) Modifying or replacing the receptor binding domain in order to alter the cell selectivity of these toxins away from the neuromuscular junction; or 2) Modifying or replacing the light chain in order to cleave new substrates.

##### *1.4.4.1 Retargeting to different cell types*

Early retargeting of BoNT/A to different cell types was carried out by removing the receptor binding domain from BoNT/A then chemically conjugating it to different ligands using protein cross-linkers. These were initially used as a proof of concept that the receptor binding domain is limited to cell surface binding and that it can be replaced with other cell surface binding ligands.

When conjugated to wheat germ agglutinin, a lectin which binds N-acetylglucosamine and N-acetyl sialic acid on the membrane of a variety of neuronal cell lines and non-neuronal cell types, it becomes internalised into a range of neuronal cell types as well as pancreatic beta cells (Chaddock et al., 2000b). It successfully inhibited the potassium stimulated release of radiolabelled noradrenaline or glycine from the relevant neuronal cell lines and inhibited radiolabelled insulin release from the pancreatic cells. Similarly, conjugation to NGF also allowed internalisation into PC12 cells and inhibited radiolabelled noradrenaline release (Chaddock et al., 2000a). The same group then turned the use of these retargeted BoNT conjugates to analgesia by selective targeting to nociceptors (Duggan et al., 2002). They identified *Erythrina cristagalli* lectin as a suitable ligand to bind galactose-containing carbohydrates selectively found on nociceptive neurons, but evidence for this specificity is lacking in the publication (data not shown). Substance P release from embryonic rat DRG cultures was attenuated by this ligand-conjugated BoNT. *In vivo* extracellular recordings of dorsal horn neurons showed an inhibition of C and A $\delta$  firing, but not A $\beta$  firing with transcutaneous electrical stimulation after an intrathecal injection of this construct. This shows that retargeted BoNTs are able to modify the firing of the pain signalling pathway and may be useful for enhanced analgesia.

Fully recombinant modified BoNTs were then produced, despite the challenge of producing these proteins due to their size and complexity. One study describes a novel BoNT consisting of the light chain of BoNT/C coupled to epidermal growth factor (EGF) as a receptor binding domain (Foster et al., 2015). This construct specifically targeted a human respiratory epithelial cell line rather than any neuronal-type cell, providing stronger evidence for the ability of BoNTs to be retargeted to cell types that are completely insensitive to native BoNTs. Incubation of this cell line with the EGF-BoNT/C construct inhibited the release of mucin, a principle component of mucus secretions from epithelia.

As it has been shown that BoNTs can effectively be retargeted to different cell types, there has been a move to link the BoNT light chain to ligands which specifically target receptors found on nociceptive neurons. One approach is to generate an antibody to a protein expressed on nociceptive neurons to link to the BoNT/A light chain. An antibody against an extracellular portion of the P2X3 receptor was generated and expressed as a fusion protein with BoNT/A lacking a receptor binding domain (Ma et al., 2014). This fusion protein bound to P2X3 receptors expressed by primary rat DRG neurons, as shown by Western blotting and immunocytochemistry. Incubation

with the protein also induced SNAP25 cleavage and reduced potassium-evoked CGRP release from these neurons.

Another construct was created by coupling BoNT/A domains to an anti-TrkA antibody or NGF via an immunoglobulin G (IgG) binding domain and IgG linker (Nugent et al., 2017). These were shown to deliver the SNAP25-cleaving protease into TrkA-expressing PC12 cells, unlike the control protein lacking the receptor binding ligand.

Tang et al. (2020) created two novel BoNTs with therapeutic intentions. They used a sortase-mediated protein ligation approach to covalently link their ligands of interest to the light chain and translocation domain of BoNT/D. The ligands they used were interleukin 1 beta (IL1 $\beta$ ) for inhibition of inflammatory mediators in rheumatoid arthritis, and a CGRP receptor antagonist for treatment of neuropathic pain. Once again, these retargeted BoNTs were shown to be internalised into macrophages and DRG neurons respectively, and inhibit the release of IL6 and substance P via VAMP cleavage. One limiting factor of all the studies on these nociceptor-specific ligand fusion BoNT proteins is that there appear to be no studies performed past the protein creation and basic internalisation assay stage (Ma et al., 2014; Nugent et al., 2017; Tang et al., 2020). Whether these proteins are active or have enhanced therapeutic effects beyond native BoNTs *in vivo* is not discussed. This suggests that more physiological studies (i.e. on animal models) have either not been performed or that they have failed at this stage and the negative data has not been published.

Chimeric BoNTs with selected desirable qualities from different serotypes have also been created. For example, Meng et al. (2009) published an in-depth publication on the ability of BoNT/A, BoNT/E and a chimera of these BoNTs called BoNT/EA to target and inhibit CGRP from trigeminal neurons. They demonstrated that BoNT/A was unable to abolish capsaicin-induced CGRP release due to only cleaving 9 amino acids from SNAP25. This truncation was not sufficient to prevent SNARE complex assembly, allowing CGRP release at prolonged calcium increases induced by capsaicin. BoNT/E on the other hand was unable to enter the trigeminal neurons due to a lack of expression of its receptors (synaptic vesicle glycoprotein isoforms A and B) in this particular type of neuron. By creating a fusion protein which is a chimera of the light chain of BoNT/A and the receptor binding and translocation domains of BoNT/E the group were able to overcome these

problems and create a novel toxin able to inhibit capsaicin-induced CGRP release from trigeminal neurons.

#### *1.4.4.2 Retargeting to different substrates*

Modifications have also been made to the protease structure of BoNTs, either to enhance their clinical efficacy or as a proteolytic tool to target non-SNARE proteins. In particular, there has been interest in retargeting BoNTs to SNAP23, a SNARE protein involved in secretion from cell types such as glia, exocrine cells, endocrine cells and epithelial cells (Kunii et al., 2016; Hepp et al., 1999). Two publications describe modified BoNTs that have been conferred selectivity to SNAP23 as well as SNAP25 by mutagenesis of the light chain. These toxins may be of interest to the pain community as glial cells and their secreted factors are well known to play a role in many different types of pain, but the researchers do not speculate on this aspect (Chen & Barbieri, 2009; Sikorra et al., 2016).

A more sophisticated approach to re-engineer BoNTs to specific non-SNARE targets of interest was published recently (Blum et al., 2021). Phage-assisted continuous evolution was utilised to divert BoNT proteases (BoNT/X, BoNT/F and BoNT/E) away from their natural targets towards a diverse range of proteins. They successfully targeted the protease to VAMP4, VAMP7, and phosphatase and tensin homologue. The reprogrammed toxins lost selectivity to their natural substrates as they gained specificity for the new ones. They crucially also retained the unique ability of BoNTs to self-deliver into the newly specified cells. This technique has ramifications not just for sensory neuroscience but also a vast array of bioscientific and clinical applications. For example, pain signalling peptides could be targeted, or mutated oncogenes in tumour cells, or as a research tool to investigate the functions of practically any protein in a cell. With this discovery there may be a new wave of novel BoNTs attuned to a wide variety of different proteins.

#### *1.4.5 SNARE-stapling*

There are methodological difficulties associated with producing modified BoNTs as a single construct. BoNTs are large, complex proteins and this is a limiting factor in their successful generation by traditional recombinant methods. By treating each of the three BoNT domains as

separate units, the different domains can be produced by recombinant techniques and then reassembled to form a wide variety of functioning modified toxins. A novel “protein stapling” technique has been developed by the Davletov lab to allow reassembly of the protein (Darios et al., 2010). This approach uses the self-assembling properties of SNARE proteins (SNAP25, VAMP2/synaptobrevin and syntaxin) to form a heteromeric, tetrahelical coiled coil between the recombinant domains. This forms an irreversible and stable peptide bridge linking the proteins into one functional unit. The protease and translocation domains of BoNT/A are produced with a SNAP25 linker at one end, and a receptor binding domain is produced which is attached to a VAMP2/synaptobrevin linker. When the syntaxin stapling peptide is added to the reaction then the SNARE proteins self-assemble and the protease, translocation and receptor binding domains are brought together to form a single functioning toxin that internalises into cells and cleaves SNARE proteins (Figure 1.8).



**Figure 1.8. Structure of a protein stapled botulinum neurotoxin.** Light chain (Lc, red) and translocation domain (Td, black) fused to SNAP25 (green), linked by a syntaxin (Syx, red) protein staple to a synaptobrevin (Syb, blue) fused receptor binding domain (Rbd, yellow). Figure adapted from Darios et al., 2010.

Although the protein staple is formed of SNARE proteins, themselves the target of the BoNT light chains, these stapled BoNTs do not undergo self-cleavage of the protein staple and remain functional (as detailed in the following paragraphs). Reasons for this haven’t been fully elucidated, but it has been demonstrated that BoNT/A-cleaved SNAP25 still retains the ability to assemble into a functional SNARE complex (Meng et al., 2009). This would allow even self-truncated SNAP25 to assemble into a single stapled protein. It has also been shown that complexed SNARE proteins are resistant to BoNT proteolysis, meaning that once the compound has been assembled it is unlikely to be vulnerable (Hayashi et al., 1994).

This approach has all the benefits of the retargeted BoNTs described in the previous section, with a greater ease of production and assembly. It also has an added safety benefit, as the individually

produced parts of these toxins are non-functional and therefore non-toxic prior to assembly with the linker syntaxin peptide. There is also great flexibility in the assembly of different subunits. For example, it is possible to produce chimeric toxins with the protease and targeting ability of different serotypes, or to duplicate the receptor binding domains to improve cellular targeting efficiency (Andreou et al., 2020). It is also possible to exchange the native receptor binding domain for completely different ligands in order to change the susceptible cell type (Arsenault et al., 2013). There is also evidence that by introducing the larger SNARE linker to the toxin the paralytic effect is lessened, potentially due to the steric hindrance of uptake at tight neuromuscular junctions or their small synaptic vesicles (Mangione et al., 2016; Andreou et al., 2020).

Restapled versions of BoNT/A have been shown to have comparable anti-nociceptive effects to native BoNT/A in pre-clinical pain models. BitoxA, the SNARE-stapled form of BoNT/A, was able to reverse secondary mechanical hyperalgesia after a CFA-induced joint inflammation model, peripheral capsaicin injection, and mechanical hyperalgesia after SNI neuropathy (Mangione et al., 2016). It was also able to reduce plasma extraversion caused by capsaicin-induced inflammation. Direct comparison to native BoNT/A was not discussed in this publication but its anti-nociceptive potential is promising.

A similar BoNT/A-based toxin with a duplicated receptor binding domain called BitoxAA was tested in models of migraine (Andreou et al., 2020). BitoxAA showed significantly reduced paralytic effects on muscle compared to BoNT/A, as shown by CMAP recordings following injection into the gastrocnemius muscle. BitoxAA prevented spiking activity in a rat trigeminal meningeal *ex vivo* preparation, as well as raising the mechanical and electrical threshold for firing of trigeminovascular afferents *in vivo*. It also inhibited face rubbing in a glyceryl trinitrate sensitisation with subsequent orofacial formalin model of migraine.

Chimeric toxins have also been produced with this method. One published toxin involves the stapling of the light chain and translocation domains of BoNT/A to the receptor binding domain of tetanus toxin, a related clostridial neurotoxin (Ferrari et al., 2013). Rather than acting peripherally, tetanus toxin is internalised and transported back to the CNS where its receptor binding domain selectively targets it to internalisation into spinal cord inhibitory neurons. This causes VAMP2/synaptobrevin cleavage in these neurons, leading to spastic paralysis. By creating this chimera it is possible to create a SNAP25-cleaving BoNT that targets CNS neurons. When this toxin

is delivered intrathecally it does not cause paralysis, either flaccid or spastic, and is able to reduce mechanical sensitivity in a CFA-induced inflammatory model.

Due to the flexibility of production of these SNARE-stapled BoNTs it is possible to create novel toxins specifically designed with pain treatment in mind. Two such toxins were given the names SP-Bot and Derm-Bot (Mairù et al., 2018). SP-Bot is the enzymatic and translocation domains of BoNT/A stapled to the substance P ligand. This targeting domain allows internalisation and silencing of neurokinin 1 receptor (NK1R)-expressing neurons in the spinal cord which are involved in pain signalling. An intrathecal injection of this construct reduces mechanical hyperalgesia in many different pain states, including CFA-induced joint inflammation, CFA-induced peripheral inflammation and SNI neuropathy. This effect was not present in NK1R knockout mice. Derm-bot is also a BoNT/A-based conjugate, but stapled to the dermorphin peptide as its receptor binding domain. When injected intrathecally this construct silences spinal neurons which express mu-opiate receptors, providing a similar effect to traditional opiates. Derm-bot injection is able to reverse SNI-induced hyperalgesia with equivalent potency to a morphine injection, but was shown to last over 25 days rather than hours. An injection of morphine also had no additive effects to the analgesia shown with Derm-bot, suggesting that they are indeed acting on the same neurons in the spinal cord which have already been silenced by Derm-bot. These studies give strong evidence that retargeted BoNT proteases can be used to specifically silence carefully selected neurons within spinal cord nociceptive pathways and may be more effective analgesics than the relatively non-specific native BoNTs.

#### 1.4.5.1 ChoBot

Cholera toxin is produced by some strains of *Vibrio cholerae*, and infects the intestinal mucosa leading to intense diarrhoea and dehydration via ionic imbalance and osmosis. This 84kDa toxin is formed of an A subunit and a B subunit. The cholera toxin B subunit (CTB) is a homo-pentamer forming the targeting portion of the toxin which binds to GM1 gangliosides on intestinal epithelial cell membranes (Holmgren et al., 1975). This CTB pentamer-GM1 complex facilitates the internalisation and retrograde translocation of the enzymatic A subunit into the endoplasmic reticulum of the cell. The A subunit is made up of two chains, A1 and A2, which are attached by a disulphide bond. The A1-chain is the enzymatic portion of the toxin, and the A2 chain is a linker region bridging A1 and the B subunit. When the toxin reaches the endoplasmic reticulum the A1

and A2 chains are separated by proteolytic cleavage and breaking of the disulphide bond and the enzymatic A1 toxin is translocated into the cytosol (Wernick et al., 2010).

Intestinal epithelial cells are not the only cells which express the GM1 ganglioside which CTB binds to; GM1 is also expressed on the surface of neurons. Recombinantly expressed CTB with no A subunit is non-toxic and is able to bind to peripheral neurons (Mekalanos et al., 1977). CTB labelled with fluorescent molecules, biotin or horseradish peroxidase (HRP) have been used as neuronal tracers for decades due to the ability of CTB to bind to GM1 gangliosides on the cell surface and internalise the tracer molecule, which is then able to undergo trans-synaptic retrograde transport to connecting neurons. After intraperitoneal injection or intramuscular injection into the tongue both motor and sensory ganglia in the brain are heavily labelled by CTB-HRP, as are motor neurons in the spinal cord and sensory axons entering the dorsal horn, demonstrating the ability of peripheral neurons to take up the toxin (Alisky et al., 2002). Injection into the sciatic nerve also was shown to label motor neurons in the ventral spinal cord and sensory afferents of the dorsal horn (Rivero-Melián et al. 1992).

However, doubts of CTB's ability as a universal peripheral tracer for sensory neurons was brought into doubt when it became clear that not all types of neuron are labelled equally.

When CTB (also referred to as cholera toxin B subunit) is injected and subsequently detected using an anti-cholera toxin B subunit antibody it was shown that only certain layers of the dorsal horn became CTB immunoreactive. After injection into the footpad there is only weak CTB labelling of laminae I and II, the substantia gelatinosa which is the location of nociceptive afferent input (Rivero-Melián & Grant, 1991). There is also no colocalisation of CGRP or substance P positive afferents in the spinal cord following sciatic nerve injection, further substantiating this suggestion (Rivero-Melián et al. 1992). Similar layered labelling of the spinal cord was also shown with an CTB-HRP conjugate when injected into the L5 DRG. This also demonstrated labelling of the deeper dorsal horn and other regions that are known to receive large fibre afferent inputs (Robertson & Grant, 1985). These studies suggested that only the thicker myelinated fibres that project to the deeper regions of the spinal cord take up and transport CTB.

Investigation of CTB labelling of the DRG was then used to confirm that uptake of CTB is indeed not universal across all sensory neurons. An injection of HRP-CTB into peripheral nerves was shown to distinctly label only a subpopulation of sensory neurons (LaMotte et al., 1991). The

labelled neurons were primarily larger, and 98% were myelinated as shown by electron microscopy. This population was in contrast to another co-injected neuronal label, wheat germ agglutinin-HRP. Another group used the detection of CTB immunoreactivity directly on fixed L5 DRG sections to show labelling of only 34% of the sensory neurons (Robertson & Grant, 1989). They also showed that the labelled population were large neurons that were also primarily immunoreactive for RT97, a neurofilament antibody that detects myelinated A fibre neurons. 97% of the CTB positive neurons were RT97-positive, whereas only 5% and 3% of CGRP and substance P positive neurons colocalised with CTB binding respectively. A follow up study using the same technique demonstrated again that the vast majority of labelled neurons were large and reactive for RT97 (Robertson et al., 1991). This publication attempted to characterise the small percentage of CTB positive neurons that were RT97-negative but no hard conclusions could be made due, presumably, to the lack of specific subpopulation marking antibodies available at the time. From these extensive studies it can be determined that it is indeed primarily larger, myelinated sensory neurons that take up CTB in naïve animals.

The binding of CTB to sensory neurons becomes complicated further in injured states. Several high profile publications had shown that nerve injury changed the CTB labelling in the spinal cord to include lamina II, which is mostly innervated by C fibres (Woolf et al., 1992; Lekan et al., 1996). As they were assuming that the CTB was still labelling myelinated fibres it was taken to mean that A fibre terminals were redistributing to the nociceptive laminae of the spinal cord and proposed this as a mechanism of neuropathic allodynia. However, this turned out to be more likely to result from CTB binding specificity changing with injury states. One study used perineural capsaicin around a transected sciatic nerve to selectively ablate TRPV1-expressing sensory neurons and showed that this prevented CTB from labelling laminae II (Sántha & Jancsó, 2003). This suggests that it is not A fibres sprouting but instead TRPV1-expressing C fibres taking up CTB following injury which is responsible for this effect. Electron microscopy of the dorsal root of the spinal cord showed no difference in the proportion of myelinated and unmyelinated fibres between the ipsilateral and contralateral side yet the CTB labelling of unmyelinated axons was increased 6-fold.

The labelling of DRG neurons by CTB also changes after nerve injury. Tong et al. (1999) demonstrated in both rat and monkey that sciatic nerve transection dramatically changes the DRG population that labels with CTB-HRP, or CTB detected with cholera toxin B subunit antibody, after injection into the proximal part of the transected nerve. The proportion of L5 DRG neurons labelled

increased from 45% to 81% with the antibody and from 54% to 87% with CTB-HRP, and this was driven by the increased labelling of smaller DRG neurons. This was also associated with CTB labelling of laminae II in the spinal cord. Another publication showed the same finding, also using CTB injection and antibody labelling following sciatic nerve transection (Shehab et al., 2003). Cholera toxin immunoreactivity became present in more neurons following transection and included smaller-diameter neurons. These smaller neurons that newly bind CTB colocalised with the peptidergic marker vasoactive intestinal peptide (VIP), which is upregulated in small-diameter sensory neurons after injury.

Damage to the nerves doesn't have to be physical to induce an upregulation of CTB labelling. Perineural capsaicin or resiniferatoxin prior to CTB-HRP injection into the intact sciatic nerve also broadened the population of sensory neurons labelled (Oszlács et al., 2015). This chemical damage also increased the proportion of DRG neurons labelled with CTB, and shifted them to smaller cell types which were unmyelinated as shown by electron microscopy, and also led to labelling of lamina II of the spinal cord.

Due to the ability of CTB to bind to DRG neurons in the periphery, and its increased labelling of C fibres following damage of the nerves, a SNARE-stapled botulinum toxin called ChoBot was created with CTB as its targeting domain. Theoretically this toxin may be damage specific, targeting only damaged C fibres and silencing them, for example in neuropathic pain states. The cholera toxin was truncated to contain only the A2 chain and the B subunit pentamer and this was expressed attached to synaptobrevin. The light chain-translocation domains (LcTd) of BoNT/A attached to  $\alpha$ -SNAP25 was then separately expressed. When these two separately expressed peptides are attached with the stapling peptide, syntaxin, the SNARE staple forms between them to create a chimera with the targeting B subunit of cholera, the linking A2 chain of cholera, the translocation domain of BoNT/A and the SNAP25-cleaving region of BoNT/A.

## **1.5 Hypothesis and aims**

From the literature discussed in this introduction, it was hypothesised that the chimeric toxin ChoBot may direct BoNT/A's analgesic effects to a different subpopulation of sensory neurons which are sensitive to CTB binding, leading to analgesia. One aim of this thesis is to assess whether this chimeric toxin is able to bind, internalise into and cleave SNAP25 in sensory neurons, and

whether SNAP25 cleavage has a functional effect that can be detected. Another aim is to assess whether the altered targeting specified by the cholera receptor binding domain is beneficial in a pain therapeutic over and above the native, unmodified toxins, both in terms of enhanced silencing of nociceptors and decreased potency at the neuromuscular junction. In order to investigate this, the action of ChoBot will be tested with respect to the first line BoNT used in the clinic, BoNT/A. The action of ChoBot will be assessed *in vitro* using primary rat DRG cultures, and a supplementary aim of this thesis is to develop an entirely *in vitro* model of CIPN using the chemotherapy drug paclitaxel as a way to test the action of novel BoNTs as therapeutics for CIPN. Following *in vitro* testing, this thesis also aims to show an *in vivo* action of ChoBot using behavioural testing in neuropathic rat models and pre-clinical evidence for ChoBot as a future therapy for chronic pain.

## 2. Materials and methods

### 2.1 Frequently used reagents

Reagent	Product code	Stock
Phosphate-buffered saline (PBS)	BP399-4, Fisher Scientific	10x solution, RT
Dimethyl sulfoxide, anhydrous (DMSO)	276855, Sigma	Room temperature
Veratridine	Ab120279, Abcam	Solid in desiccated conditions, -20°C
$\alpha,\beta$ -Methyleneadenosine 5'-triphosphate lithium salt ( $\alpha,\beta$ -methylene-ATP)	M6517, Sigma	10mM in ultrapure H <sub>2</sub> O, -20°C
Trans-cinnamaldehyde	C80687, Sigma	200mM in DMSO, -20°C
Capsaicin	M2028, Sigma	10mM in DMSO, -20°C
Bovine serum albumin (BSA)	A2153, Sigma	4°C
Fish skin gelatin	G7765, Sigma	4°C
Triton X-100	BP151, Fisher Scientific	Room temperature
Tween-20	BP337, Fisher Scientific	Room temperature
Sucrose	S/8600/53, Fisher Scientific	Room temperature
Paraformaldehyde	158127, Sigma	4°C
Picric acid	P6744, Sigma	Room temperature
Isoflurane (Isoflo)	988-3245, Henry Schein	Room temperature
Ethylene glycol	324558, Sigma	Room temperature
Glycerol	G/0650/17, Fisher Scientific	Room temperature
Paclitaxel	10461, Cayman Chemical	Solid in desiccated conditions, -20°C for <i>in vivo</i> injection; 10mM in DMSO, -20°C for <i>in vitro</i> use
Botulinum neurotoxin A (BoNT/A)	Isolated Toxin (150kDa), Metabionics	-80°C
4-(2-hydroxyethyl)-1-piperazineethanesulfonic acid (HEPES)	H3375, Sigma	Room temperature

#### 2.1.1 Solutions and buffers

Ringer (pH 7.4)	
NaCl	140mM
KCl	4mM
CaCl <sub>2</sub>	2mM
MgCl <sub>2</sub>	1mM
HEPES	10mM
NaOH	4.54mM
Glucose	10mM

<b>High potassium Ringer (pH 7.4)</b>	
NaCl	104mM
KCl	40mM
CaCl <sub>2</sub>	2mM
MgCl <sub>2</sub>	1mM
HEPEs	10mM
NaOH	pH to 7.4
Glucose	10mM

<b>HEPEs buffered Tyrodes solution (HBTS) (pH 7.4)</b>	
NaCl	140mM
KCl	5mM
CaCl <sub>2</sub>	2mM
MgCl <sub>2</sub>	2mM
HEPEs	25mM
NaOH	pH to 7.4
Glucose	10mM

<b>High potassium HEPEs buffered Tyrodes solution (pH 7.4)</b>	
NaCl	85mM
KCl	60mM
CaCl <sub>2</sub>	2mM
MgCl <sub>2</sub>	2mM
HEPES	25mM
NaOH	pH to 7.4
D-(+)-Glucose	10mM

<b>Buffer A</b>	
NaCl	100mM
HEPES	20mM
NaOH	pH to 7.3

<b>Immunocytochemistry blocking solution</b>	
Fish skin gelatin	2%
BSA	2%
Tween-20	0.1%
PBS	

<b>Immunohistochemistry blocking solution</b>	
Goat serum	5%
Fish skin gelatin	1%
BSA	5%
Triton X-100	0.3%
PBS	

<b>Cryoprotectant solution</b>	
Ethylene glycol	30%
Glycerol	30%
Phosphate buffer	20mM
dH <sub>2</sub> O	

### 2.1.2 Antibodies and fluorescent molecules

<b>Antibody</b>	<b>Species raised in</b>	<b>ICC dilution</b>	<b>IHC dilution</b>	<b>Code</b>	<b>Source</b>
<b>Primary antibodies</b>					
Cleaved SNAP25	Rabbit (polyclonal)	1.5000	1.5000	In-house	Davletov lab
Cleaved SNAP25	Mouse (monoclonal)	1.1000	-	Ab635	Allergan
SNAP25	Rabbit (polyclonal)	1.500	-	SYSY1110 02	Synaptic Systems
Beta-III-tubulin	Mouse (monoclonal)	1.2000	1.500	MAB1195	R&D systems
CGRP	Mouse (monoclonal)	1.1000	1.2000	C7113	Sigma
Neurofilament 200 (NF200)	Mouse (polyclonal)	1.200	1.200	In-house	Davletov lab
Peripherin	Mouse (monoclonal)	1.500	1.500	MAB1527	Millipore
ATF3	Rabbit (polyclonal)	1.500	1.500	HPA00156 2	Atlas Antibodies
TRPV1 (extracellular epitope)	Rabbit (polyclonal)	1.50	-	ACC-029	Alomone
TRPV1	Rabbit (polyclonal)	1.500	-	ACC-030	Alomone
GM1a	Rabbit (polyclonal)	1.200	-	orb6099	Biorbyt
<b>Secondary antibodies</b>					
Goat anti-Rabbit IgG (H+L) Highly Cross-Adsorbed Secondary Antibody, Alexa Fluor 488	Goat (polyclonal)	1.2000	1.500	A11034	Invitrogen

Goat anti-Rabbit IgG (H+L) Cross-Adsorbed Secondary Antibody, Alexa Fluor 594	Goat (polyclonal)	1.2000	1.500	A11012	Invitrogen
Goat anti-Mouse IgG (H+L) Highly Cross-Adsorbed Secondary Antibody, Alexa Fluor 488	Goat (polyclonal)	1.2000	1.500	A11029	Invitrogen
Goat anti-Mouse IgG (H+L) Cross-Adsorbed Secondary Antibody, Alexa Fluor 594	Goat (polyclonal)	1.2000	1.500	A11005	Invitrogen
<b>Fluorescent molecules</b>					
Isolectin B4-FITC conjugate (IB4-FITC)	-	1.300	-	L2895	Sigma
Cholera toxin subunit B-FITC conjugate (CTB-FITC)	-	1.250	-	C1655	Sigma
4',6-diamidino-2-phenylindole (DAPI)	-	1.10,000	1.10,000	D9542	Sigma

The antibody for the BoNT/A-truncated version of SNAP25 was produced and purified by the Davletov lab. Validation of the antibody showing specificity for cleaved SNAP25 was performed by Western blot (Figure 2.1). In lysed rat DRG cultures, untreated conditions showed no immunoreactivity to this antibody, despite the presence of uncleaved, total SNAP25. Treatment with BoNT/A for 24 hours produced an immunoreactive band using the cleaved SNAP25 antibody at the relevant molecular weight for cleaved SNAP25, demonstrating its specificity for the cleaved protein product.

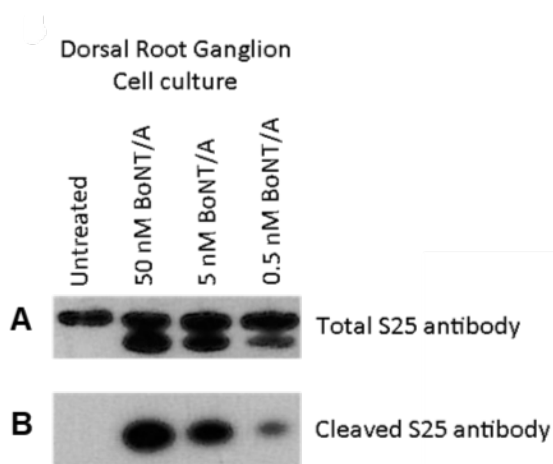


**Figure 2.1. Western blot demonstrating specificity of the in-house rabbit cleaved SNAP25 antibody to BoNT/A light chain cleavage. a)** Western blot of a rat DRG culture treated for 24 hours with BoNT/A and probed for all SNAP25 protein. This blot shows a concentration dependent increase in the amount of protein detected in a second band representing a truncated, BoNT/A-cleaved SNAP25 product. This second band is not detected when there is no BoNT/A treatment. **b)** When the blot is probed with the BoNT/A cleavage product specific antibody for SNAP25 (cS25), there is no band present in the absence of BoNT/A treatment. There is also a concentration-dependent increase in the amount of cS25 protein as BoNT/A concentration increases. Data provided courtesy of Dr Charlotte Leese.

## 2.2 Primary culture of dorsal root ganglion neurons

### 2.2.1 Animals

All procedures were conducted under UK Home Office Project, Personal and Institutional Licenses and complied with the UK Animals (Scientific Procedures) Act, 1986. Experiments were conducted on male Sprague Dawley rats purchased from Charles River. All animals were housed in a 12 hour light/dark cycle at 21°C and in 55% relative humidity. Food and water was available ad libitum.

### 2.2.2 Coating of 96-well plates and coverslips

Black 96-well polystyrene high-binding microplates (Greiner Bio-One, 355090) were coated with 40µL of 20µg/ml laminin in PBS (L2020, Sigma-Aldrich) for at least 2 hours at 37°C, before washing twice in PBS without being allowed to dry. Any empty wells were filled with PBS to prevent evaporation.

Sterile 16mm coverslips were coated first with poly-D-lysine (PDL) then with laminin. A 10 $\mu$ L dot of 50 $\mu$ g/ml PDL (P6407, Sigma) was placed directly in the middle of the coverslip, then the coverslips were placed at 37°C for at least 2 hours. The PDL was then washed twice with ultrapure H<sub>2</sub>O and allowed to dry. The coverslips were then stored at 4°C until use. Prior to cell plating, the coverslips were then coated with a 10 $\mu$ L dot of 20 $\mu$ g/ml laminin in PBS (L2020, Sigma-Aldrich) for at least 2 hours at 37°C. The laminin was then washed twice with PBS without being allowed to dry.

### *2.2.3 Dissociation of dorsal root ganglion neurons*

3-8 week old male Sprague Dawley rats were sacrificed by Schedule 1 method (cervical dislocation or CO<sub>2</sub> overdose, confirmed by exsanguination) in accordance with the UK Animals (Scientific Procedures) Act 1986. The animals were decapitated, and the skin overlying the spinal cord cut from the neck to the tail to expose the vertebral column. The spinal column was then removed by cutting along both sides using iris scissors, lifting and then releasing any tissues and organs from beneath it, and finally cutting through it at the caudal end. Excess muscle and connective tissue was cut away. The dorsal roof of the spinal column was removed using microscissors to expose the spinal cord. The ventral side of the spinal column was then bisected, to produce a bisected spinal column. The spinal cord was pulled away to reveal the DRG. Each DRG was dissected out using fine tweezers and microscissors by cutting the central and peripheral spinal root close to the body of the ganglion. DRG were collected into PBS or F12 media.

Depending on the place of work, two different dissociation protocols were followed (Method 1 and Method 2 below). All solutions and media were warmed to 37°C. In a culture hood, the medium was removed from the DRG and replaced with warmed digestion enzyme.

**Method 1:** Digestion enzyme consisting of 1mg/ml Dispase II (D4693, 0.85 U/mg, Sigma) and 0.6 mg/ml Collagenase XI (C7657, 1594 U/mg, Sigma) in HEPES-buffered dissociation solution was added to the DRG for between 1 and 1.5h at 37°C. The DRG were then dissociated in the enzyme mix by trituration with a P1000. The 1ml of cell suspension was then layered on top of 4ml 15% bovine serum albumin (BSA) in DRG wash media and centrifuged for 5 minutes at 1000 RPM with the brake turned off. The supernatant was removed and the cells were resuspended in 5ml of wash media and centrifuged again. The supernatant was removed and the pellet of dissociated

DRG neurons was resuspended in the appropriate amount of DRG media to allow either 200µl per well in a 96-well plate or a 3µl dot in the middle of a coverslip. Cells were allowed to attach to coverslips for 30 minutes at 37°C and 5% CO<sub>2</sub> in a covered 12-well plate, before being flooded with 1ml of DRG media. Neurons were maintained at 37°C and 5% CO<sub>2</sub>. Half media changes were performed every 2-3 days using warmed complete DRG media.

<b>HEPES-buffered dissociation solution (sterile, pH 7.3)</b>	
NaCl	155mM
KH <sub>2</sub> PO <sub>4</sub>	1.5mM
HEPES	5.6mM
HEPES sodium salt	4.8mM
D-(+)-Glucose	10mM
NaOH	pH to 7.3

<b>DRG wash media (method 1)</b>		
DMEM/F12 with Glutamax	31331, Gibco	
Heat-inactivated horse serum	26050, Gibco	10%
Penicillin-streptomycin	P0781, Sigma	1%

<b>DRG media (method 1)</b>		
Neurobasal A	10888, Gibco	
Heat-inactivated horse serum	31331, Gibco	1%
Penicillin-streptomycin	26050, Gibco	1%
Nerve growth factor (NGF) β	SRP4304, Sigma	20ng/ml
B27	17504-044, Gibco	1x
Glutamax	35050-061, Gibco	1%
Uridine	U3003, Sigma	20µM
5'-Fluoro-2'-deoxyuridine	F0503, Sigma	20µM

**Method 2:** Digestion enzyme consisting of 0.125% Collagenase (C0130, Sigma) in DMEM/F12 was applied for 1 h at 37°C, followed by 3 washes with warmed PBS. 0.25% trypsin (T0303, Sigma) in PBS was then applied for 10 minutes at 37°C. 2ml of wash media was added to stop the digestion and the DRG were triturated with a P1000. The suspension was passed through a 100µm cell strainer and centrifuged at 900 RPM for 3 minutes before being resuspended in 1ml of wash media. The cell suspension was then layered on top of 2ml of 15% BSA in wash media and centrifuged at 900 RPM for 10 minutes. The supernatant was then removed, and the pellet of DRG neurons was resuspended in 200µl of wash media and 3µl of this suspension was spotted into the centre of a 96-well plate. Cells were allowed to attach for 1h at 37°C before being flooded with

200µl of full DRG media per well. Neurons were maintained at 37°C and 5% CO<sub>2</sub>. Half media changes were performed every 2-3 days using warmed complete DRG media.

<b>DRG wash media (method 2)</b>		
DMEM/F12 with Glutamax	31331, Gibco	
Heat inactivated fetal bovine serum	10500064, Gibco	10%
Penicillin-streptomycin	26050, Gibco	1%

<b>DRG media (method 2)</b>		
DMEM/F12 with Glutamax	31331, Gibco	
Heat inactivated fetal bovine serum	10500064, Gibco	10%
Penicillin-streptomycin	26050, Gibco	1%
Nerve growth factor (NGF) β	N1408, Sigma	50ng/ml
Uridine	U3003, Sigma	60µM
5'-Fluoro-2'-deoxyuridine	F0503, Sigma	143µM

### **2.3 Stapled botulinum toxin production**

All botulinum toxin preparation and protein analysis was performed by Dr Charlotte Leese.

Preparation of ChoBot involved production of 3 structurally independent units (Figure 2.2): 1) The light chain-translocation domain of BoNT/A (LcTd/A) fused to SNAP25 as described previously in Darios et al., (2010) to form LcTd/A-S25; 2) The syntaxin helix peptide (AEDAEIIKLENSIRELHDMFMDMAMLVESQGEMIDRIEYNVEHAVDYVE); 3) The cholera binding domain (AB5) fused to the Synaptobrevin (syb) helix (Synaptobrevin 2, aa 2-84).

The syntaxin peptide was synthesised by Peptide Synthetics. The LcTd/A-S25 was expressed by the Davletov group in BL21 strain of E. coli as a glutathione S-transferase N-terminal fusion. Proteins fused to glutathione S-transferase were purified on Glutathione Sepharose beads (GE Healthcare, Buckinghamshire, United Kingdom) and eluted from beads in 20 mM HEPES, pH 7.3, 100 mM NaCl (Buffer A) using thrombin. Further purification was achieved by gel filtration using a Superdex 200 10/200GLcolumn (GE Healthcare).

The Syb-AB5 binding domain was co-expressed in E.coli in two parts by Matthew Balforth at the University of Leeds. The first part consisted of the 25 C-terminal amino acids of the CTA2 subunit fused to the Syb SNARE helix (2-84) with a 5 amino acid linker in between them and an N-terminal Maltose binding protein (MBP) affinity tag for ease of purification, which could be removed by a

TEV protease site. The second co-expressed part was the CTB subunit. When coexpressed in E.coli, the CTB forms a pentamer around the CTA2 part of the brevin-fused protein, forming MPB-Syb-AB5 which was purified by NiNTA affinity purification. The MPB was then removed by TEV proteolysis and Syb-AB5 was further purified by another round of NiNTA affinity purification.

The full Chobot construct was assembled by mixing the three fusion proteins for 60 minutes at 20°C, each component at 1µM concentration, in Buffer A containing 0.4% octyl glucoside (OG). After confirmation of the assembly by SDS-PAGE and Coomassie staining, the protein was aliquoted and stored at -80°C before functional experiments.

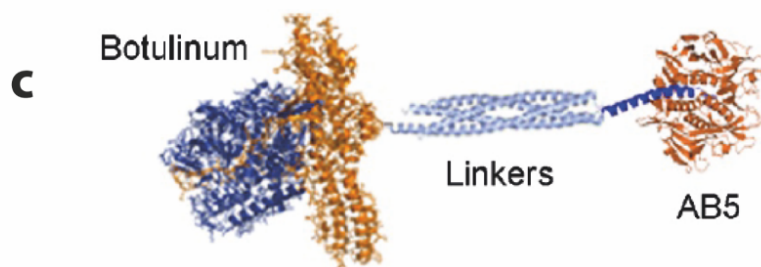
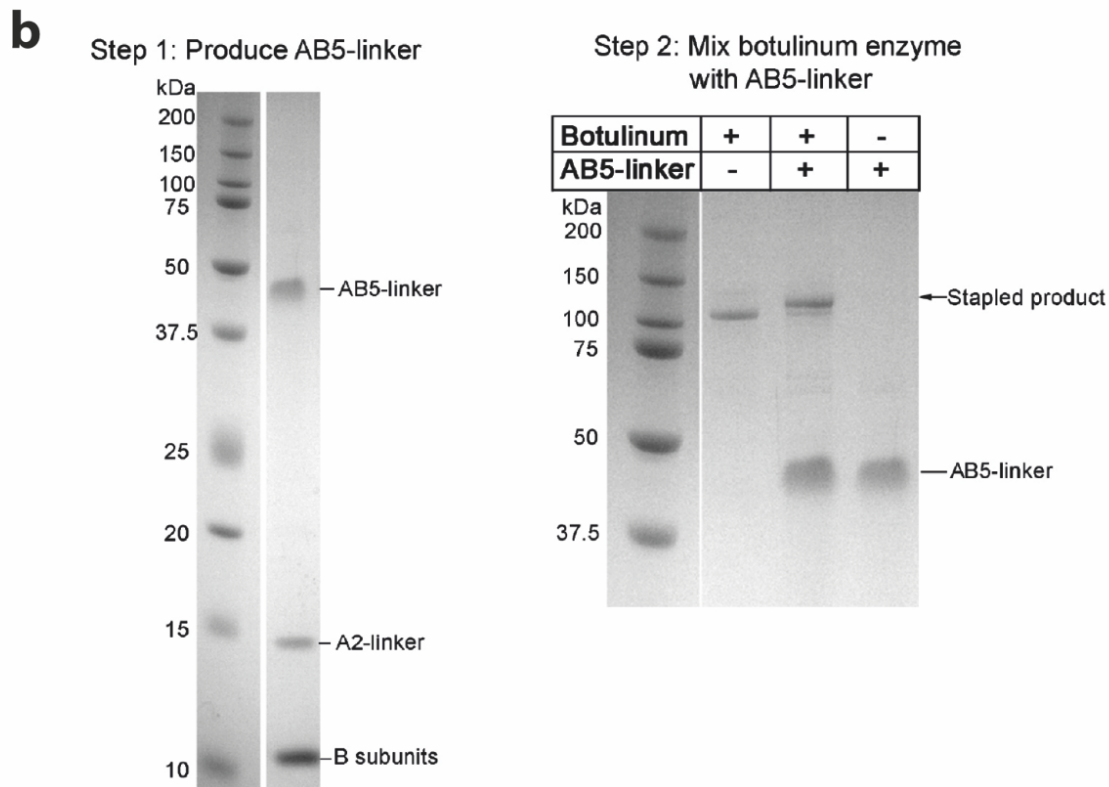
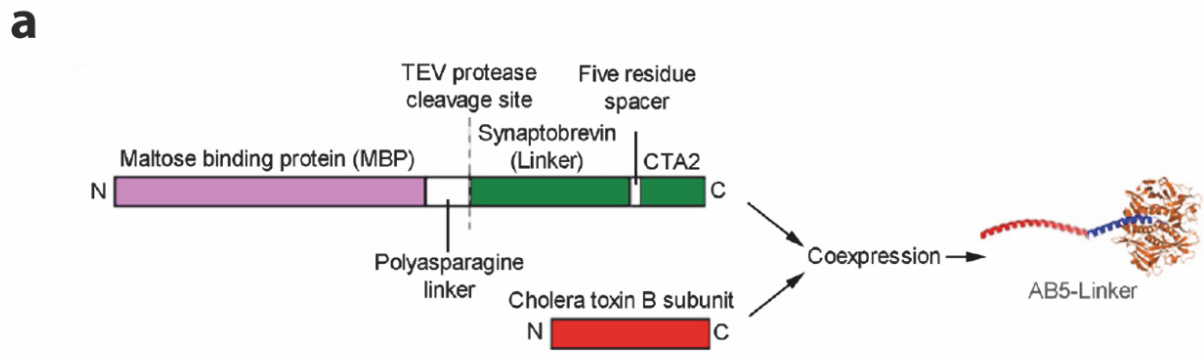


**Figure 2.2. Production of ChoBot. a)** Self-assembly of the pentameric cholera toxin B (CTB) subunit attached to the synaptobrevin linker protein (AB5-Linker). After coexpression, the maltose binding protein is removed by cleavage at the TEV site. CTA2=cholera toxin A2 subunit. **b)** Western blot showing production of the AB5-linker (Step 1) and production of ChoBot from mixing (1) the AB5-linker (2) the BoNT/A translocation and light chain domains attached to SNAP25 and (3) the syntaxin stapling protein (Step 2). **c)** Final combined structure of ChoBot. Data provided courtesy of Dr Charlotte Leese.

Bitox/AA was prepared as described in Andreou et al. (2020). Preparation of BiTox/AA involved recombinant production of 3 structurally independent units (Figure 2.3): 1) The receptor binding domain (HcA, BoNT/A 874–1296, UniProt K4LN57) independently fused to synaptobrevin (rat syb2 25–84, UniProt P63045); 2) The receptor binding domain independently fused to syntaxin (rat syx 3, 195–253, UniProt Q08849); 3) The light-chain translocation domain (LHn) fused to SNAP25. These recombinant proteins were expressed in bacteria, purified, and then mixed to form BiTox/AA. Specifically, proteins were expressed in a BL21 strain of *Escherichia coli* as glutathione S-transferase C-terminal fusions. Proteins fused to glutathione S-transferase were purified on Glutathione Sepharose beads (GE Healthcare, Buckinghamshire, UK) and eluted from beads in 20 mM HEPES, pH 7.3, and 100 mM NaCl (buffer A) using thrombin. Further purification was achieved by gel filtration using a Superdex 200 10/200 GL column (GE Healthcare). BiTox/AA was assembled by mixing the three fusion proteins for 60 min at 20°C, each component at 1µM concentration, in buffer A containing 0.4% OG. After confirmation of the assembly by SDS-PAGE and Coomassie staining, the protein was aliquoted and stored at –80°C before functional experiments.

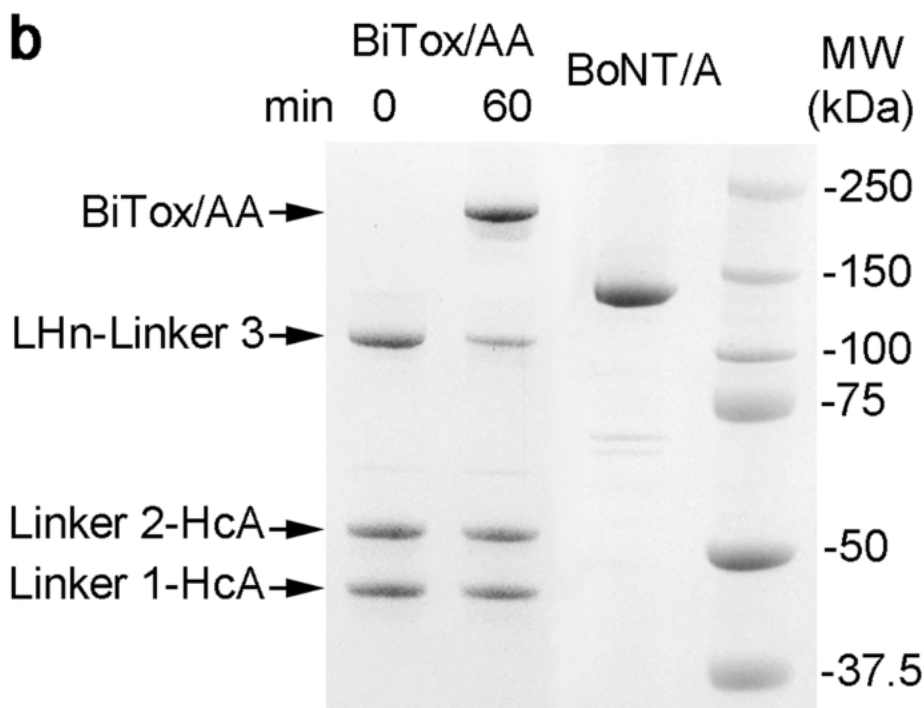
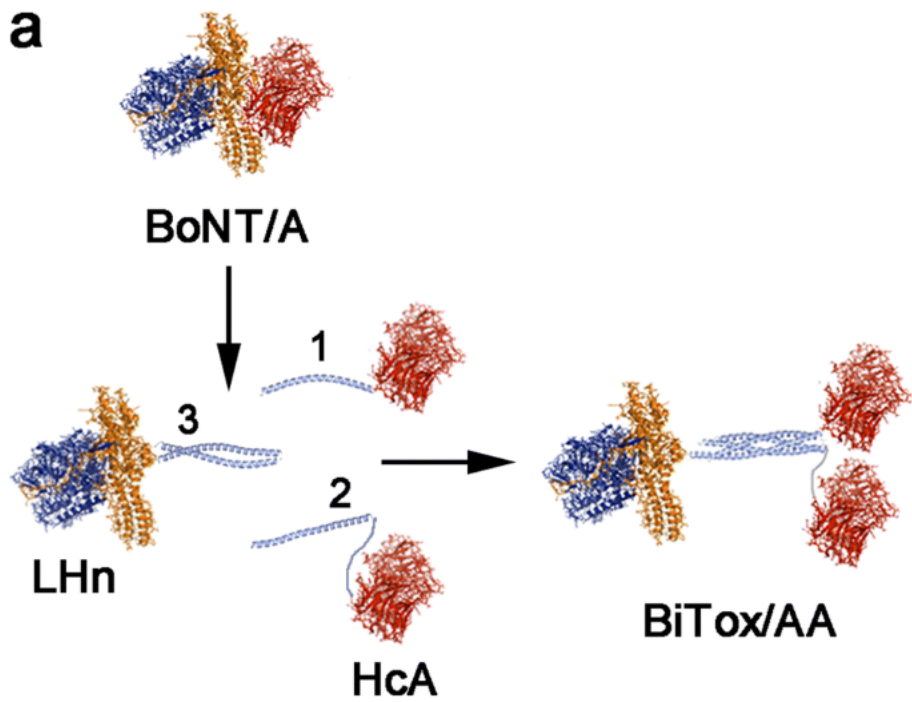


**Figure 2.3. Production of BiTox/AA.** **a)** Schematic of native BoNT/A toxin and formation of BiTox/AA from three separate fusion proteins. LHN is the BoNT/A light chain and translocation domains attached to SNAP25 (3), HcA is the receptor binding domain of BoNT/A, one which is linked to synaptobrevin (1) and the other to syntaxin (2). SNAP25, syntaxin and synaptobrevin self-assemble to form a SNARE complex, leading to formation of BiTox/AA. **b)** Coomassie-stained SDS-PAGE gel showing the formation of BiTox/AA after the 60-min assembly reaction. The lane indicating 0 min demonstrates the initial protein amounts used in the BiTox/AA assembly reaction. BiTox/AA exhibits higher molecular weight compared to the native BoNT/A molecule. Excess amounts of HcA with linkers 1 and 2 in the lane 60 min migrate at their original positions. Figure copied from Andreou et al. (2020) under a Creative Commons Attribution 4.0 International License.

OG is a detergent which was originally used to disrupt lipid bilayers in SNARE complex formation experiments (Hu et al., 2002). It is used in the reaction mix when producing SNARE-stapled botulinum toxins because it increases the speed of SNARE complex formation, potentially by disrupting their initial folding enough to allow them to complex with each other (Figure 2.4).

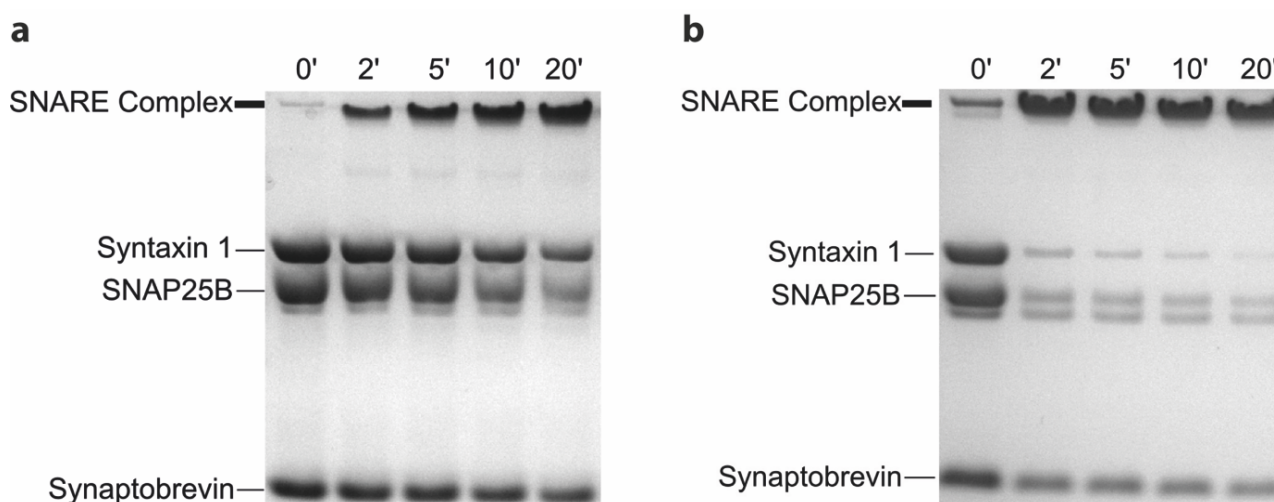


**Figure 2.4. Effect of octyl glucoside (OG) on the speed of SNARE complex formation. a)** In the absence of OG it takes many minutes for the SNARE complex to assemble in a reaction mixture of syntaxin 1, SNAP25 and synaptobrevin/VAMP2. Even at 20 minutes, there is still significant banding at molecular weights representing the individual SNARE proteins which have still failed to form complexes with each other. **b)** When 0.8% OG is added to the reaction mix, SNARE complex assembly is significantly more complete, even at the 2 minute timepoint. Data provided courtesy of Dr Charlotte Leese.

## 2.4 Treatment of cultured dorsal root ganglion neurons

### 2.4.1 Paclitaxel treatment

At either 2 or 6 days *in vitro* (DIV), DRGs were treated with paclitaxel. Paclitaxel was dissolved in dimethyl sulfoxide (DMSO) then diluted to 2x concentration in media, and a half media change was then used to apply the drug to the wells or coverslips resulting in a 1x concentration. All conditions involving DMSO had a final concentration of 0.1% DMSO. Experiments were performed 24h after addition of paclitaxel.

Initial *in vitro* experiments were performed with paclitaxel dissolved in a 50/50 mix of Kolliphor EL (C5135, Sigma) and ethanol (E/0665DF/17, Fisher Scientific), as this is the vehicle used in patients and animal models. However, Fluorescent Imaging Plate Reader (FLIPR) calcium imaging showed

that Kolliphor/ethanol suppressed calcium responses to potassium chloride and, to a lesser extent, cinnamaldehyde in a neuronal cell line (Figure 2.5). It was therefore decided to use DMSO as the solvent for *in vitro* paclitaxel experiments.

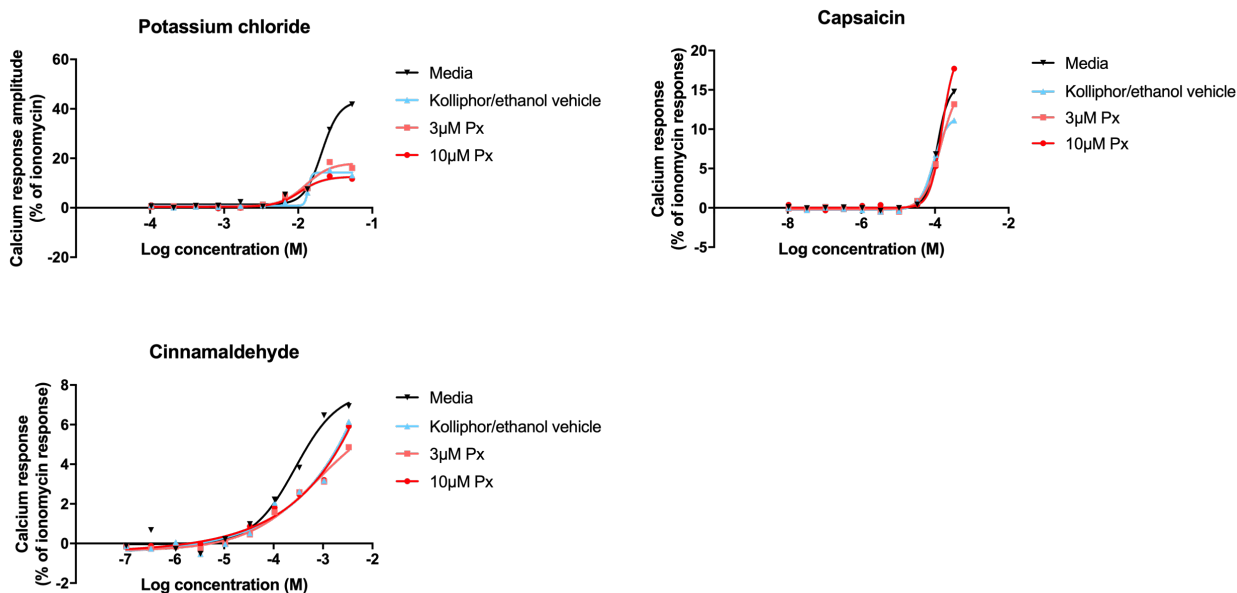


**Figure 2.5. Effect of Kolliphor/ethanol vehicle on calcium responses of neuronally differentiated IMR32 cells assayed by FLIPR.** Dose responses of calcium response amplitude for different chemical stimuli was carried out in differentiated IMR32 cells. IMR32 cells had been subjected to a 24 hour treatment with paclitaxel (Px), an equivalent concentration of Kolliphor/ethanol vehicle, or a media change only.

#### 2.4.2 Toxin treatment

Stapled botulinum toxins were diluted in buffer A with 0.4% OG (to keep the final OG concentration consistent between different toxins and batches) to 20x final concentration. This stock was then diluted in warmed complete media to 2x final concentration. A half media change was then used to apply the toxin to the wells or coverslips resulting in a 1x concentration. The final concentration of OG was therefore 0.02% in all conditions except media change only controls.

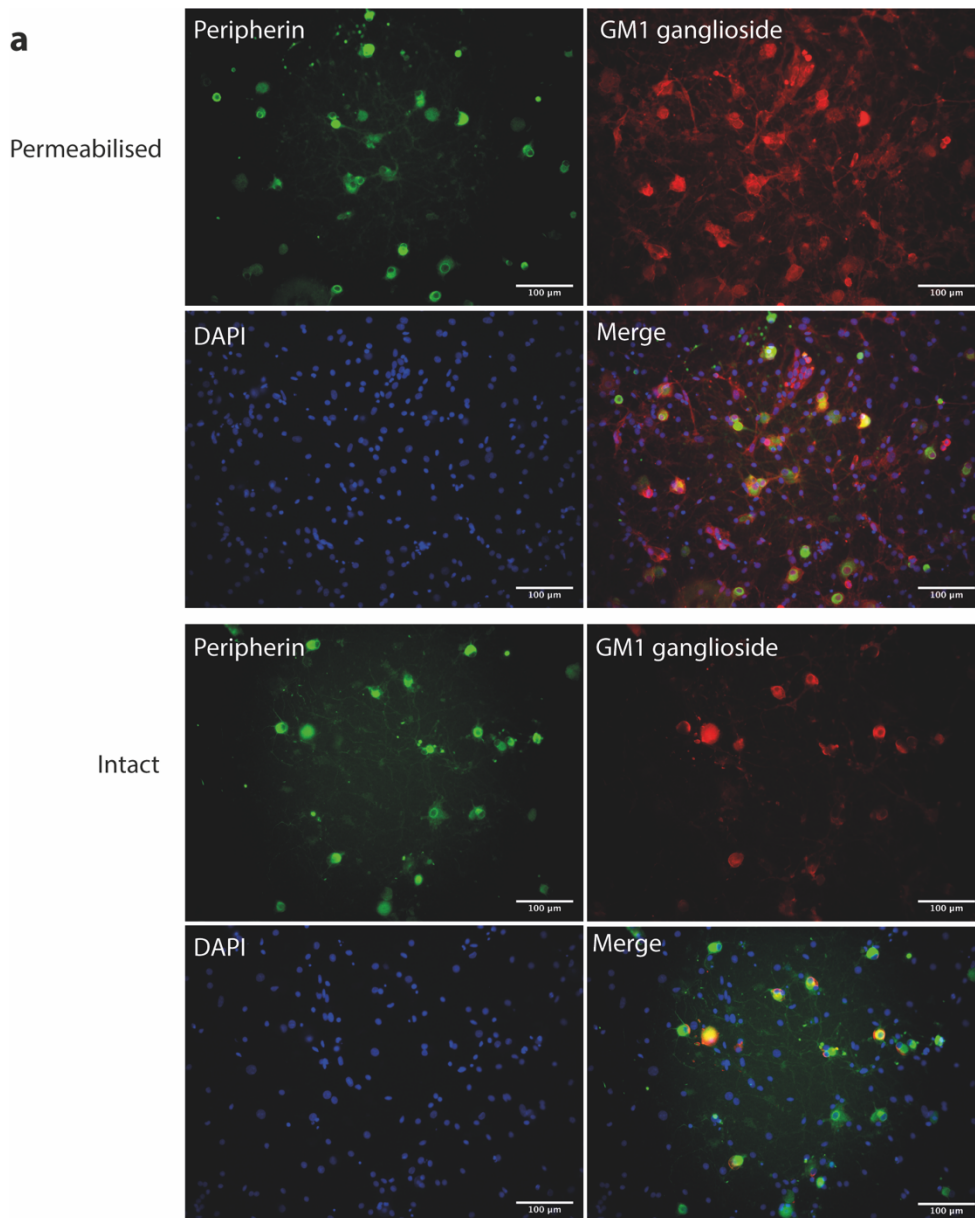
## **2.5 Immunocytochemistry and imaging of dorsal root ganglion neurons**

### **2.5.1 Fixation and immunocytochemistry**

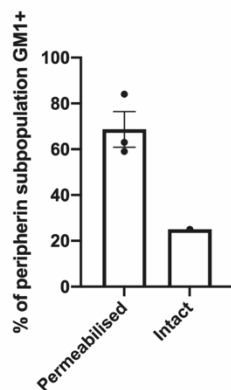
If CTB or IB4 fluorescent conjugates were used, these were applied for 30 minutes on live cells at 37°C then washed twice with PBS prior to fixation. Fixation was performed on ice. Wells were washed once with ice cold PBS for 2 minutes, then fixed for 10 minutes with ice cold 4% PFA in PBS. The PFA was then washed from the wells with PBS. The cells were then permeabilised with 0.1% triton X-100 for 15 minutes before being washed again with PBS. Blocking solution was added to the wells at room temperature for 1 hour. Primary antibodies were diluted in blocking solution then applied to the wells for 1 hour at room temperature. Primary antibodies were washed 3 times with PBS. Fluorescent secondary antibodies and DAPI were diluted in blocking solution and applied to the cells for 45 minutes at room temperature in the dark before being washed 3 times with PBS.

Immunocytochemistry for the GM1 ganglioside was performed on cultures prior to permeabilisation. This was in order to only mark ganglioside at the membrane and avoid any immunoreactivity of internal GM1 gangliosides which are due to be processed into more complex gangliosides rather than being expressed at the membrane as GM1 itself (Figure 2.6c). When applied to permeabilised cultures there was widespread immunofluorescence of peripherin-expressing neurons. When cultures were not permeabilised prior to immunolabelling, the percentage of GM1-labelled neurons decreased dramatically, presumably by labelling only the ganglioside functionally inserted into the membrane (Figure 2.6c).

If labelling for GM1 was required, cells were fixed then blocked in blocking solution without Tween-20 for 1 hour. The GM1 antibody was applied for 1 hour, diluted in blocking solution without Tween-20, washed with three PBS washes, then the secondary antibody was applied for 45 minutes in blocking solution without Tween-20. The plate was kept protected from light from this point. The wells were washed 3 times with PBS again, then the neurons were permeabilised with 0.1% triton X-100 and immunocytochemistry for any other antigens proceeded as detailed above.



**b** Effect of cell permeabilisation on GM1 immunoreactivity



**c**



**Figure 2.6. Effect of cell permeabilisation with triton on immunocytochemistry of the GM1 ganglioside.** **a)** Representative images showing co-localisation of the small C fibre population marker peripherin with GM1 ganglioside when immunocytochemistry was performed either following permeabilisation or on non-permeabilised cells. **b)** Co-localisation of peripherin and the GM1 antibody was decreased in non-permeabilised cultures, suggesting that only a subpopulation

*of neurons that express the GM1 ganglioside have it functionally inserted in the membrane. c) The GM1 ganglioside synthesis pathway. The GM1 ganglioside lies in the middle of the synthesis of the  $\alpha$ -series gangliosides (Yu et al., 2011). As there are multiple more complex gangliosides further along in the pathway, membrane specific immunocytochemistry was required in order to only mark GM1 ganglioside at the membrane and avoid any GM1 that was destined for further processing into a different ganglioside before expression at the membrane.*

### *2.5.2 Epifluorescent microscopy of cell cultures*

Immunocytochemistry images were either automatically taken using an InCell Analyser 2200 (GE Healthcare) or manually using a Leica DMI8 microscope, Leica DFC3000G camera and CoolLED pE-300 Ultra light source using Leica Application Suite X.

When using the InCell Analyser 2200, a 20x air objective (numerical aperture 0.45) was used to image relevant wells of the 96-well plate. Between 10 and 12 fields of view were pre-defined to evenly cover the entire well before imaging, eliminating bias involved in choosing fields. Excitation was performed with a 561nm laser for AlexaFluor 594 secondaries, a 488 laser for AlexaFluor 488 secondaries and a 405 laser for DAPI excitation. FITC, TexasRed and DAPI emission filters were used to filter the emitted light. Laser and software autofocuses were used to automatically focus on the DAPI image, then this focal plane was applied to images taken with other wavelengths.

When manually imaging DRG neurons with the Leica DMI8, 6 fields of view were randomly imaged from across the well using a Leica 20x air objective (numerical aperture 0.4). Cells were excited at the relevant wavelength for AlexaFluor-488, AlexaFluor-594 and DAPI, and emission filters were used to filter the emitted light at the relevant wavelength.

### *2.5.3 Image analysis for ChoBot, cholera toxin subunit B and GM1 ganglioside subtyping*

Image analysis and quantification was performed using FIJI. Circular regions of interest (ROIs) were drawn around cell bodies of neurons (as marked by either pan-neuronal markers or markers of certain neuronal populations). The Multi Measure function was then used to measure the fluorescent intensities (either mean grey value or min & max grey value depending on experiment) of the relevant wavelength of the image. These were then copied into Microsoft Excel for analysis.

Thresholds for positivity were set by measuring the fluorescent intensities of cell bodies of a negative control for each culture (i.e. wells that were not treated with toxin for cleaved SNAP25 quantification, or a secondary only control for other markers). A threshold was then set for each culture at the mean + 2 standard deviations of the negative control intensities measured.

#### *2.5.4 Image analysis for ATF3 expression and area covered by neuronal processes*

All ATF3 image analysis of DRG cultures was performed blinded to treatment condition by undergraduate project student Jemimah Suratos. Image analysis and quantification was performed using FIJI. Thresholding was performed to produce a mask of DAPI, ATF3 and  $\beta$ -III-tubulin. First, the brightness and contrast of the DAPI image was adjusted, then thresholding was applied to highlight all nuclei present in the culture before a binary mask was created. The 'despeckle' function was used to remove noise and the 'watershed' function was used to divide any merged nuclei with a line of one pixel thickness. Any fused nuclei that remained following these functions were ignored by adding a size threshold of 0-128 $\mu\text{m}^2$  to the 'analyse particles' function used to then measure the intensities of the nuclei.

The ATF3 intensity associated with each DAPI stained nucleus was then measured by redirecting the DAPI mask onto the ATF3 image and measuring the mean pixel intensity using the 'analyse particles' function, again with a size threshold of 0-128 $\mu\text{m}^2$ . A threshold intensity for a nucleus to be classified as ATF3 positive was set at a mean intensity of 10816 by visually assessing a composite of the DAPI and ATF3 channel images.

The  $\beta$ -III-tubulin image was then used to determine which nuclei are associated with neurons in the culture. The brightness and contrast were adjusted to best show the soma and a binary mask was created. The 'watershed' function was applied to separate any touching cell bodies. The 'analyse particles' function was used with a size threshold of 60-infinity  $\mu\text{m}^2$  to create ROIs marking individual cell bodies. The area of these cell bodies was measured and converted into a circular diameter by the equation  $D=2\sqrt{(A/\pi)}$ . Each individual ROI was then manually assessed to check it corresponded to one single cell body. The DAPI outline was then overlaid onto the  $\beta$ -III-tubulin outline and any neurons with multiple nuclei, or no nucleus, were rejected. The ATF3

intensity for the remaining  $\beta$ -III-tubulin ROIs was recorded, giving a cell body diameter, associated ATF3 intensity and whether that ATF3 intensity reached the threshold to be classified as positive.

The area covered by neuronal processes in the culture was also measured. The brightness and contrast of the  $\beta$ -III-tubulin image was adjusted to show the processes clearly, and a rectangular ROI covering a tenth of the area of the image was placed in an area without cell bodies. This ROI was duplicated and the image was thresholded to mark neurites. This threshold was analysed to determine what proportion of the image the processes covered.

### *2.5.5 Extracellular TRPV1 immunocytochemistry*

For cell surface labelling of TRPV1 with an extracellular epitope-recognising antibody (Alomone, ACC-029) a live cell approach was taken. Wells had been treated with paclitaxel, DMSO or a media change only for 24 hours prior to experiments. This treatment and all imaging was performed blinded. DRG neurons were incubated in primary antibody diluted in warmed complete media for 10 minutes at 37°C. They were then washed 5 times in warmed media and then incubated in a fluorescent secondary antibody, also diluted in warmed media. The secondary antibody was applied for 10 minutes at room temperature, sometimes alongside a proprietary cell membrane stain from a Neurite Outgrowth Staining Kit (A15001, Invitrogen) used at 1 in 5000 dilution. The wells were then washed 3 times with media before being washed twice with PBS and fixed with PFA as above. DAPI was then applied to the wells for an hour diluted in PBS, then washed three times with PBS.

If a capsaicin TRPV1 internalisation protocol was to be used, either 10 $\mu$ M or 1 $\mu$ M capsaicin in Ringer solution with 0.1% DMSO final concentration was applied to the cells for 1 minute and washed with media twice prior to applying the antibodies to the cells (based on Tian et al., 2019).

### *2.5.6 Confocal microscopy*

Neurons were imaged on an inverted Nikon A1 confocal microscope with a CFI Plan Achromat VC 60x oil objective (NA 1.4) using Nikon Elements software. When a neuron to image had been identified in the full field of view (Figure 2.7a), the Nyquist XY function was used to reduce the

scan area and increase the optical resolution to achieve the maximum resolution that achieves Nyquist sampling (Figure 2.7b,c). This increased the resolution from 2.4195 pixels/ $\mu\text{m}$  to 10.0387 pixels/ $\mu\text{m}$ . x4 line averaging was applied to reduce noise. Only neurons which had clear membrane only TRPV1 staining at intensities higher than secondary only controls were imaged. Some neurons were also shown to take the membrane stain up into the cytosol (Figure 2.7c). The membrane of these neurons was considered to be compromised so these were excluded from imaging and analysis. An intact, clearly defined nucleus shown by DAPI staining was also required for the neuron to be imaged. 10 neurons per well were imaged, with two wells per condition, giving a total n number of 20 neurons per condition.

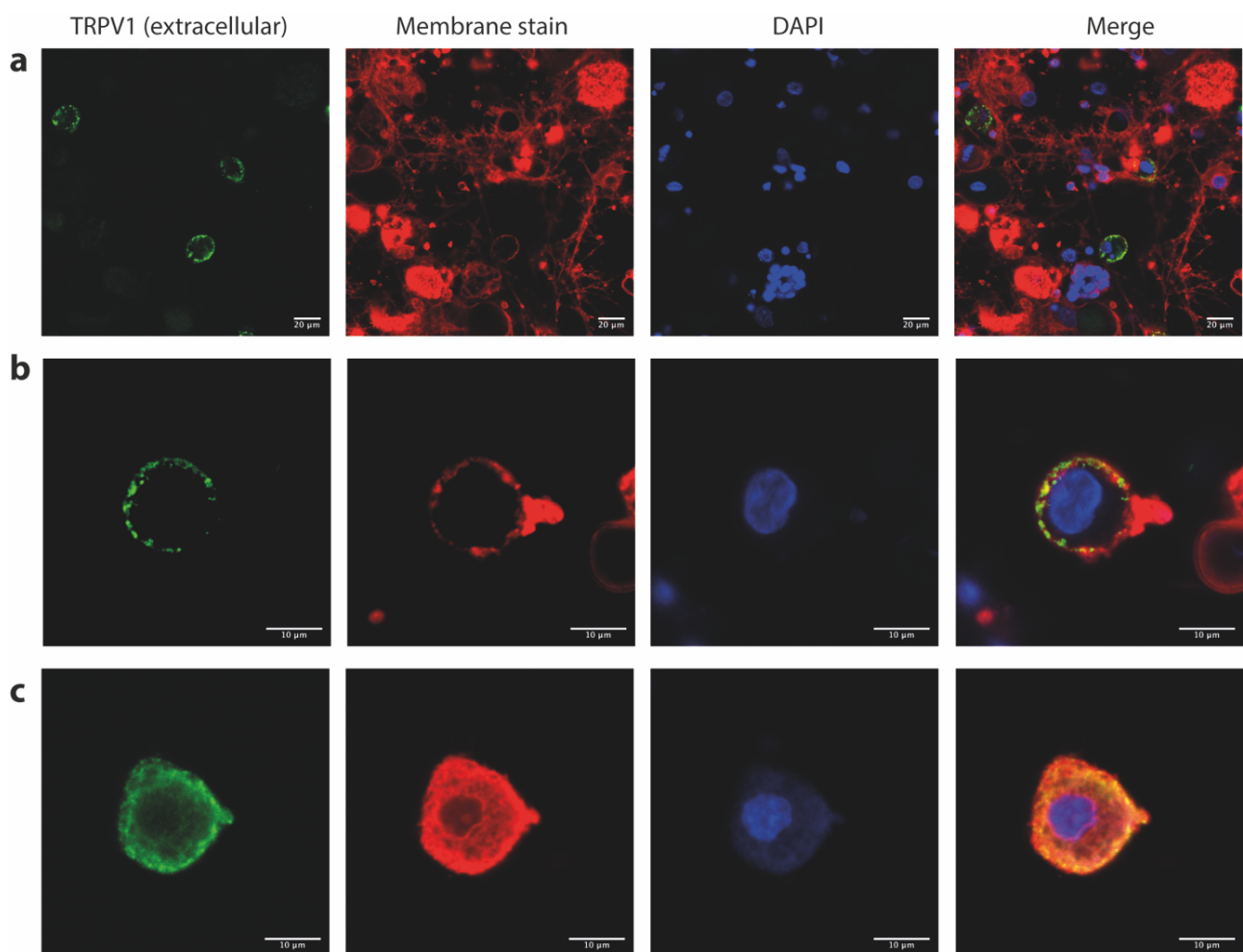


**Figure 2.7. Imaging of TRPV1 extracellular antibody immunocytochemistry of dorsal root ganglion cultures. (a)** Full field view of stained and fixed cultures showing membrane-isolated staining of TRPV1 (green), membrane stain (red) and DAPI (blue). **(b)** Only neurons with membrane-bound TRPV1 and membrane stain with an intact nucleus were imaged for analysis. **(c)** Some DRG neurons took the membrane stain up into the cytosol. These were presumed to not have an intact membrane and therefore likely to be compromised or dead so were not imaged.

### 2.5.7 Extracellular TRPV1 image analysis

Image analysis and quantification was performed using FIJI. Only the extracellular TRPV1 channel was quantified. A ROI was drawn by hand around the outside of the cell membrane using the freehand selection tool as initial automatic thresholding approaches to do this were inconsistent (Figure 2.8b). A macro written by Dr Darren Robinson was then used to create a new ROI that encompassed a fixed 2 $\mu$ m diameter towards the middle of the cell from the original ROI (Figure 2.8a,c). It then measured the mean intensity of this ring, now encompassing the majority of the membrane staining.

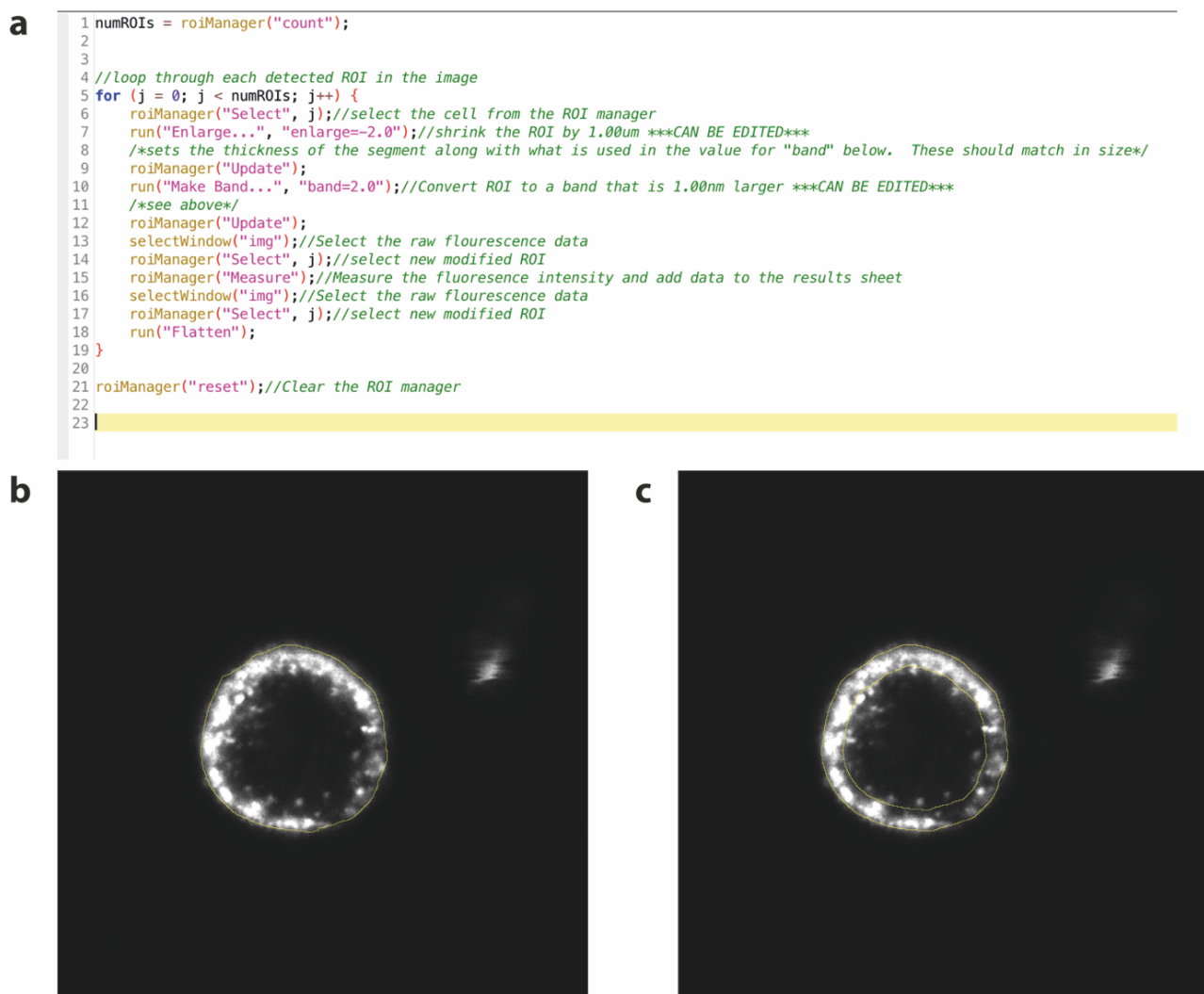


**Figure 2.8. Analysis of TRPV1 extracellular antibody immunocytochemistry. a)** A macro was used to automatically create a 2 $\mu$ m diameter ring ROI around the membrane of each cell. **b)** An ROI was first drawn by hand around the outside of the cell membrane (yellow). **c)** The macro then applied a ring shape ROI to encompass the whole membrane and measured the mean intensity within this ring (yellow).

## **2.6 Live cell assays**

### **2.6.1 Calcitonin gene-related peptide release assay**

CGRP release was assayed using an acetylcholinesterase based enzyme-linked immunoassay (ELISA) kit from Bertin Bioreagent (A05482). Briefly, wash buffer, enzyme immunoassay buffer and anti-CGRP tracer were made according to kit instructions. Stimulating compounds were made up at working concentration in HEPES-buffered Tyrodes solution (HBTS) with 10 $\mu$ M DL-Thiorphan (Bachem, N-11950025) and warmed to 37°C. An CGRP standard concentration curve was made up in enzyme immunoassay buffer from the highest concentration of 500 pg/ml with 7 subsequent 1:2 serial dilutions. Just before stimulation, ELISA plates were washed 5 times with wash buffer, then 100 $\mu$ l of anti-CGRP tracer was added to each well. The CGRP concentration curve was added to relevant wells.

Media was removed from DRG neurons in a 96-well plate. Wells were washed once with warmed HBTS and thiorphan, then warmed compounds were added to the wells and the plate was incubated at 37°C for 10 minutes. The supernatant was then carefully removed from the wells and placed into the ELISA plate with the tracer. ELISA plates were sealed and placed at 4°C overnight.

On the second day, Ellman's reagent was made up per kit instructions. ELISA plates were washed 5 times with wash buffer and then 200 $\mu$ l of Ellman's reagent was added. The plates were left to develop at room temperature on an orbital plate shaker in the dark for between 30 and 60 minutes. Absorbance was then measured at 405nm using a plate reader (PerkinElmer Enspire or FLUOstar Optima). The mean absorbance of the blank well controls was subtracted from the absorbance of each well and the optical density of the standard curve was plotted to convert the absorbance into CGRP concentration.

### **2.6.2 Fura2-AM single cell calcium imaging**

DRG neurons were cultured on coverslips as above. Fura2-AM (Invitrogen, F1221) stock was made up at 2mM in DMSO and stored in aliquots at -20°C in desiccating conditions. On the day of imaging, Fura2-AM was made up to 2 $\mu$ M in Ringer solution with 0.02% Pluronic F-127 (P6867,

Molecular Probes) added to enhance dispersal. Mixing was done by vigorous pipetting at the surface of the solution for approximately a minute. Coverslips were loaded for 30 minutes with Fura2-AM in a 37°C incubator, after which the solution was replaced with Ringer solution. Coverslips were then kept in the incubator for between 15 and 60 minutes, after which they were taken out to settle at room temperature for 15 minutes before imaging.

Coverslips were imaged using a Zeiss 40x air objective (numerical aperture 0.75) on an Axiovert S100TV microscope. Images were sequentially acquired at 340nm and 380nm excitation wavelengths using a Polychrome IV monochromator from T.I.L.L. Photonics. An emission filter was used to filter only the correct emission wavelength for Fura2-AM. Images were taken at a rate of 1fps on Metamorph software, using a Photometrics Cascade 512B camera. Coverslips were perfused at a rate of 3ml/min with a Multichannel Systems PPS2 peristaltic perfusion system.

Compounds were diluted in Ringer solution from stock immediately prior to imaging. For veratridine assay experiments, the perfusion protocol was as follows: 1 minute Ringer solution, 3 minutes 30µM veratridine, 10 minutes Ringer solution, 1 minute 10µM  $\alpha,\beta$ -Methyleneadenosine 5'-triphosphate lithium salt ( $\alpha,\beta$ -Methylene ATP), 4 minutes Ringer solution, 1 minute 200µM cinnamaldehyde, 4 minutes Ringer solution, 1 minute 200nM capsaicin, 4 minutes Ringer solution, 1 minute high potassium (40mM) Ringer solution. The final concentration of DMSO was 0.1% when the stock compounds were solubilised in DMSO.

Image analysis was performed in ImageJ. Regions of interest were drawn around each cell body, and a ROI was used to measure the background in the absence of a neuron. The average intensity of the background ROI of each image was subtracted from the average intensity of each cell body for both the 380nm and 340nm excitations. R at each timepoint was calculated by calculating the ratio of the signal at 340 and 380nm for each ROI. The  $R_0$  calcium signal of each neuron was then calculated as the mean 340/380 ratio in the first 30 seconds of recording, in the absence of stimulation.  $\Delta R/R_0$  was then calculated as  $(R-R_0)/R_0$ . Calcium signal over time was then analysed in Graphpad Prism.

Only neurons that responded to potassium chloride depolarisation were used for analysis. For the veratridine assay, neurons were grouped into one of four distinct veratridine response profiles, the oscillatory (OS), slow decay (SD), intermediate decay (ID) and rapid decay (RD) profiles, as

described in Mohammed et al. (2017). Briefly, a multi-peak veratridine response was classed as OS, whereas a single peak response was classed as SD, ID or RD based on whether it took over 15 minutes, 2-5 minutes or less than 2 minutes to revert back to baseline respectively. Whether the neuron subsequently responded to  $\alpha,\beta$ -Methylene ATP, cinnamaldehyde, capsaicin or 40mM KCl, and the response amplitude was also recorded. A response to any of the stimuli was classed as a  $\Delta F/F_0$  increase above 6 standard deviations at baseline.

For area under the curve calculations, as not every response reached baseline by the end of the wash period, the area under the curve to the half decay point was analysed. The X coordinate corresponding to the half amplitude was found. The area of the calcium response peak to this point was then analysed with Graphpad Prism.

### *2.6.3 Fluorescent Imaging Plate Reader calcium imaging*

DRG were cultured for 7 days before 24 hours of paclitaxel or vehicle treatment. At 8 DIV, the media was tipped off the plate and the neurons were loaded with 100 $\mu$ l per well of Calcium 6 (Molecular devices, R8191), made up to kit instructions in HBTS for 2 hours at room temperature protected from light. Stimulating compounds were made up in a flat bottom 96-well plate (Nunc Microwell, Thermofisher) in HBTS at 3x concentration with 0.3% DMSO. A second plate containing the calcium ionophore ionomycin (Tocris, 1704) was made up at 4x concentration with 0.4% DMSO.

After loading, the plates were placed into the FLIPR. A mask was used to read from only the centre of each well, as DRG neurons were spotted in the middle for these experiments. A baseline read of 10 seconds was performed before 50 $\mu$ l of the stimulating compound was added to the respective DRG wells, diluting the compound down to 1x working concentration with 0.1% DMSO in the well. After a 5 minute read, 50 $\mu$ l of ionomycin was added to the DRG wells, diluting down to 1 $\mu$ M and 0.1% DMSO in the well. A further 5 minute read was then performed. A read was performed every second for the duration of the experiment.

<b>FLIPR calcium imaging settings</b>	
Gain	150
Exposure	0.4
Intensity	80
Excitation	470-495 nm
Emission	515-575 nm
Stimulation addition rate	40 $\mu$ l/s

The amplitude of the calcium response to the stimuli was then exported, by exporting the max-min read between read 10 and 300 (amplitude to stimulating compound) and 310 and 610 (amplitude to ionomycin). Ionomycin was used to induce calcium influx over the whole neuronal population in a way that should not be affected by ion channel changes, to normalise and control for varying plated neuronal densities between repeats and individual wells. For each well, the amplitude of response to an addition of buffer was subtracted from the amplitude of the stimulating compound. This buffer subtracted value was then normalised as a percentage of the amplitude of the subsequent ionomycin addition.

#### 2.6.4 Incucyte

Brightfield phase images of live DRG cultures were taken using an Incucyte SX1 live-cell analysis system with a 20x objective. DRG neurons at 7 DIV were treated with different concentrations of paclitaxel or DMSO, or a half media change control was performed. The treated plate was placed in the Incucyte and a brightfield image was taken immediately, after 4 hours, then every 12 hours until 64 hours. NeuroTrack software was used to apply a mask to the cell bodies and neurites in the culture. A set of 120 images was used to train the Neurotrack software.

<b>Incucyte Neurotrack settings</b>	
Segmentation mode	Brightness
Segmentation adjustment	1
Hole fill ( $\mu\text{m}^2$ )	100
Adjust size (pixels)	0
Min cell width ( $\mu\text{m}^2$ )	7
Cell-body cluster filter area ( $\mu\text{m}^2$ )	Min: 200 Max: 200
Neurite filtering	Best
Neurite sensitivity	0.5
Neurite width ( $\mu\text{m}$ )	1

## **2.7 *In vivo* experiments**

### **2.7.1 *Paclitaxel injections***

A rat model of CIPN was induced according to a well-established protocol (Polomano et al., 2001). Paclitaxel was dissolved to 6mg/ml in a 1:1 ratio of Kolliphor EL (C5135, Sigma) and ethanol (E/0665DF/17, Fisher Scientific). Aliquots were then frozen at for storage at -20°C if required. The paclitaxel was then diluted to 2mg/ml in 0.9% saline solution (12446-01, Dechra). Rats were anaesthetised with 4% isoflurane in oxygen in an induction chamber for paclitaxel injections. Injections were given at 2mg/kg via an intraperitoneal injection using a 23 gauge needle coupled to a 1ml syringe. 4 injections were given every other day over 8 days, to give a total cumulative dose of 8mg/kg per rat. Vehicle groups received equivalent injections of Kolliphor EL/ethanol/saline. Animals were observed until recovered from anaesthesia.

### **2.7.2 *Spared nerve injury***

The SNI model was used as a model of peripheral neuropathic pain as described in Decosterd & Woolf, 2000). Briefly, rats were anaesthetised using 4% isoflurane in oxygen then maintained at 2%. All surgery was performed aseptically. The left hindleg was shaved and wiped with iodine solution. An approximately 1cm incision was made longitudinally through the skin on the lateral surface of the thigh to expose the muscles using a scalpel. Blunt dissection was used to separate the muscle layer to reveal the sciatic nerve. Using a stereomicroscope, Mersilk sutures (W580) were tightly ligated around the tibial and common peroneal branches of the sciatic, leaving the smallest sural branch intact. The ligated nerves were then axotomised distally to the ligation using microscissors. The muscle layer was closed and the skin incision closed with Vicryl sutures (W9831T). 0.05mg/kg Vetergesic was then administered for pain relief. Animals were observed until recovered from anaesthesia.

### **2.7.3 *Intraplantar injection of botulinum toxin***

Rats were anaesthetised with 4% isoflurane in oxygen for injections. Toxins were diluted in 0.4% OG in buffer A to allow a 30µl injection volume. The left hindpaw was cleaned using 70% ethanol.

The toxin was injected subcutaneously in the middle of the footpads of the plantar surface of the left hindpaw using a BD Micro-Fine 0.5-ml insulin syringe. The animal was then observed until recovered from anaesthesia.

#### 2.7.4 Von Frey testing

Behavioural testing was performed blinded to BoNT injection. Mechanosensitivity thresholds were measured using the simplified up-down method (SUDO) described in Bonin et al. (2014). This technique estimates paw withdrawal threshold by the application of von Frey monofilaments (Touch Test Sensory Evaluator Kit of 20, Stoelting) of logarithmically increasing force. The SUDO method differs from traditional measurements of paw withdrawal threshold as exactly 5 von Frey filament stimulations are used per measurement, thereby standardising any sensitisation through repeated monofilament application.

Testing occurred between 9am and 12pm each day. Briefly, rats were placed in chambers above a wire mesh grid and allowed to acclimatise for 30 minutes. When the animals were at rest but not asleep, monofilament 4.31 (number 10) was applied to the centre of the hindpaw footpad until it buckled and was held for 3 seconds. Whether there was a swift paw withdrawal reflex or not was recorded. If there was a response, the next lower force filament was then tested, if there was no response the next higher force filament was applied. At least 1 minute was given between monofilament applications for each animal. Testing progressed in this up-down manner until 5 filaments had been applied and the responses recorded.

The 50% withdrawal threshold for each animal, in grams, was estimated by the formula:

$$50\% \text{ threshold } (g) = (10^{x+B})/10,000$$

where x is the logarithmic value of the final filament applied (e.g. 4.31) and B is an adjustment value equal to half the mean logarithmic interval between filaments of the set. The mean logarithmic interval between filaments is 0.176 so the adjustment value used was 0.088. This adjustment value was either negative or positive based on whether there was a positive withdrawal response to the final filament applied or not.

Two withdrawal threshold estimates were recorded per hindpaw per animal each day, and the mean of these were taken as the 50% withdrawal threshold. At the end of the experiment the animals were sacrificed by Schedule 1 method and tissue was taken for processing.

### *2.7.5 Dry ice cold allodynia testing*

Behavioural testing was performed blinded to retargeted BoNT injection. Dry ice was used as a cold stimulus for a behavioural read-out of cold allodynia, based on the method published by Brenner et al. (2012). A 3ml syringe was adapted by cutting off the end for the needle and small holes made in up the barrel of the syringe. Dry ice was ground into a fine powder and packed into a compressed pellet by loading into the syringe, pressing it against a flat surface and depressing the plunger. The rats were placed on a glass surface (originally intended for Hargreaves thermal testing) and allowed to acclimatise for 30 minutes. Testing occurred between 9am and 12pm each day. When the rats were at rest but not asleep, the pellet of compressed dry ice was applied to the glass surface beneath the hindpaw, and the latency to withdraw the foot was measured with a stopwatch. The dry ice pellet against the glass produces a consistently ramping cold stimulus, therefore the latency to withdrawal is correlated to the temperature for withdrawal. Approximately 5 minute intervals were allowed before retesting of the same paw. 5 latencies were recorded for each hindpaw per animal per day. A mean of these latencies was then used as the final latency to withdrawal for each animal. At the end of the experiment the animals were sacrificed by Schedule 1 method and tissue was taken for processing.

### *2.7.6 Compound muscle action potential recordings*

CMAP recordings from rat gastrocnemius muscle was performed as detailed in Andreou et al. (2020). Rats were anaesthetised with 4% isoflurane and maintained at 2%. Stimulating needle electrodes (ELSTM2; Biopac, Goleta, CA) were inserted perpendicularly into the muscle approximately 0.5 cm from the fifth lumbar vertebrae on either side. The anode was always placed distally and the cathode placed proximally to the recording leg. A ground electrode (EL452, Biopac) was placed in the base of the tail. A reference recording needle electrode (EL450, Biopac) was placed over the tendon of the gastrocnemius muscle, and a recording electrode was placed in the belly of the medial gastrocnemius muscle.

CMAP measurements were performed using a Biopac system with a bandpass of 30–9999 Hz and 200× gain, running AcqKnowledge software. A 0.2-ms pulse stimulation was performed with a voltage stimulator (BSLSTMB). Supramaximal stimulation was determined for each recording. The amplitude of the CMAP waveform was then measured (Figure 2.9). Eight recordings per leg were performed, replacing the recording electrode each time, and the largest three recordings were averaged.



**Figure 2.9. CMAP recording using AcqKnowledge software.** Example trace showing the recorded CMAP waveform (above, red) and the amplitude measured (arrow). The blue trace (below) shows the stimulating voltage spike.

Baseline CMAP recordings were determined for the gastrocnemius of each hind limb. Rats were then each injected with 30µl of a botulinum construct subcutaneously over the recording site of the left gastrocnemius muscle using a BD Micro-Fine 0.5-ml insulin syringe immediately after baseline recording. All injections and recordings were performed blinded to the toxin and concentration given. CMAPs were then recorded from both gastrocnemius muscles again on days 1, 2, 3, and 7, and the fold-change to the baseline CMAP at each time point was calculated for each rat. At the end of the experiment the animals were sacrificed by Schedule 1 method.

## 2.8 Immunohistochemistry and imaging of sections

### 2.8.1 Tissue preparation, fixation and sectioning

Rats were sacrificed by cervical dislocation and death was confirmed by exsanguination. The lumbar DRG (L1-L6) were dissected as detailed in Section 2.2.3. The plantar surface of the hindpaw

was dissected by cutting round the footpads with a scalpel and using blunt dissection to remove the skin. DRG were fixed in 4% PFA in PBS at 4°C for 2-4 hours before being placed at 4°C overnight in 30% sucrose in PBS. The hindpaw skin was fixed in Zamboni's solution (a phosphate-buffered solution of 2% PFA and 15% picric acid) before being transferred into 30% sucrose in PBS at 4°C.

For sectioning, tissue was embedded in Cryo-M-Bed OCT medium (53581-1, Bright) and frozen on dry ice. Sections were prepared using a cryostat (OFT5000, Bright Instruments). DRG were sectioned at 13µm thickness and collected directly onto SuperFrost Plus slides (J1830AMN2, ThermoScientific) and stored at -20°C until use. Skin sections were cut at 30µm and collected as free-floating sections into cryoprotectant solution and stored at -20°C until use.

### *2.8.2 Immunohistochemistry*

Immunohistochemistry was all performed at room temperature. Sections on slides were drawn around with a hydrophobic barrier PAP pen. Slide-mounted sections or free-floating sections were washed for 10 minutes with PBS three times. They were then blocked with immunohistochemistry blocking solution for 1 hour. Primary antibodies were then diluted in blocking solution and applied to the sections for 2 hours before being washed off with three 10 minute washes in PBS. Sections were then incubated with secondary antibodies and DAPI diluted in blocking solution for 2 hours in the dark. Sections were again washed with three 10 minute washes of PBS. Free-floating sections were then mounted onto SuperFrost Plus slides (J1830AMN2, ThermoScientific) and allowed to partially air dry in the dark. Slides were finally coverslipped using Fluoromount-G mounting medium (00-4958-02, Invitrogen) and #1.5 thickness 24 mm x 60 mm coverslips (631-0853, ThermoScientific).

### *2.8.3 Epifluorescent microscopy of tissue sections*

Tissue sections were imaged using a Leica 20x air objective (numerical aperture 0.4), Leica DMI8 microscope, Leica DFC3000G camera and CoolLED pE-300 Ultra light source. Sections were excited at the relevant wavelength for AlexaFluor-488, AlexaFluor-594 and DAPI, and emission filters were

used to filter the emitted light at the relevant wavelength. Images were acquired using Leica Application Suite X.

#### *2.8.4 Image analysis of tissue sections*

Co-localisation analysis of paw tissue sections was performed in FIJI. The brightness and contrast of neuronal subtype and cleaved SNAP25 images was adjusted to pick up just the positively stained processes. A ROI was then drawn freehand around the dermis and epidermis. The Co-localisation Threshold function was then run, including zero-zero pixels. Percentage co-localisation is reported as the percentage volume that is co-localised within each channel (%Ch1 Vol and %Ch2 Vol).

#### *2.8.5 Statistical analysis*

All statistical analysis was performed in Graphpad Prism. Details of each individual statistical test is detailed in figure legends. Statistical significance was defined as a null-hypothesis probability of  $P < 0.05$ . Results are presented as mean  $\pm$  the standard error of the mean (SEM). N refers to the number of biological replicates (i.e. 1 culture from one animal or 1 animal tested), n refers to individual measurements such as number of cells analysed.

### 3. *Characterisation of an in vitro model of chemotherapy-induced peripheral neuropathy*

#### 3.1 *Introduction*

Animal studies have been invaluable for understanding some of the mechanisms that lead to CIPN. However, these are ethically dubious and expensive, and despite these drawbacks often still do not translate to successful drug discovery for patients. A robust *in vitro* model would be advantageous in order to study the structural, electrophysiological, and neurotransmission changes that lead to CIPN, as well as to screen compounds such as novel botulinum toxins as potential treatments.

The vast majority of *in vitro* studies of CIPN have used cultured primary rodent DRG neurons, presumably due to easy access and physiological relevance. Paclitaxel has been shown to induce functional changes when applied directly to the DRG neurons in the media, making it a promising candidate for an *in vitro* model of CIPN. One of the most widely reported features of this is the inhibition of neurite outgrowth and the degeneration of neurites in the culture. When DRG neurons are cultured for between 5 and 7 days they develop extensive neuritic processes which undergo a reduction in length as soon as 24 hours after paclitaxel addition to the culture conditions (Yang et al., 2009; James et al., 2008). This echoes the retraction of epidermal nerve fibres observed in CIPN animal models (Boyette-Davis et al., 2011; Wozniak et al., 2018). Whether or not the mechanism is conserved is unclear, however, and whether it is a causal factor of the sensory symptoms of CIPN is yet to be determined.

*In vitro* paclitaxel exposure also causes changes in the release of the neuropeptides CGRP and substance P from cultured DRG neurons (Section 1.3.2.4). In the case of CGRP there are discrepancies as to whether paclitaxel attenuates or enhances release. This appears to be dependent on the concentration and the time-course of paclitaxel exposure, with acute exposure (10 minutes) enhancing release in a concentration dependent manner, and longer exposure (days) enhancing release at lower concentrations and attenuating it at higher concentrations (He & Wang 2015; Pittman et al., 2014).

As the use of cell cultures lends itself well to electrophysiological recordings, there has been literature published on the effect of paclitaxel on ion channel expression and the consequences of this on electrical activity (Section 1.3.2.3). For example, the sodium ion channel NaV1.7, which is heavily implicated in pain processing, is upregulated in dissociated DRG neurons of rats injected with paclitaxel (Li et al., 2018; Zhang & Dougherty, 2014). This is associated with hyperexcitability of the neurons, manifesting as spontaneous firing and reduced thresholds for activation. However, the protocols that produced these effects did require *in vivo* paclitaxel exposure injection protocols, and did not focus on *in vitro* exposure only. An entirely *in vitro* approach with paclitaxel applied directly to the neurons would be much more applicable for high throughput, screening experiments. Changes to ion channels and electrical activity has been demonstrated following entirely *in vitro* chemotherapy exposure. TRPV1-mediated activity is shown to be altered by direct perfusion of paclitaxel onto DRG neurons (Li et al., 2015). Acute paclitaxel exposure induces spontaneous action potentials and a reduced rheobase, and also prevented desensitisation of repeated capsaicin stimulated calcium responses.

Calcium imaging can be used as a way of assessing the activity of DRG cultures in naïve and pained conditions. One example of an assay to characterise the proportion and activity of different types of neurons in culture is the veratridine response profile assay. Veratridine is a compound that binds to open VGSCs and holds them in the active state, preventing deactivation and subsequently leading to depolarisation and calcium influx (although this does require depolarisation and VGSC activation in the first instance). Veratridine gives 4 characteristic profiles of responses in mouse DRG (oscillatory, slow decay, intermediate decay, rapid decay), which are differentially emblematic of nociceptors and non-nociceptors in the culture. Putative nociceptors are defined by their response to any of the agonists  $\alpha,\beta$ -methylene ATP, cinnamaldehyde or capsaicin. This combination of stimuli should activate all nociceptors, as capsaicin activates peptidergic C fibres,  $\alpha,\beta$ -Methylene ATP activates non-peptidergic C fibres and cinnamaldehyde was used to activate C-low threshold mechanoreceptors which express TRPA1 but not TRPV1 or P2X3 (Mohammed et al., 2017). Putative nociceptors are more likely to respond to veratridine with a multi-peak oscillatory (OS) calcium response and non-nociceptors are more likely to respond with a slowly rectifying slow decay (SD) response (Mohammed et al., 2020). The proportion of these veratridine responses that occur is a readout of the activity of nociceptors and non-nociceptors within the culture, and can be used as an assay of nociceptor activity and silencing by analgesics. Cultures from NaV1.7 knockout mice have a lower proportion of OS-responding neurons and NaV1.8 knockouts have a

higher proportion of OS-responding neurons. NaV1.7 and NaV1.8 antagonists also act to reduce the number of OS-responding neurons, demonstrating the applicability of this assay to drug screening for nociceptor silencing.

### **3.2 Summary and objectives**

An entirely *in vitro* model would give a higher-throughput system to screen compounds such as novel BoNTs to prevent or reverse changes associated with CIPN as an assay of their analgesic potential.

Experimental objectives:

- To investigate paclitaxel-induced neurotoxicity *in vitro* using DRG cultures and study whether some sensory neuron subpopulations are more susceptible to this toxicity than others using the damage-responsive transcription factor ATF3.
- To study whether the veratridine response profile assay (Mohammed et al., 2017) can be applied to detect changes to nociceptors in rat DRG cultures following paclitaxel exposure.
- Consider whether *in vitro* paclitaxel changes the functional activity of DRG cultures in response to stimulation with nociceptive agonists using calcium imaging and CGRP release assays.
- Investigate if the expression of TRPV1 at the membrane is upregulated by *in vitro* paclitaxel exposure.

### **3.3 Results**

#### **3.3.1 Paclitaxel induces expression of a stress-response transcription factor in a subset of sensory neurons**

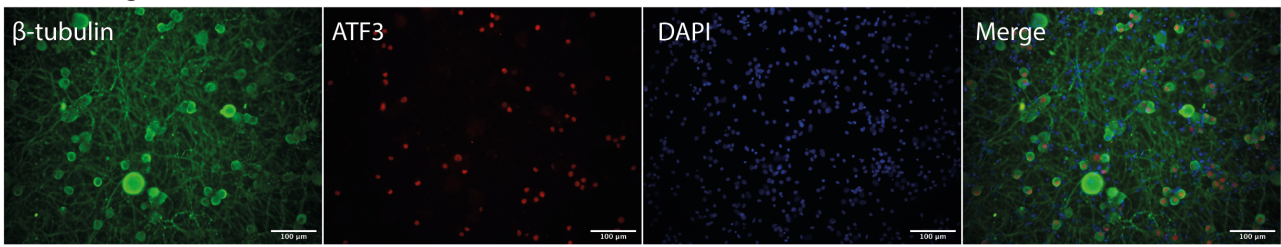
The initial experiments in this chapter aim to understand the toxic effects of *in vitro* paclitaxel on DRG neurons by using neuronal diameter as a broad-strokes tool to separate different neuronal populations. Two parameters were assessed, (1) an overall size distribution analysis to determine whether certain size neurons in the population are diminished via toxic mechanisms following paclitaxel exposure, and (2) expression of the stress responsive transcription factor ATF3 in

different sizes of neurons. Nuclear ATF3 expression is well established in rodent DRG neurons in response to peripheral damage or toxicity, such as following axotomy, crush injury, paclitaxel exposure, or diabetic neuropathy models (Anderson, 2012). Expression of this marker has also been shown to be induced *in vivo* in paclitaxel-induced CIPN models, though the degree of expression varies widely (Makker et al., 2017; Jamieson et al., 2007; Flatters & Bennett, 2006; Peters et al., 2007).

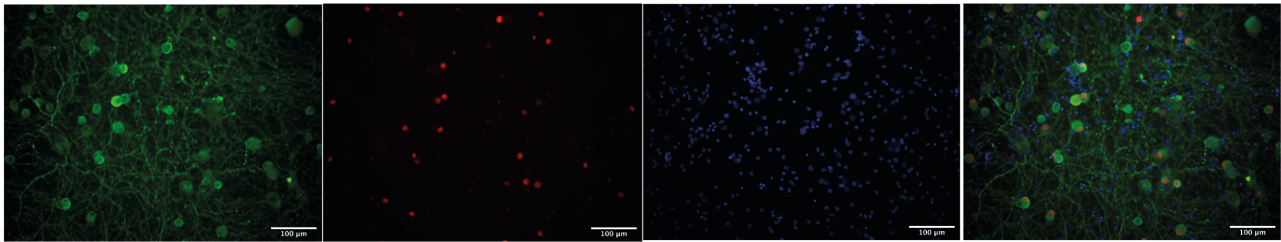
Paclitaxel was applied to neurons at both 2 and 6 days after dissociation and experiments were performed at 3 and 7 DIV, in order to assess whether age of cultures (and therefore development of dendrites) has any bearing on paclitaxel-induced changes. Paclitaxel was diluted in culture media and applied to the cells for 24 hours, before they were fixed and stained with the pan-neuronal marker  $\beta$ -III-tubulin and ATF3 (Figure 3.1, Figure 3.2). Two concentrations of paclitaxel were used in these experiments, 3 $\mu$ M and 10 $\mu$ M. These were chosen because this corresponds to the peak blood serum concentration of patients that have an estimated 15% and 100% probability of developing CIPN respectively (Hertz et al., 2018). A DMSO only control as well as a media change only control were used. The final concentration of DMSO was kept consistent in all conditions.

### 3DIV

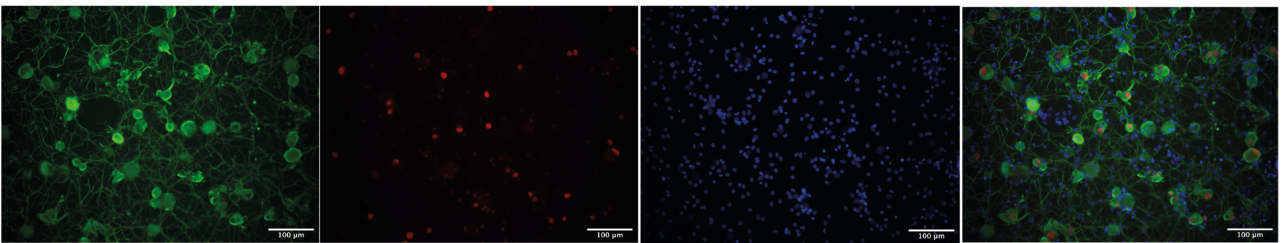
Media change



DMSO



3μM paclitaxel



10μM paclitaxel

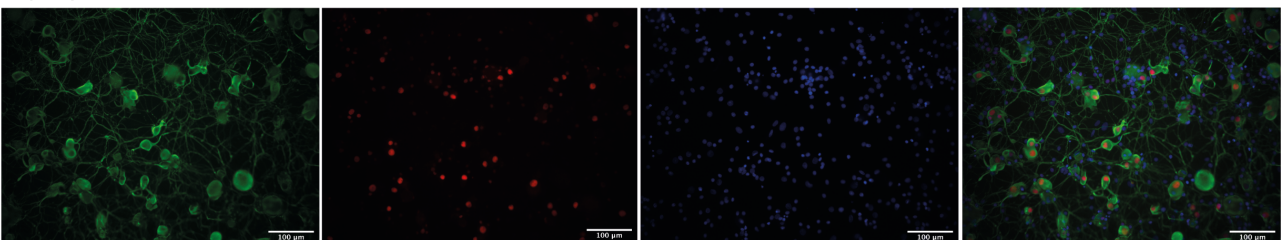
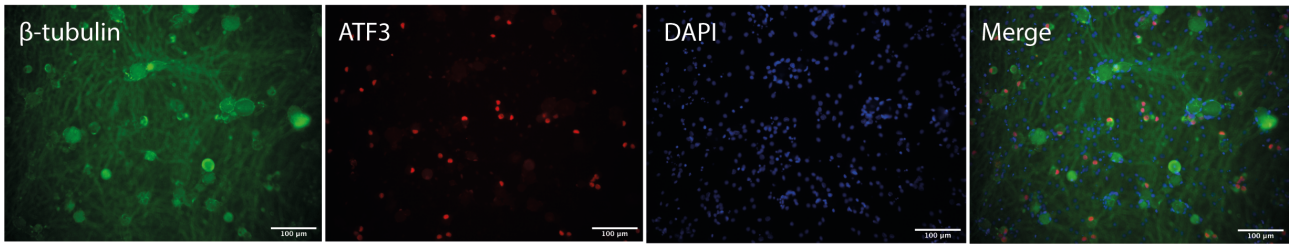


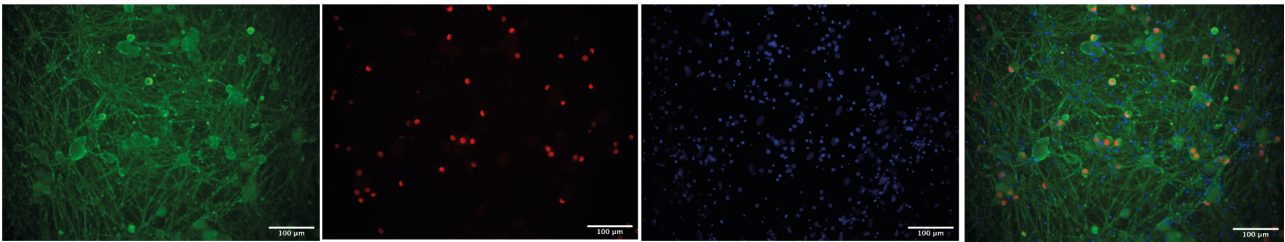
**Figure 3.1.  $\beta$ -III-tubulin and Activating Transcription Factor 3 (ATF3) expression in 3 day-old dorsal root ganglion cultures exposed to paclitaxel. Cultures at 2 days in vitro (DIV) were exposed to different concentrations of paclitaxel or an equivalent concentration of DMSO in the media for 24 hours before fixation. Representative images of immunofluorescence for the pan-neuronal marker  $\beta$ -III-tubulin (green), ATF3 (red), and the nuclear stain DAPI (blue).**

## 7DIV

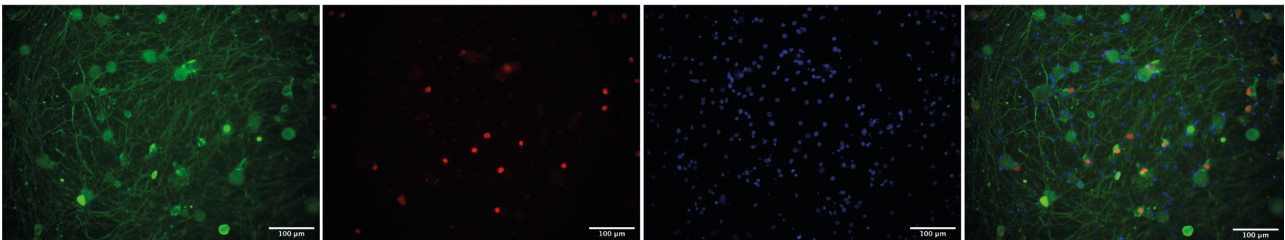
Media change



DMSO



3 $\mu$ M paclitaxel



10 $\mu$ M paclitaxel

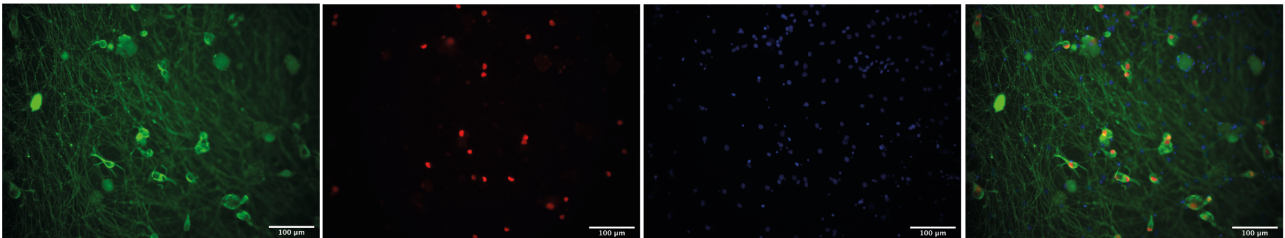


**Figure 3.2.  $\beta$ -III-tubulin and Activating Transcription Factor 3 (ATF3) expression in 7 day-old dorsal root ganglion cultures exposed to paclitaxel. Cultures at 6 days in vitro (DIV) were exposed to different concentrations of paclitaxel or an equivalent concentration of DMSO in the media for 24 hours before fixation. Representative images of immunofluorescence for the pan-neuronal marker  $\beta$ -III-tubulin (green), ATF3 (red), and the nuclear stain DAPI (blue).**

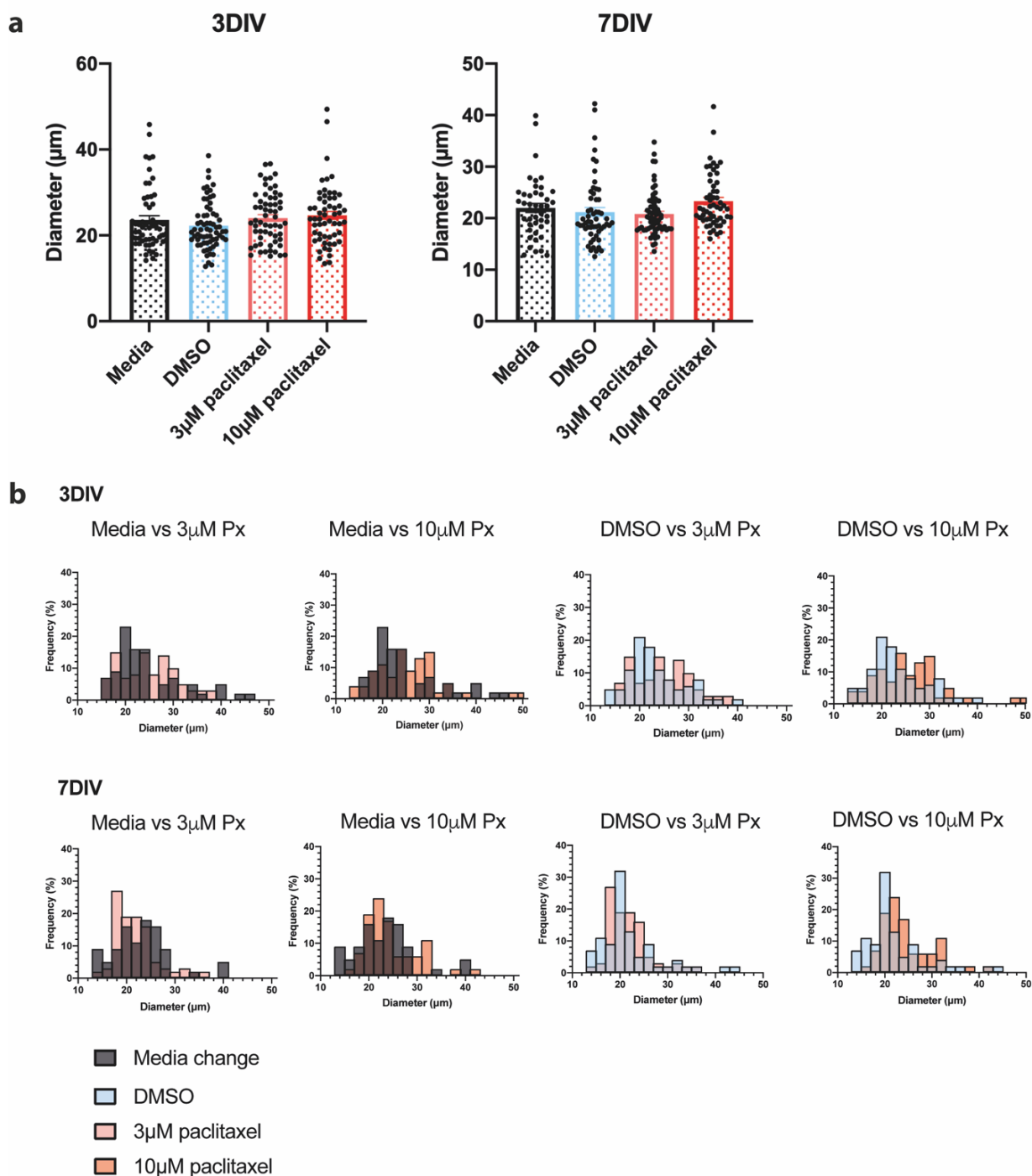


**Figure 3.3. Size frequency distributions of dorsal root ganglion (DRG) neurons exposed to paclitaxel in vitro. a)** The diameters of  $\beta$ -III-tubulin-visualised DRG neurons were measured at 3 or 7 days in vitro (DIV) after exposure to paclitaxel (Px), DMSO, or a media change control for 24 hours. No significance of ordinary one-way ANOVA. **b)** Diameter histograms are shown as a percentage of neurons analysed per condition, with a bin width of  $2\mu\text{m}$ . All paclitaxel-treated conditions (pink/red) and control conditions (black/blue) are plotted against each other.  $N=1$  culture, 2 images per condition.  $n=44-66$  neurons measured per condition. No significance of ordinary one-way ANOVA of diameters at each timepoint. Images analysed by project student Jemimah Suratos.

In order to determine whether the survival of a particular sensory subtype was being reduced by paclitaxel exposure, the diameters of the cell bodies marked with  $\beta$ -III-tubulin were analysed. To

be a useful model for evaluation of an analgesic, it is important to first establish that the treatment did not adversely affect the survival of sensory neurons. Rodent DRG neurons can be crudely classified into large neurons (>26µm), of which 90% express the myelination marker NF200, and small neurons (<26µm), which are largely unmyelinated (Lawson & Waddell, 1990; Yousuf et al., 2019). Smaller diameter neurons are more likely to be nociceptors and thermoreceptors than larger neurons, which are more likely to function as proprioceptors and low threshold mechanoreceptors (Usoskin et al., 2015). From *in vivo* animal model studies there is evidence that larger, myelinated populations are most strongly affected by the axonal toxicity of paclitaxel, as shown by ATF3 expression and morphological changes (Makker et al., 2017; Jamieson et al., 2007; Boehmerle et al., 2014). A shift towards smaller diameter neurons in the culture may therefore be caused by the death or detachment of these larger diameter populations.

There was no significant difference in the neuron diameters measured between conditions at either timepoint (Figure 3.3a). However, when histograms of neuron diameter from paclitaxel-treated and control conditions at 3 DIV are plotted against each other, the paclitaxel treated conditions consistently had peaks shifted towards larger diameter neurons than control conditions (Figure 3.3b). What this shows is that any particular vulnerability of certain diameter populations to paclitaxel is subtle for the time frame and conditions tested, and may not lead to cell death in most cases. Though not significant (potentially due to a fairly small number of cells measured), if there is a true shift to larger diameters following paclitaxel exposure then this is not easily explained by findings from *in vivo* studies, which would predict the neurotoxic loss of larger neurons, leading to a shift towards smaller neurons in culture. Findings may also be confounded by the particular enrichment of certain subpopulations of neurons in the culture, due to the dissociation process being particularly damaging to larger diameter neurons. Rather than cell death, this could be explained by a global cell swelling effect following paclitaxel exposure, potentially due to membrane retracting to the soma as the neurites degenerate. Therefore the expression of ATF3, another indicator of cell stress which could be associated with a pain phenotype, was investigated in these DRG cultures.

The expression of the stress responsive transcription factor ATF3 in different diameter neurons was investigated using the same images (Figure 3.1, Figure 3.2). This marker is most commonly used *in vivo* but there are a limited number of studies using it on DRG *in vitro* (Peeraer et al., 2011;

Wang et al., 2011). The expression of ATF3 was high even in naïve cultures, with 47% of neurons expressing it at 3 DIV, and 48% expressing it at 7 DIV (Figure 3.4a). Presumably this is due to cellular stress associated with the axotomy, dissociation and artificial culture environment of using primary neurons. This is a regular feature of ATF3 expression *in vitro*, with one study reporting levels of 20% and another even reporting 94% of DRG neurons expressing ATF3 in naïve conditions in culture (Peeraer et al., 2011; Wang et al., 2011). There was no difference in ATF3 expression in 3 day old cultures compared to 7 days old, suggesting that this time difference does not either reduce or increase cellular stress in the culture. Notably, this proportion of ATF3-positive neurons did not change following paclitaxel exposure (Figure 3.4a). Thus the unphysiologically high level of ATF3 expression in cultures, even without treatment, may be masking any overall effect of paclitaxel.

The diameters of neurons expressing ATF3 were then measured, in order to ascertain whether a particular subtype of DRG neuron was particularly sensitive to cell stress induced by paclitaxel. At 3 DIV, ATF3-positive neurons exposed to 10 $\mu$ M paclitaxel were significantly larger than media only control neurons (Figure 3.4b). This finding replicates what is reported in the literature, with larger diameter subpopulations of DRG neurons expressing ATF3 following CIPN induction in animal models (Makker et al., 2017; Jamieson et al., 2007; Peters et al., 2007). This was not replicated in cultures used at 7 DIV. Neuron diameter histograms of all the neurons in the culture versus ATF3-positive neurons were plotted for each treatment condition at each timepoint (Figure 3.4c). The ATF3-expressing neurons had the same size distribution as the overall culture in all conditions.

These experiments demonstrate that there is no significant loss of any particular diameter of DRG neuron induced by paclitaxel. In terms of cellular damage rather than loss, ATF3 is more likely to be expressed by larger diameter neurons following paclitaxel exposure, potentially highlighting a particular vulnerability of larger, NF200-expressing neurons. Further experiments would be required to ascertain this fully as only one culture and therefore biological replicate was performed for these experiments. The high overall expression of ATF3 in naïve cultures throws some doubt on the suitability of using primary DRG cultures to explore neuropathic conditions like CIPN, as these cultures may already have some features of neuropathy resulting from the dissociation process.

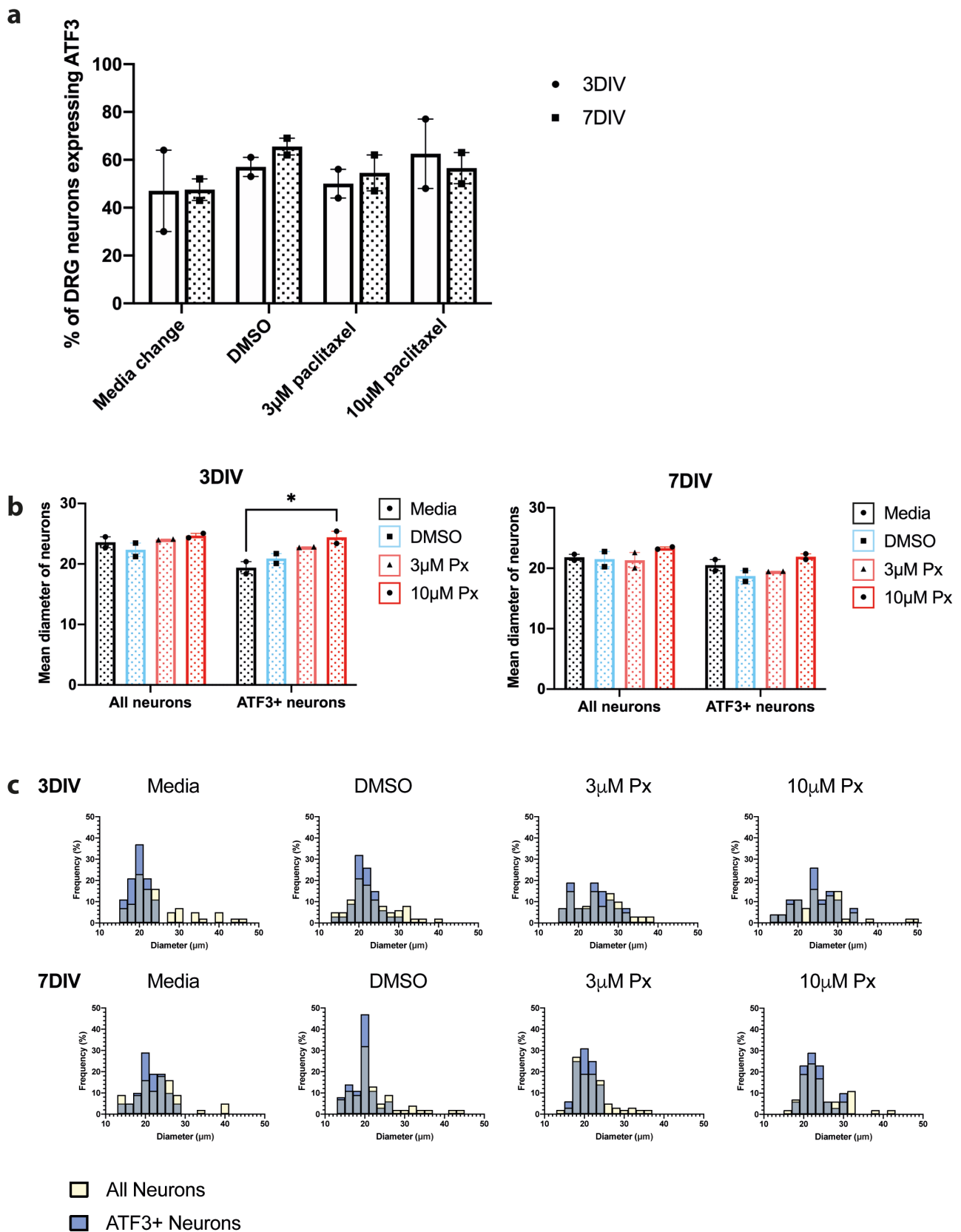


**Figure 3.4. Proportion and size distribution of dorsal root ganglion (DRG) neurons expressing the neuronal damage marker Activating Transcription Factor 3 (ATF3) after in vitro paclitaxel exposure.** **a**) Percentage of neurons at 3 or 7 days in vitro (DIV) expressing ATF3 after exposure to paclitaxel, DMSO, or a media change control for 24 hours. Data points plotted are the percentage of  $\beta$ -III-tubulin-visualised DRG neurons that express ATF3 per image analysed. No significance of ordinary one-way ANOVA of ATF3 positive percentage at either timepoint. **b**) Diameter of all

neurons in the culture and neurons that express ATF3 after paclitaxel or control treatment at 3 or 7DIV. Data points plotted are the mean diameter of  $\beta$ -III-tubulin-visualised DRG neurons per image analysed. Data presented as mean  $\pm$  SEM. Two-way ANOVA of 3DIV, effect of ATF3 expression  $P=0.0113$ , effect of paclitaxel treatment  $P=0.0113$ , no significant effect of interaction. Followed by Šídák's multiple comparisons test, ATF3+ media vs ATF3 10 $\mu$ M paclitaxel,  $P=0.0488$ . Two-way ANOVA of 7DIV, effect of ATF3 expression  $P=0.0129$ , no significant effect of paclitaxel treatment, no significant effect of interaction. Followed by Šídák's multiple comparisons test, no significance. **c)** Size frequency distribution of all  $\beta$ -III-tubulin-visualised DRG neurons in the culture (yellow) compared to those that also express ATF3 (blue). Diameter histograms are shown as a percentage of neurons analysed per condition, with a bin width of 2 $\mu$ m. For all figure data,  $N=1$  culture, 2 images per condition.  $n=44-66$  neurons analysed per condition. All grouped data presented as mean  $\pm$  SEM. \*  $P<0.05$ . Images analysed by project student Jemimah Suratos.

### 3.3.2 Paclitaxel induces the retraction of neurites in dorsal root ganglion cultures

There are multiple publications indicating that the application of paclitaxel and other CIPN-inducing chemotherapy drugs inhibits outgrowth and induces retraction of neurites from DRG cultures and neuronal cell lines (Yang et al., 2009; James et al., 2008). Incucyte Neurotrack live cell imaging was used to track the area of the culture covered by cell bodies and the length of neurites in the culture over time in the presence of different concentrations of paclitaxel to confirm this finding (Figure 3.5a). There was no change in the cell body area with increasing paclitaxel concentrations (Figure 3.5b). This supports the conclusion from the previous section that these concentrations of paclitaxel do not directly induce neuronal death or detachment. Neurite length present in the culture decreased over time in a concentration dependent manner, becoming significantly different from DMSO at 300nM, demonstrating neurite degeneration at these concentrations and timeframes (Figure 3.5c).

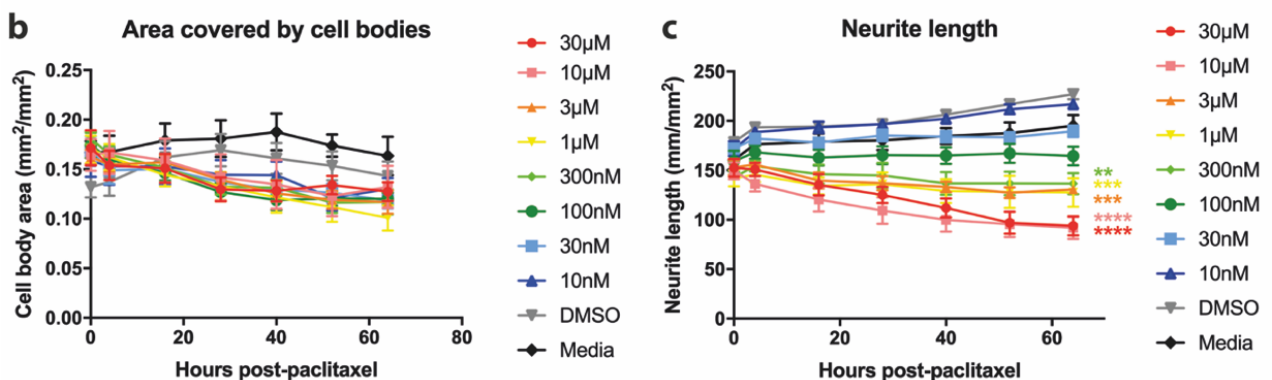
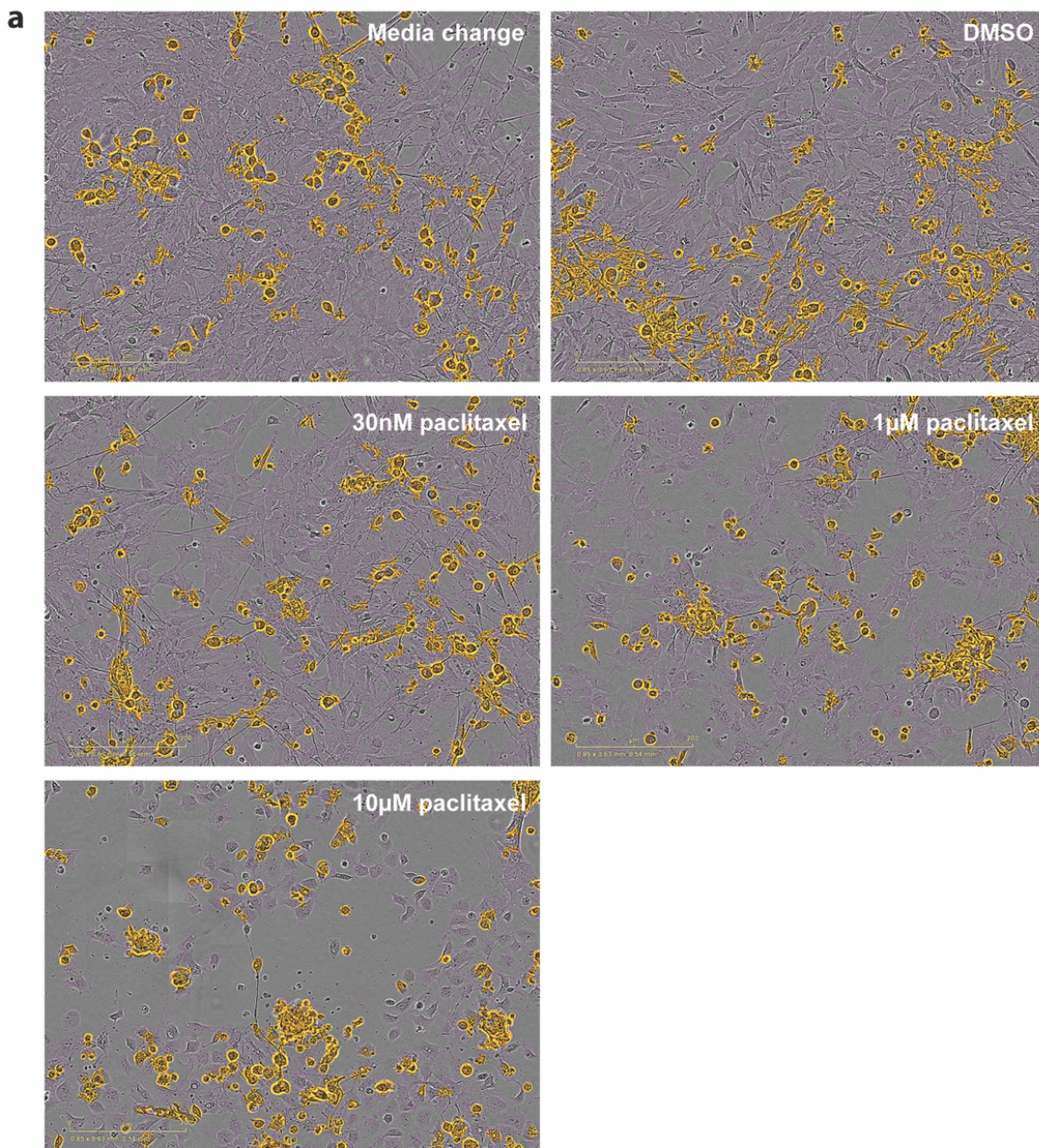


**Figure 3.5. Incucyte Neurotrack imaging of dorsal root ganglion (DRG) cultures exposed to paclitaxel in vitro. a)** Representative images of DRG neurons after 64 hours of exposure to different concentrations of paclitaxel, or an equivalent concentration of DMSO. The yellow mask is cell bodies, the purple mask is neurite processes. **b)** The area of the image covered by neuronal cell bodies over time is not affected by different paclitaxel concentrations. No significance of ordinary one-way ANOVA. **c)** The total length of neurites in the image decreases over time as concentration

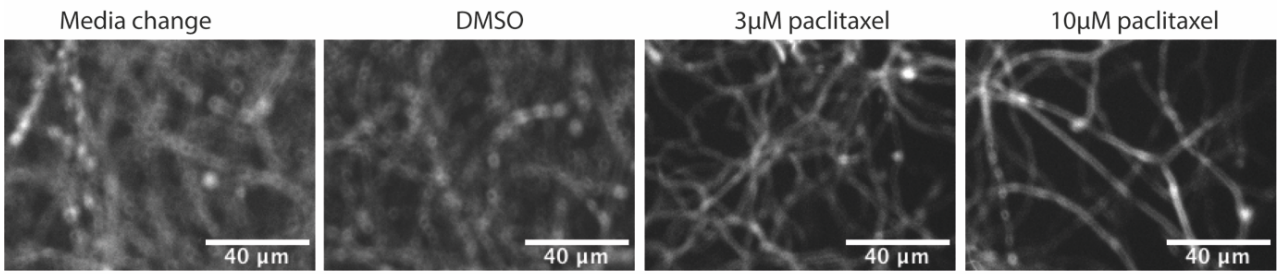
of paclitaxel increases. Ordinary one-way ANOVA  $P < 0.0001$ . Followed by Dunnett's multiple comparisons test, comparing each concentration to the DMSO control.  $30\mu\text{M}$   $P < 0.0001$ ,  $10\mu\text{M}$   $P < 0.0001$ ,  $3\mu\text{M}$   $P = 0.0002$ ,  $1\mu\text{M}$   $P < 0.0002$ ,  $0.3\mu\text{M}$   $P < 0.0016$ . For all figure data,  $N = 1$  culture, 6 images per condition. All grouped data presented as mean  $\pm$  SEM. \*\*\*\* $P < 0.0001$  \*\*\*  $P < 0.001$  \*\*  $P < 0.01$ .

As Incucyte imaging relies on brightfield images, the processes of supporting cells and glia may inaccurately be included in the neurite mask. Immunocytochemistry of  $\beta$ -III-tubulin was therefore also used to quantify the area covered by neurites in DRG cultures treated with paclitaxel for 24 hours at 3 and 7 DIV, as this isoform of  $\beta$ -tubulin is considered to be expressed by neurons only (Figure 3.6a) (Moskowitz et al., 1993). At both timepoints the paclitaxel-treated cultures had significantly reduced coverage of  $\beta$ -III-tubulin-marked neuronal processes, though only one culture was performed, so further biological replicates would be required to confirm this finding (Figure 3.6b).  $3\mu\text{M}$  and  $10\mu\text{M}$  concentrations of paclitaxel caused the same degree of neurite loss.

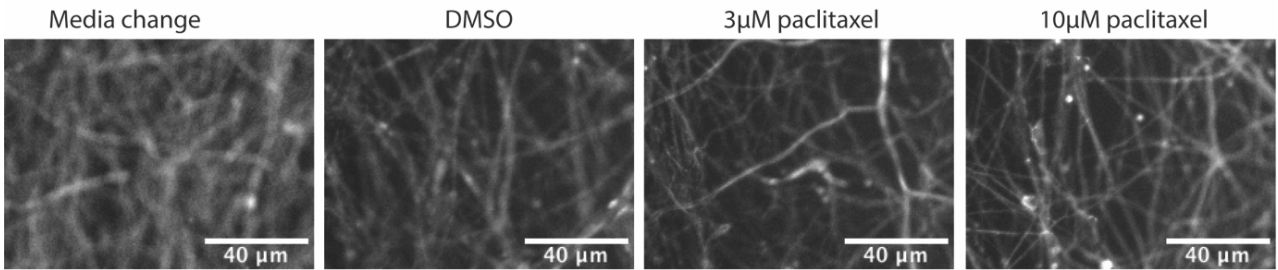
These data confirm previously published work showing that a key feature of *in vitro* paclitaxel is the degeneration of neurites from DRG neurons, and that this can be replicated using the concentrations and conditions of these experiments. These conditions will therefore be used for further functional experiments.

**a**

**3DIV**



**7DIV**



**b**

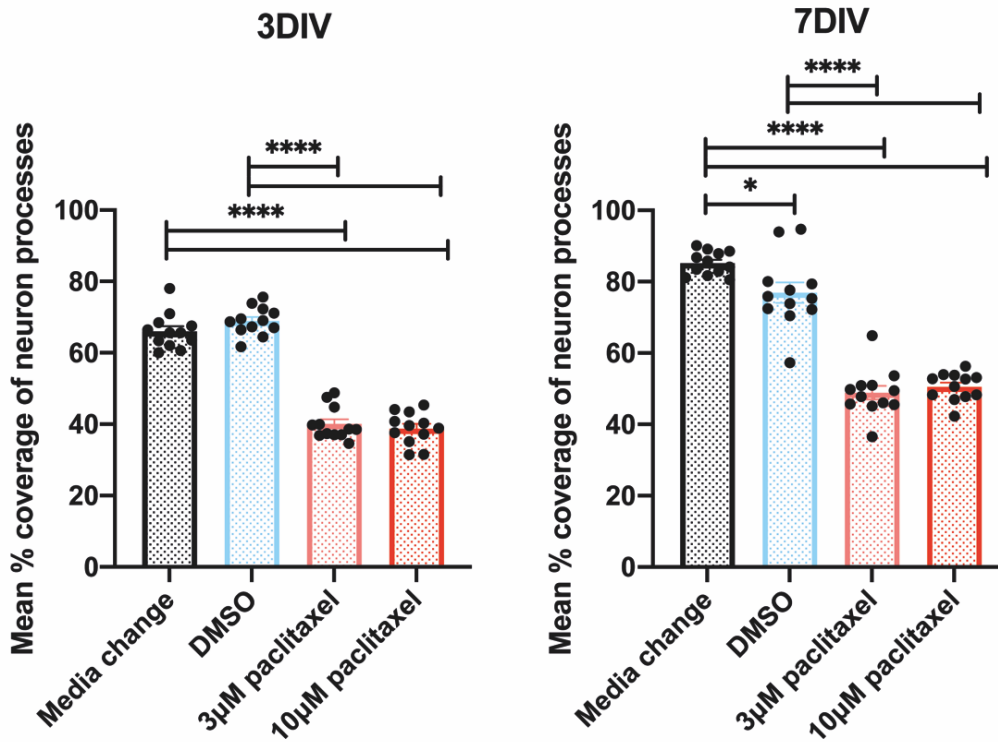


**Figure 3.6. Neuronal processes of dorsal root ganglion neurons marked with  $\beta$ -III-tubulin following exposure to paclitaxel in vitro. a)** Representative images analysed for area coverage of neuronal processes following 24 hours of exposure to paclitaxel, DMSO or a control media change. An area of set dimension was placed on each  $\beta$ -III-tubulin image, avoiding any cell bodies. This was then thresholded and the area masked by  $\beta$ -III-tubulin immunofluorescence was measured. **b)** The area covered by neuronal processes was measured at 3 or 7 days in vitro (DIV). Ordinary one-way ANOVA of 3DIV,  $P < 0.0001$ . Followed by Tukey's multiple comparisons test, Media vs 3µM,  $P < 0.0001$ , Media vs 10µM,  $P < 0.0001$ , DMSO vs 3µM,  $P < 0.0001$ , DMSO vs 10µM,  $P < 0.0001$ .

Ordinary one-way ANOVA of 7DIV,  $P < 0.0001$ . Followed by Tukey's multiple comparisons test, Media vs DMSO,  $P = 0.0177$ , Media vs  $3\mu\text{M}$ ,  $P < 0.0001$ , Media vs  $10\mu\text{M}$ ,  $P < 0.0001$ , DMSO vs  $3\mu\text{M}$ ,  $P < 0.0001$ , DMSO vs  $10\mu\text{M}$ ,  $P < 0.0001$ . For all figure data,  $N = 1$  culture, 2 wells per condition, 6 images per well. Data presented as mean  $\pm$  SEM. \*\*\*\* $P < 0.0001$  \*  $P < 0.05$ .

### 3.3.3 Paclitaxel exposure has no effect on whole population calcium responses to certain nociceptive agonists

So far in these experiments, no functional changes to DRG exposed to paclitaxel in terms of their signalling and ion channel expression have been assessed. This is vital to understanding CIPN in terms of pain signalling. In order to attempt this, calcium imaging was used to assess electrical activity and ion channel activation to a certain degree. Hypothetically, calcium imaging would be able to detect changes such as: (1) Increased expression of a chemosensitive ion channel, (2) expression of a chemosensitive ion channel in a wider population of neurons than in naïve conditions, (3) Increased sensitivity of a chemosensitive ion channel, (4) increased action potential firing in response to depolarisation.

Initially, FLIPR calcium imaging was used to investigate DRG cultures exposed to paclitaxel at 6 DIV. FLIPR records the fluorescence of neurons loaded with the calcium indicator Calcium 6. The fluorescence change in response to a chemical stimulus is recorded from over the whole well, and therefore provides an average response representing the whole heterogeneous population of DRG neurons. Potassium chloride was used to depolarise the neurons. Veratridine, a compound that holds VGSCs in their open state, cinnamaldehyde, a TRPA1 agonist, and capsaicin, a TRPV1 agonist were used to activate subpopulations of chemosensitive sensory neurons. Surprisingly, 24 hours of treatment with  $10\mu\text{M}$  paclitaxel in the media had no significant effect on the peak calcium response amplitude to any of these stimuli considering that both NaV1.7 and TRPV1 activity is reported to be enhanced in CIPN (Figure 3.7a). This may again be a feature of already damaged, cultured DRG neurons, due to the lack of an intact sensory system featuring both peripheral and central sensitisation, or that the mechanism of paclitaxel-induced CIPN cannot be replicated by *in vitro* exposure.

In order to investigate whether *in vivo* paclitaxel exposure is required to observe effects, DRG were then cultured from rats that had been given *in vivo* paclitaxel injections. Behavioural studies confirm that the injection protocol used establishes a pain phenotype at the time of sacrifice

(Section 6.3.4). The cultures were analysed with FLIPR the day after dissociation. However, *in vivo* paclitaxel exposure also had no effect on the peak calcium response to these stimuli (Figure 3.7b).

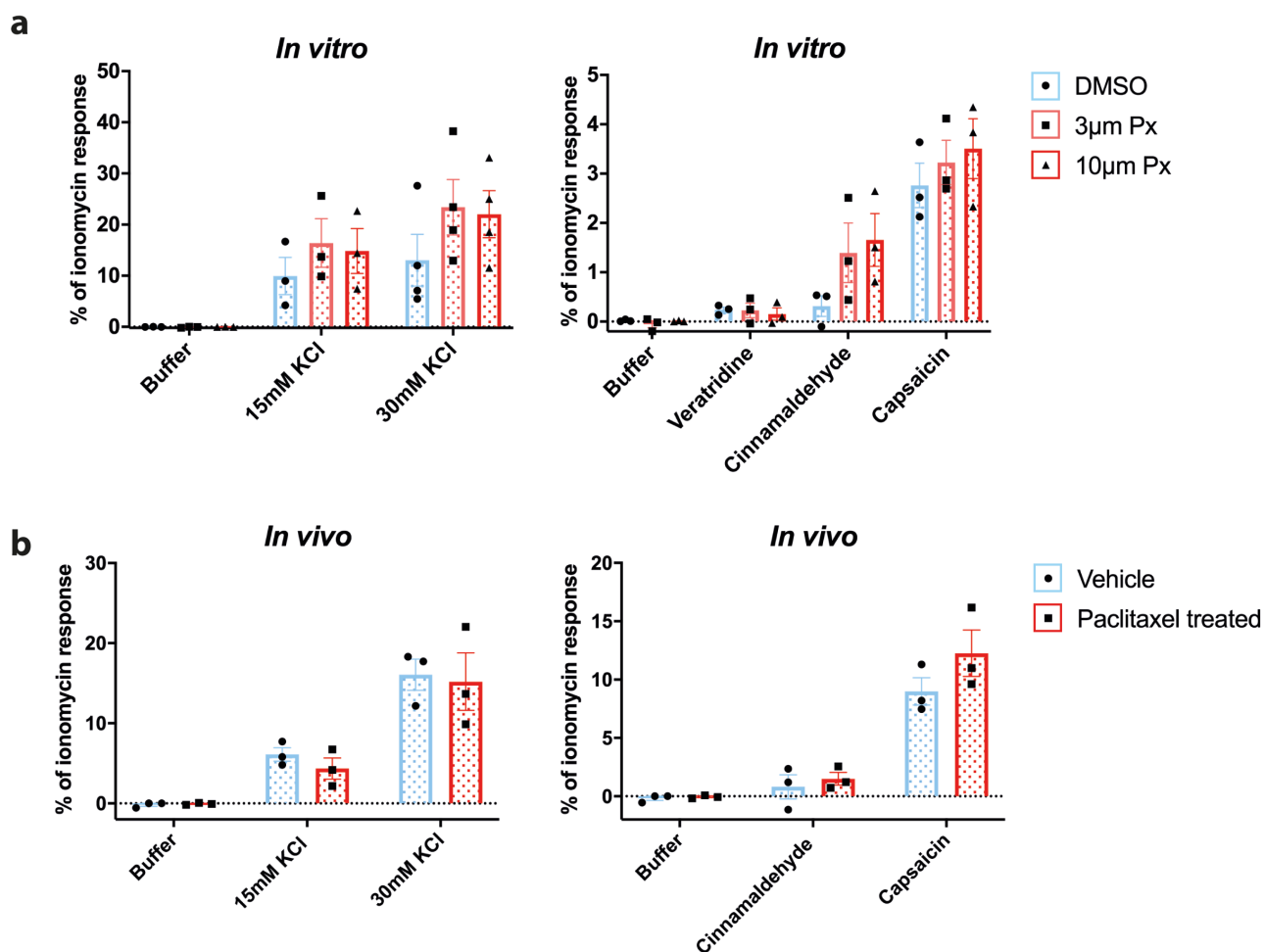


**Figure 3.7. FLIPR calcium imaging of dorsal root ganglion (DRG) neurons exposed to paclitaxel *in vitro* or *in vivo*.** **a)** DRG cultures from naïve rats were exposed to paclitaxel (Px) or DMSO for 24 hours at 6 days *in vitro* then stimulated with potassium chloride (KCl), 10µM veratridine, 100µM cinnamaldehyde or 30nM capsaicin. The increase in intracellular calcium concentration over the whole population of neurons was recorded during the stimulation, and the amplitude of the response normalised to a subsequent ionomycin response was calculated. No significance of ordinary one-way ANOVA. **b)** Rats were given 4 injections of paclitaxel or the equivalent vehicle on alternate days then sacrificed for DRG culture 7 days later. The following day the neurons were stimulated with various compounds and the amplitude of calcium signal was recorded. No significance of ordinary one-way ANOVA. For all figure data, N=3-4 cultures, 4 wells stimulated with each compound per condition per culture. Data presented as mean ± SEM.

From these experiments it could be concluded that paclitaxel has no effect on these particular chemosensitive subpopulations of sensory neurons, or that axotomy and dissociation masks any pertinent changes. Capsaicin responses after paclitaxel exposure have often been shown to be potentiated in the literature, and one publication has observed this using calcium imaging (Li et al., 2015). It was therefore disappointing that no effect was detected for capsaicin in these

experiments. As FLIPR doesn't record the calcium responses from individual cells, it may also be the case that two opposing effects are cancelling out, or that any change to a subset of neurons is masked by a lack of response from the rest of the neurons in the well. It was therefore decided to pursue single-cell calcium imaging to investigate this further.

### *3.3.4 Veratridine responses are not a valid assay of nociceptive populations in rat dorsal root ganglion cultures*

In order to subsequently assess the functional effect of paclitaxel on nociceptors in culture on an individual cell level, the veratridine nociceptor screening assay described in Mohammed et al., 2017 was replicated in rat DRG.

Before applying this assay to paclitaxel-induced changes, naïve rat DRG cultures were first used as a comparison to the published mouse response profiles. DRG neurons were imaged at 2 and 3 DIV, the same as was used in the published experiments. As expected, a proportion of the rat DRG neurons responded to veratridine, and these responses all fell into one of the four distinct profiles (Figure 3.8b). However, when compared to the published mouse data, significantly fewer rat neurons respond to 30 $\mu$ M veratridine, with only 27% of DRG neurons responding compared to 77% in mouse (Figure 3.8c). The distribution of the response profiles also differed slightly, with the SD profile being the most prevalent in rat DRG, but the OS profile was the most common in mouse (Figure 3.8d). Crucially, in mouse DRG stimulated with veratridine the OS profile is found more often in neurons responding to at least one of the subsequent nociceptive agonists, and the SD, ID and RD profiles found less often (Figure 3.8e). This suggests that distinct profiles are characteristic of nociceptive and non-nociceptive populations in mouse. However, when repeated with rat DRG no such associations were present, with nociceptors and non-nociceptors falling into each of the four veratridine response categories with equal probability (Figure 3.8f).



oscillatory (OS) was not significantly different between rat and mouse. Ordinary one-way ANOVA  $P < 0.0001$ . Followed by Šidák's multiple comparisons test, SD rat vs mouse,  $P = 0.0132$ .  $N = 8$  cultures,  $n = 494$  neurons for mouse,  $N = 3$  cultures,  $n = 78$  neurons for rat. **e)** The OS profile is enriched and the SD profile diminished in putative nociceptors that respond to at least one of the agonists capsaicin, cinnamaldehyde or  $\alpha$ - $\beta$ -methylene-ATP in mouse DRG cultures. Ordinary one-way ANOVA followed by Šidák's multiple comparisons test.  $N = 7$  cultures,  $n = 671$  neurons. **f)** No particular veratridine response profiles were enriched or diminished in putative nociceptors in rat DRG cultures. No significance of ordinary one-way ANOVA.  $N = 3$  cultures,  $n = 279$  neurons. All mouse data reproduced from Mohammed et al., 2017. All data presented as mean  $\pm$  SEM. \*\*\*\* $P < 0.0001$  \*  $P < 0.05$ .

From this it can be determined that in rat DRG neurons using this particular culture protocol and timeframe, the veratridine response assay is not a useful output for nociceptor activity. Whether this is due to a difference in dissociation procedure, or whether there is a fundamental difference in physiology between rat and mouse DRG is responsible for this is not known. Considering that there was no association with veratridine response and nociceptor/non-nociceptor activity, it is therefore possibly not surprising that *in vitro* paclitaxel exposure had no effect on the distribution of veratridine responses, at 2/3 or 7 DIV (Appendix Figure 0.1).

### 3.3.5 Paclitaxel increases the amplitude of calcium response to capsaicin, but not other nociceptive agonists

Although the veratridine response assay itself did not provide a convenient method for assaying the activity of DRG subtypes from rat, the experimental paradigm is still useful as the responses to each of the three nociceptive agonists ( $\alpha$ - $\beta$ -methylene-ATP, cinnamaldehyde and capsaicin) can be individually analysed. The proportion of neurons responding to each of these agonists was analysed after paclitaxel exposure, compared to untreated controls. There was no change in the proportion of putative nociceptors (responding to any of the agonists) in cultures at 2/3 or 7 DIV in response to paclitaxel, nor a change in the proportion of neurons responding to each agonist individually (Figure 3.9a/b).

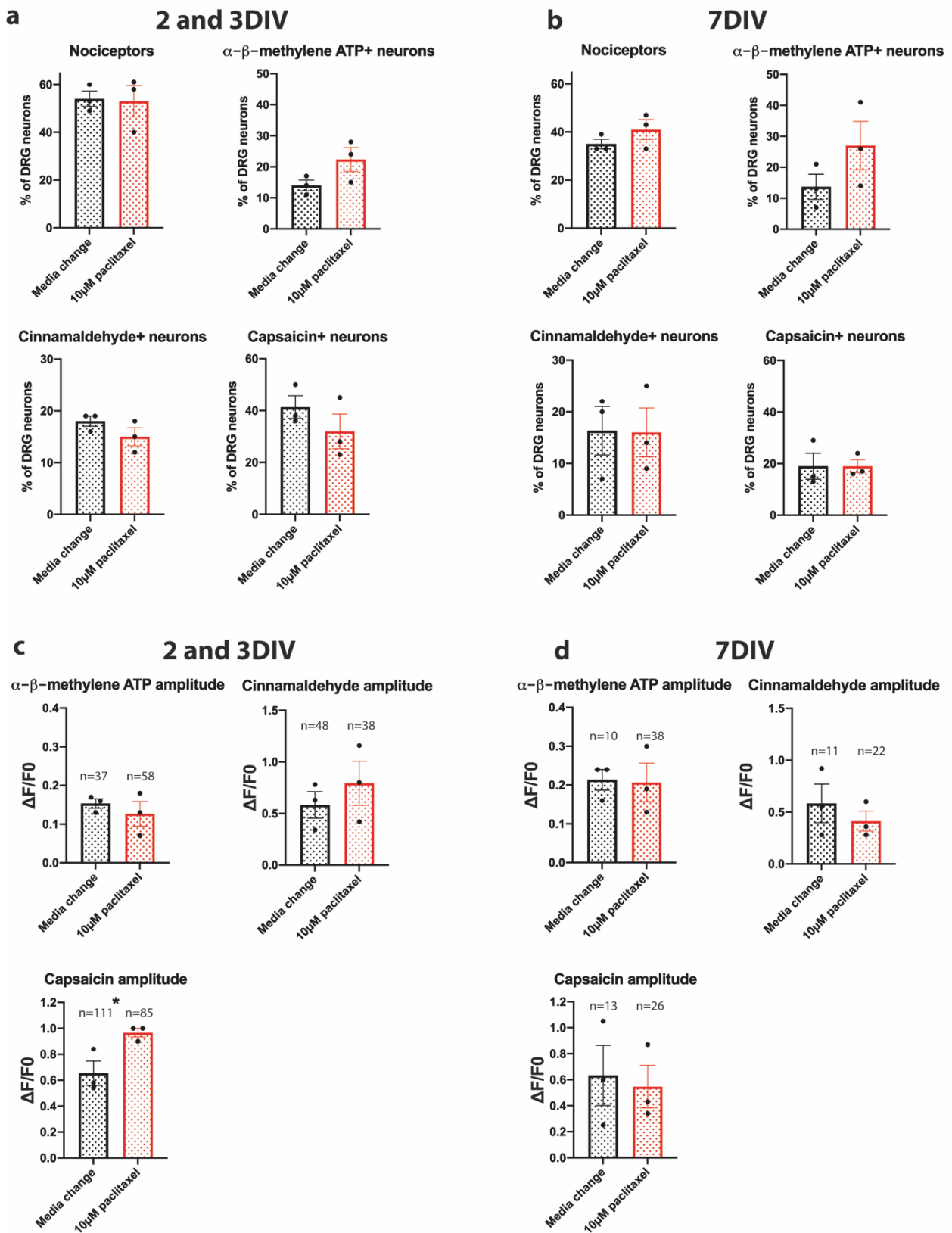


**Figure 3.9. Effect of in vitro paclitaxel exposure on the proportion of rat dorsal root ganglion (DRG) neurons responding to nociceptive agonists and the amplitude of responses. a)** The percentage of DRG neurons responding to the common nociceptive agonists  $\alpha$ - $\beta$ -methylene-ATP, cinnamaldehyde and capsaicin was recorded at 2 and 3 days in vitro (DIV). DRG neurons responding to any of these agonists are considered putative nociceptors. Paclitaxel exposure had no effect on the number of neurons responding to any of these agonists. No significance of two tailed unpaired t test. N=3 cultures, n=279 media change neurons, n=266 paclitaxel treated

neurons. **b)** There was also no effect of the percentage of neurons responding to each agonist at 7DIV. No significance of two tailed unpaired *t* test. *N*=3 cultures, *n*=70 media change neurons, *n*=136 paclitaxel treated neurons. **c)** The peak amplitude of calcium response to each agonist ( $\Delta F/F_0$ ) was measured. At 2 and 3 DIV there was no significant change in the amplitude of calcium responses to  $\alpha$ - $\beta$ -methylene-ATP or cinnamaldehyde after paclitaxel exposure. No significance of two-tailed unpaired *t* test. The amplitude of capsaicin calcium responses was significantly increased following paclitaxel exposure. *P*=0.0348. *N*=3 cultures. **d)** However, at 7DIV there was no difference in calcium response amplitude to any of the three agonists used. No significance of two-tailed unpaired *t* test. *N*=3 cultures. All data presented as mean  $\pm$  SEM. \* *P*<0.05.

The peak amplitude of the calcium response to each agonist was also analysed between paclitaxel and control conditions. There was no significant difference in response for any of the agonists at 7 DIV (Figure 3.9d). At 2/3 DIV the amplitude of responses to  $\alpha$ - $\beta$ -methylene-ATP and cinnamaldehyde also showed no change due to paclitaxel exposure. However, the peak amplitude due to capsaicin stimulation was significantly larger in the paclitaxel-treated cultures than the untreated cultures (Figure 3.9c).

Increased calcium amplitudes in response to capsaicin is consistent with previous publications reporting evidence for changes in the expression and function of the TRPV1 channel following paclitaxel exposure (Section 1.3.2.3). Monitoring changes in capsaicin responses and/or TRPV1 expression could therefore provide a convenient *in vitro* assay for monitoring CIPN, and subsequent experiments in this chapter will investigate this further.

### *3.3.6 Capsaicin-induced release of calcitonin gene-related peptide from DRG cultures is potentiated by in vitro paclitaxel exposure*

In order to probe the effect of paclitaxel on the exocytosis of a nociceptive neuropeptide, the release of CGRP from DRG cultures was assayed using an ELISA. DRG neurons were taken from naïve rats and cultured for 6 days before 24 hours of *in vitro* paclitaxel treatment. The neurons were then stimulated for 10 minutes with veratridine, cinnamaldehyde or capsaicin, the supernatant taken and the CGRP concentration analysed. Veratridine did not induce release of CGRP over basal levels (Figure 3.10a). Cinnamaldehyde induced CGRP release over basal levels but paclitaxel had no effect on the degree of release. Capsaicin did not significantly increase CGRP release over basal levels in the DMSO treated controls. CGRP release was only successfully induced by capsaicin stimulation after exposure to paclitaxel. In order to account for intra-culture

variability, CGRP release in paclitaxel-treated conditions was then normalised to DMSO control conditions for each culture (Figure 3.10b). Capsaicin-induced CGRP release was significantly potentiated in both the 3 $\mu$ M and 10 $\mu$ M paclitaxel-treated cultures.

From these results it appears that there is a subtle potentiation of capsaicin-induced CGRP release by paclitaxel. Taken together with increased capsaicin amplitudes detected by single-cell calcium imaging, these experiments suggest that *in vitro* paclitaxel may potentiate TRPV1-mediated responses in cultured DRG neurons. The function and expression of TRPV1 has previously been implicated in animal models of CIPN *in vivo*, so may be a key factor in the development of CIPN. One finding from animal models is that levels of TRPV1 in the DRG are increased by paclitaxel treatment (Li et al., 2015; Hara et al., 2013). An upregulation of TRPV1 at the membrane of paclitaxel-exposed DRG neurons is one possible explanation for the potentiated capsaicin responses observed in this chapter on cultures at 2/3 DIV.

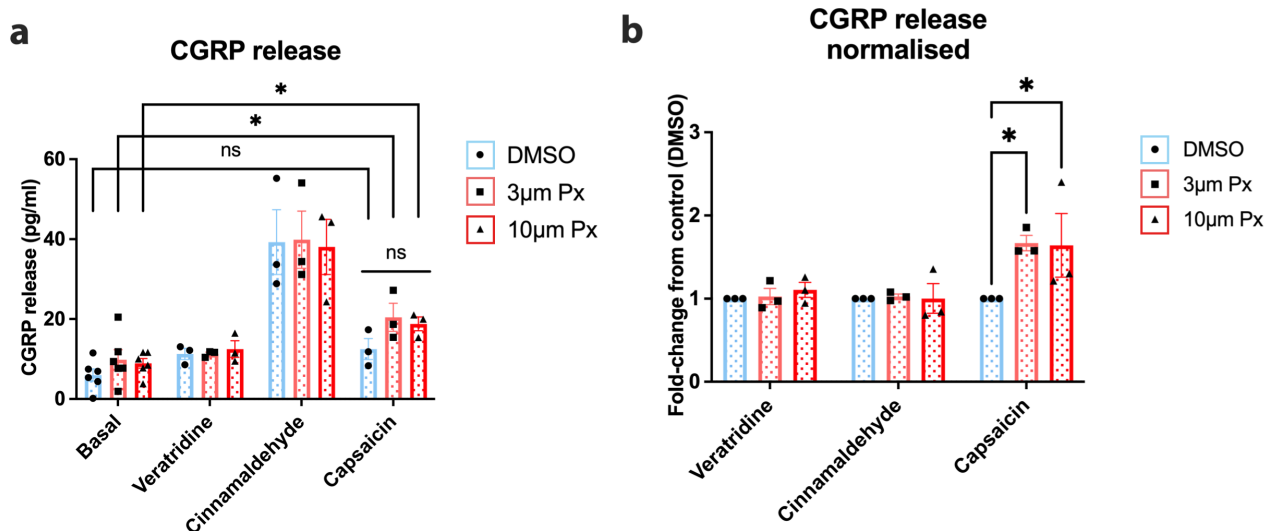


**Figure 3.10. The effect of paclitaxel on the release of calcitonin gene-related peptide.** Dorsal root ganglion (DRG) cultures were prepared from naïve rats and treated *in vitro* with paclitaxel (Px) or DMSO at 6 days *in vitro* for 24 hours. The release of CGRP to a 10 minute stimulation with 30nM capsaicin, 100 $\mu$ M cinnamaldehyde or 10 $\mu$ M veratridine was then quantified with an enzyme-linked immunoassay (ELISA). There was no significant difference between control and paclitaxel-treated conditions for each stimulus. Two-way ANOVA of paclitaxel concentration and stimulus, followed by Tukey's multiple comparisons test. DMSO basal release is not significantly different from DMSO capsaicin stimulated release. 3 $\mu$ M and 10 $\mu$ M paclitaxel basal release are significantly different from the equivalent paclitaxel concentration capsaicin stimulated release. Two tailed paired t test, 3 $\mu$ M  $P=0.0415$ , 10 $\mu$ M  $P=0.0462$ . **b**) CGRP release was then normalised to the control DMSO condition. Capsaicin release was significantly increased in paclitaxel-treated conditions. Two-way ANOVA of paclitaxel concentration and stimulus, followed by Tukey's multiple comparisons test. Capsaicin concentration DMSO vs 3 $\mu$ M  $P=0.015$ , DMSO vs 10 $\mu$ M  $P=0.0202$ .  $N=6$  cultures for basal release,  $N=3$  cultures for stimulated release, 4 wells stimulated with each compound per condition per culture. Data presented as mean  $\pm$  SEM. \*  $P<0.05$ .

### 3.3.7 *The density of TRPV1 at the membrane of dorsal root ganglion neurons is not affected by in vitro paclitaxel exposure*

As both the calcium response amplitude to capsaicin and capsaicin-stimulated CGRP release were potentiated after *in vitro* paclitaxel treatment, experiments were performed which sought to determine whether this was due to an increased density of TRPV1 receptor at the membrane. In an attempt to quantify the levels of TRPV1 inserted in the cell membrane, paclitaxel-treated or control neurons were labelled live with an extracellular epitope-recognising TRPV1 antibody before being fixed and imaged with a confocal microscope. The extracellular-epitope labelling property of this antibody theoretically gives it the ability to only label the TRPV1 receptors inserted into the membrane when used on live, non-permeabilised cells.

In order to validate the antibody, the blocking peptide provided and secondary-only controls were used. TRPV1 immunoreactivity was seen as a ring of fluorescence at the somatic membrane of a subpopulation of smaller-diameter neurons (Figure 3.11a). When the primary antibody was applied alongside an excess of blocking peptide provided by the manufacturer, this immunoreactivity disappeared (Figure 3.11b). There was also no reactivity when the primary antibody was omitted (Figure 3.11c).

High concentrations of capsaicin have been shown to induce TRPV1 internalisation in DRG neurons. In an attempt to demonstrate that this live immunolabelling approach is able to detect a functional TRPV1 downregulation, capsaicin was applied to the neurons prior to live staining and fixation in an attempt to induce internalisation of the receptor. Either 1 $\mu$ M or 10 $\mu$ M of capsaicin in a calcium containing buffer was applied to the neurons for 1 minute. It has been published that this is sufficient to induce the internalisation of a TRPV1-pHluorin from the membrane via a capsaicin desensitisation mechanism (Tian et al., 2019). 10 $\mu$ M was reported to reduce the channel fluorescence intensity to approximately 40% of baseline at 5 minutes. In these experiments, DRG neurons at 3 and 7 DIV were imaged. The mean fluorescence intensity of a 2 $\mu$ m diameter ringed ROI around the membrane was analysed after exposure of the DRG to capsaicin at the concentrations and timeframes detailed in Tian et al. (2019). There was no significant decrease in the TRPV1 membrane intensity in capsaicin-exposed, DMSO or buffer only controls (Figure 3.11d).

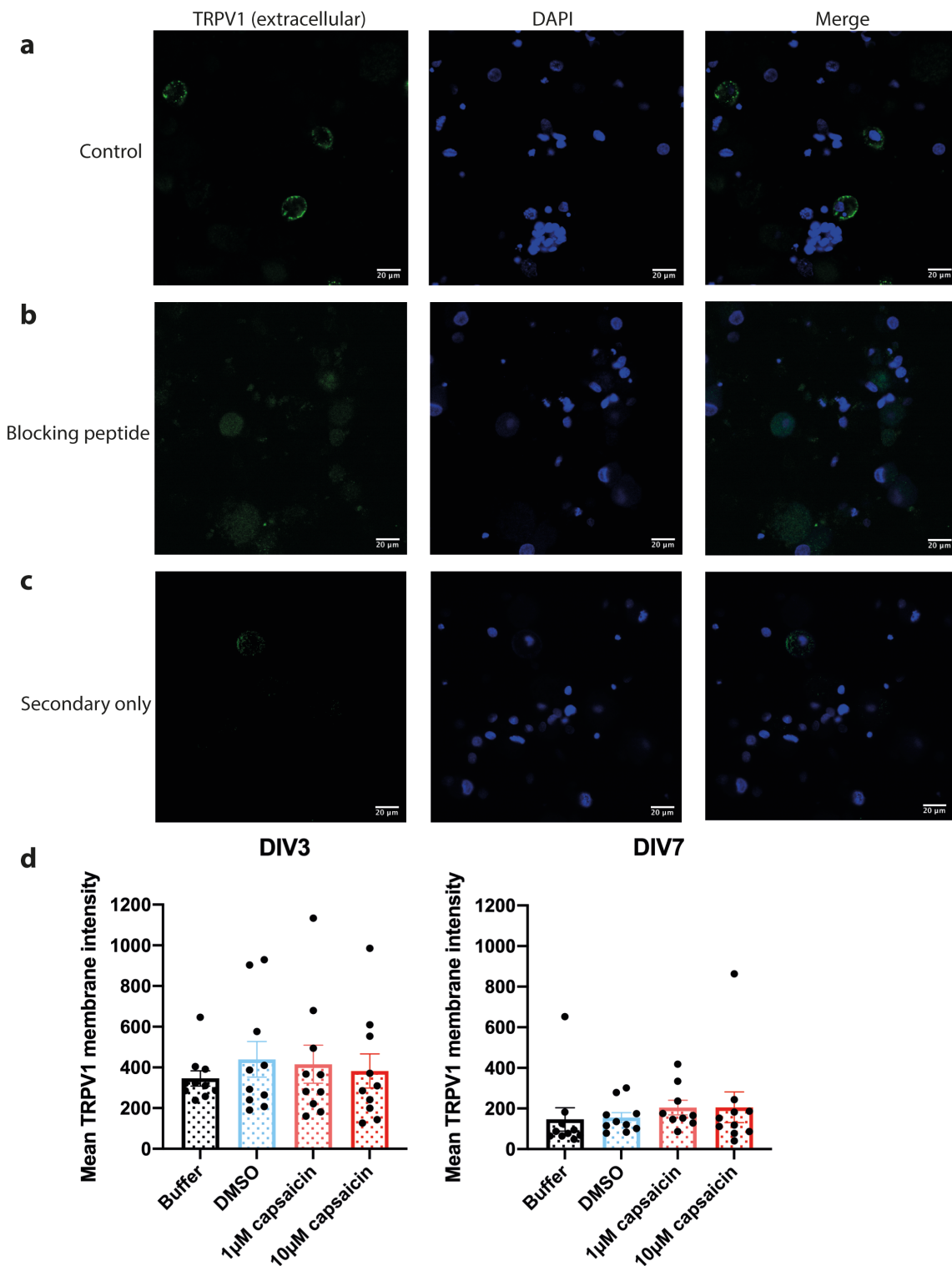


**Figure 3.11. Validation of TRPV1 extracellular antibody and effect of capsaicin-induced TRPV1 internalisation.** **a**) Extracellular TRPV1 antibody staining of dorsal root ganglion (DRG) neuron cultures in control conditions. **b**) Extracellular TRPV1 incubated with a 10x excess of blocking peptide prevented immunolabelling of TRPV1 positive cells. **c**) Incubation without the primary TRPV1 antibody also prevented immunolabelling. **d**) DRG neurons were stimulated with either 1µM or 10µM capsaicin for 1 minute prior to live immunolabelling and fixation in an attempt to induce TRPV1 internalisation. The control conditions were a 1 minute addition of the relevant buffer only or an equivalent concentration of DMSO in buffer. These experiments were performed on DRG cultures at 3 or 7 days in vitro (DIV). N=1 culture per timepoint, n=10 neurons per condition. Data presented as mean ± SEM. No significance of ordinary one-way ANOVA.

Although capsaicin-induced TRPV1 internalisation couldn't be distinguished with antibody fluorescence, this may have been due to the capsaicin internalisation protocol rather than the immunolabelling approach itself. The protocol used was shown to induce internalisation of an overexpressed, modified TRPV1 channel, so internalisation of the endogenously expressed receptor may not behave the same way. Whether an upregulation of the density of membrane-inserted TRPV1 could be observed following *in vitro* paclitaxel exposure was subsequently still investigated.

The mean membrane intensity of TRPV1 positive DRG neurons was analysed after 24 hours of paclitaxel or control treatment (Figure 3.12a). There was no significant difference in extracellular TRPV1 immunoreactivity between any conditions, although a slight trend may be present (Figure 3.12b).

From this it could be concluded that either there is no upregulation of TRPV1 at the membrane following paclitaxel exposure, and any increase in capsaicin responses may be due to sensitisation or reduced desensitisation. It may be the case that this antibody-based approach is not sensitive enough to detect any changes in membrane expression that have occurred. The potentiation of capsaicin calcium amplitudes was from a  $\Delta F/F_0$  of 0.65 to 0.96 after paclitaxel, and capsaicin-induced CGRP release was increased to 165% of the control condition. It may be that this fluorescence imaging approach is not sensitive enough to pick up this degree of TRPV1 upregulation if this is indeed the mechanism of potentiation. A more functional, calcium imaging-based approach was therefore used to further clarify whether TRPV1 membrane expression is increased by paclitaxel exposure.

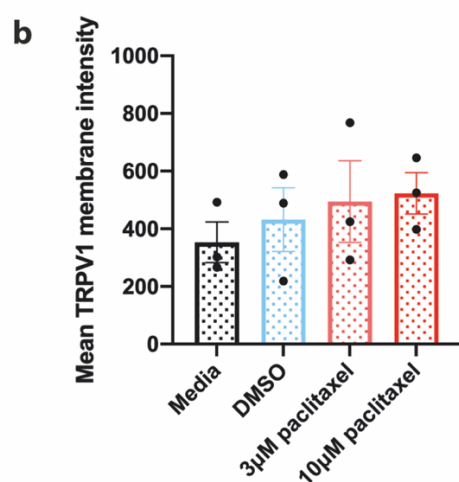
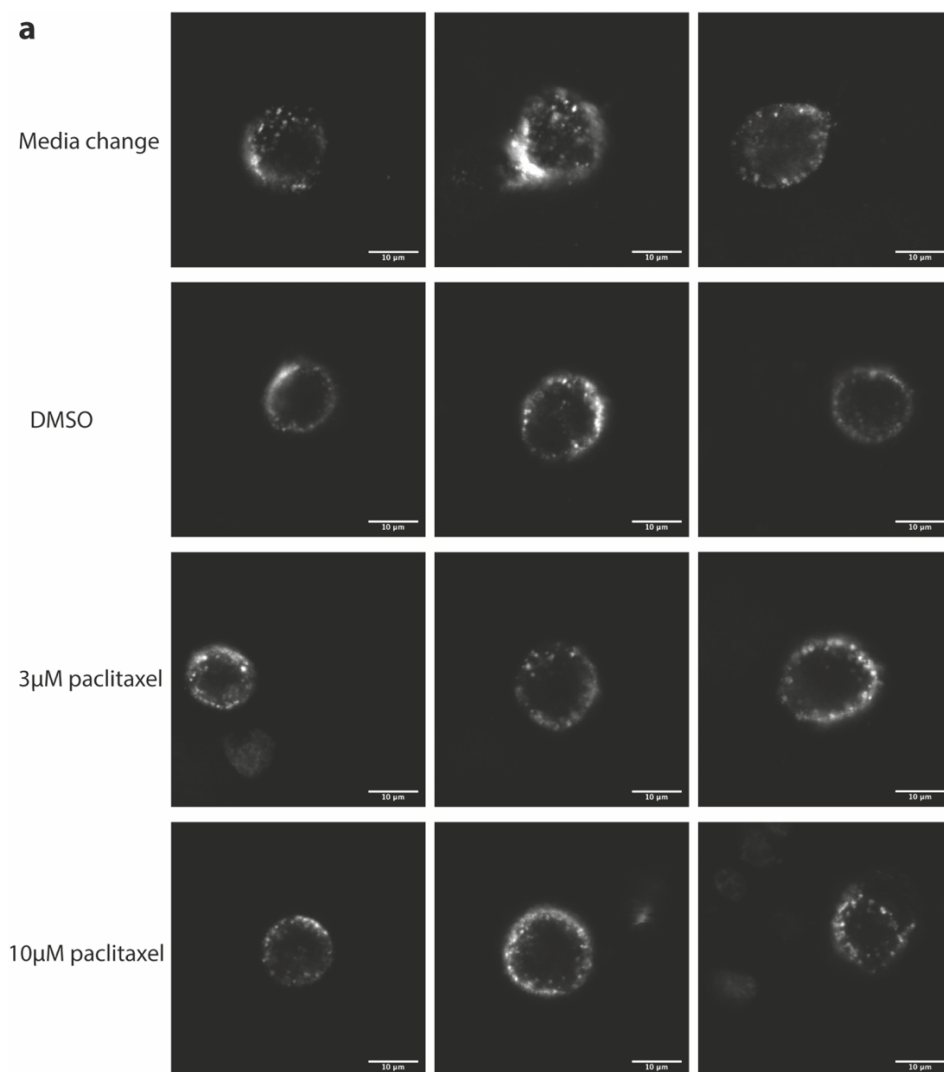


**Figure 3.12. Effect of *in vitro* paclitaxel exposure on extracellular TRPV1 membrane intensity immunolabelling of dorsal root ganglion (DRG) cultures. a)** Representative images of TRPV1 positive DRG neurons analysed. Neurons were imaged at 3 days *in vitro* (DIV). **b)** Mean TRPV1 fluorescence intensity of the membrane was analysed for each neuron imaged. N=3 cultures, n=20 neurons per condition per culture. Data presented as mean  $\pm$  SEM. No significance of ordinary one-way ANOVA.

### *3.3.8 Cadmium block of voltage-gated calcium channels alters the time-course of capsaicin responses but has no effect on the amplitude in the presence or absence of paclitaxel*

In another attempt to quantify the activity of TRPV1 at the membrane of DRG neurons following paclitaxel exposure, cadmium chloride was used to block VGCCs while repeating the calcium imaging experiment from section 3.3.5.

100µM cadmium has been used as a VGCC blocker, including in DRG neurons, for decades (Gross & Macdonald, 1987). As TRPV1 channels are non-selective cation channels, when they are activated by capsaicin, calcium flows in through the TRPV1 channels themselves. However, calcium influx can also occur through VGCCs as a result of the subsequent depolarisation caused by TRPV1 activation. In order to separate out the effect of capsaicin to that through TRPV1 channels only, VGCC blockade would be used to limit calcium influx after capsaicin application to the calcium that is directly through the TRPV1 channel, rather than as a result of depolarisation and action potential firing. To test successful VGCC blockade in these experiments, the effect of cadmium on potassium chloride evoked depolarisation responses was investigated. The presence of cadmium drastically reduced the amplitude of calcium responses to potassium chloride, providing evidence that 100µM cadmium chloride is sufficient to block calcium influx through VGCCs (Figure 3.13a).

Interestingly, there was no significant effect on capsaicin response amplitude between cadmium and cadmium-free solutions, suggesting that the vast majority of the calcium response is mediated directly through TRPV1 channels (Figure 3.13c). However, cadmium chloride did alter the time-course of the response, preventing it from reversing back to baseline even after cadmium washout (Figure 3.13b). This was associated with the blockade or masking of potassium responses, which became absent or much smaller than cadmium free solutions. It's not clear whether this is due to some interaction of cadmium with Fura-2 AM, blockade of calcium pumps that are required to bring intracellular calcium concentration back to baseline, or some other mechanism. One effect of this was that it was no longer possible to analyse just the neurons that respond to potassium chloride as a cellular quality control process, so all capsaicin calcium responses were analysed.

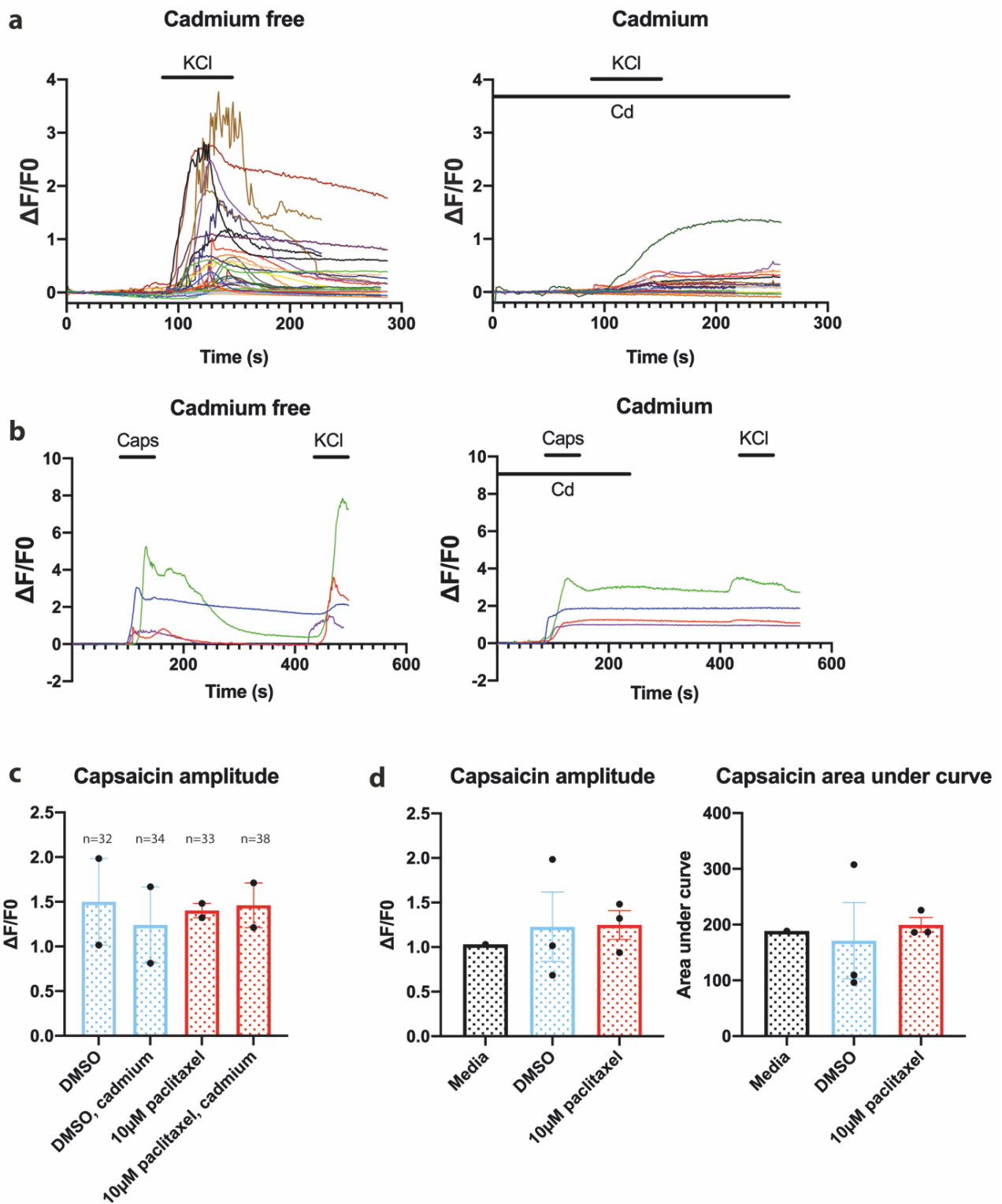


**Figure 3.13. Effect of voltage gated calcium channel (VGCC) block with cadmium chloride on calcium responses to capsaicin. a)** Dorsal root ganglion (DRG) neurons were imaged at 2 and 3 days in vitro. Representative single cell calcium imaging traces of potassium chloride (KCl) response in the presence and absence of cadmium chloride (Cd). 100 $\mu$ M cadmium chloride was added to perfusing solutions to block VGCCs. In order to test successful VGCC blockade, the effect of cadmium chloride on depolarisation-evoked calcium responses to KCl was recorded. The presence of cadmium chloride successfully blocked the vast majority of KCl response. **b)** Cadmium chloride was then used to assess the contribution of calcium influx directly through TRPV1 receptors and calcium influx through VGCCs as a result of electrical activity following capsaicin stimulation. **c)** The

*amplitude of capsaicin response in the presence and absence of cadmium following paclitaxel exposure or DMSO control was measured. No significance of ordinary one-way ANOVA. N=2 cultures per condition. d) The experiment examining the effect of paclitaxel exposure on capsaicin response amplitude in the absence of cadmium was repeated. The peak amplitude of the response was analysed as in the earlier experiment. The area under the curve to the half decay point was also analysed for this experiment. No effect of ordinary one-way ANOVA. Media, N=1 culture, n=15 neurons. DMSO, N=3 cultures, n=47 neurons. 10 $\mu$ M paclitaxel, N=3 cultures, n=52 neurons. All data presented as mean  $\pm$  SEM.*

Paclitaxel treatment also had no effect on the amplitude of capsaicin responses in the presence of cadmium (Figure 3.13c). However, in this experiment paclitaxel also failed to affect capsaicin amplitude in the absence of cadmium, in contrast to the earlier experiments described in section 3.3.5. In order to clarify this discrepancy, further biological replicates were included to increase to an N of 3 (Figure 3.13d). Still, the increased capsaicin calcium response amplitude observed in earlier experiments was not observed. The area under the calcium response was also analysed, and paclitaxel also had no effect on this.

The failure to replicate the earlier finding of increased amplitudes of capsaicin-induced calcium signals could be put down to various factors. It could be due to the original experiment returning a false positive or the experimental repeat failing for another reason. Some differences that could account for the discrepancy are the control condition for the original experiment being a media change whereas in the repeated experiment a 24 hour DMSO exposure was used instead. Also, cultures were not matched in the original experiment, which may make the chance of a falsely significant result more likely. In the second experiment all conditions were imaged from each of the three cultures which may reduce variability. Whether capsaicin-induced calcium signals are potentiated by paclitaxel or not in this chapter remains ambiguous.

### **3.4 Discussion**

This chapter aimed to evaluate whether CIPN could be reproduced *in vitro* as a way to quickly and efficiently test the ability of novel botulinum constructs to reverse or prevent this pain state. In order to achieve this, the effect of *in vitro* paclitaxel on morphology, calcium responses, neuropeptide release and ion channel expression was investigated.

Paclitaxel had no effect on cell survival and didn't increase ATF3 expression above naïve levels, but did cause the retraction of neurites from DRG neurons, as reported previously in the literature. Neurite retraction is likely to be caused directly by paclitaxel's effects on microtubules, *in vivo* (manifesting as the loss of intraepidermal nerve fibre density) as well as *in vitro* (Boyette-Davis et al., 2011; Yang et al., 2009; James et al., 2008). How this links to a painful phenotype is unclear, however. It has been hypothesised that the severity of CIPN caused by different chemotherapeutic agents correlates with how much they disrupt fast axonal transport (LaPointe et al., 2013). The link between this transport disruption and the generation of painful spontaneous discharges and lower thresholds for activation in the nociceptive system hasn't been elucidated. Altered transport could potentially account for the decrease in membrane expression of ion channels contributing to hyperpolarisation, such as potassium channels. However, this needs to be reconciled with the equivalent upregulation of excitatory ion channels such as NaV1.7 and TRPV1 (Section 1.3.2.3), which isn't as easily accounted for by trafficking defects.

Multiple experiments in this chapter point to potentiated signalling of TRPV1 following paclitaxel exposure. Early experiments showed that *in vitro* paclitaxel increased capsaicin-induced calcium amplitudes, though this was unable to be replicated in a subsequent experiment. Capsaicin-induced CGRP release was shown to be potentiated following paclitaxel exposure. Taken together, these findings suggest increased TRPV1 expression or activity induced by this *in vitro* CIPN model. Increased surface TRPV1 expression was not significant as detected using an immunolabelling approach, though there was a trend towards increased TRPV1 labelling in the paclitaxel treated conditions. It is possible that there is increased trafficking of TRPV1 to the membrane but that a fluorescent antibody-based approach is not sensitive enough to detect it. TRPV1 activity is complex, so there are a few different mechanisms by which potentiation could occur that does not involve translocation to the membrane. Firstly, this could be due to an increased density of TRPV1 receptors at the membrane caused by decreased recycling from the membrane. Secondly, paclitaxel may be sensitising the TRPV1 receptors via phosphorylation by kinases, specifically PKA, PKC, CaMKII, Src or Cdk5 (Malek et al., 2015). These kinases can be activated by the binding of inflammatory mediators to their receptors, and paclitaxel is known to have pro-inflammatory effects *in vivo* (Section 1.3.2.5) (Joseph et al., 2019). A lack of pro-inflammatory signalling may not be present due to the simplified cellular nature of DRG cultures, which may explain the lack of *in vitro* paclitaxel effects. Thirdly, paclitaxel could be preventing capsaicin-induced desensitisation, resulting in an increased response to sustained stimulation. Therefore TRPV1 upregulation at the

membrane may not be responsible for potentiated capsaicin responses, and paclitaxel may induce it by one of the mechanisms outlined above. There is evidence for increased TRPV1 sensitisation (Chen et al., 2011) as well as inhibited desensitisation of TRPV1 (Adamek et al., 2019) following paclitaxel *in vivo*. It may be possible that there is a change to TRPV1 function present in DRG neurons following *in vitro* paclitaxel administration as well, but that this is not being directly mediated by upregulation of the ion channel to the membrane.

The lack of an unambiguous effect of paclitaxel on DRG cultures may mean that mechanisms that lead to CIPN *in vivo* do not have a conserved mechanism *in vitro*. This could be due to pharmacokinetics and pharmacodynamics not being replicated, or that a culture of **only neurons and glia at the level of the DRG** is not sufficient to replicate CIPN in a functioning sensory system. The rat DRG cultures used in this experiment were also shown to have a very high expression of ATF3 even in control conditions, so it is possible that these are not a good model system to study neuropathic conditions as they are already mimicking a neuropathic state due to the dissociation protocol.

Dissociation causes cellular damage and stress which alters gene expression and may put the neurons in a neuropathic state that could mask pain-related effects (Frey et al., 2015; Zheng et al., 2007). The main argument for using DRG neurons at longer culture times is that these axotomy and dissociation-related changes have had enough time to stabilise or return back to baseline, putting them back in a “naïve” state once again. The earlier experiments in this chapter utilised ATF3 expression to look at cellular stress within DRG cultures. What was clear is that a large percentage of the neurons express ATF3, with 47% of neurons expressing it at 3 DIV, and 48% expressing it at 7 DIV. This supports the hypothesis that DRG cultures are not a particularly good model for the un-pained sensory system, which has practically no ATF3 expression *in vivo* (Bráz & Basbaum, 2010). It also does not support the theory that 7 days is sufficient to revert the neurons back to a more physiologically normal state, as ATF3 expression had not decreased at all at this timepoint.

From the results of this chapter it has evolved that paclitaxel administration directly to rat DRG neurons using the conditions and time frames detailed is unlikely to be a robust model of CIPN. Potential pitfalls could include the relatively acute exposure to paclitaxel of 24 hours, when it takes days to develop in animal models and patients. The issue may lie in the use of dissociated

DRG neurons which have been shown in this chapter to already express a damaged phenotype. It may also be a wider issue with the mechanism of paclitaxel on sensory neurons, which may not be possible to be replicated *in vitro* without the much longer axons which are the most vulnerable to toxicity *in vivo*. The testing of novel botulinum constructs in rodent models is therefore required to understand its potential use as an analgesic for CIPN and other chronic pain disorders further.

## 4. *In vitro* characterisation of a novel chimeric botulinum toxin, ChoBot

### 4.1 Introduction

The perfect peripheral analgesic for a pain condition would silence only the nociceptors that are mediating the aberrant, painful signalling in that particular condition, leaving all other sensation intact. However, the sensory system is complex and the subtypes of DRG neurons that mediate different modalities of sensation, from low threshold to nociception, is far from fully understood. Genetic and transcriptomic studies in recent years have begun to elucidate the molecular and functional diversity of different sensory neuron subtypes.

Arguably the lowest level physiological and functional characterisation of a rodent DRG neuron is its degree of myelination. Myelination can be assessed by looking at the expression of NF200, which is only expressed in myelinated neurons in rodents. Myelinated neurons that express NF200 are classified (by conduction velocity) either into larger A $\beta$ -fibres or smaller A $\delta$ -fibres (Lawson & Waddell, 1991). In the skin, these myelinated neurons can be classified into low threshold mechanoreceptors, generally involved in touch sensation, and high threshold and large dynamic range mechanoreceptors which may be involved in mechanical nociception (Adelman et al., 2019). A $\delta$  nociceptors have also been demonstrated to mediate noxious heat responses (Treede et al., 1998).

C-fibres are generally NF200 poor, being either unmyelinated or very weakly myelinated (Lawson & Waddell, 1991). Expression of the cytoskeletal filament protein peripherin can be used to distinguish these smaller, NF200-negative C-fibre populations (Goldstein et al., 1991). A basic categorisation of C-fibres can be into those that express the neuropeptides CGRP and/or substance P and the NGF receptor TrkA, and those that bind IB4 and express the c-Ret receptor for GDNF (Averill et al., 1995). However, there is some overlap between these so-called peptidergic and non-peptidergic C-fibre groups, with approximately 10% of CGRP-positive neurons also binding IB4 in mouse (McCoy et al., 2013). CGRP is also expressed in neurons with A-fibres, and is not limited to a purely C-fibre population (Ruscheweyh et al., 2007). C-fibres are generally nociceptive, responding to mechanical, heat or cold stimuli, or a combination of these as polymodal nociceptors. However, the proportion of modality specific to polymodal C-fibre

nociceptors is debated (Emery et al., 2016). One study performed intracellular recordings of lumbar DRG neurons as different modalities were used to stimulate the skin (Lawson et al., 2019). From this it was deduced that IB4-positive neurons include most polymodal nociceptors and some mechanospecific nociceptors, and possibly some silent nociceptors. TrkA-expressing, presumed peptidergic, neurons are mostly classified as high threshold mechanoreceptors. Most cold sensitive C-fibres were IB4 negative and CGRP and TrkA positive. The expression of particular ion channels can also give clues to the function of a nociceptor. For example, the expression of TRPV1 is restricted to a subpopulation of mechanically insensitive C-fibres, that instead respond to heating (Lawson et al., 2008).

Subpopulations of sensory neurons have been shown to express different gangliosides as components of their cell membrane (Gong et al., 2002). One of these gangliosides, the GM1 ganglioside, is the site of binding for cholera toxin. In disease pathogenesis, cholera binds to the GM1 ganglioside to internalise into intestinal epithelial cells (Holmgren et al., 1975). GM1 is also expressed by peripheral neurons, and the ability of labelled CTB to internalise into these neurons has been exploited to trace neuronal pathways for decades (Mekalanos et al., 1997). CTB without the enzymatic A subunit is non-toxic and can be labelled with HRP, biotin or fluorescent molecules for this use.

The uptake of CTB via the GM1 ganglioside is not equal across all subpopulations of DRG neurons (Section 1.4.5.1). In naïve conditions, the vast majority of neurons that are labelled by CTB are large diameter, NF200-positive neurons, rather than smaller CGRP and substance P-expressing neurons (Robertson & Grant, 1989). However, this CTB-susceptible subpopulation changes following neuropathic injury such as nerve transection or chemical damage (Shehab et al., 2003; Tong et al., 1999; Oszlács et al., 2015). After injury, the overall proportion of DRG neurons that take up CTB is increased. This increase is driven by recruitment of smaller diameter neurons, including nociceptive peptidergic populations (Tong et al., 1999; Shehab et al., 2003; Oszlács et al., 2015). Presumably, this is caused by changes of expression of the GM1 ganglioside induced by neuropathic damage, due to GM1's role in neuronal regeneration and plasticity (Mocchetti, 2005).

## 4.2 Summary and objectives

As CTB so effectively internalises into DRG neurons, it may be useful to target these neurons with compounds designed for analgesia via binding to the GM1 ganglioside. Specifically, SNARE cleavage within these neurons using a BoNT light chain may prove efficacious if the subpopulation targeted is nociceptive in nature. A chimera of the BoNT/A light chain and translocation domains linked to the CTB pentamer of cholera toxin was therefore created using SNARE stapling, named ChoBot (Section 2.3).

The novel property of altered CTB binding following nerve injury is also an interesting prospect for an analgesic. The changes that take place following injury to confer CTB selectivity to more neurons isn't known, but if damaged neurons can be specifically targeted by this mechanism then this may prove an effective analgesic.

Research aims:

- Demonstrate that ChoBot is proteolytically active in DRG cultures.
- Investigate the subpopulation(s) of neurons that are targeted by ChoBot, and compare to CTB binding and GM1 ganglioside expression in sensory neurons.
- Evaluate whether ChoBot functionally inhibits the stimulated release of the pain-related neuropeptide CGRP.
- Assess whether damage by the chemotherapy drug paclitaxel *in vitro* confers ChoBot susceptibility to a wider range of neurons.

## 4.3 Results

### 4.3.1 *The botulinum A light chain-translocation domain that has not undergone stapling to a receptor binding domain is not internalised into sensory neurons*

In order to trace the action of the BoNT protease, antibodies that are specific to the cleaved form of the SNARE protein can be used. As ChoBot is a BoNT/A chimera, if functional it would cleave 9 amino acids from the C-terminus of the SNARE protein SNAP25 to give a SNAP25<sub>197</sub> protein. From this, the activity of ChoBot can be localised to subpopulations of DRG neurons.

In order to determine whether the BoNT/A light chain-translocation domain with protein staple attachment (LC-TD-SNAP25) can be internalised without SNARE stapling to a receptor binding domain, this protein product was applied to cultured DRG neurons without having undergone a SNARE stapling reaction. LC-TD-SNAP25 was applied for 24 hours. Cultures were then fixed and immunocytochemistry for the pan-neuronal marker  $\beta$ -III-tubulin and BoNT/A-truncated SNAP25 protein (cleaved SNAP25, cS25) was carried out. A threshold for cS25 positivity was set at the mean + 2 standard deviations above the relevant secondary-only intensities measured from all soma marked by  $\beta$ -III-tubulin. Cleavage of SNAP25 could be seen in very few neurons, and only 10 out of 751 neurons passed the positive intensity threshold (Figure 4.1). Therefore internalisation of the BoNT/A light chain via mechanisms such as bulk endocytosis is not sufficient to induce SNAP25 cleavage in sensory neurons, and receptor mediated exocytosis is required to allow sufficient targeting.

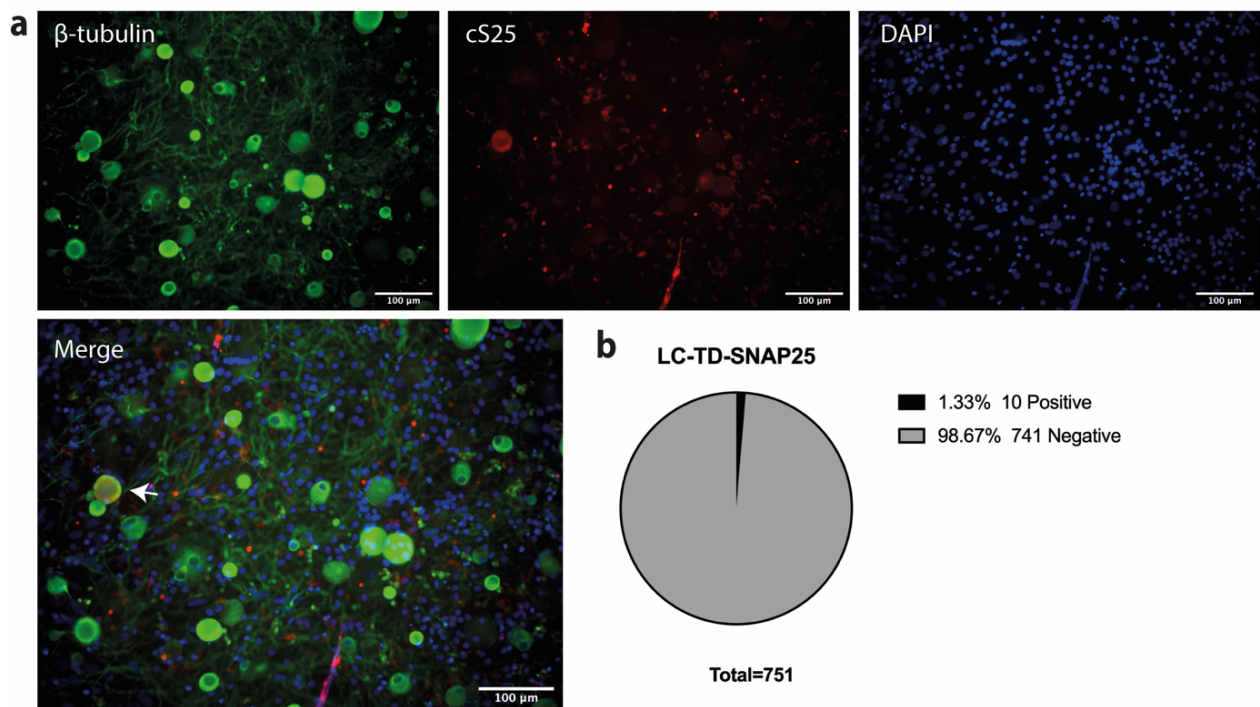


**Figure 4.1. The effect of light chain-translocation domain-SNAP25 (LC-TD-SNAP25) on SNAP25 cleavage. a)** 1nM of LC-TD-SNAP25 was applied to DRG cultures for 24 hours, then the immunofluorescent intensity of cleaved SNAP25 (cS25) in  $\beta$ -III-tubulin-marked neurons was measured. Arrow shows a rare example of a cS25-positive cell body. **b)** A positive threshold intensity for cS25 was set at the mean+2 standard deviations of the vehicle-only cS25 intensities. Fewer than 2% of neurons in the culture passed the threshold for cS25 positivity. N=3 cultures, 2 wells per condition, 2-6 images per well.

#### 4.3.2 *A subpopulation of sensory neurons express the ganglioside target of ChoBot and bind fluorescent cholera toxin subunit B*

In order to assess a cholera toxin-based targeting system for BoNT retargeting, the subpopulations of sensory neurons that bind Alexafluor 488-conjugated CTB was investigated. NF200 was used as a marker of myelinated (A $\beta$  and A $\delta$ ) DRG neurons, peripherin was used as a marker of smaller diameter C-fibre neurons, CGRP was used as a marker of the peptidergic C-fibre population. IB4 binding would also have been used as a marker of non-peptidergic C-fibres, however the IB4-488 conjugate wavelength overlapped with CTB and could not be assessed. CTB was shown to co-localise with 33% of the NF200-expressing population, 26% of the peripherin-expressing population and 42% of the CGRP-expressing population (Figure 4.2).

As another marker for potential cholera subunit B binding and subsequent ChoBot targeting, the localisation of the GM1 ganglioside receptor at the membrane of DRG neurons was investigated. Subtyping of the sensory neurons that express the GM1 ganglioside was carried out using the same subpopulation markers as above (Figure 4.3). GM1 immunocytochemistry was carried out on unpermeabilised cultures, due to issues presumably caused by labelling of internal GM1 rather than just functional, membrane-inserted GM1 in permeabilised cells (Section 2.5.1). GM1 expression was highest in the NF200-positive subpopulation at 38%. 25% of the peripherin-positive subpopulation, 27% of the CGRP-positive subpopulation and 21% of the IB4-binding subpopulation co-localised with GM1.

The results of these experiments show that a proportion of DRG neurons express both the GM1 ganglioside receptor for cholera toxin, and bind fluorescent CTB. This is in agreement with data published *in vivo*. However, one discrepancy is that the vast majority (85%) of NF200-expressing rat DRG neurons become CTB-positive following injection compared to just 5% of CGRP-expressing neurons (Robertson et al., 1989). In the experiments of this thesis, the selectivity is not as strong for myelinated subpopulations, also including a percentage of putative nociceptors that express peripherin, CGRP, or bind IB4. This could be attributed to cultured DRG neurons behaving more like an axotomised sensory pathway due to dissection and dissociation.

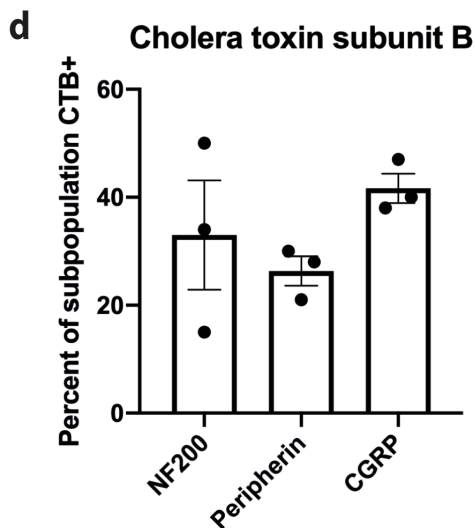
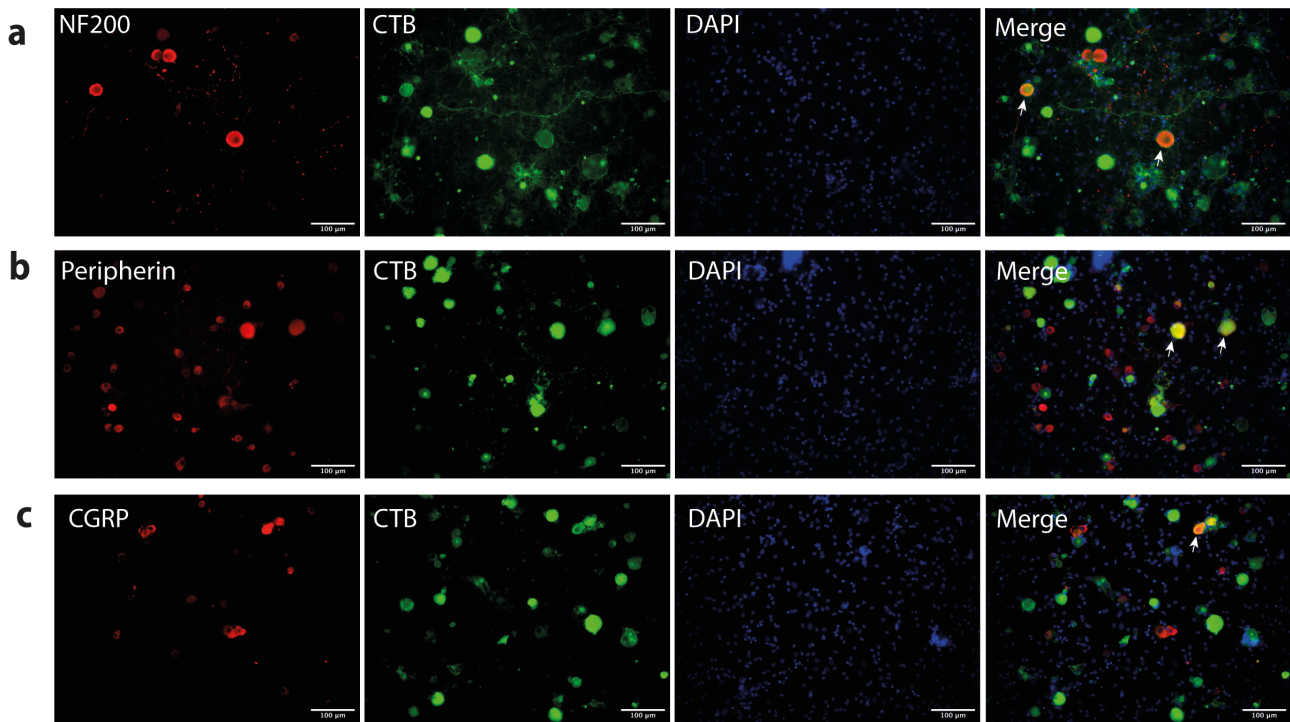


**Figure 4.2. Subtypes of sensory neurons that bind fluorescent cholera toxin subunit B.** Dorsal root ganglion cultures at 3 days *in vitro* were labelled with a fluorescently conjugated cholera toxin B (CTB) subunit live for 30 minutes prior to fixation and immunocytochemistry. Representative images showing CTB co-localisation with the markers of sensory neuron subpopulations: **(a)** NF200, **(b)** peripherin, **(c)** CGRP. **Arrowheads show examples of colocalised neurons.** **d)** The percentage of neurons in each subpopulation that were also positive for CTB was analysed, as defined by an intensity above the mean + 2 standard deviations of the secondary only conditions. N=3 cultures, 2 wells per condition, 6 images per well. NF200 n=586, peripherin n=842, CGRP n=223. No significance of ordinary one-way ANOVA. Data presented as mean  $\pm$  SEM.

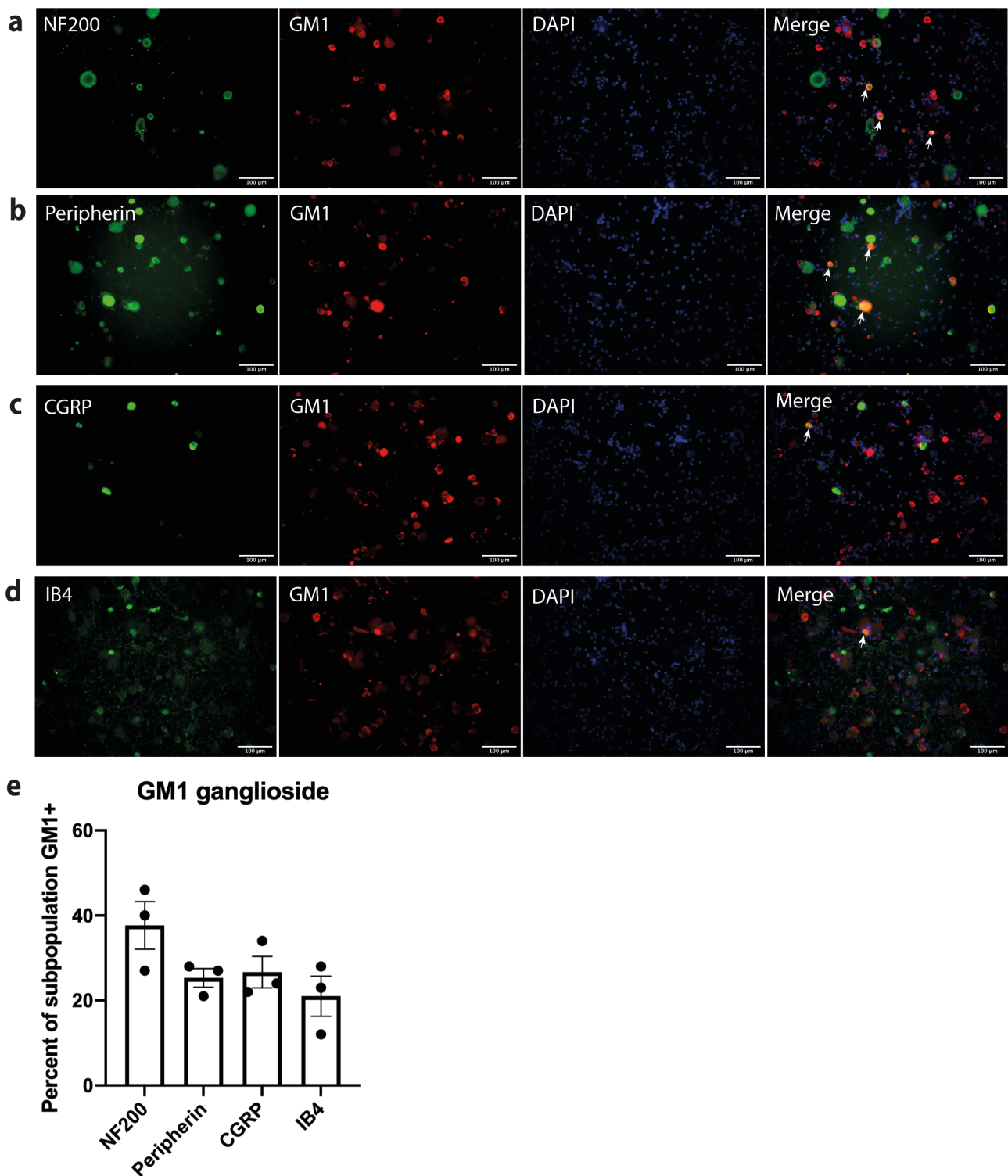


**Figure 4.3. Subtypes of sensory neurons that express extracellular GM1 ganglioside.** Dorsal root ganglion cultures at 3 days *in vitro* were fixed for analysis of expression of the GM1 ganglioside. Representative images showing GM1 ganglioside co-localisation with the markers of sensory neuron subpopulations: **(a)** NF200, **(b)** peripherin, **(c)** CGRP, **(d)** IB4. **Arrowheads show examples of colocalised neurons.** **e)** The percentage of neurons in each subpopulation that were also positive for the GM1 ganglioside was analysed, as defined by an intensity above the mean + 2 standard deviations of the secondary only conditions. N=3 cultures, 2 wells per condition, 6 images per well. NF200 n=222, peripherin n=252, CGRP n=146, IB4 n=246. No significance of ordinary one-way ANOVA. Data presented as mean  $\pm$  SEM.

### *4.3.3 ChoBot cleaves SNAP25 in a subpopulation of dorsal root ganglion neurons over a 1000-fold concentration range*

The SNAP25-cleaving ability of ChoBot in cultured DRG neurons was assessed following a 24-hour exposure to different concentrations of ChoBot. As a control, all conditions contained the same concentration of the vehicle detergent OG, which is used in the SNARE-stapling reaction to facilitate coiled coil formation (Section 2.3). Immunocytochemistry for  $\beta$ -III-tubulin and cS25 was carried out. In agreement with predictions from GM1 and CTB localisation, imaging showed the presence of cS25 in a subpopulation of DRG neurons at all ChoBot concentrations tested (Figure 4.4a).

Very few neurons passed the threshold for cS25-positivity in control conditions, with 3 out of 204 neurons after the media change and 3 out of 180 neurons in the vehicle-only conditions (Figure 4.4b). ChoBot was applied at 10pM, 100pM, 1nM and 10nM concentrations. At all these concentrations, the cS25 intensities were significantly increased compared to the control groups. However, there was no significant difference between the different ChoBot concentrations, suggesting that even 10pM concentration is sufficient to induce maximal SNAP25 cleavage. This is not necessarily surprising due to the potency of the BoNT/A light chain once internalised. This potency is conferred by the ability of one light chain to target many SNAP25 molecules, and by resistance to proteosomal degradation over time (Matak & Lacković, 2014). Therefore in these cultures, as long as sufficient ChoBot is binding to receptors and being internalised, even very low numbers of internalised light chains are likely to be sufficient to cleave all available SNAP25 over a 24 hour period. Taking the average of all the concentrations used in this experiment, 28% of DRG neurons analysed were sensitive to SNAP25 cleavage by ChoBot, showing a sensitive and insensitive subpopulation of neurons.

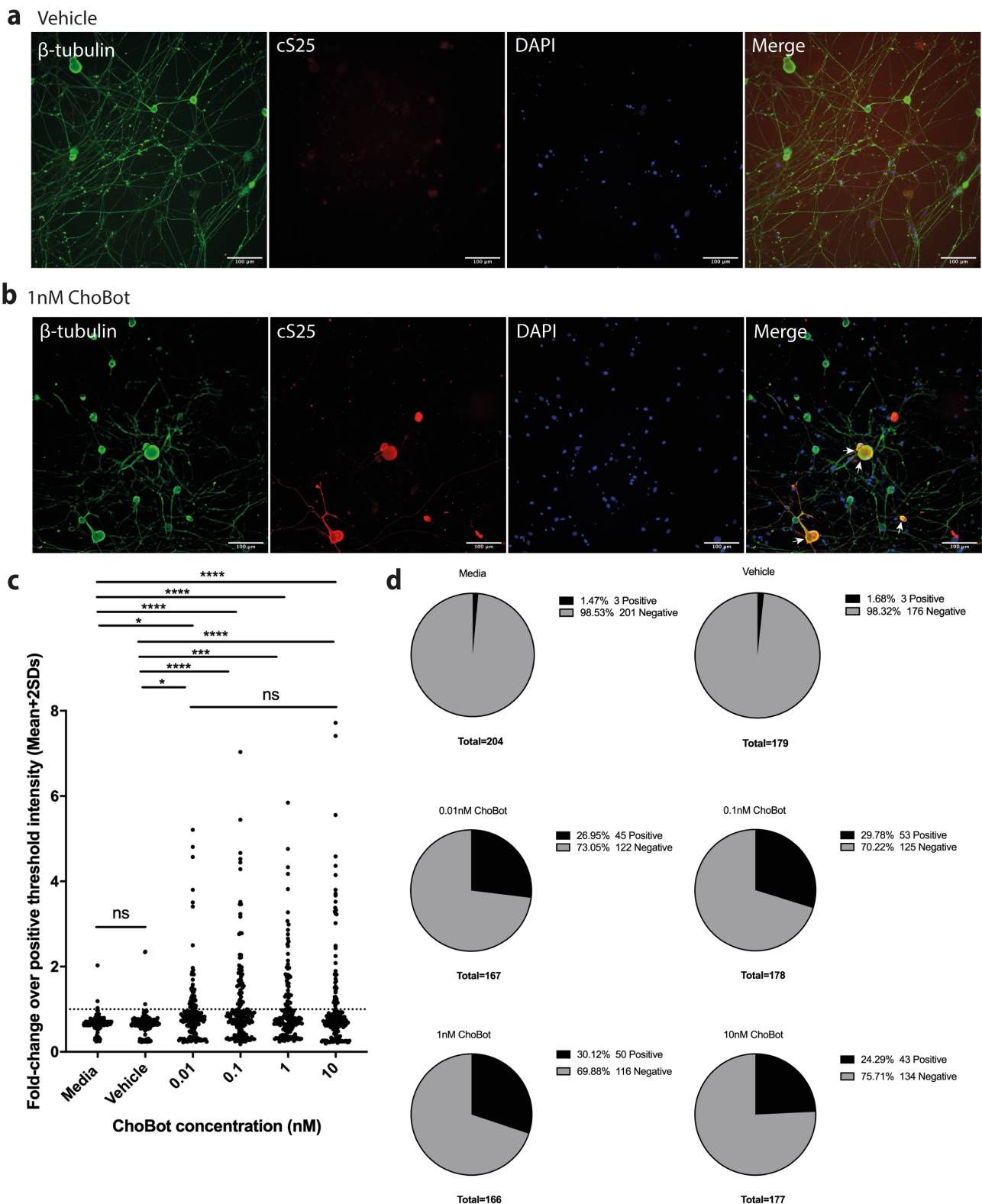


**Figure 4.4. ChoBot cleaves SNAP25 in dorsal root ganglion cultures at concentrations from 10pM to 10nM.** Cultures at 6 days *in vitro* were exposed for 24 hours to different concentrations of ChoBot. Representative images showing immunocytochemistry for the pan-neuronal marker  $\beta$ -III-tubulin and the BoNT/A-cleaved SNAP25 (cS25) protein after exposure to (a) vehicle only or (b) 1nM ChoBot. Arrowheads show examples of colocalised neurons. c) The fluorescent intensity of cS25 was measured from each  $\beta$ -III-tubulin positive cell body following 24 hours of treatment with different concentrations of ChoBot, a media change control or a vehicle-only control. Cells were deemed positive for cS25 with intensities over the mean +2 standard deviations of intensity

measurements of control wells from the same experiment. Ordinary one-way ANOVA  $P < 0.0001$ . Followed by Tukey's multiple comparisons test. **d)** Proportion of DRG neurons classed as positive for cS25 at each concentration of ChoBot. For all figure data,  $N=2$  cultures, 2 wells per condition, 6 images per well. Media change  $n=204$ , vehicle  $n=179$ , LC-TD-SNAP25  $n=751$ , 0.01nM  $n=167$ , 0.1nM  $n=178$ , 1nM  $n=166$ , 10nM  $n=177$ . \*\*\*\* $P < 0.0001$  \*\*\* $P < 0.001$  \*  $P < 0.05$ .

#### *4.3.4 Myelinated and peptidergic neurons are more susceptible to SNAP25-cleavage by ChoBot than other subpopulations*

Immunocytochemistry for markers of sensory neuron subpopulations and cS25 was carried out to determine whether there is a particular subpopulation that is susceptible to ChoBot binding, light chain internalisation and SNAP25 cleavage (Figure 4.5). Most co-localisation of cS25 was seen in the NF200 and CGRP-positive DRG population, at 35% and 30% cleavage respectively. In contrast, only 11% of peripherin-positive neurons and 10% of IB4 positive neurons were positive for cS25. The targeting of the TRPV1-expressing population was also investigated, with 23% of this population positive for cS25 after ChoBot treatment.

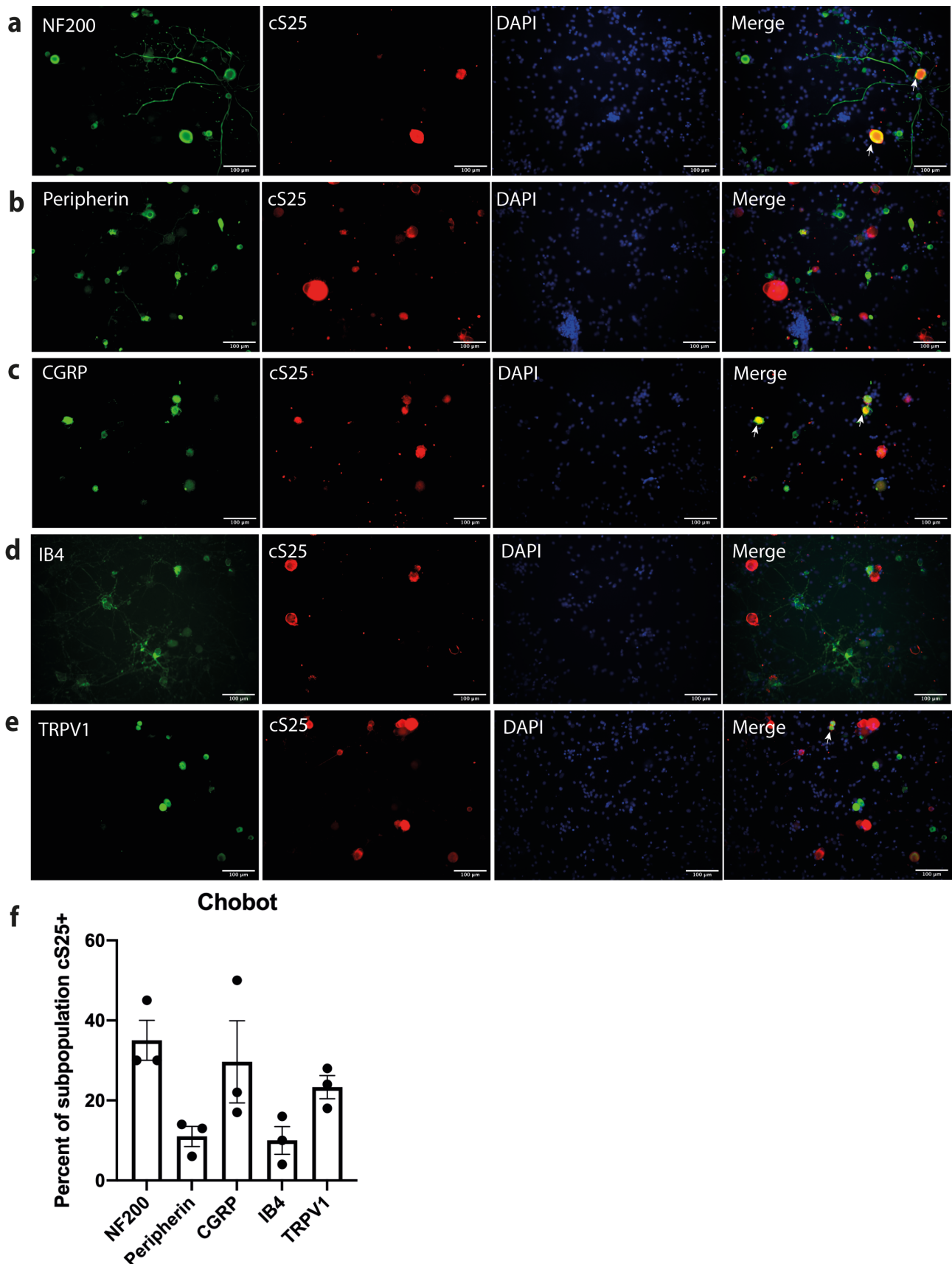


**Figure 4.5. Subtypes of sensory neurons susceptible to SNAP25 cleavage by Chobot.** Dorsal root ganglion cultures were treated with 1nM ChoBot for 24 hours at 2 days in vitro (DIV), then fixed for immunocytochemistry at 3 DIV. Representative images showing cleaved SNAP25 (cS25) co-localisation with the markers of sensory neuron subpopulations: **(a)** NF200, **(b)** peripherin, **(c)** CGRP, **(d)** IB4, **(e)** TRPV1. **Arrowheads show examples of colocalised neurons.** **f)** The percentage of

neurons in each subpopulation that were immunoreactive for cS25 was analysed, as defined by a cS25 intensity above the mean + 2 standard deviations of the untreated media and vehicle-only control conditions. N=3 cultures, 2 wells per condition, 6 images per well. NF200 n=406, peripherin n=514, CGRP n=191, IB4 n=410, TRPV1=261. No significance of ordinary one-way ANOVA. Data presented as mean ± SEM.

As 1nM ChoBot was shown to cleave SNAP25 in 30% of CGRP-expressing DRG neurons by immunocytochemistry, whether this caused a functional change in the stimulated release of CGRP was investigated. Cultures were stimulated with a 40mM potassium chloride solution to depolarise all electrically active neurons, and capsaicin to stimulate TRPV1-expressing neurons. Both potassium chloride and capsaicin induced the release of CGRP concentrations above basal in all conditions. There was no significant difference between control and ChoBot treated wells when raw data was plotted, though there was significant variability in CGRP levels between cultures (Figure 4.6a). When data was normalised to the media change only condition for each culture, potassium chloride-evoked CGRP release was significantly reduced by ChoBot (Figure 4.6b). This provides further evidence that ChoBot is able to successfully intoxicate a subpopulation of the nociceptive CGRP-expressing neurons. It also provides evidence for a functional effect in this population of DRG neurons, demonstrating that cleavage of SNAP25 is able to inhibit exocytosis of a pain-relevant neuropeptide by preventing the formation of SNARE complexes.

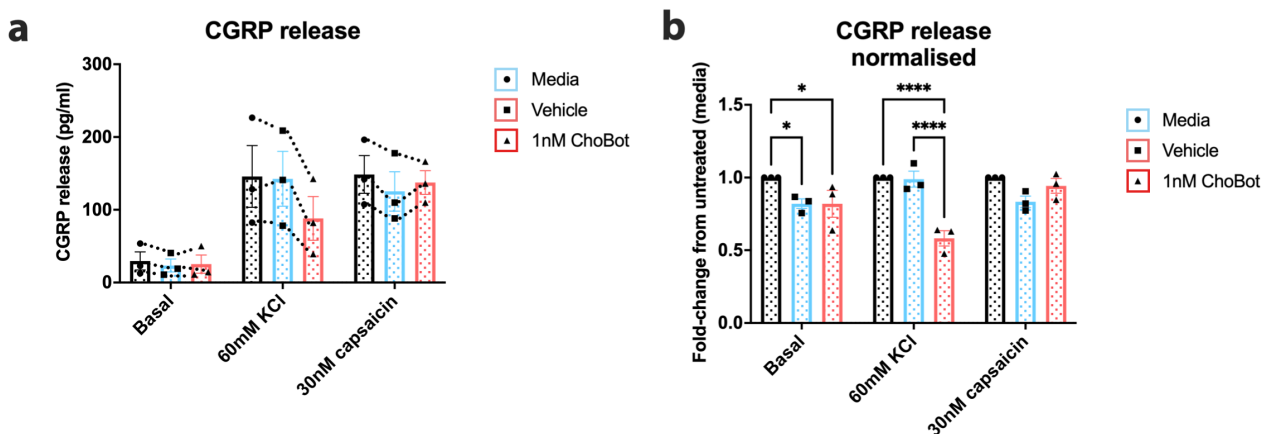


**Figure 4.6. ChoBot inhibits depolarisation-induced calcitonin gene-related peptide release.** DRG neurons at 6 DIV were exposed to ChoBot, vehicle, or a media change 24 hours prior to a calcitonin gene-related peptide (CGRP) release assay. They were stimulated with potassium chloride (KCl) or capsaicin. **a**) When raw data was plotted, there was no effect of ChoBot in naïve (DMSO) or paclitaxel sensitised conditions. **b**) When data was normalised to the untreated media change condition for each separate culture, 1nM ChoBot significantly reduced KCl-evoked CGRP release. Two-way ANOVA of treatment and stimulus. Followed by Tukey's multiple comparisons test. For all data, N=3 cultures, 2 wells per stimulus per condition. Data presented as mean ± SEM. \*\*\*\*p<0.0001 \* P<0.05.

#### *4.3.5 Comparison of ChoBot selectivity to cholera toxin subunit B binding and GM1 expression in neuronal subpopulations*

The subpopulation selectivity of ChoBot, and the subpopulations that express GM1 and bind CTB were compared in order to confirm that ChoBot susceptibility is being conferred by GM1 expression and subsequent binding of the CTB receptor binding domain (Figure 4.7). These markers were not used in conjunction with each other due to initial data suggesting competition for the same receptors and binding sites. It was initially hypothesised that the subpopulations would be the same between these groups, due to ChoBot having a receptor binding domain that is the same as CTB, which binds the GM1 ganglioside. Indeed, there was no significant difference in the proportion of myelinated NF200-positive, peptidergic CGRP-positive, or non-peptidergic IB4-binding DRG neurons targeted by each of these markers. However, there was a significant difference within the peripherin-expressing subpopulation. ChoBot cleaved SNAP25 in a lower proportion of peripherin-expressing neurons than bound CTB or were immunoreactive for GM1.

There are many steps in the mechanism of ChoBot intoxication that could cause a disconnect between GM1 expression and successful cleavage of SNAP25 in peripherin-expressing subpopulations. For example, there could be a lack of expression of SNAP25 in this subpopulation. To account for this unexpected observation of lower ChoBot susceptibility compared to GM1 expression and CTB binding in peripherin-expressing neurons, it was investigated whether expression of the full-length target protein, SNAP25, is diminished in this population of neurons. Immunocytochemistry for full-length SNAP25 within neurons marked by  $\beta$ -III-tubulin or peripherin was performed (Figure 4.8). SNAP25 expression was clearly differentially expressed over the DRG population, with very strong fluorescence in certain neurons and weak in others (Figure 4.8a).

## Subpopulation selectivity of ChoBot in relation to CTB binding and GM1 expression

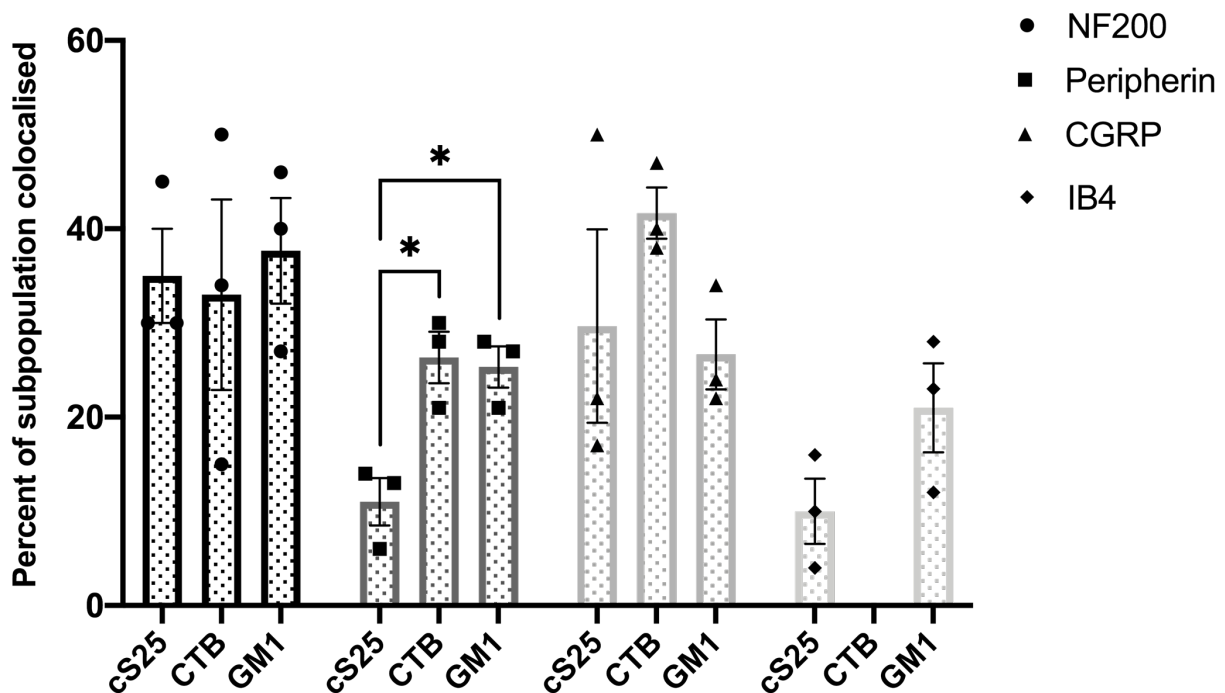


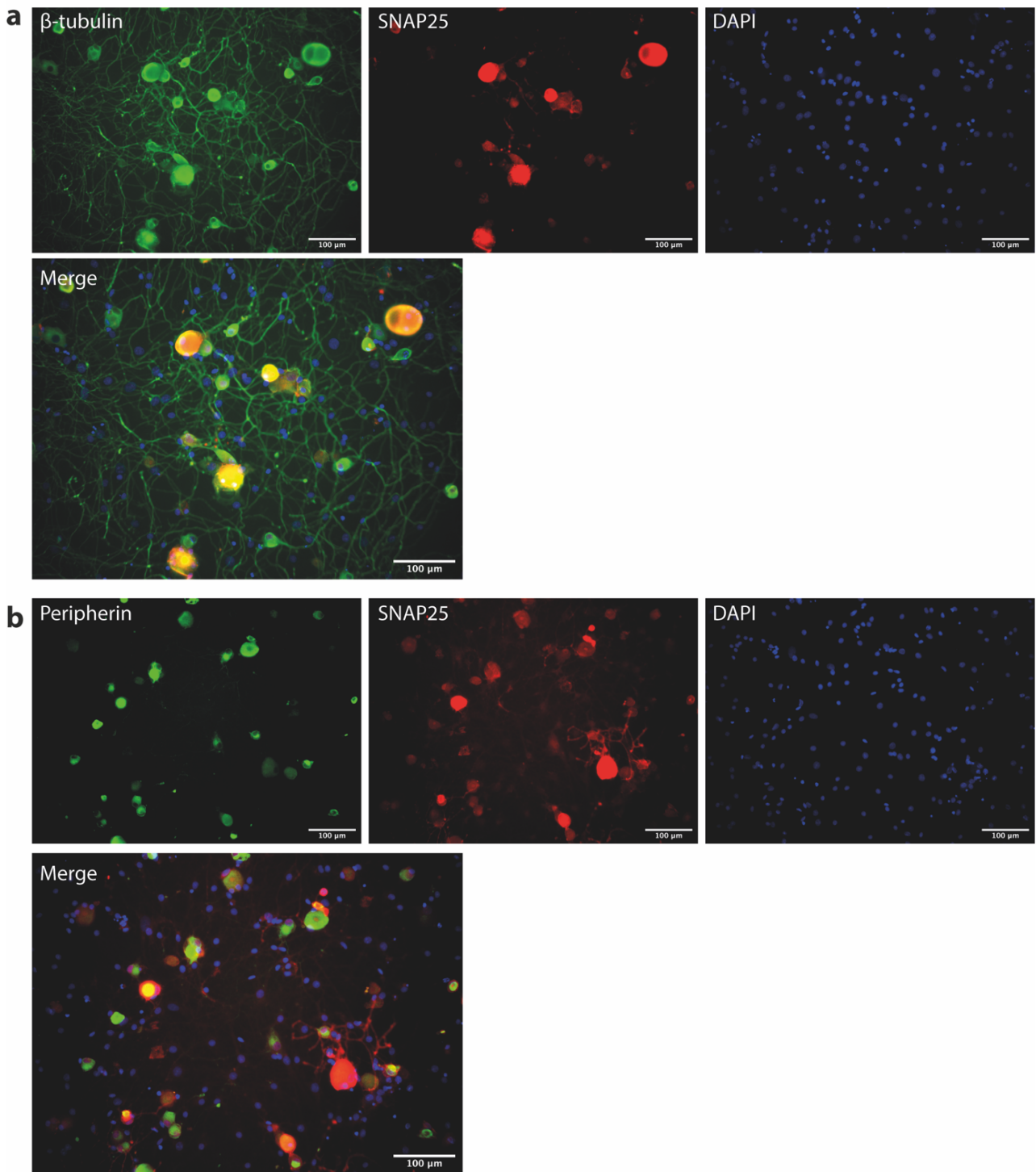
**Figure 4.7. Subtyping of neurons susceptible to SNAP25 cleavage by ChoBot, CTB binding and GM1 expression.** The proportions of neurofilament 200 (NF200)-expressing neurons, peripherin-expressing neurons, calcitonin gene-related peptide-expressing neurons and isolectin IB4-binding neurons that are positive for cleaved SNAP25 (cS25), fluorescent cholera toxin subunit B (CTB) binding and uptake, and for membrane GM1 ganglioside expression. The expression/binding of these three markers was significantly different in the peripherin positive subpopulation. Ordinary one-way ANOVA  $P=0.0082$ . Followed by Tukey's multiple comparisons test. cS25 vs. CTB,  $P=0.0013$ , cS25 vs. GM1,  $P=0.0154$ . NF200 and CGRP, no significance of ordinary one-way ANOVA. IB4, no significance of two-tailed unpaired t test.  $N=3$  cultures, 2 wells per condition, 6 images per well. Data presented as mean  $\pm$  SEM. \*  $P<0.05$ .

The SNAP25 fluorescence intensity from DRG neurons marked with  $\beta$ -III-tubulin was then compared to those marked with peripherin, to ascertain whether overall SNAP25 expression was lower in this subpopulation. A threshold for SNAP25 expression was set at the mean + 2 standard deviations above the secondary only intensities, in order to determine whether some neurons lack SNAP25 expression entirely. 7% of  $\beta$ -III-tubulin-positive neurons and 10% of peripherin-positive neurons fell below this threshold, suggesting that a small percentage of DRG neurons may lack the SNAP25 protein entirely, or in such low densities as to not be detected by immunocytochemistry (Figure 4.9a). When each individually analysed neuron was plotted, SNAP25 intensity was indeed lower in the peripherin subpopulation compared to the overall population (Figure 4.9a). However, when the SNAP25 intensities were averaged per culture, there was no significant decrease in peripherin-positive neurons compared to the pan-neuronal  $\beta$ -III-tubulin (Figure 4.9b). This

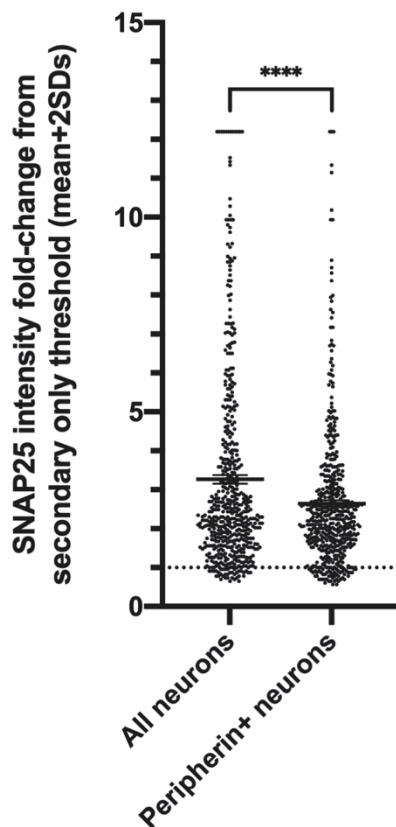
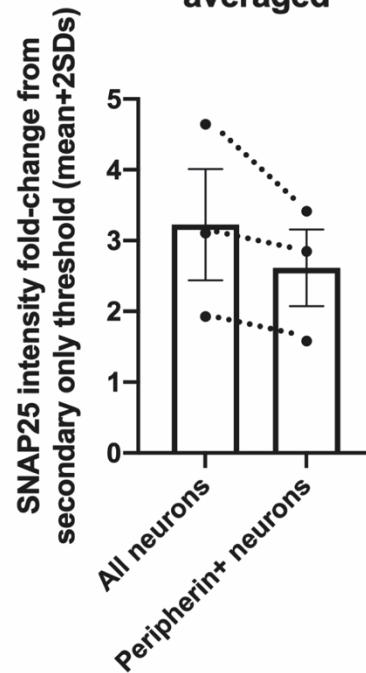
suggests that there is a slightly differential expression of SNAP25 within the peripherin-expressing class of neurons compared to the whole DRG neuron population.

The mean intensity of SNAP25 in peripherin neurons was 19% lower than the mean intensity measured from the whole population of DRG neurons. This relatively subtle change is not enough to entirely account for the disconnect observed between cS25 positivity following ChoBot treatment and CTB binding/GM1 expression (58% and 57% lower respectively), so must be mediated by some other mechanism (Figure 4.7).

Another question arising from these experiments is which type of peripherin-expressing subpopulation is driving this difference. Peripherin is a marker of small diameter, C-fibre neurons including both peptidergic and non-peptidergic marked by CGRP and IB4 respectively. A significantly lower cleavage rate was not detected in either of these subgroups. There was a trend towards fewer cS25 positive neurons compared to GM1 expressing neurons in the IB4 subpopulation (unpaired t test,  $P=0.1337$ ). It may be that ChoBot is failing to cleave SNAP25 in both the peptidergic and non-peptidergic populations but that this effect size is not large enough to be significant until the two subgroups are combined. It may also be complicated by the imperfect use of CGRP as a peptidergic C-fibre marker only, diluting the effect size within the C-fibre population by also labelling a CGRP-expressing A $\delta$ -fibre population.



**Figure 4.8. Expression of full-length SNAP25 in dorsal root ganglion neurons. a)** Representative image showing SNAP25 immunoreactivity in all neurons, marked by  $\beta$ -III-tubulin. **b)** Representative image showing SNAP25 immunoreactivity in the subpopulation of neurons marked with peripherin.

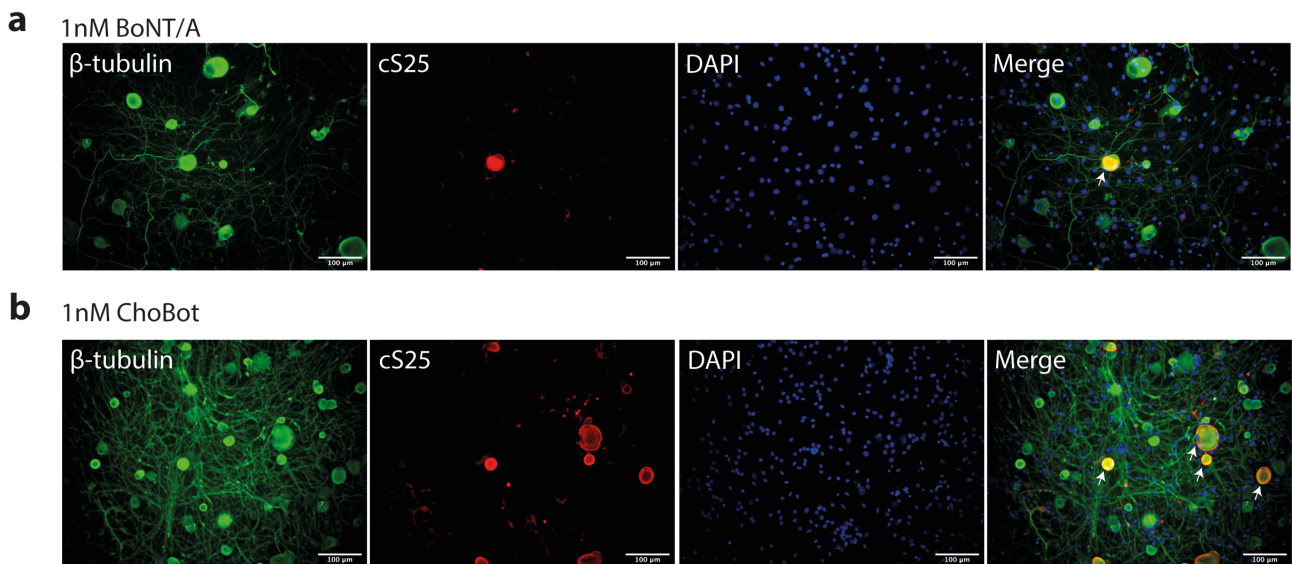
**a SNAP25 immunofluorescence****b SNAP25 immunofluorescence averaged**

**Figure 4.9. SNAP25 immunofluorescence is decreased in peripherin-expressing neurons compared to the total population. a)** The immunofluorescence intensity of SNAP25 was measured in the soma of neurons marked by  $\beta$ -III-tubulin (all neurons) and in the soma of neurons that express peripherin. These intensities were normalised to a SNAP25 positivity threshold that was set at the mean intensity + 2 standard deviations of the secondary only conditions (dotted line). The normalised intensity of each measured neuron was plotted. Unpaired two-tailed t test  $P < 0.0001$ . **b)** The SNAP25 intensities of neurons measured for each culture were then averaged. No significance of unpaired two-tailed t test.  $N = 3$  cultures, 2 wells per condition, 6 images per well.  $\beta$ -III-tubulin neurons  $n = 543$ , peripherin neurons  $n = 518$ . Data presented as mean  $\pm$  SEM. \*\*\*\*  $P < 0.0001$ .

#### 4.3.6 *ChoBot has a higher targeting efficacy of sensory neurons in vitro than BoNT/A*

In terms of its clinical use, one important question is whether ChoBot has a more favourable activity profile than the current most commonly used botulinum toxin for pain treatment, BoNT/A. In order to address this, the percentage of neurons that are susceptible to SNAP25 cleavage by ChoBot and BoNT/A was directly compared.

As in earlier experiments, toxins were applied for 24 hours, then the cS25 intensities of soma marked by  $\beta$ -III-tubulin were measured (Figure 4.10). 0.1nM BoNT/A cleaved SNAP25 in 10% of DRG neurons, compared to 30% by 0.1nM ChoBot in an earlier experiment (Figure 4.4c,d). 1nM BoNT/A also caused SNAP25 cleavage in just 13% of neurons compared to 32% of neurons by 1nM ChoBot within the same culture-matched experiment (Figure 4.10c). As with ChoBot, higher concentrations of BoNT/A did not increase the number of cS25-positive DRG neurons, suggesting that a more limited subpopulation of neurons is sensitive to BoNT/A intoxication. This supports the further investigation of ChoBot as an analgesic as it appears from *in vitro* experiments to target a wider proportion of sensory neurons than the currently clinically used BoNT/A. However, further experiments must be performed in order to demonstrate that silencing of these particular neurons by ChoBot would be beneficial for pain treatment.



**c** **SNAP25 cleavage by ChoBot and BoNT/A**

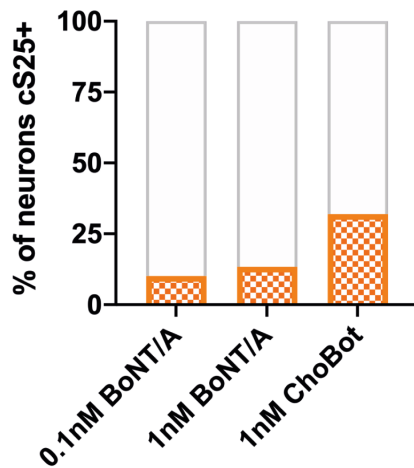


**Figure 4.10. ChoBot cleaves SNAP25 in a larger proportion of dorsal root ganglion neurons than BoNT/A. a,b,c)** Representative images showing immunocytochemistry for the pan-neuronal marker  $\beta$ -III-tubulin and the BoNT/A-cleaved SNAP25 (cS25) protein. Cultures at 6 days in vitro were treated for 24 hours with **(a)** 1nM BoNT/A or **(b)** 1nM ChoBot. **Arrowheads show examples of colocalised neurons.** **c)** The fluorescent intensity of cS25 was measured from each  $\beta$ -III-tubulin positive cell body after treatment with each toxin. Cells were deemed positive for cS25 with intensities over the mean +2 standard deviations of intensity measurements of control wells from the same experiment. The proportion of DRG neurons classed as positive for cS25 for each toxin is shown.  $N=3$  cultures for 0.1nM BoNT/A and 1nM Chobot,  $N=1$  for 1nM BoNT/A. Unpaired t test  $P=0.0368$ . For each culture, 2 wells per condition, 6 images per well. 0.1nM BoNT/A  $n=643$ , 1nM BoNT/A  $n=179$ , 1nM ChoBot  $n=119$ . \*  $P<0.05$ . Data presented as mean  $\pm$  SEM.

#### 4.3.7 Comparison of BoNT/A and ChoBot subpopulation selectivity

In order to compare ChoBot to the current most commonly clinically used BoNT, subtyping of BoNT/A cleavage was performed using the same markers. Co-localisation of cS25 following 24h of 0.1nM BoNT/A treatment was performed with NF200, peripherin, CGRP and IB4-positive populations (Figure 4.11). SNAP25 cleavage was predominately in the myelinated NF200 group, which had significantly higher co-localisation with cS25 than peripherin-expressing and IB4-binding neurons (Figure 4.11e).

SNAP25 cleavage was higher following ChoBot treatment than BoNT/A treatment in all subpopulations investigated (Figure 4.11f). This shows that rather than a particular new population being targeted by ChoBot, there is overall improved targeting of all subpopulations. However, this increased targeting by ChoBot was only significant for NF200 and CGRP. As myelinated sensory neurons comprise low threshold mechanoreceptors as well as A $\delta$ -nociceptors, *in vivo* studies would be required to determine whether improved targeting of NF200-expressing neurons enhances analgesia. However, enhanced targeting of CGRP-expressing neurons is likely beneficial as CGRP-expressing neurons are generally considered to be nociceptive.

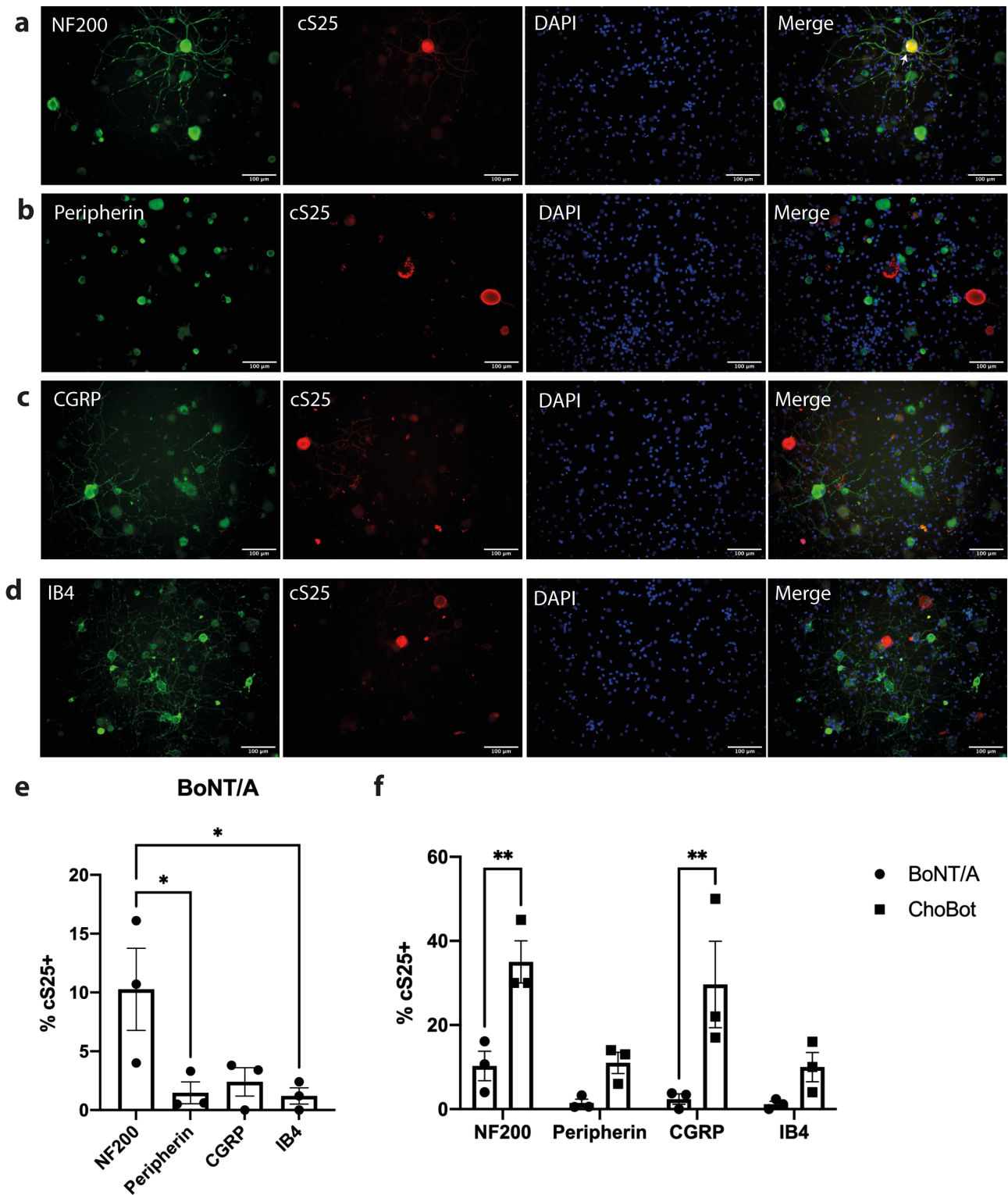


**Figure 4.11. Subtypes of sensory neurons susceptible to SNAP25 cleavage by BoNT/A.** Dorsal root ganglion cultures were treated with 0.1nM BoNT/A for 24 hours at 2 days in vitro (DIV), then fixed for immunocytochemistry at 3 DIV. Representative images showing cleaved SNAP25 (cS25) co-localisation with the markers of sensory neuron subpopulations: **(a)** NF200, **(b)** peripherin, **(c)** CGRP, **(d)** IB4. **Arrowheads show examples of colocalised neurons.** **e** The percentage of neurons in each subpopulation that were immunoreactive for cS25 was analysed, as defined by a cS25 intensity above the mean + 2 standard deviations of the untreated media and vehicle-only control conditions. N=3 cultures, 2 wells per condition, 6 images per well. NF200 n=381, peripherin n=563, CGRP n=146, IB4 n=338. Ordinary one-way ANOVA P=0.0311, followed by Tukey's multiple

comparisons test. NF200 vs peripherin  $P=0.0494$ , NF200 vs IB4  $P=0.0431$ . **f)** The percentages of each subpopulation to SNAP25 cleavage by either BoNT/A or ChoBot were directly compared. Two-way ANOVA of toxin and subpopulation marker, followed by Sidak's multiple comparisons test.  $**P<0.01$ . All figure data presented as mean  $\pm$  SEM.

#### 4.3.8 Paclitaxel co-applied with ChoBot does not widen the susceptible subpopulation

Published *in vivo* studies show an increased internalisation of CTB in more DRG neurons after neuropathic injury such as nerve transection, capsaicin or resiniferatoxin damage (Section 1.4.5.1). In order to understand whether ChoBot shares this mechanism, and therefore targets a wider population of DRG neurons in culture after an *in vitro* neuropathic insult, was investigated. *In vitro* paclitaxel exposure was combined with ChoBot intoxication to ascertain whether neuronal targeting is affected. If ChoBot targeting is the same as described by *in vivo* studies on CTB, it would be expected that in a neuropathic state a larger proportion of sensory neurons would have SNAP25 cleavage induced by ChoBot, and that this would be driven primarily by cleavage of SNAP25 in smaller diameter neurons.

In this initial experiment, 10 $\mu$ M paclitaxel or an equivalent DMSO concentration was applied at the same time as 1nM ChoBot. After 24 hours, the neurons were fixed and immunocytochemistry for  $\beta$ -III-tubulin and cS25 was carried out (Figure 4.12). The proportion of  $\beta$ -III-tubulin labelled cell bodies that were positive for cS25 was analysed. Data was plotted as the percentage of cS25-positive neurons within each image (Figure 4.12c) and as an averaged percentage per culture (Figure 4.12d). There was no significant difference in the proportion of DRG neurons that were susceptible to SNAP25 cleavage by ChoBot when paclitaxel was applied at the same time as ChoBot. This suggests that when paclitaxel is co-applied with ChoBot, paclitaxel is either not able to induce GM1 expression in a further subpopulation of neurons following damage (possibly due to already being maximal due to culture methods), or that ChoBot does not act like CTB in widening its susceptible subpopulation following damage.

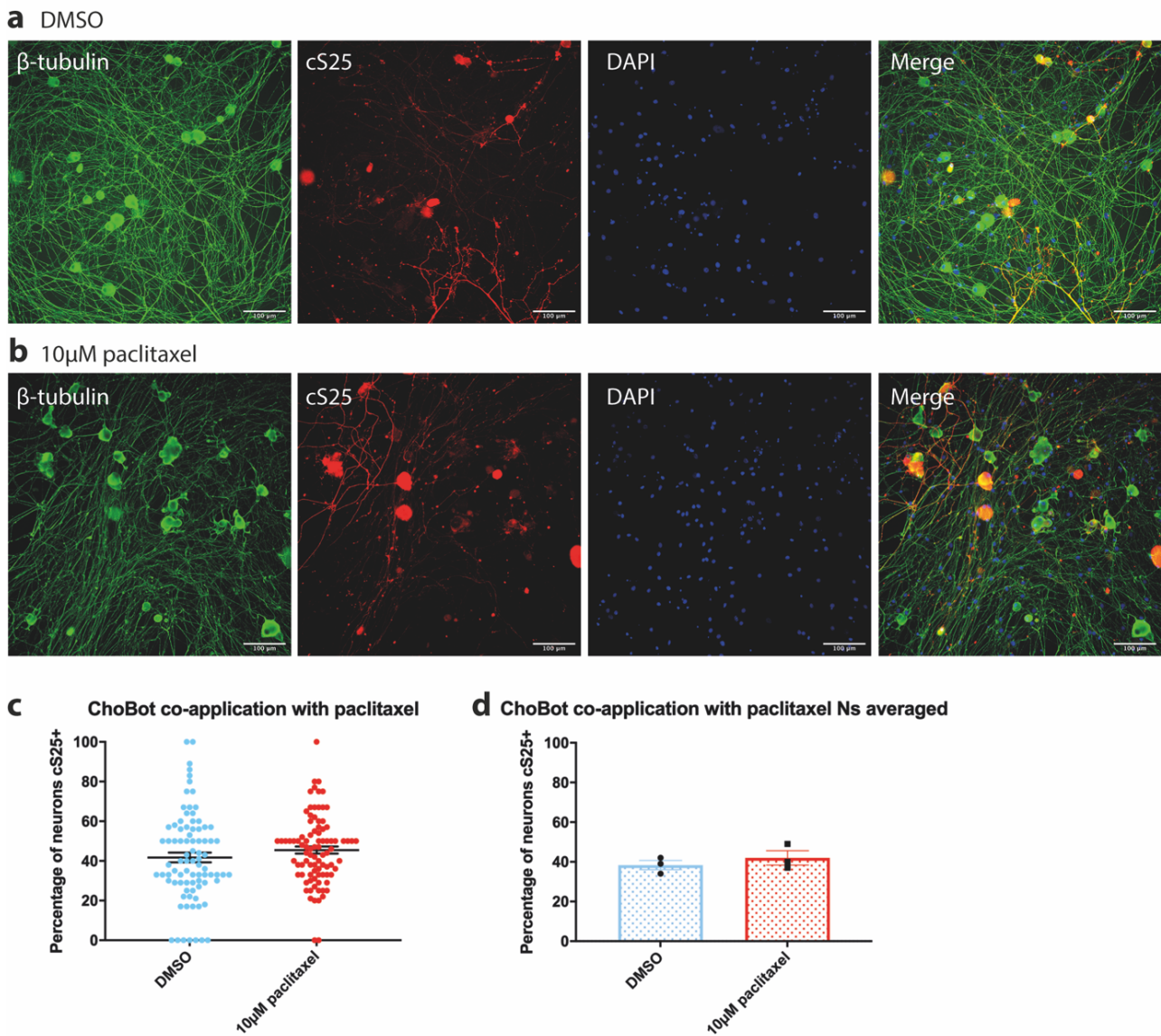


**Figure 4.12. The effect of paclitaxel co-application on SNAP25 cleavage by ChoBot. a,b)** Cultures at 6 days *in vitro* were treated with 10 $\mu$ M paclitaxel (or relevant DMSO concentration) alongside 1nM ChoBot for 24 hours before fixation. Representative images show the cleavage of SNAP25 in  $\beta$ -III-tubulin positive neurons in paclitaxel- or DMSO-treated conditions. **c)** The proportion of  $\beta$ -III-tubulin positive neurons that co-localised with cleaved SNAP25 was analysed, defined as a threshold intensity above the mean + 2 standard deviations of the untreated control intensities. The percentage of neurons positive for cS25 in each image was plotted. No significance of two-tailed paired *t* test. **d)** The data was then averaged to give a percentage for each separate culture. No significance of two-tailed paired *t* test. N=3 cultures, 2-3 wells per condition, 10-14 images per well. DMSO n=810, 10 $\mu$ M paclitaxel n=960. Data presented as mean  $\pm$  SEM.

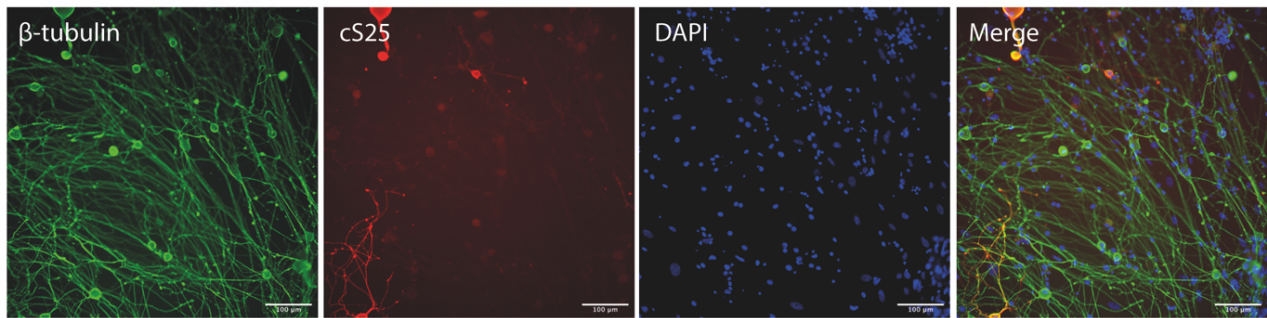
#### *4.3.9 Exposure to paclitaxel prior to ChoBot increases the proportion of neurons that are susceptible to cleavage of SNAP25*

As co-application of paclitaxel with ChoBot had no effect on the proportion of DRG neurons that become cS25 positive, it was investigated whether damage and subsequent downstream mechanisms may be required to be induced prior to ChoBot application in order to enhance uptake of the toxin. A 24 hour pre-treatment with paclitaxel was therefore applied prior to ChoBot application. Neurons were either treated with paclitaxel for 24 hours then the paclitaxel was removed and ChoBot was applied for 24 hours, or paclitaxel was applied for 24 hours then ChoBot and paclitaxel were applied together for 24 hours. The DRG were then fixed and stained for  $\beta$ -III-tubulin and cS25 as before (Figure 4.13).

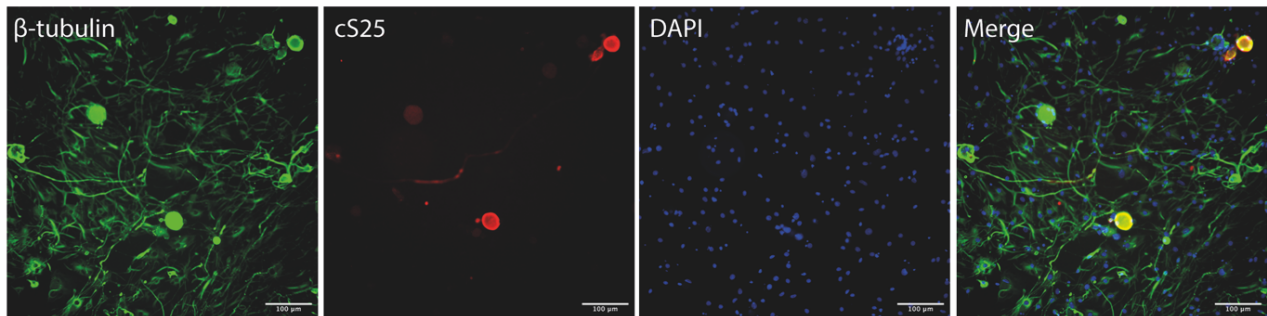
In both the paclitaxel-exposed conditions (24 and 48 hours) there was a small but significant increase in the proportion of cS25-positive neurons when the percentage per image was plotted (Figure 4.13d). 47% of the neurons were cS25 positive in the DMSO control condition, compared to 57% and 56% in the 24 and 48 hour paclitaxel conditions. However, when the percentages for each individual culture were plotted, this small increase was not significant (Figure 4.13e).

In order to test whether this effect was specific to ChoBot or was due to a more general effect of BoNT action or an artefact of immunocytochemistry, the same experiment was performed with the stapled BoNT/A analogue BitoxAA (Figure 4.14a). BitoxAA is formed by stapling of the BoNT/A light chain to a duplicated BoNT/A receptor binding and translocation domain (Section 2.3). With this toxin, there was no significant increase in the proportion of cS25-positive neurons in paclitaxel-treated conditions, whether the percentages for each individual image (Figure 4.14b) or the average were plotted (Figure 4.14c).

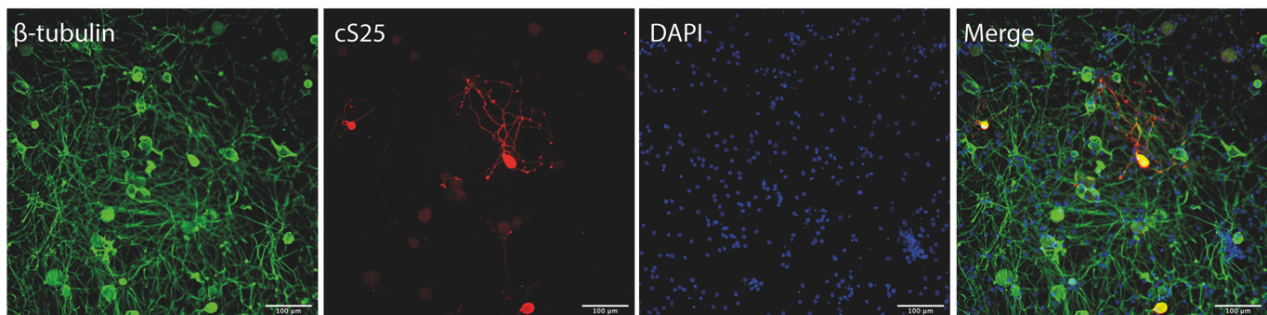
**a** DMSO



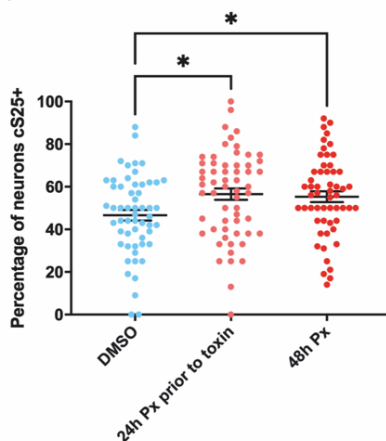
**b** 24h Px prior to toxin



**c** 48h Px



**d** ChoBot after paclitaxel treatment



**e**

ChoBot after paclitaxel treatment Ns averaged

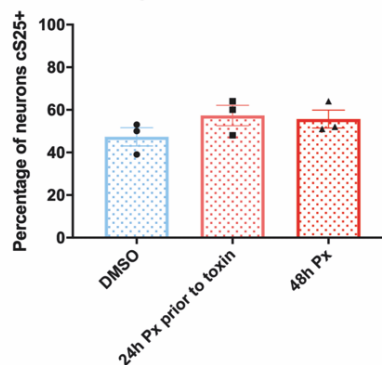


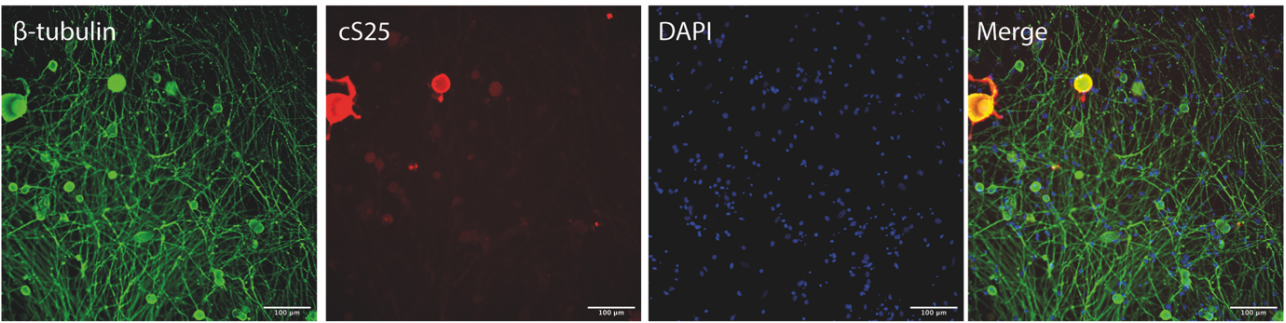
**Figure 4.13. Effect of paclitaxel pre-treatment on SNAP25 cleavage by ChoBot.** Cultures at 6 days *in vitro* were treated with 10 $\mu$ M paclitaxel. 24 hours later this was removed and they were then treated with ChoBot and DMSO (**b**, 24h Px prior to toxin), or Chobot and paclitaxel (**c**, 48h Px) for another 24 hours before fixation. Control conditions had 48 hours of DMSO exposure (**a**, DMSO). Representative images show the cleavage of SNAP25 in  $\beta$ -III-tubulin positive neurons in these conditions. **d**) The proportion of  $\beta$ -III-tubulin positive neurons that were co-localised with cleaved SNAP25 was analysed, defined as a threshold intensity above the mean + 2 standard deviations of

*the untreated control intensities. The percentage of neurons positive for cS25 in each image was plotted. Ordinary one-way ANOVA  $P=0.0128$ . Followed by Dunnett's multiple comparisons test, comparing each concentration to the DMSO control. 24h Px prior to toxin  $P=0.0120$ , 48h Px  $P=0.0346$ . e) The data was then averaged to give a percentage for each separate culture. No significance of ordinary one-way ANOVA.  $N=3$  cultures, 2 wells per condition, 10-12 images per well. DMSO  $n=1051$ , 24h Px prior to toxin  $n=690$ , 48h Px  $n=659$ . Data presented as mean  $\pm$  SEM. \*  $P<0.05$ .*

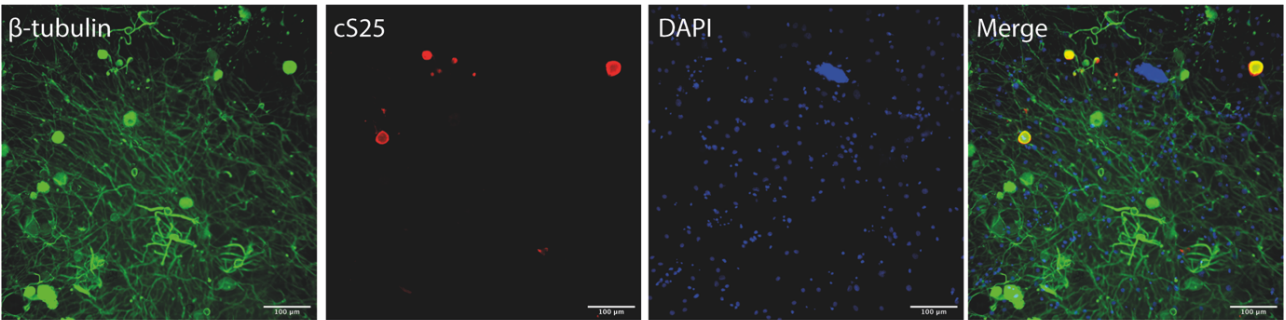
As no damage-related effect was detected with BitoxAA it is likely that the increased cleavage of SNAP25 detected with ChoBot is directly due to its receptor binding CTB domain, rather than a general effect of stapled BoNTs, experimental bias or artefacts. It therefore seems plausible that paclitaxel is increasing GM1 expression and ChoBot uptake in a small additional percentage of DRG neurons *in vitro*.

However, the effect of paclitaxel on increased ChoBot targeting shown in this experiment is much more subtle than the published data on increased CTB targeting of DRG neurons after damage. There are a few potential explanations for this. One is that the *in vitro* paclitaxel model used may not be as damaging as its *in vivo* counterparts, or that the mechanism increasing uptake is not conserved *in vitro*. Another is that, as discussed in the previous chapter, DRG cultures may be a better model of neuropathic injury than the naïve state due to the stress and damage caused by axotomy and dissociation (Section 3.3.1). Paclitaxel may only induce a small additional effect on an already neuropathic model, failing to induce a significant additional neuropathic effect.

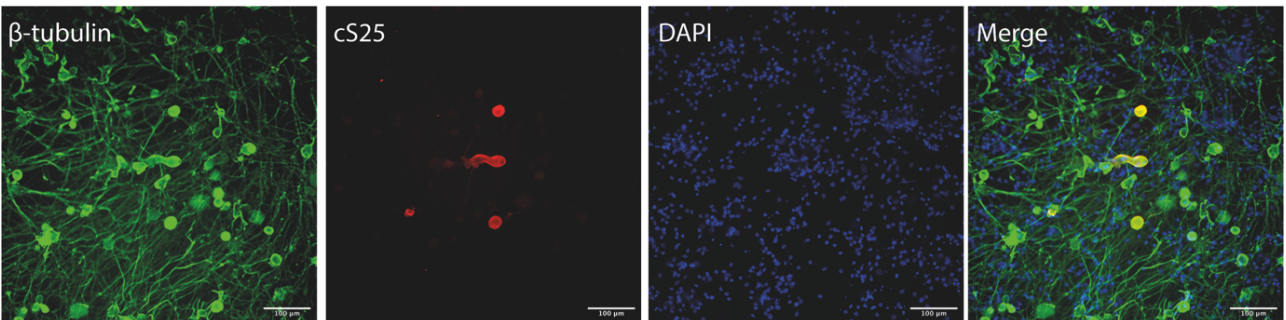
**a** DMSO



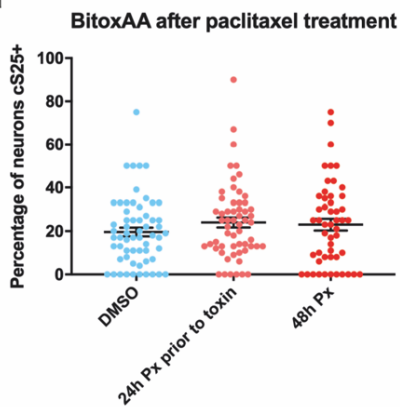
**b** 24h Px prior to toxin



**c** 48h Px



**d**



**e**

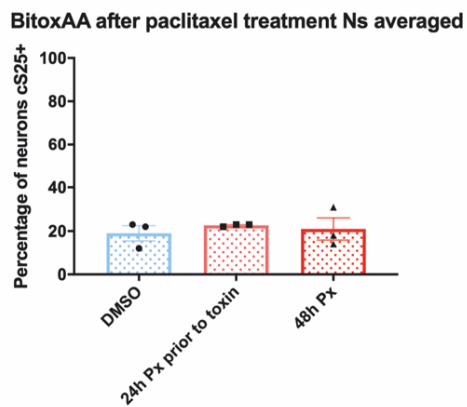


**Figure 4.14. Effect of paclitaxel pre-treatment on SNAP25 cleavage by BitoxAA.** Cultures at 6 days *in vitro* were treated with 10 $\mu$ M paclitaxel. 24 hours later this was removed and they were then treated with 2nM BitoxAA and DMSO (**b**, 24h Px prior to toxin), or BitoxAA and paclitaxel (**c**, 48h Px) for another 24 hours before fixation. Control conditions had 48 hours of DMSO exposure (**a**, DMSO). Representative images show the cleavage of SNAP25 in  $\beta$ -III-tubulin positive neurons in these conditions. **d**) The proportion of  $\beta$ -III-tubulin positive neurons that were co-localised with cleaved SNAP25 was analysed, defined as a threshold intensity above the mean + 2 standard

deviations of the untreated control intensities. The percentage of neurons positive for cS25 in each image was plotted. No significance of ordinary one-way ANOVA. e) The data was then averaged to give a percentage for each separate culture. No significance of ordinary one-way ANOVA. N=3 cultures, 2 wells per condition, 10-12 images per well. DMSO n=822, 24h Px prior to toxin n=724, 48h Px n=686. Data presented as mean  $\pm$  SEM.

#### 4.4 Discussion

Initial experiments in this chapter confirmed the expression of GM1 and the ability of rat DRG neurons in culture to bind fluorescent CTB. It was therefore worthwhile to investigate whether ChoBot, a novel chimera of BoNT/A with a CTB receptor-binding domain, is functional in the same neurons and predict its likelihood as a successful analgesic. Functionality of a BoNT in this situation depends on successful membrane and vesicle receptor binding, membrane translocation to the cytosol via the translocation domain pore, expression of the cleavage substrate in the neuron, and the proteolytic cleavage of that substrate by the light chain (Lacy et al., 1998; Rummel, 2013). After 24 hours of exposure to ChoBot in the media, it is clear that a distinct subpopulation of DRG neurons become immunoreactive for cS25, demonstrating that ChoBot is functional *in vitro*. It also cleaved SNAP25 in a larger percentage of neurons than BoNT/A. Depending on the additional neurons intoxicated, this may lead to improved analgesia by ChoBot than the most commonly used BoNT in clinic.

A comparison of the subpopulation subtypes affected by BoNT/A and ChoBot was performed. ChoBot caused cleavage of SNAP25 in a significantly higher proportion of NF200-expressing and CGRP-expressing DRG neurons than BoNT/A. NF200, a marker of myelination, is expressed by the A $\beta$  and A $\delta$  subpopulations of neurons. Although low threshold mechanoreceptors fall into this category, it also includes high threshold and large dynamic range mechanoreceptors as well as thermal nociceptors, particularly in the A $\delta$  subpopulation (Adelman et al., 2019; Treede et al., 1998). The targeting of this population may also explain the high cS25 rate in CGRP-positive neurons, and the ability of ChoBot to inhibit depolarisation-evoked CGRP release. Although CGRP is often expressed by neurons in the peptidergic C-fibre population, substance P expression is considered a better marker. This is because CGRP has also been shown to be expressed by a significant proportion (approximately 40%) of myelinated A $\delta$ -fibre neurons (Ruscheweyh et al., 2007). As a novel toxin, from these experiments the analgesic potential of ChoBot isn't clear. The DRG neurons targeted may indeed include nociceptive subpopulations, especially considering the

enhanced targeting of CGRP-expressing neurons. However, the high SNAP25 cleavage rate in myelinated neurons could theoretically affect low threshold mechanoreceptors. If neuronal silencing is achieved by ChoBot in these mechanoreceptors then this would impair touch sensation, which could be a barrier to clinical acceptance.

The experiments in this chapter showed a low rate of SNAP25 cleavage by BoNT/A in CGRP-expressing populations, at less than 3%. However, publications report successful inhibition of potassium-evoked CGRP release by BoNT/A, at least in cultured trigeminal sensory neurons (Meng et al., 2007; Meng et al., 2009). This chapter did not investigate the ability of BoNT/A to inhibit CGRP release from cultures due to the low targeting efficacy shown by immunocytochemistry, and high likelihood of failure. The disconnect between the literature and the targeting of BoNT/A in this chapter's experiments may be due to trigeminal cultures versus DRG cultures. The vast majority of trigeminal neurons are reported to express CGRP (Meng et al., 2007). However, CGRP is expressed in only a small subpopulation of DRG neurons. This may account for a large enough effect size to be demonstrated by inefficient targeting of a large population of neurons in trigeminal cultures, but would be unlikely to be observed in the small subpopulation of CGRP-expressing DRG neurons.

One interesting finding from this chapter was the observation of the BoNT/A, /C and /E target protein, SNAP25, being differentially expressed by different subpopulations of DRG neurons. This has ramifications for analgesia using SNAP25-cleaving BoNTs. Using immunocytochemistry, the experiments in this chapter provided evidence for decreased SNAP25 expression in the peripheral-expressing class of DRG neurons compared to the total population. In order to confirm and understand this differential expression further in different subpopulations, a publicly available single cell RNA-seq dataset was utilised (Usoskin et al., 2015). In agreement with the experiments in this chapter, the expression of SNAP25 differed across subpopulations, and was highest in the NF (NF200-expressing) class compared to the nociceptive classes (NP and PEP) (Figure 4.15). Bearing this in mind, a SNAP25-cleaving BoNT may not be ideal as an analgesic, as the myelinated, less nociceptive DRG neurons have the highest expression of its target protein. A VAMP2-cleaving light chain (such as BoNT/B or /F) may be more useful as the expression of this SNARE protein is more equally distributed over the subpopulations (Figure 4.15).

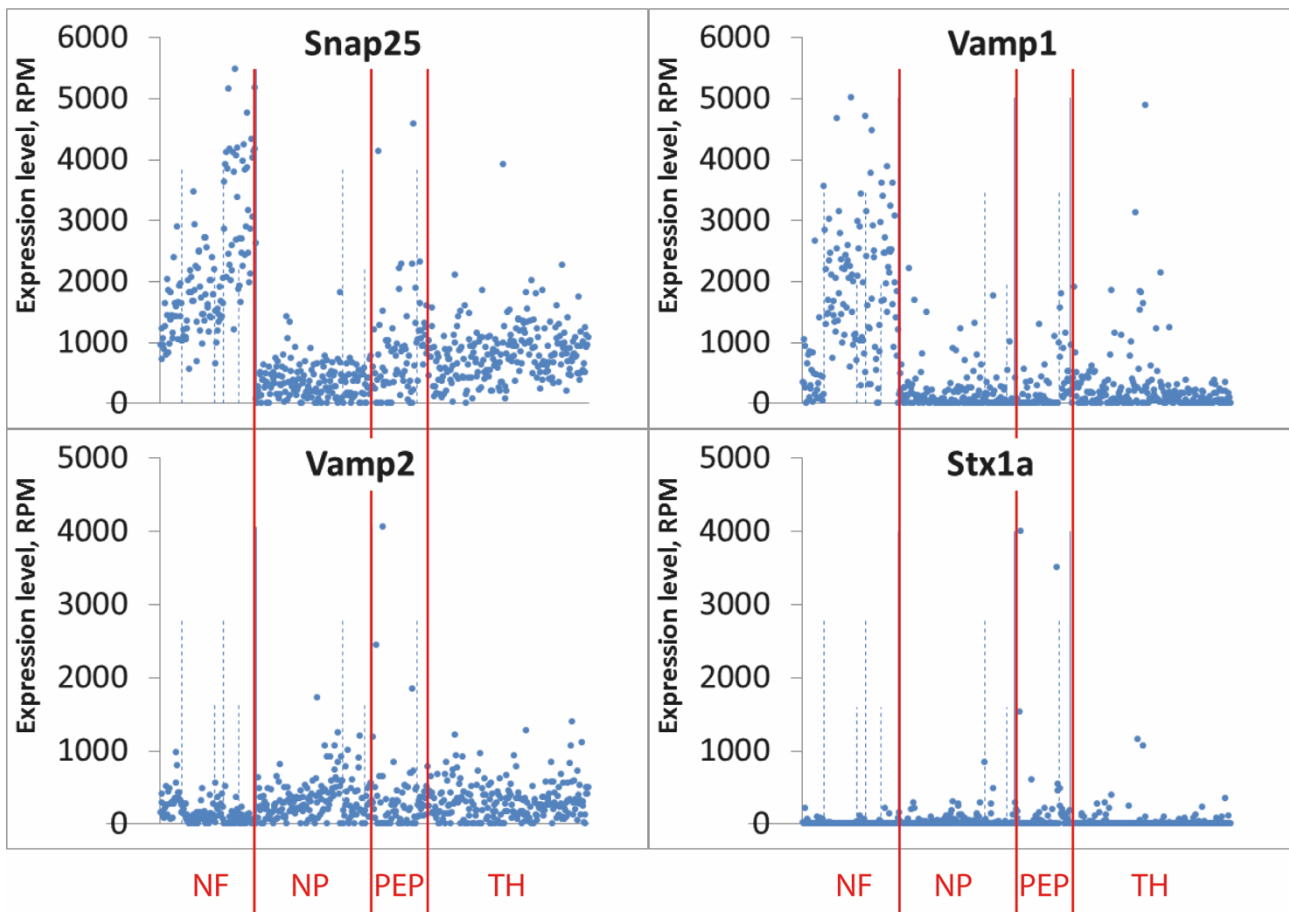


**Figure 4.15. Distribution of SNARE RNA expression in dorsal root ganglion subpopulations.** Reads-per-million (RPM) of RNA encoding different BoNT-sensitive SNARE proteins in single mouse dorsal root ganglion neurons. Vertical lines separate the major subtypes, neurofilament containing (NF), non-peptidergic nociceptors (NP), peptidergic nociceptors (PEP) and tyrosine hydroxylase containing (TH). Data and figure adapted from Usoskin et al., 2015.

Another question arising about the action of ChoBot is whether it retains the same properties as CTB binding following neuropathic injury, in that new subpopulations of DRG neurons become susceptible after nerve injury. It appears that there is a small but significantly increased proportion of DRG neurons becoming intoxicated by ChoBot following exposure to the CIPN-inducing drug paclitaxel. The mechanisms governing enhanced uptake of CTB in a wider population of DRG neurons following nerve injury haven't been well investigated in the literature. It therefore isn't clear if enhanced targeting is specifically localised to damaged sensory neurons or if enhanced targeting is being induced by a more global effect. If the GM1 ganglioside is upregulated specifically in damaged, hyperexcitable DRG neurons and ChoBot is preferentially targeting these neurons then this could potentially be a very beneficial prospect in an analgesic. Even if this is not the case, these experiments show that ChoBot has more widespread targeting of rat sensory neurons *in vitro* than BoNT/A. ChoBot's potency at the neuromuscular junction will next be

assessed in order to further understand its potential utility as a peripherally administered analgesic.

## 5. *Comparison of the paralytic properties of native and engineered botulinum toxins*

### 5.1 *Introduction*

Muscle contraction is initiated when an action potential reaches the presynaptic terminal of a motor neuron. The voltage change activates VGCCs, allowing the influx of calcium ions into the presynaptic terminal, triggering the release of acetylcholine into the synapse and subsequent depolarisation and contraction of the associated muscle fibre. Exocytotic release of acetylcholine is dependent on formation of the SNARE protein coiled coil to bring the vesicle into apposition with the membrane to fuse and release its contents (Martyn et al., 2009). This pathway is the natural target of native BoNTs which induce flaccid muscle paralysis by the proteolytic cleavage of SNARE proteins. Which SNARE is targeted depends on the particular BoNT isoform.

For pain management, the paralysis of muscles is the biggest drawback of BoNT use as it limits the therapeutic doses that can be safely used in clinic. When developing novel BoNTs it is therefore essential to understand the safe therapeutic dose window. It is also necessary to understand how analgesia correlates with paralysis, and whether a toxin can be produced that has increased potency in terms of analgesia without increased potency at the neuromuscular junction.

The postsynaptic activity of muscle fibres can be measured quantitatively with electromyography. The CMAP is the current generated by the simultaneous depolarisation of many muscle fibres in the same area. This depolarisation can be induced by electrical stimulation of the motor nerve innervating the muscle. The amplitude of the CMAP response is proportional to the number of muscle fibres activated (Karup, 1983). When stimulation current is large enough to elicit the maximal response possible, the CMAP amplitude is proportional to the number of functional muscle fibres present. Supramaximal CMAP amplitude has therefore been used to assess the paralytic effect of botulinum toxin injection in a quantitative manner.

The gold standard method of measuring potency of BoNTs is by measuring the intraperitoneal dose required to kill 50% of a cohort of mice, the LD<sub>50</sub>. There are other behavioural assays such as the digital abduction score (DAS) assay which involves scoring a startle-induced flexion of the

hindpaw following an intramuscular injection of BoNT on a scale of 0-4 (Broide et al., 2013). However, CMAP amplitude measurements are much more aligned to modern 3Rs principles of animal research compared to the LD<sub>50</sub>, and are more sensitive and informative compared to DAS assay scoring.

There have been no published studies using CMAP amplitude to compare different BoNT serotypes or to better understand novel or retargeted toxins. To date, all studies using CMAP amplitudes examined the effect of BoNT/A (BOTOX) as a toxicity assay to replace the traditional LD<sub>50</sub> injection test (Cichon et al., 1995; Sakamoto et al., 2009; Torri et al., 2014). These experiments involve the injection of BoNT/A into the large gastrocnemius muscle of the hindleg of rats. The gastrocnemius is then stimulated by current flow through electrodes placed either by the spinal cord or the sciatic nerve. Supramaximal stimulation voltages are determined and the CMAP amplitude is recorded.

As these studies use BoNT/A, the doses are reported in Units (U), a specific measure of potency which is tested for each batch. 1U is defined as the LD<sub>50</sub> (the dose lethal to 50% of the animals in the study) following intraperitoneal injection **in a cohort of mice** (Jankovic, 2004). Doses used in CMAP studies **in rat** range from 0.01U to 30U, **higher than the LD<sub>50</sub> in mice due to their larger size and peripheral administration of toxin** (Table 5.1). CMAP amplitude is reduced significantly by 24 hours post-injection of BoNT/A (approximately 80% to the final maximum reduction achieved at 4 days), with a maximum reduction reached by 4 days that remains static until at least 10 days post-injection (Cichon et al., 1995; Sakamoto et al., 2009).

Publication	Range	Dose (Units, U)	Approximate CMAP change (mV)
Cichon et al., 1995	Minimum dose	0.5	38 to 8
	Maximum dose	5	38 to 3
Sakamoto et al., 2009	Minimum dose	0.01	74 to 65
	Maximum dose	30	70 to 2
Torri et al., 2014	Minimum dose	0.04	60 to 52
	Maximum dose	1.28	60 to 8

**Table 5.1. BoNT/A doses used in published compound muscle action potential studies.**

## 5.2 Summary and objectives

A primary aim of this project was to assess the utility of novel BoNTs as non-paralytic analgesics. The aim of this chapter therefore is to quantify and compare the paralytic activity of native and retargeted toxins using CMAP amplitude measurements. This is the first data using this technique to compare native BoNT serotypes, BoNT/A and BoNT/C. It also aims to understand the neuromuscular activity of the novel stapled toxins Bitox/AA and ChoBot and how they compare to the native toxins.

Research aim:

- To compare the neuromuscular blocking ability of various native and stapled BoNTs in a quantitative manner using CMAP recordings.

## 5.3 Results

### 5.3.1 Effect of BoNT/A injection on compound muscle action potential amplitude

As BoNT/A is the most commonly used BoNT clinically, its effect on the gastrocnemius CMAP amplitude was first investigated. This was to allow subsequent comparison to other BoNT serotypes as well as novel stapled BoNTs. BoNT/A was purchased as an isolated toxin (150kDa) from Metabionics. Injection doses increased on a half  $\log_{10}$  scale. In order to allow comparisons in true concentrations, the activity Unit (U) was converted to amount of toxin in picograms (Table 5.2).

Amount injected in Units (U)	Amount injected in picograms
2	7.4
6.3	23.3
20	74
63	233

**Table 5.2. BoNT/A doses used in this chapter in Units and picograms.**

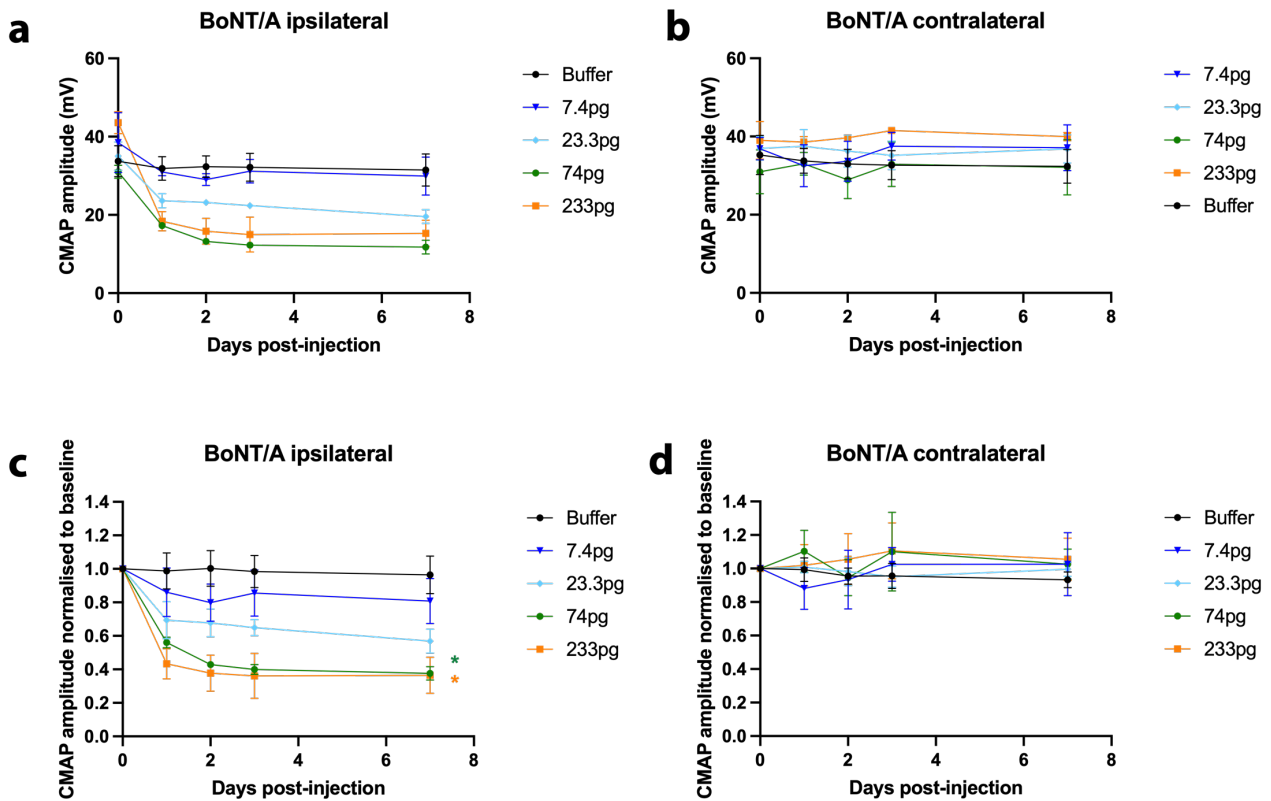


**Figure 5.1. Compound muscle action potential recordings following a subcutaneous injection of BoNT/A over the gastrocnemius muscle.** Recordings from the belly of both left and right medial gastrocnemius muscles were made during a supramaximal electrical stimulation of the muscle. **a, b)** The amplitude of the compound muscle action potential (CMAP) of both gastrocnemius muscles was measured immediately prior to and at intervals following a single subcutaneous injection of BoNT/A above the left (ipsilateral) gastrocnemius. **c,d)** The amplitude of the CMAP for each day post-injection was normalised to each individual animal's baseline CMAP amplitude pre-injection for the injected and contralateral leg. Repeated measures two-way ANOVA of time and toxin, followed by Dunnett's multiple comparisons test to buffer control, reported on graph for 7 days post-injection. No significance of repeated measures two-way ANOVA of contralateral CMAPs.  $N=5$  for buffer control,  $N=3$  for all other concentrations. Data presented as mean  $\pm$  SEM. \*\*\* $P<0.001$  \* $P<0.05$ .

Naïve, baseline CMAP amplitudes lay in the 30-45mV range for all animals tested. This is on the same order of magnitude as reported in the literature, and is particularly close to reported in Cichon et al., 1995 (Table 5.1). Immediately after baseline recordings, toxin was injected subcutaneously above the area of gastrocnemius muscle being recorded from. BoNT/A reduced the amplitude of the CMAP in a dose- and time-dependent manner, with a decrease clearly observable within 24h post-injection, increasing to a maximum 3 days after injection, a timescale which also matches that reported in the literature (Figure 5.1a,c). No effect was present when recording from the gastrocnemius of the un-injected contralateral leg (Figure 5.1b,d).

One discrepancy between the published effect of BoNT/A and the results of this thesis are the doses shown to affect CMAP amplitude. One publication showed that 0.5U reduced the CMAP amplitude to roughly 21% of baseline (Cichon et al., 1995) and another showed a reduction to approximately 71% of baseline with an injection of 0.03U (Sakamoto et al., 2009). Another publication reported a significant reduction beginning at 0.04U (Torri et al., 2014). The amounts of BoNT/A used in this chapter are significantly higher than this, with 6.3U (23.3pg) required to significantly reduce CMAP compared to control. The dose required to reduce the CMAP to 50% was approximately 0.1U in one report (Sakamoto et al., 2009) and 0.19U in another (Torri et al., 2014). This is in comparison to 17U (63pg) in the experiments in this chapter (Table 5.3). Potential causes of this discrepancy are the addition of human serum albumin to the toxin in the published studies, in order to stabilise the neurotoxin complex and prevent binding to surfaces (Malhotra et al., 2003). The injections of toxin in this chapter were given subcutaneously rather than intramuscularly directly into the gastrocnemius as in the published literature, due to limitations of the animal project licence these experiments were performed under. Either one of these could increase the amount of BoNT/A required to see an effect on CMAP amplitude. However, toxin formulation and injection site were kept consistent throughout all the experiments in this chapter, still allowing direct comparison between different toxins.

### 5.3.2 *Effect of Bitox/AA injection on compound muscle action potential amplitude*

The stapled BoNT/A analogue with duplicated receptor binding domain, Bitox/AA (Section 2.3), was injected into the hindleg and the CMAP was recorded. This comparison to BoNT/A was used to investigate whether the stapling reaction decreases potency, or whether duplication of the targeting domain increases potency compared to native BoNT/A. Doses that had a significant effect on the CMAP ranged from 16 to 160ng (Figure 5.2a,c). 1.6ng was sufficient to induce a decrease to approximately 60% of the baseline CMAP amplitude. This is approximately 100-fold higher than required for a similar CMAP amplitude reduction using BoNT/A, suggesting decreased potency of Bitox/AA at the neuromuscular junction compared to native toxin, presumably due to some property of the protein staple. The amplitude decreased further with increasing dose. There was no significant effect on the contralateral muscle (Figure 5.2b,d).

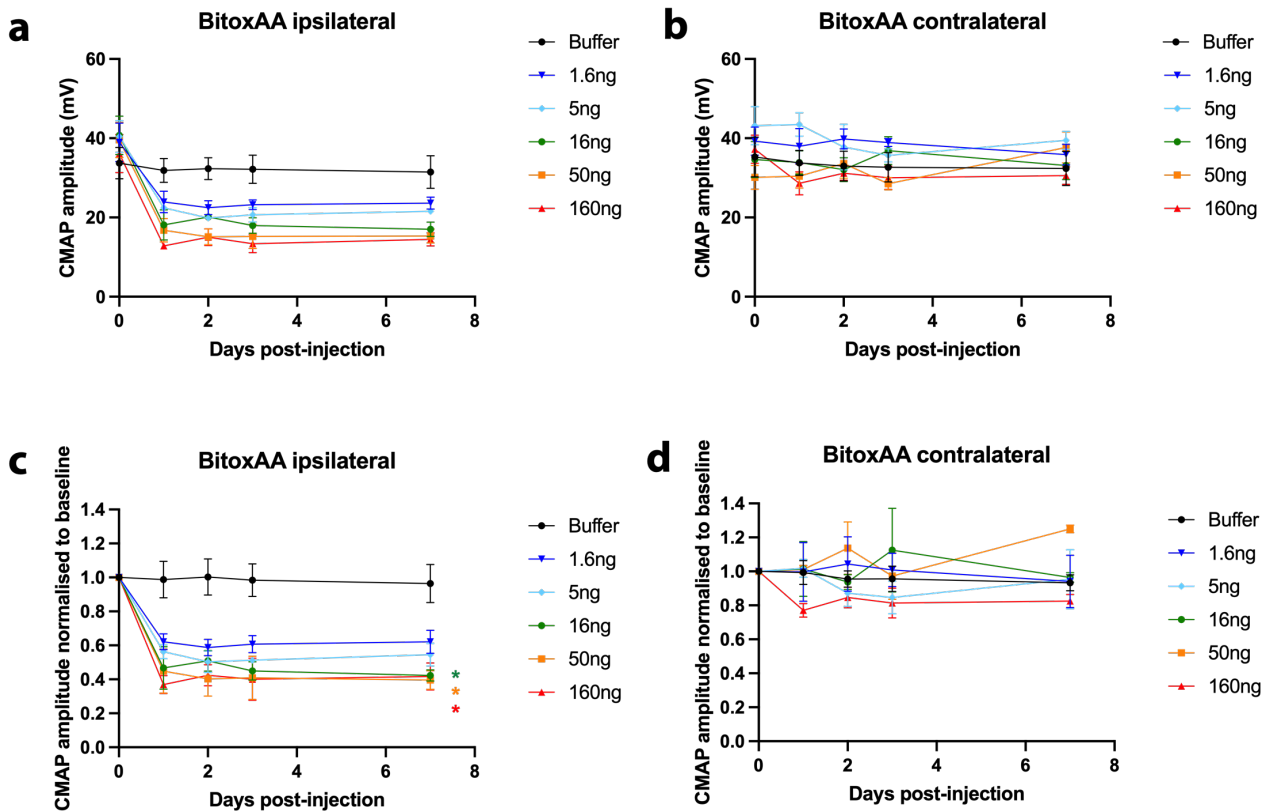


**Figure 5.2. Compound muscle action potential recordings following a subcutaneous injection of Bitox/AA over the gastrocnemius muscle.** Recordings from the belly of both left and right medial gastrocnemius muscles were made during a supramaximal electrical stimulation of the muscle. **a, b)** The amplitude of the compound muscle action potential (CMAP) of both gastrocnemius muscles was measured immediately prior to and at intervals following a single subcutaneous injection of Bitox/AA above the left (ipsilateral) gastrocnemius. **c, d)** The amplitude of the CMAP for each day post-injection was normalised to each individual animal's baseline CMAP amplitude pre-injection for the injected and contralateral leg. Repeated measures two-way ANOVA of time and toxin, followed by Dunnett's multiple comparisons test to buffer control, reported on graph for 7 days post-injection. No significance of repeated measures two-way ANOVA of contralateral CMAPs. N=5 for buffer control, N=3 for all other concentrations. Data presented as mean  $\pm$  SEM. \*\*P<0.01 \* P<0.05

### 5.3.3 Effect of BoNT/C injection on compound muscle action potential amplitude

The ability of the native BoNT serotype BoNT/C to inhibit the CMAP was next evaluated. BoNT/C was produced as an isolated toxin (150kDa) that was purified by the Binz lab. BoNT/C cleaves two SNARE proteins, SNAP25 and syntaxin. Whether the potency of this toxin at the neuromuscular junction differs from BoNT/A (which cleaves only SNAP25) was investigated.

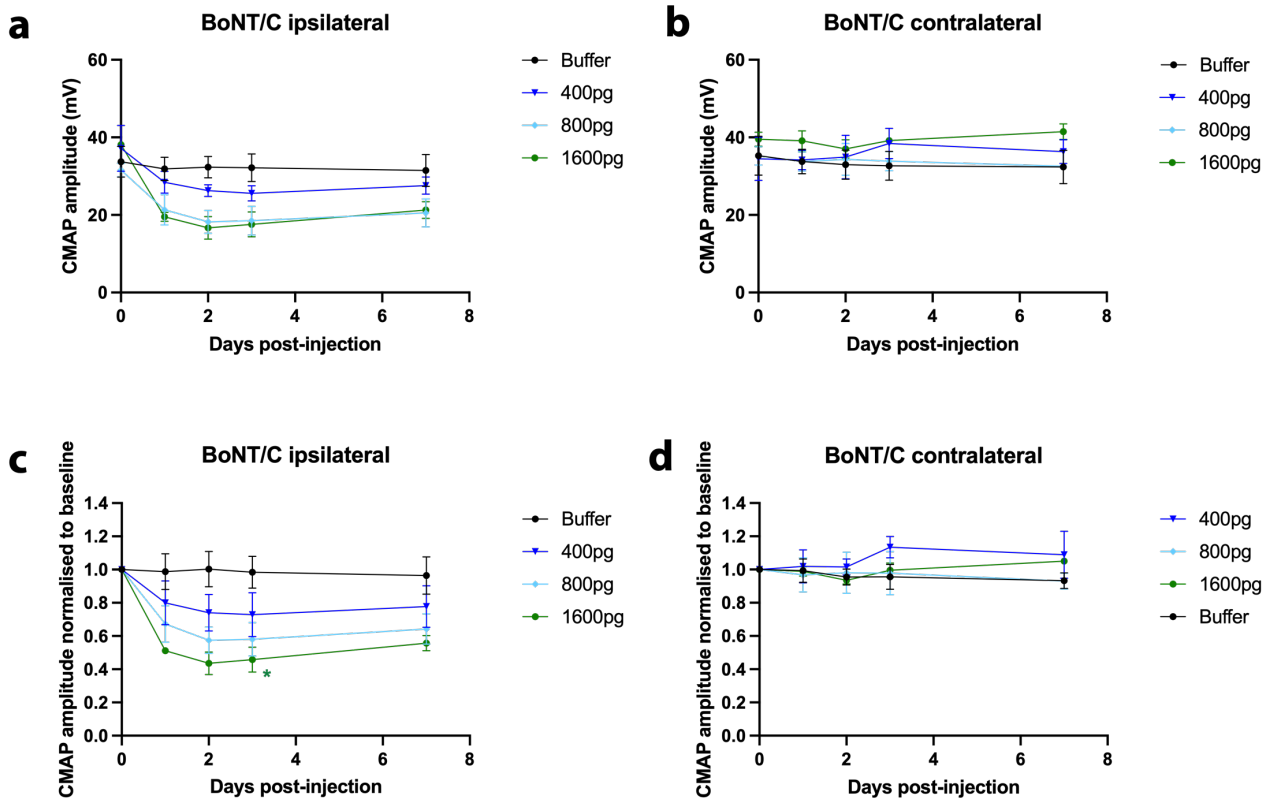


**Figure 5.3. Compound muscle action potential recordings following a subcutaneous injection of BoNT/C over the gastrocnemius muscle.** Recordings from the belly of both left and right medial gastrocnemius muscles were made during a supramaximal electrical stimulation of the muscle. **a, b)** The amplitude of the compound muscle action potential (CMAP) of both gastrocnemius muscles was measured immediately prior to and at intervals following a single subcutaneous injection of BoNT/C above the left (ipsilateral) gastrocnemius. **c, d)** The amplitude of the CMAP for each day post-injection was normalised to each individual animal's baseline CMAP amplitude pre-injection for the injected and contralateral leg. Repeated measures two-way ANOVA of time and toxin, followed by Dunnett's multiple comparisons test to buffer control, reported on graph for 3 days post-injection. No significance of repeated measures two-way ANOVA of contralateral CMAPs.  $N=5$  for buffer control,  $N=3$  for all other concentrations. Data presented as mean  $\pm$  SEM.

BoNT/C doses from 400 to 1600pg were shown to decrease the CMAP amplitude in a dose dependent manner, with 1600pg being significantly different from buffer at 3 days post-injection (Figure 5.3a,c). This is significantly less potent than BoNT/A which showed CMAP inhibition at the much lower dose of 74pg. Again, there was no effect on the contralateral side (Figure 5.3b,d). However, none of the concentrations of toxin caused a significant reduction of the CMAP from buffer control by 7 days. On the ipsilateral side, the CMAP reduction appears to already be reversing back towards baseline at just 7 days post-injection, an effect not observed with any of the other toxins in this chapter. This suggests a shorter duration of action of neuromuscular blockade by BoNT/C. This may be due to the different light chain of BoNT/C, as all other toxins investigated in this chapter contain the light chain of BoNT/A. Whether this is an effect of syntaxin

cleavage reversal compared to just SNAP25 cleavage reversal, or whether this is due to the BoNT/C light chain cleaving only 8 amino acids from SNAP25 compared to the 9 cleaved by BoNT/A is unclear (von Berg et al., 2019).

#### *5.3.4 Effect of ChoBot injection on compound muscle action potential amplitude*

ChoBot was also assessed for its potency to block the neuromuscular junction. ChoBot is the only toxin assessed in this chapter which does not contain the receptor binding domain of a native BoNT, instead carrying the cholera toxin receptor binding domain which targets the GM1 ganglioside (Section 2.3). ChoBot was the least neuromuscular blocking toxin assessed, with doses of 630ng inducing only a reduction to approximately 70% of the baseline CMAP amplitude in the ipsilateral leg, an effect too small to be significantly different from buffer injection (Figure 5.4a,c).

200pg appeared to have a small effect on the CMAP at 1 and 2 days post-injection, but this was no longer present at 3 days. ChoBot activity was unique in that as the dose injected increased, there was no subsequent further reduction to CMAP amplitude. All 3 concentrations from 63ng to 630ng induced a reduction to roughly 60-70% of the baseline CMAP amplitude. Saturation at the neuromuscular junction may have already been reached by the relatively high dose of 63ng (compared to other toxins), but that this saturation is limited to only a partial reduction of CMAP amplitude. This could be attributed to the GM1-targeting ability of ChoBot cleaving SNAP25 in just a subpopulation of motor neurons, compared to non-selective specificity of the native toxin specificity to the pre-synapses of all neuromuscular junctions.

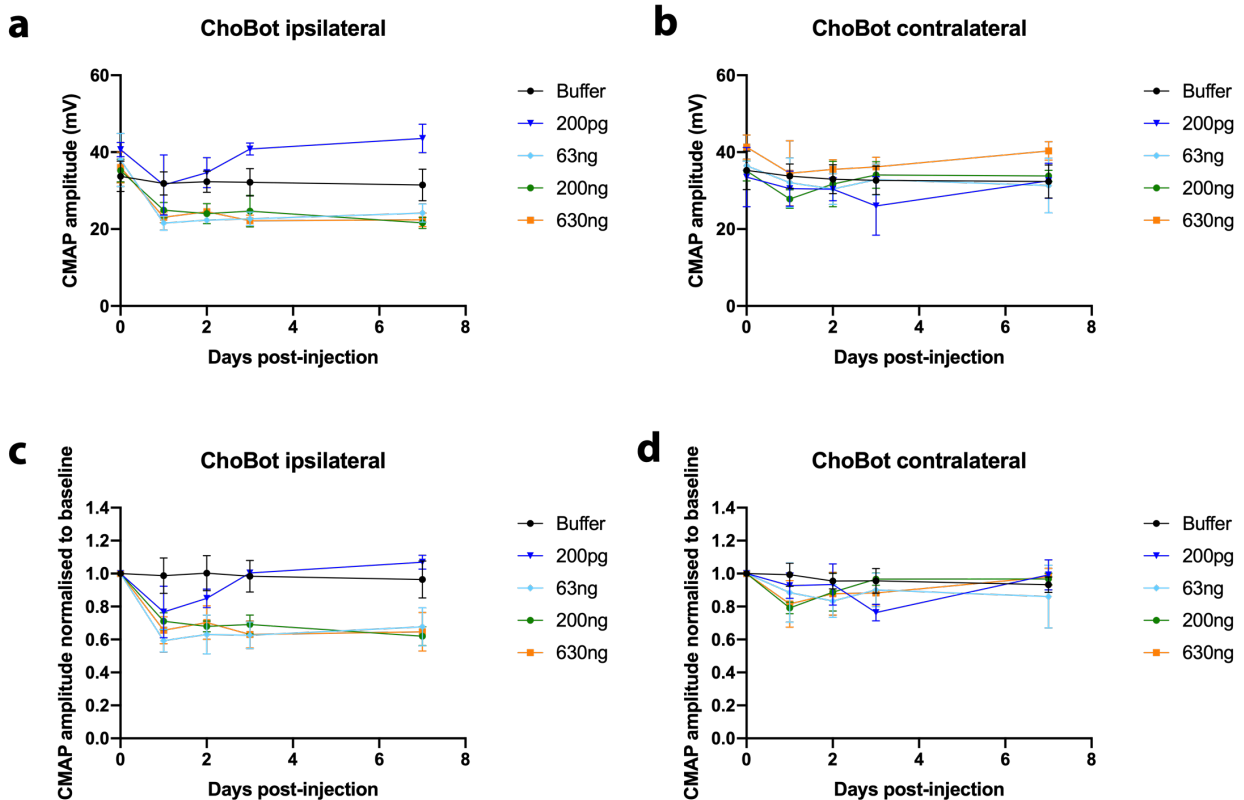


**Figure 5.4. Compound muscle action potential recordings following a subcutaneous injection of ChoBot over the gastrocnemius muscle.** Recordings from the belly of both left and right medial gastrocnemius muscles were made during a supramaximal electrical stimulation of the muscle. **a, b)** The amplitude of the compound muscle action potential (CMAP) of both gastrocnemius muscles was measured immediately prior to and at intervals following a single subcutaneous injection of ChoBot above the left (ipsilateral) gastrocnemius. **c, d)** The amplitude of the CMAP for each day post-injection was normalised to each individual animal's baseline CMAP amplitude pre-injection for the injected and contralateral leg. **No effect of toxin on repeated measures two-way ANOVA of time and toxin. No significance of repeated measures two-way ANOVA of contralateral CMAPs.**  $N=5$  for buffer control,  $N=3$  for all other concentrations except  $N=2$  for 200pg. Data presented as mean  $\pm$  SEM.

### 5.3.5 Comparison of the effect of native and engineered botulinum toxins on the compound muscle action potential

In order to more easily compare the specificity and potency of the toxins investigated in this chapter, the normalised CMAP amplitudes for each concentration of each toxin were plotted on a logarithmic scale of concentration (Figure 5.5). Although a full dose response up to complete paralysis was not performed due to ethical reasons, a linear regression analysis was applied as a rough guide of potency for each toxin. This was plotted for the CMAPs recorded at 24h and 72h post-injection (Table 5.3). The paralytic effects of the toxins varied greatly, from BoNT/A as the most potent to ChoBot as the least potent. BoNT/C had the steepest CMAP amplitude reduction

with increasing dose, followed by BoNT/A then BitoxAA. ChoBot was the only toxin which showed the same degree of CMAP inhibition at all doses injected above 63ng, with a regression expression gradient close to 0.

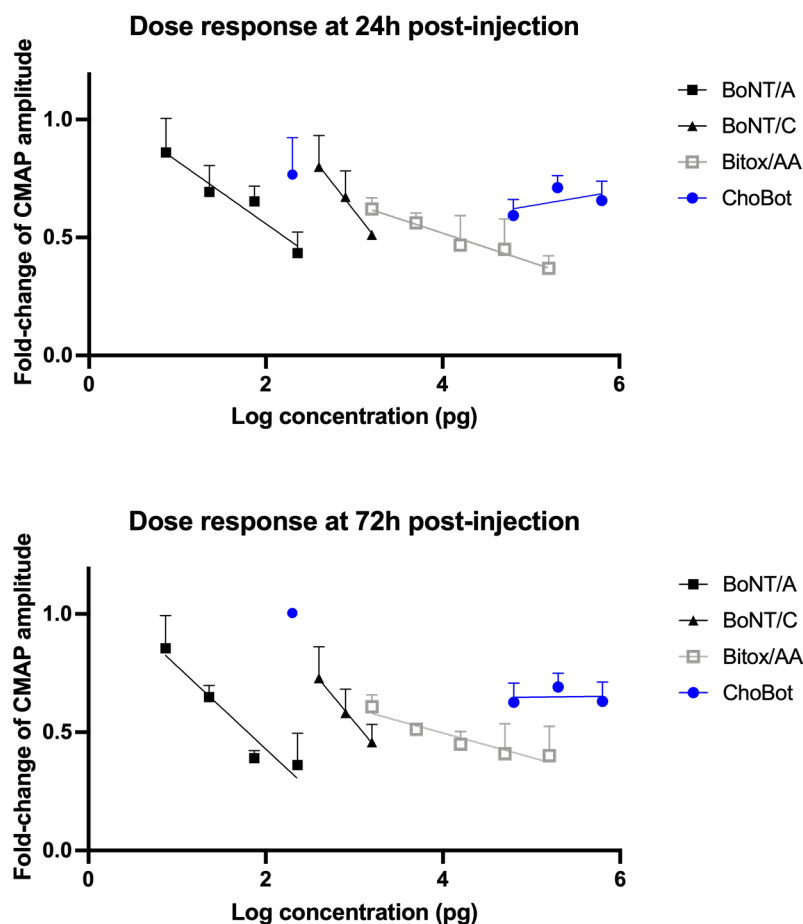


**Figure 5.5. Dose response of native and retargeted botulinum toxins on compound muscle action potential amplitude.** The normalised to baseline compound muscle action potential (CMAP) amplitudes were plotted on a log<sub>10</sub> scale of concentration. Amplitudes at 24h and 72h post-injection were plotted. A linear regression analysis was applied for each toxin. N=3 per concentration per toxin except N=2 for 200pg ChoBot. Data presented as mean ± SEM.

Toxin	Timepoint (h)	Regression expression	R <sup>2</sup>	50% CMAP reduction dose (pg)
BoNT/A	24	Y = -0.2645*logX + 1.087	0.4721	166
	72	Y = -0.3497*logX + 1.129	0.6210	63
Bitox/AA	24	Y = -0.1232*logX + 1.011	0.3222	14,051
	72	Y = -0.1033*logX + 0.9101	0.2574	9332
BoNT/C	24	Y = -0.4805*logX + 2.054	0.4080	1714
	72	Y = -0.4515*logX + 1.899	0.3538	1255
ChoBot	24	Y = 0.06344*logX + 0.3174	0.05716	N/A
	72	Y = 0.004399*logX + 0.6263	0.001892	N/A

**Table 5.3. Regression expressions and doses required to reduce the compound muscle action potential amplitude by 50%.**

## 5.4 Discussion

There have been three reported studies published on the effect of a BoNT, specifically BoNT/A, on CMAP amplitude of the gastrocnemius muscle (Cichon et al., 1995; Sakamoto et al., 2009; Torri et al., 2014). In order to use BoNT/A as a standard toxin to compare novel toxins to, this chapter also investigated the effect of different doses of BoNT/A on CMAP amplitude. The main limiting factor of BoNT use for pain conditions is their unwanted paralysis of muscle. Therefore, if a toxin could be developed with less potency at the muscle but retained action on sensory neurons this would be an advantage over the currently used native serotypes. Incidentally, all the other toxins investigated in this chapter were shown to be less paralytic than BoNT/A, but further testing for their effects on the nociceptive pathways would be required before being able to determine whether one of these would be more useful than BoNT/A for treating chronic pain conditions.

In all the experiments within this chapter, the maximum doses used were generally kept conservative and full inhibition of the CMAP was not attempted. This was to avoid systemic effects on the contralateral leg and to preserve the welfare of the animals over the course of the study.

In general, the safety of BoNT use is improved when a wider range of doses can be given without a quickly ramping paralytic effect at increased doses. In these experiments, BoNT/C had the steepest regression gradient, suggesting a smaller potential therapeutic window than BoNT/A and therefore a reduced safety profile. On the other hand, Bitox/AA had a better safety profile than BoNT/A, with increasing dose only inducing a modest increase in CMAP amplitude reduction.

The novel chimeric toxin ChoBot had a unique dose response profile of all the tested toxins, as CMAP inhibition was stable at 60-70% of the baseline CMAP response for all the different doses within the 63-630ng range. These amounts were the largest amount injected of all the toxins investigated. This was not an artefact of the injection or another compound in the formulation as a 200pg injection did not affect the CMAP amplitude by 3 days post-injection. Why the dose response of ChoBot on muscle doesn't appear to follow a traditional dose response curve isn't clear, but it appears as if neuromuscular blockade is already saturated by these larger doses, but that saturation occurs at a maximum of only 30-40% inhibition. ChoBot is the only toxin in this chapter which has a specific ganglioside binding receptor binding domain rather than a native BoNT receptor binding domain. It is known that certain gangliosides are found at the presynaptic

terminal of the neuromuscular junction, and have even been shown to act as receptors for native BoNT binding (Hotta et al., 2013; Bullens et al., 2002). However, there is little research on the degree of expression of GM1 by motor neurons which ChoBot is presumably acting on. Theoretically, if the GM1 ganglioside is only expressed by 30-40% of these neurons then even high doses of ChoBot would not be able to cause complete neuromuscular blockade.

This chapter looked only at BoNT potency at the muscle. It does not address the question of whether a particular BoNT's potency at the muscle is correlated with its potency at sensory neurons. If it is presumed that the two are highly correlated, the usefulness of BoNTs as analgesics is generally limited. However, the incomplete action of ChoBot at the neuromuscular junction makes it an interesting candidate for a lack of correlation between muscle paralysis and sensory neuron silencing. If paralysis is limited by differential expression of its ganglioside receptor at neuromuscular junctions then high doses could be well tolerated. If ChoBot successfully acts on nociceptors to silence pain signalling then there could be a disconnect between paralytic potency and analgesic potency, making a promising candidate for the clinic. It also would be a very safe toxin to use as the therapeutic window is much larger than that of native toxins, and the other novel toxins investigated in this chapter. Considering the action of ChoBot on sensory neurons in culture detailed in the previous chapter, its unique muscle response profile provides further evidence for interest in it as a treatment for chronic pain. The action of ChoBot in the context of the intact sensory system of the rat will next be investigated.

## 6. *In vivo* testing of ChoBot as an analgesic agent

### 6.1 Introduction

As with any potential new therapeutic, *in vitro* investigation can only give so much information about the action of BoNTs on the sensory system. BoNTs in particular require investigation in model organisms such as rodents due to their effects on muscle. Even if a toxin was able to block exocytosis from all nociceptive neurons, if it also potently blocks exocytosis at the neuromuscular junction then it is no longer likely to be a useful analgesic in the clinic. A rodent model is therefore required to be able to determine a BoNT's potency on the sensory and neuromuscular systems simultaneously. Linking *in vitro* concentrations to safe human doses is also difficult, and animal model doses are the necessary intermediary between the two.

There are clear differences between the exposure of dissociated neurons in a plate and the exposure of functional neurons *in situ* to a compound. In culture, the neurons are directly exposed to a BoNT in the media, which may allow more efficient internalisation. However, when a BoNT is injected into an animal it must diffuse from the site of injection to the neuronal processes, be internalised into the neuron via its receptors, and then transported within that neuron to its site of action which may be a significant distance away. Retrograde trafficking and transcytosis of the light chain to dorsal horn spinal cord neurons has been hypothesised to be important for the analgesic action of BoNTs, and this transport only exists in an intact peripheral and central nervous system (Section 1.4.3.1) (Matak et al., 2012; Bach-Rojecky & Lacković, 2009; Matak et al., 2011). It is also difficult to model the long-term effects of BoNT treatment in culture as the lifetime of cultured neurons is limited. Indeed, the *in vitro* experiments in this thesis uses just a 24 hour exposure of toxin, which may not be ideal for modelling the months-long effect of BoNTs *in vivo*.

For all the reasons outlined above, it was necessary to investigate the action of the retargeted toxin ChoBot in the intact, functioning nervous system of the rat. Immunohistochemistry of cS25 allows the localisation of ChoBot action in specific sensory neurons at all levels of the nervous system. Rat pain models also allow initial testing of ChoBot as an analgesic agent in a behavioural context. As ChoBot was designed to be injected peripherally to act on the same neurons as CTB

(which internalises into peripheral sensory neurons), peripheral neuropathic pain models were used.

CIPN is a common type of peripheral neuropathy which ChoBot may be a useful treatment for. An established *in vivo* rat model of peripheral CIPN involves four intraperitoneal injections of 2mg/kg paclitaxel on alternate days (Polomano et al., 2001). This has been shown to cause mechanical allodynia and hyperalgesia, thermal hyperalgesia and cold allodynia in the hindpaws and tail. This appears to mimic some of the commonly reported symptoms of CIPN in patients, which include pain in response to touch and cold sensitivity in the hands and feet (Toftthagen et al., 2013). More traditional neuropathic models may also be useful to study ChoBot as an analgesic. These commonly involve crush injury, ligation or transection of nerves. The SNI model involves the ligation and transection of two of the three major branches of the sciatic nerve (Decosterd & Woolf, 2000). Similarly to CIPN, this also leads to mechanical allodynia and hypersensitivity, cold allodynia and thermal hyperalgesia in the ipsilateral paw.

Using animal models to study novel analgesics relies on behavioural testing of nociceptive reflexes, notably the hindpaw withdrawal reflex. Mechanical sensitivity is tested by applying von Frey filaments of increasing forces to the hindpaw until a withdrawal reflex is elicited. Up-down methods are used to then estimate a force that elicits a withdrawal 50% of the time (Chaplan et al., 1994; Bonin et al., 2014). Thermal thresholds can be estimated by measuring the latency to withdraw from a radiant heating laser applied to the glass underneath the hindpaw (Hargreaves et al., 1988). Similarly, cold thresholds can be estimated by measuring the latency to withdraw to a cold stimulus applied to the glass, such as a pellet of dry ice (Brenner et al., 2012). However, scoring or timing the animals' reaction to a cooling chemical such as acetone applied to the hindpaw may also be used (Choi et al., 1994).

Behavioural tests such as these are vital in pain research as they give a quantitative assessment of the sensitivity of different modalities of sensation after a pain-inducing injury or insult. This then allows preclinical testing of compounds or therapies in a quantifiable way. However, it is important to remember that reflex reactions may not correlate to the aversive and affective aspects of pain which are the most distressing. It must also be remembered that many compounds which are successful at reversing pain behaviours in preclinical models do not succeed in human trials (Berge, 2011).

Multiple studies have investigated the use of BoNT/A's ability to reverse the allodynic and hyperalgesic consequences of neuropathic injury in rat models (Table 6.1). Many claim a complete or almost complete reversal of altered nociceptive thresholds following a single intraplantar injection of BoNT/A. However, the doses used are far higher than shown to have an effect on CMAP amplitudes summarised in Table 5.1 of the previous chapter, which show significant muscle inhibition at doses as low as 0.5U (Cichon et al., 1995). The authors of these BoNT/A pain model studies often do not directly address potential paralytic effects altering the animal's ability to withdraw from the stimulus. Only a single study used rotarod testing to rule out overt adverse motor effects (Park et al., 2006). It is therefore important to note that the doses used in these studies may be too high for a true therapeutic effect with no effect on muscle. In order to accurately compare therapeutic effects of BoNT/A with novel BoNT constructs such as ChoBot, direct comparison using CMAP-verified doses would be required in the future.

Reference	Model	Dose	Behavioural test	Effect
Bach-Rojecky et al., 2005	Partial sciatic nerve transection	7U/kg	Randall-Selitto paw-pressure (mechanical)	Complete reversal to baseline
			52°C hotplate (thermal)	Complete reversal to baseline
Park et al., 2006	L5/L6 spinal nerve ligation	20U/kg	Von Frey (mechanical)	Reduction from 100% to 50% withdrawal frequency to 35.6 mN von Frey stimulus
			Acetone (cold)	Reduction from 100% to 70% withdrawal frequency to acetone
Favre-Guilnard et al., 2009	Paclitaxel, 2mg/kg x4	20U/kg	Randall-Selitto paw-pressure (mechanical)	Complete reversal to baseline bilaterally
Marinelli et al., 2010	Chronic constriction injury of sciatic nerve	18.75 and 75pg/paw (approx. 5U and 20U/paw)	Dynamic plantar aesthesiometer (mechanical)	18.75pg, 50% reversal; 75pg, 80% reversal back to baseline
			5°C coldplate (cold)	Both doses, increase in withdrawal latency compared to saline injection
Xiao et al., 2011	L5 ventral root transection	7U/kg	Von Frey (mechanical)	Almost complete reversal to baseline bilaterally
Wang et al., 2017	Spared nerve injury	15U/kg (0.5% bovine serum albumin)	Von Frey (mechanical)	25% reversal back to baseline
			4°C coldplate (cold)	50% reversal back to baseline

**Table 6.1. Published effects of intraplantar botulinum toxin A injection in rat models of neuropathy.**

## 6.2 Summary and objectives

The testing of novel BoNT constructs in animal models is required to demonstrate their safety and functional action in sensory neurons in an intact model system. In the previous chapter, ChoBot was shown to be the least potent blocker of the neuromuscular system of multiple BoNTs tested,

but also had improved SNAP25-cleaving ability in DRG cultures over BoNT/A, as discussed in Chapter 4. The function of ChoBot in the sensory system *in vivo* will now be assessed.

Research aims:

- To characterise the activity of ChoBot in adult rat sensory neurons after a peripheral injection.
- Assess ChoBot's ability to reverse behavioural hypersensitivity in neuropathic pain models.

## **6.3 Results**

### **6.3.1 *ChoBot cleaves SNAP25 in nerve fibres innervating the skin at the site of injection***

Immunohistochemistry of cS25 was used to determine whether ChoBot was functionally active after injection into the plantar surface of the hindpaw. 200ng was injected subcutaneously into the left paw and rats were sacrificed 7 days after injection. At this dose, animals were behaviourally normal, with no observable motor effects and no changes to the Digit Abduction Score (DAS) of the injected paw (Broide et al., 2013). At 200ng the effect on the CMAP amplitude was saturated, and reduced to 64% of baseline at the 7 day timepoint, an effect size not significantly different from the buffer control injection (Figure 5.4). Immunoreactivity of cS25 was observed in the ipsilateral paw tissue at the site of injection (Figure 6.1a). Different structures in the skin and the corresponding innervation were identified by their location in the tissue and their gross morphology. cS25 was detected in the sensory afferents of the dermis, but very rarely in the epidermis. It was also observed deeper in the paw tissue, in afferents innervating blood vessels and motorneurons innervating muscle fibres. There was no immunoreactivity observed in the contralateral paw. There was also no cS25 detected in animals injected with vehicle only (Figure 6.1b). ChoBot is therefore proteolytically active in peripheral afferents after injection *in vivo*, including within sensory neurons innervating the dermis.

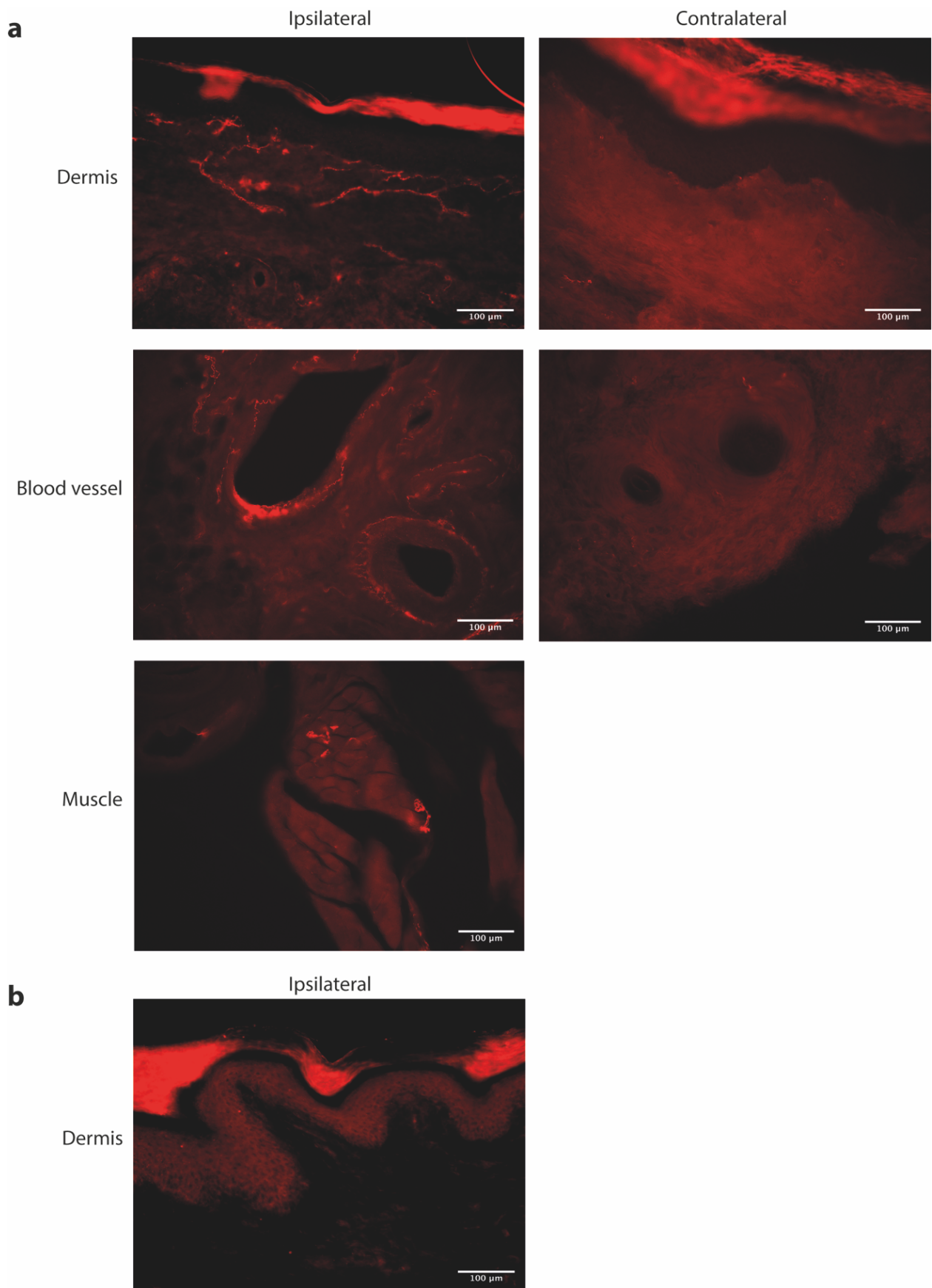


**Figure 6.1. ChoBot cleaves SNAP25 in dermal sensory fibres, fibres innervating blood vessels, and motor neurons. a)** Immunoreactivity for cleaved SNAP25 (cS25) was observed in the ipsilateral paw following a 200ng intraplantar injection of ChoBot. cS25 was seen in dermal sensory neurons, neurons innervating blood vessels and neurons innervating striated muscle. No significant

*immunoreactivity was observed in the contralateral paw. b) No immunoreactivity was observed in the ipsilateral paw of control animals injected with vehicle (0.4% octyl glucoside in buffer A). ChoBot injected animals N=2. Vehicle injected animals N=1.*

### 6.3.2 *ChoBot cleaves SNAP25 in a subpopulation of NF200- and CGRP-expressing fibres in the dermis*

Subtyping of the sensory neurons in the dermis and epidermis that are susceptible to ChoBot intoxication is necessary to assess its utility as an analgesic. However, this does have its limitations due to the physiology of skin tissue. It is impossible to know what proportion of the fibres in one section are provided by a single neuron's branching, making it seem like there is SNAP25-cleavage in many neurons when in reality it may be that one susceptible neuron is providing a lot of innervation. It can also be difficult to tell whether neurites are un-encapsulated free nerve endings or are innervating other structures such as sensory receptors or hair follicles. This limits the knowledge of what functions the susceptible subpopulations are performing in the sensory system. Finally, it is also difficult to take tissue only from the injection site precisely, which may affect analysis of SNAP25 cleavage due to tissue being taken that had not been fully exposed to the toxin.

Data from DRG cultures showed preferential uptake of ChoBot in myelinated, NF200-expressing neurons and CGRP-expressing peptidergic neurons compared to peripherin-expressing or IB4-binding populations (Section 4.3.3). In order to ascertain whether this SNAP25 cleavage selectivity is maintained *in vivo*, immunohistochemistry for cS25 in NF200- and CGRP-expressing populations of the dermis and epidermis was performed in ChoBot-injected skin (Figure 6.2). The percentage co-localisation between sensory subpopulation marker and cS25 as area covered was analysed within the epidermis and dermis. 45% of the area covered by NF200-positive fibres was also immunoreactive for cS25; the NF200-positive area accounted for 39% of all the cS25-positive area in the images. There was less overlap in the CGRP-positive fibres, with 33% of the CGRP-positive fibre area co-localising with cS25, accounting for 44% of the area that was cS25-positive (Figure 6.2c,d). These figures are similar to the proportion of NF200 and CGRP-expressing DRG neurons in culture in which ChoBot was found to be active. In culture, 35% of NF200-expressing neurons and 30% of CGRP-expressing neurons are susceptible to SNAP25 cleavage by ChoBot (Figure 4.5).

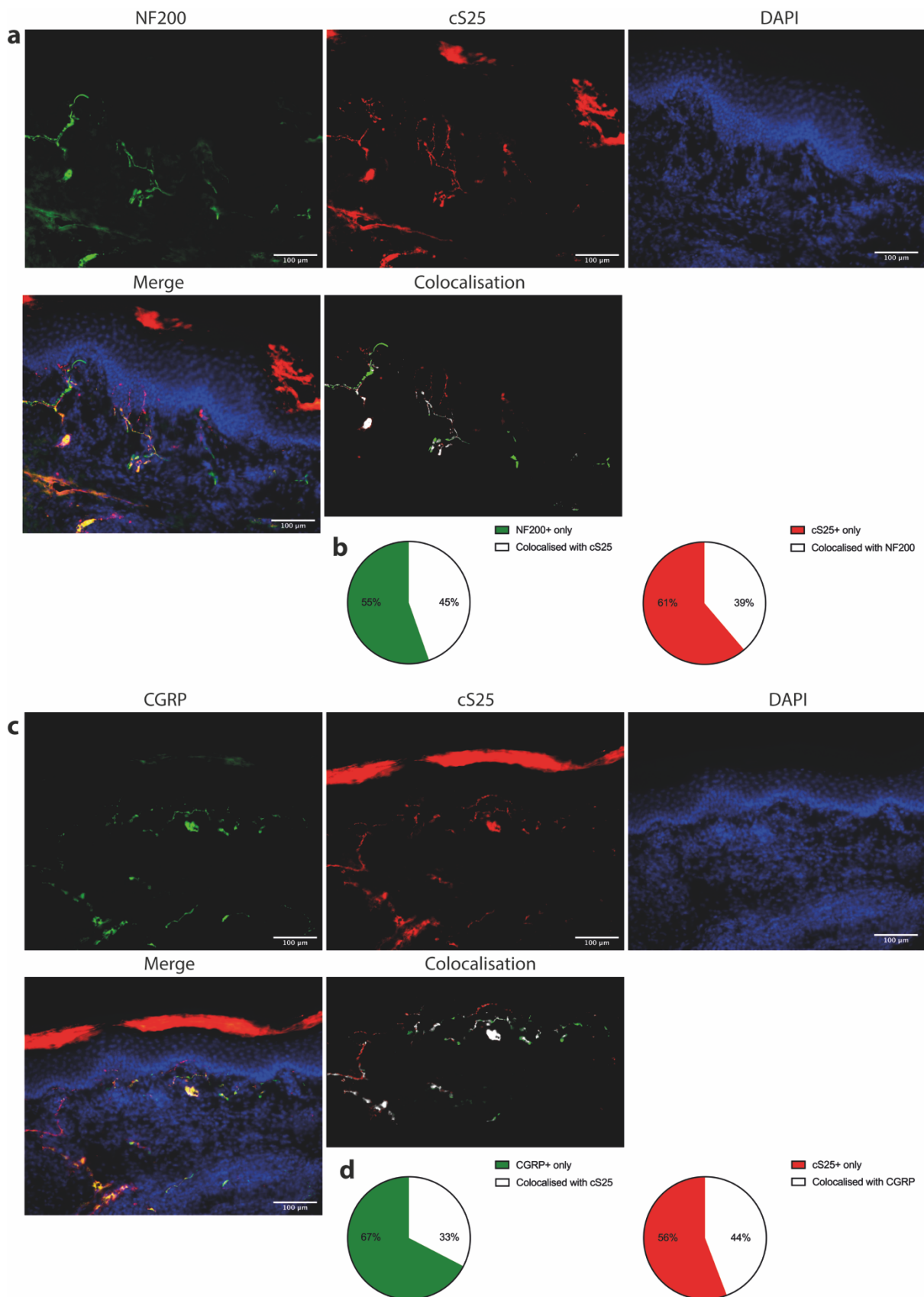


**Figure 6.2. SNAP25 cleavage in the dermis of ChoBot injected footpad. a)** Immunohistochemistry of myelinated NF200 fibres and cleaved SNAP25 (cS25) 7 days after an intraplantar injection of 200ng ChoBot. A co-localisation analysis was performed, with co-localised areas shown in white. **b)** Percentage volume of the NF200 channel co-localised with the cS25 channel, and percentage volume of the cS25 channel co-localised with the NF200 channel. **c)** Immunohistochemistry and co-

*localisation of of CGRP and cS25 was also performed. d) Percentage volume of the CGRP channel co-localised with the cS25 channel, and percentage volume of the cS25 channel co-localised with the CGRP channel. N=2, 5 images analysed per animal.*

These experiments confirm that ChoBot successfully targets sensory neurons as marked by particular subpopulation markers in the dermis at the site of injection. Overall, it appears that ChoBot targeting *in vivo* is not significantly different from that shown in primary DRG cultures, and that there is a degree of SNAP25 cleavage in both NF200- and CGRP-expressing fibres in the dermis.

### *6.3.3 SNAP25 cleavage can be detected at the level of the dorsal root ganglia after ChoBot injection*

BoNTs appear to be able to undergo retrograde transport to the CNS following peripheral injection, and there is a theory that this is necessary for its analgesic action. There is evidence that unilateral BoNT injection reverses hyperalgesia bilaterally in certain pain models, including acidic saline injections, formalin-induced facial pain and paclitaxel-induced peripheral neuropathy, but not when retrograde transport is prevented (Bach-Rojecky & Lacković, 2009; Matak et al., 2011; Favre-Guilmond et al., 2009). It was therefore investigated whether SNAP25 cleavage could be detected away from the site of injection in the soma of the DRG following a peripheral injection of ChoBot.

Lumbar DRG were dissected ipsilaterally to the ChoBot injected footpad and sections underwent immunohistochemistry for cS25 (Figure 6.3). No cS25-positive soma were detected in lumbar DRG 1 and 2. However, cS25-immunoreactive DRG neurons were observed in lumbar DRG 3-5, corresponding to DRG that innervate the hindleg via the sciatic nerve. From the presence of cS25-positive soma it appears that ChoBot has proteolytic action beyond the site of injection.

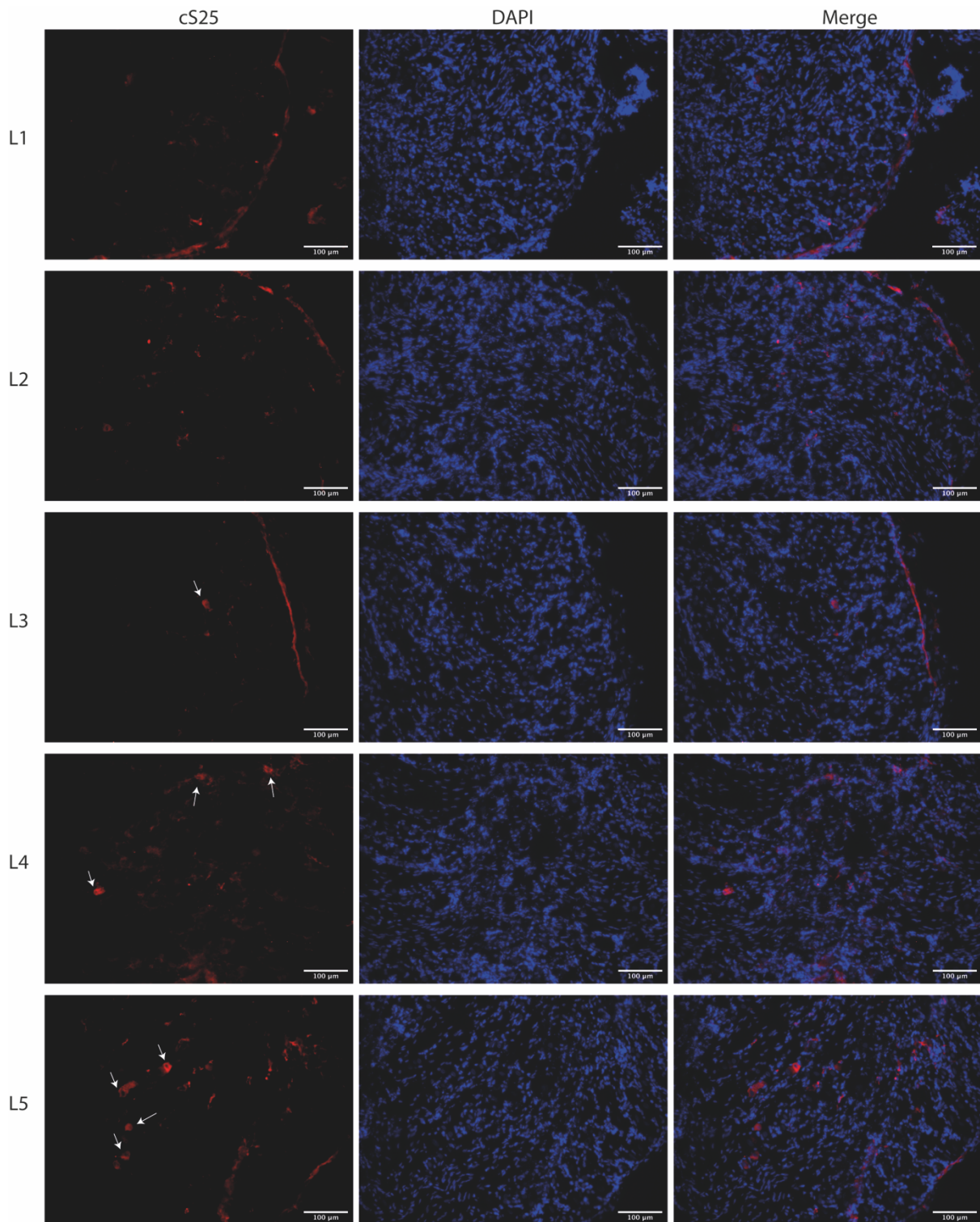


**Figure 6.3. SNAP25 cleavage in the dorsal root ganglia (DRG) ipsilateral to the ChoBot injected footpad.** Immunohistochemistry of cleaved SNAP25 (cS25) in lumbar DRG 1-5 (L1-L5) 7 days after an injection of 200ng ChoBot to the ipsilateral hindpaw. Arrows denote cS25-immunoreactive soma. N=2.

#### *6.3.4 ChoBot has no effect on mechanical or cold allodynia in a model of chemotherapy-induced peripheral neuropathy*

The ability of ChoBot to reverse pain behaviours in neuropathic rat models was assayed, to give the best preclinical evidence of ChoBot's use as an analgesic in neuropathic pain. The first model was a paclitaxel CIPN model. This involves 4 intraperitoneal injections of 2mg/kg paclitaxel, given every other day over 7 days (Polomano et al., 2001). The effect of paclitaxel injections on mechanical withdrawal threshold and cold withdrawal threshold was assessed. Von Frey filaments were used to estimate a 50% mechanical withdrawal threshold. Both paws were tested and the result averaged for each animal. Following the course of the paclitaxel injections, the force required to elicit a withdrawal reflex was significantly reduced compared to each animal's baseline testing levels (Figure 6.4a). This effect was also present when the threshold for each animal was normalised to its own baseline threshold (Figure 6.4b). The latency to withdraw from a compressed pellet of dry ice placed on glass below the hindpaw was also measured as a correlate of cold withdrawal threshold. Again, both paws were tested. The latency to withdraw from the cold stimulus was significantly reduced on the testing day immediately following paclitaxel injections (Figure 6.4c). When each animal's threshold was normalised to its baseline, withdrawal latency was significantly reduced for the rest of the testing period (Figure 6.4d).

A blinded injection of 200ng ChoBot or equivalent vehicle was then given to the plantar surface of the left hindpaw and mechanical and cold testing continued for another week. Thresholds were split into ipsilateral and contralateral to the side of injection. ChoBot had no significant effect on mechanical thresholds compared to vehicle, either ipsilaterally or contralaterally (Figure 6.5a,b). This did not change when the data was normalised to each animal's baseline (Figure 6.5c,d). There was also no difference between the ChoBot- and vehicle-injected groups in the cold allodynia behavioural test, either on the ipsilateral or contralateral sides (Figure 6.6a,b). This did not change when the data was normalised to baseline (Figure 6.6c,d). These data suggest that ChoBot has no effect on the mechanical or cold allodynia induced by a paclitaxel injection protocol to model CIPN, at least in a pre-clinical rodent model. Whether ChoBot has an effect on a more classical model of neuropathy was therefore tested.

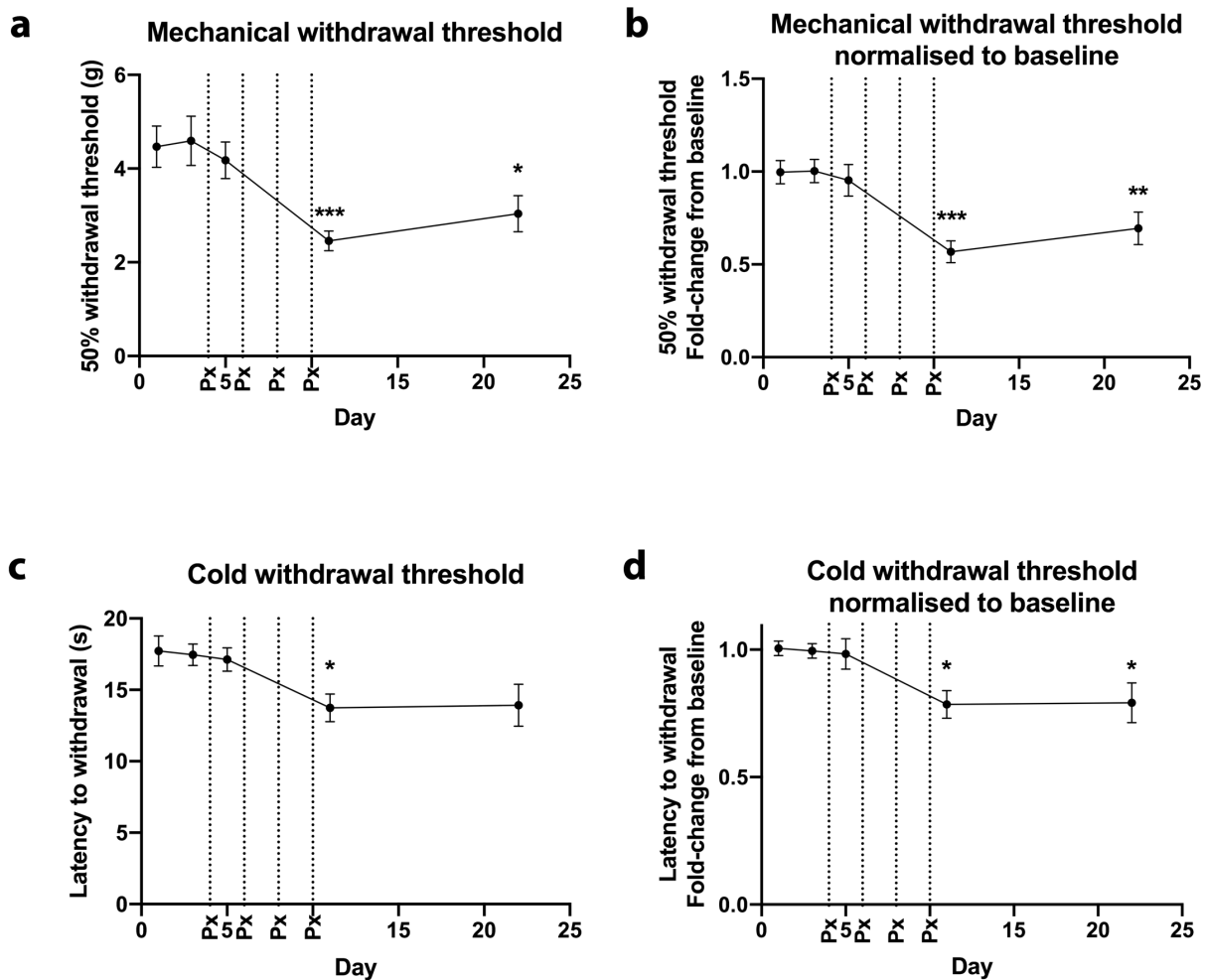


**Figure 6.4. Effect of paclitaxel injections on mechanical and cold withdrawal thresholds.** Male rats were given four intraperitoneal injections of paclitaxel (Px) on alternate days. **a)** A 50% mechanical withdrawal threshold was determined using von Frey filaments of varying forces before the injection protocol, one day after the first injection, and after the injection protocol. Two thresholds were determined for each hindpaw per animal and averaged.  $N=12$ . Ordinary one-way ANOVA of mechanical thresholds on each day compared to the average of the two baseline testing days  $P=0.0004$ . Followed by Dunnett's multiple comparisons test. **b)** The mechanical threshold for each animal was then normalised to the averaged baseline threshold from the first two days of testing. Two thresholds were determined for each hindpaw per animal and averaged.  $N=12$ . Ordinary one-way ANOVA of mechanical thresholds on each day compared to the average of the two baseline testing days  $P<0.0001$ . Followed by Dunnett's multiple comparisons test. **c)** A cold withdrawal threshold was assayed by the latency to withdraw from a dry ice stimulus placed against the glass below the hindpaw before the injection protocol, one day after the first injection, and after the injection protocol. Five thresholds were determined for each hindpaw per animal and averaged.  $N=6$ . Ordinary one-way ANOVA of cold thresholds on each day compared to the average of the two baseline testing days  $P=0.0271$ . Followed by Dunnett's multiple comparisons test. **d)** The cold threshold for each animal was then normalised to the averaged baseline threshold from the first two days of testing. Five thresholds were determined for each hindpaw per animal and averaged.  $N=6$ . Ordinary one-way ANOVA of cold thresholds on each day compared to the average of the two baseline testing days  $P=0.0164$ . Followed by Dunnett's multiple comparisons test. All figure data presented as mean  $\pm$  SEM. \*\*\* $P<0.001$  \*\* $P<0.01$  \*  $P<0.05$ .

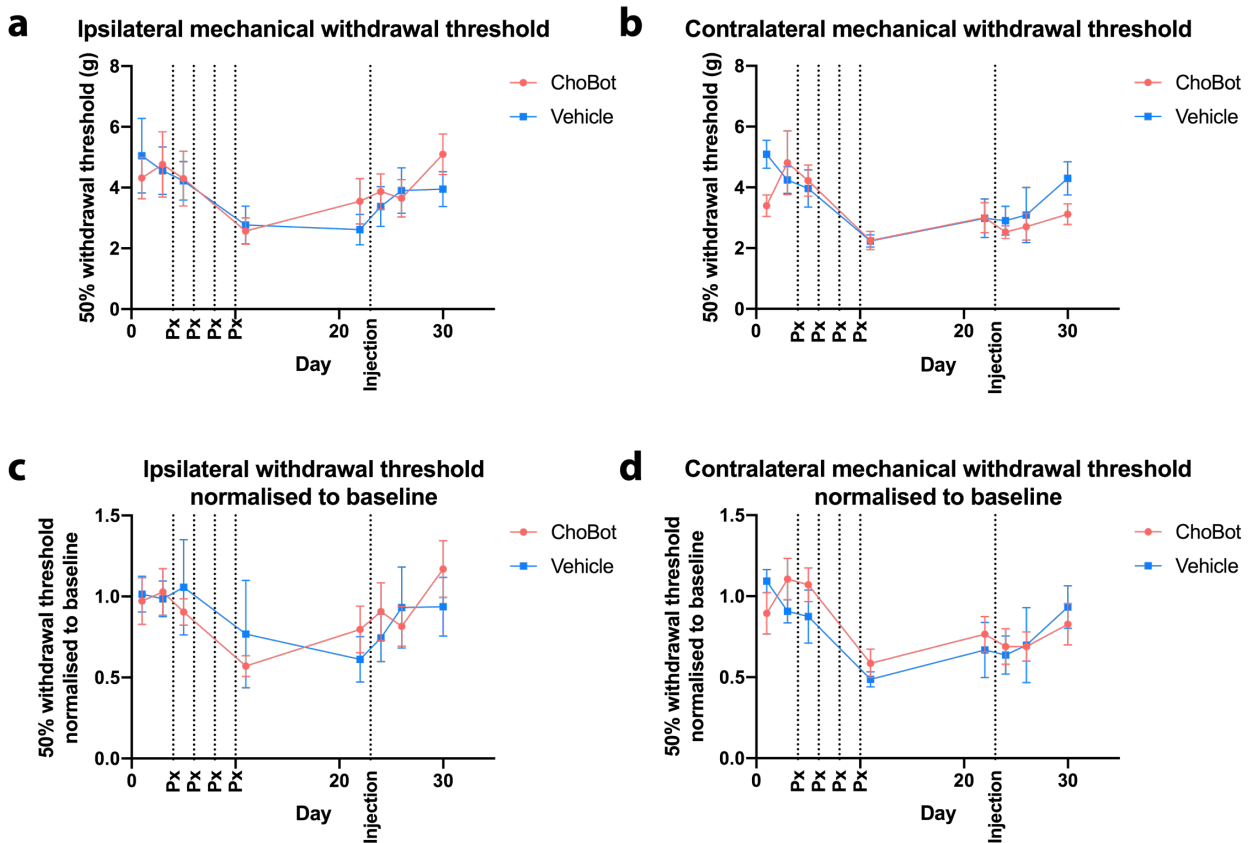


**Figure 6.5. Effect of ChoBot injection on mechanical allodynia induced by paclitaxel.** ChoBot or the equivalent buffer vehicle was injected into the plantar surface of the left (ipsilateral) hindpaw following a paclitaxel injection protocol (Px). **a)** The 50% mechanical withdrawal threshold of the injected hindpaw was tested in ChoBot-injected animals compared to vehicle-injected animals. **b)** The 50% mechanical withdrawal threshold was also assayed for the contralateral hindpaw which received no injection. **c)** The ipsilateral mechanical threshold for each animal was then normalised to the averaged baseline threshold from the ipsilateral hindpaw on the first two days of testing. **d)** The contralateral mechanical threshold for each animal was also normalised to the averaged baseline threshold from the contralateral hindpaw on the first two days of testing. For all data, two thresholds were averaged per hindpaw. N=6 per injection group. No effect of injection on **repeated measures** two-way ANOVA of time and injection. All figure data presented as mean  $\pm$  SEM.

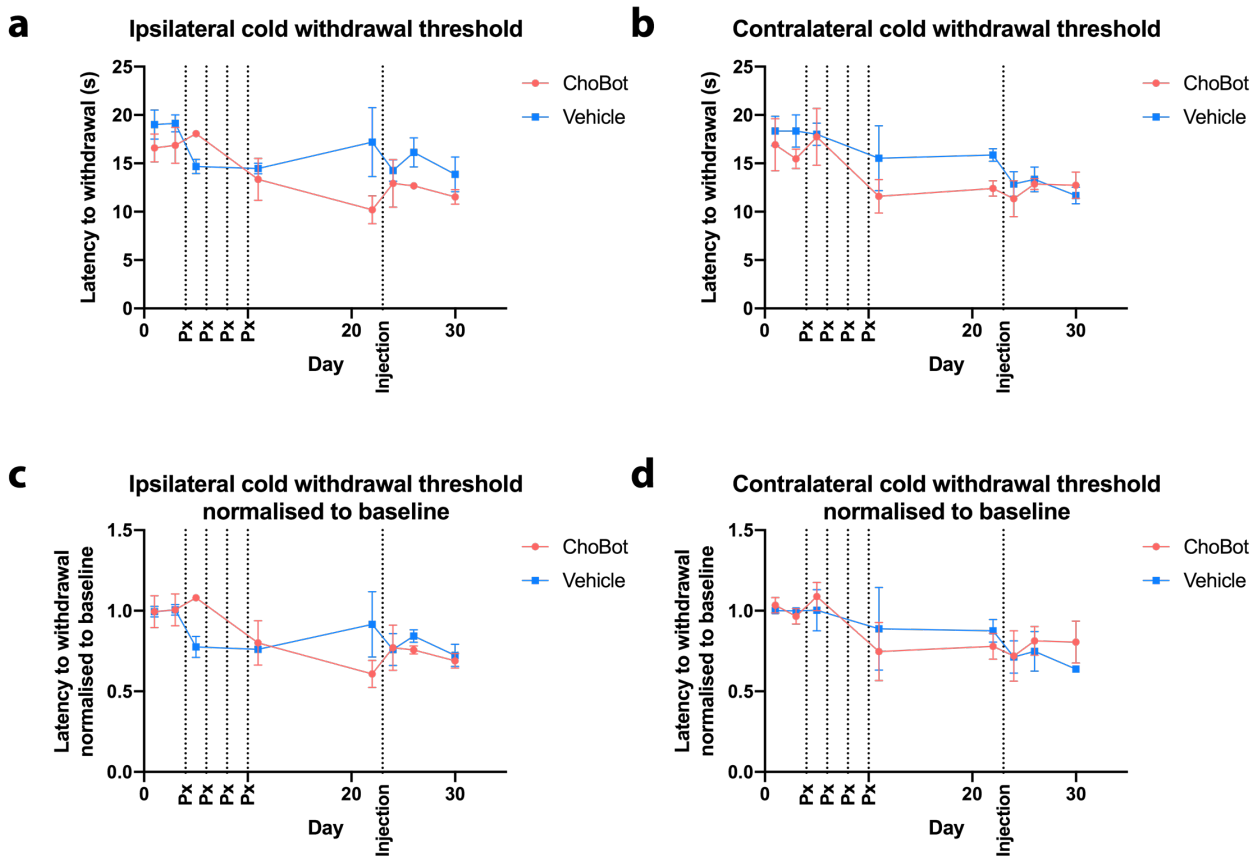


**Figure 6.6. Effect of ChoBot injection on cold allodynia induced by paclitaxel.** ChoBot or the equivalent buffer vehicle was injected into the plantar surface of the left (ipsilateral) hindpaw following a paclitaxel injection protocol (Px). **a)** The latency of cold withdrawal threshold of the injected hindpaw was tested in ChoBot-injected animals compared to vehicle-injected animals. **b)** The cold withdrawal threshold was also assayed for the contralateral hindpaw which received no injection. **c)** The ipsilateral cold threshold for each animal was then normalised to the averaged baseline threshold from the ipsilateral hindpaw on the first two days of testing. **d)** The contralateral cold threshold for each animal was also normalised to the averaged baseline threshold from the contralateral hindpaw on the first two days of testing. For all data, five thresholds were averaged per hindpaw. N=3 per injection group. No effect of injection on **repeated measures** two-way ANOVA of time and injection. All figure data presented as mean  $\pm$  SEM.

### 6.3.5 ChoBot has no effect on mechanical allodynia in the spared nerve injury model of neuropathy

ChoBot injection was also tested in the SNI model of neuropathy. In this model, the sciatic nerve is exposed and the common peroneal and tibial branches are ligated and then cut, leaving the sural nerve intact (Decosterd & Woolf, 2000). Von Frey filaments were used to test the mechanical withdrawal threshold of rats before and after SNI surgery. On the side ipsilateral to the surgery, the 50% withdrawal threshold decreased compared to baseline (Figure 6.7a). However, this was only significant when each animal was normalised to its baseline testing day (Figure 6.7b). There

was no change in mechanical threshold on the contralateral side (Figure 6.7c,d). 3 days after SNI surgery, 200ng ChoBot or the equivalent vehicle was then injected into the plantar surface of the paw ipsilateral to the surgery. Mechanical threshold testing was then carried out to determine whether ChoBot was able to reverse the mechanical allodynia caused by SNI. There was no difference in threshold between ChoBot or vehicle-only groups. As with the CIPN model, it also appears that a large, readily detectable effect on SNI-induced mechanical allodynia is not caused by ChoBot.

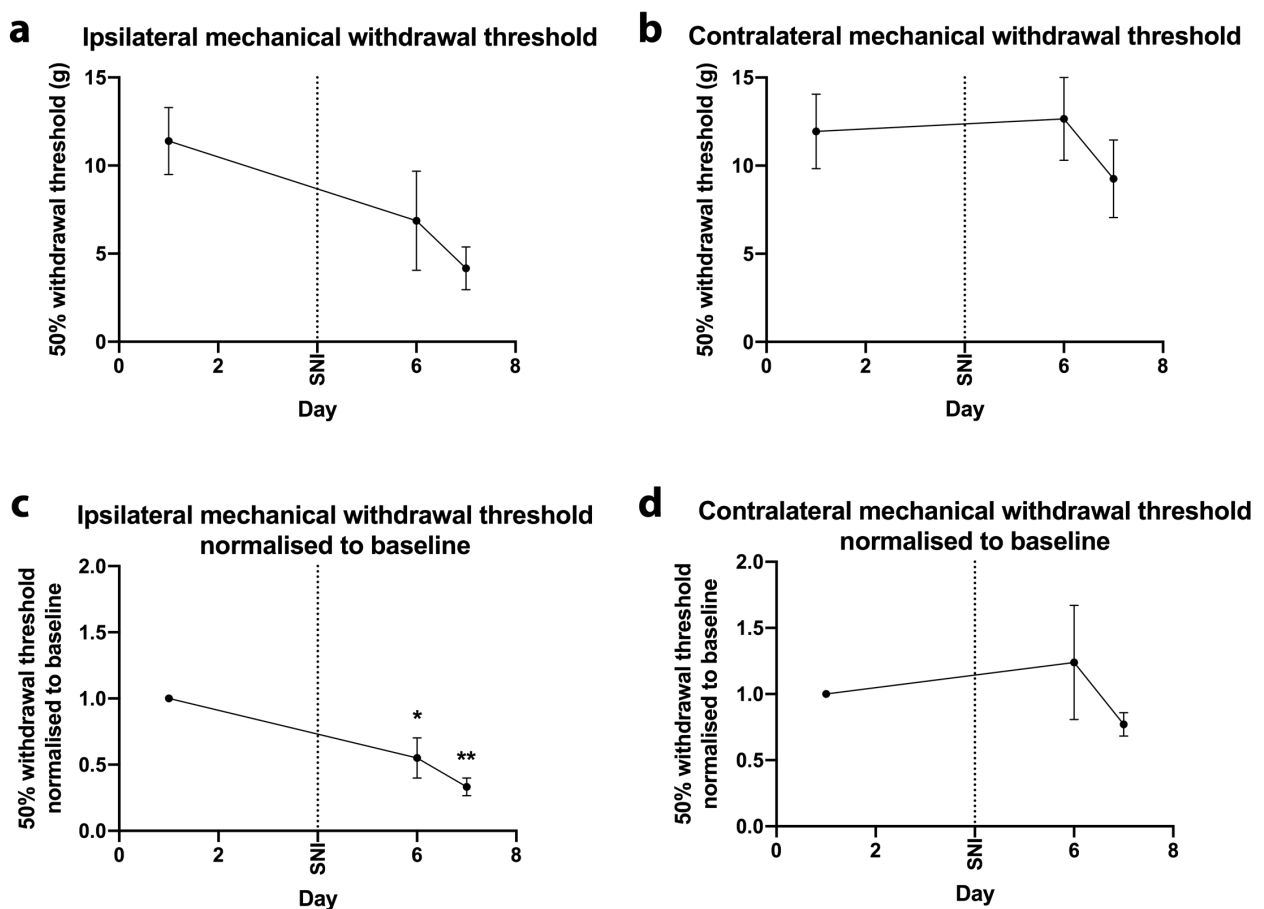


**Figure 6.7. Effect of spared nerve injury on mechanical withdrawal thresholds.** Male rats underwent the spared nerve injury (SNI) model of neuropathy and a 50% mechanical withdrawal threshold was determined using von Frey filaments of varying forces before and after the SNI protocol. **a)** The mechanical threshold was determined for the hindpaw of the leg that received the SNI. **b)** The mechanical withdrawal threshold from the contralateral leg which received no neuropathic injury was also tested. **c)** The ipsilateral mechanical threshold for each animal was then normalised to the ipsilateral baseline threshold from the first day of testing. **d)** The contralateral mechanical threshold for each animal was also normalised to the contralateral baseline threshold from the first day of testing. For all data, N=4. Ordinary one-way ANOVA of mechanical thresholds on each day compared to the baseline testing day, not significant for ipsilateral, contralateral and contralateral normalised to baseline,  $P=0.0026$  for ipsilateral normalised to baseline. Followed by Dunnett's multiple comparisons test. All figure data presented as mean  $\pm$  SEM. \*\* $P<0.01$  \*  $P<0.05$ .

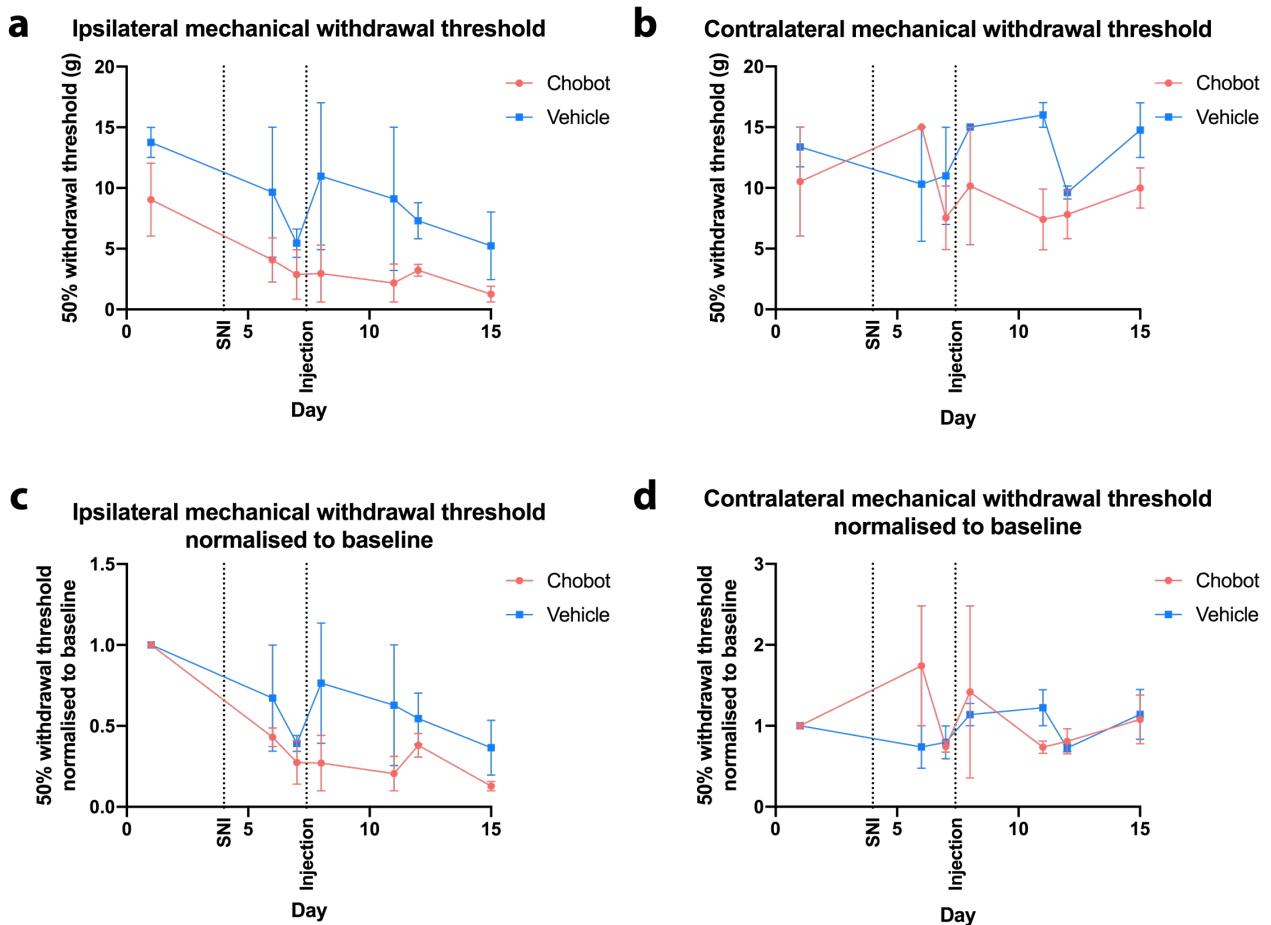


**Figure 6.8. Effect of ChoBot injection on mechanical allodynia induced by spared nerve injury.** ChoBot or the equivalent buffer vehicle was injected into the plantar surface of the left (ipsilateral) hindpaw following spared nerve injury (SNI) to the same leg and the 50% mechanical withdrawal thresholds of each hindpaw were tested. **a)** The mechanical withdrawal threshold of the injected hindpaw was tested in ChoBot-injected animals compared to vehicle-injected animals. **b)** The 50% mechanical withdrawal threshold was also assayed for the contralateral hindpaw which received no SNI or injection in either group. **c)** The ipsilateral mechanical threshold for each animal was then normalised to the baseline threshold from the ipsilateral hindpaw on the first day of testing. **d)** The contralateral mechanical threshold for each animal was also normalised to the baseline threshold from the contralateral hindpaw on the first day of testing. For all data, N=2 per injection group. No effect of injection on **repeated measures** two-way ANOVA of time and injection. All figure data presented as mean  $\pm$  SEM.

## 6.4 Discussion

This chapter investigated the action of a CMAP-verified dose of ChoBot on the intact sensory system of the rat. Although ChoBot was determined to be proteolytically active in sensory neurons both at the site of injection and more centrally at the level of the DRG, there was no clear ability of this dosage to reverse allodynia associated with neuropathic injury. This was unexpected due to the ability of BoNT/A to induce analgesia via sensory neuron intoxication, and the clear action of

ChoBot demonstrated within peripheral sensory neurons in this chapter. The variability of these behavioural experiments may have been too high to detect a subtle reversal of allodynia, or ChoBot may not target the right subpopulation of neurons for these types of pain models. ChoBot was shown to cleave SNAP25 in a proportion of CGRP-expressing fibres in the skin, and earlier *in vitro* experiments showed an inhibition of CGRP release after ChoBot exposure. CGRP upregulation and release in the spinal cord has been shown to play a role in mechanical allodynia induced by spinal nerve ligation, another model of nerve injury (Nitzan-Luques et al., 2011). It is possible that the subpopulation of CGRP-expressing neurons targeted by ChoBot *in vivo* is too limited to cause any discernible reduction of CGRP release and, subsequently, SNI-induced neuropathy.

Whereas earlier *in vitro* chapters directly compared the action of ChoBot to the most clinically used toxin, BoNT/A, due to the potency of this toxin it was decided to not risk the welfare of the animals by injecting BoNT/A for *in vivo* studies. Instead, literature-reported doses and their behavioural effects on rodent pain models have been compiled (Table 6.1). It is worth mentioning that due to the potency of BoNT/A, all the concentrations used in the literature are in the order of picograms. These are much smaller concentrations than the 200ng of ChoBot that was used with no overt effects on muscle in the experiments of this chapter. This in itself is favourable for the use of ChoBot in the clinic as the largest issue with BoNT/A injection is the difficulty in injecting minute doses of the toxin to precisely the correct area, without the local spread to neighbouring muscles (Nigam & Nigam, 2010).

All published BoNT/A papers administer toxin after the neuropathic insult. BoNTs have been shown to modulate the trafficking of pain-related ion channels to the membrane of sensory neurons (Meng et al., 2016; Nugent et al., 2018; Fan et al., 2017; Shimizu et al., 2012). Rather than attempting to reverse the changes that lead to hyperexcitability following neuropathic injury, a pre-emptive approach may be more successful for ChoBot, or indeed native BoNTs. Preventing the trafficking of these channels in the first place may be more effective than attempting to reverse them once the changes have already taken place. This would be an important area for research in the future, considering the wealth of knowledge of ion channel trafficking effects of BoNTs. Unfortunately, the time limits of this project did not allow pre-emptive BoNT treatment experiments.

The GM1 ganglioside is not only expressed by peripheral sensory neurons, it is also expressed by neurons and glia in the spinal cord (Imanaka et al., 2009). An intrathecal injection of ChoBot may therefore be a way of silencing pain pathways centrally, depending on the distribution of GM1 in the neurons and glia involved in pain signalling. Further immunohistochemical analysis of GM1 in the spinal cord would be required to analyse the potential safety of centrally administered ChoBot.

Although ChoBot did not appear to act analgesically in the pre-clinical rodent models reported in this chapter, it clearly has SNARE-cleaving action in peripheral sensory neurons at doses that do not cause significant paralysis. Moving forward, it could be beneficial to test the analgesic action of ChoBot on different types of pain model, such as inflammatory or post-surgical pain.

## 7. General discussion

### 7.1 General findings

The primary objective of this project was to characterise and assess whether a novel chimera of cholera and botulinum toxin is likely to be an effective, safe analgesic for chronic pain conditions. This toxin was created with knowledge of BoNT/A's neuronal silencing effects and knowledge of CTB's ability to target and internalise into peripheral sensory neurons, with the aim to combine both into an improved, nociceptor-silencing compound.

The first results chapter of this thesis focused on the effects of the CIPN-inducing drug paclitaxel on cultured DRG neurons as a potential assay for testing novel BoNTs such as ChoBot. *In vitro* paclitaxel was shown to affect capsaicin responses, with potentiated capsaicin-induced CGRP release and (in one experiment) capsaicin calcium response amplitude. It was unclear whether this was due to increased expression of TRPV1 at the membrane, though there was a trend towards increased surface labelling in paclitaxel-exposed conditions. The experiments in this chapter were complicated by the finding that cultured DRG neurons appeared damaged and neuropathic even in naïve conditions, as shown by the expression of the damage-response marker ATF3. This may be why any changes induced by paclitaxel were subtle and may have been masked. The effect of BoNTs on capsaicin responses in paclitaxel-treated conditions were therefore not investigated and ChoBot was instead characterised *in vitro* and *in vivo*.

The potent neuromuscular blocking effect of native BoNTs is the most limiting factor to their use in the clinic. A chapter of this thesis compared the effect of various native and engineered BoNTs on a read-out of muscle activity, the CMAP. Compared to all the other toxins tested, ChoBot was the least potent at the neuromuscular junction, and appeared to not induce complete paralysis even at nanogram doses. This development of a uniquely non-paralytic BoNT is a significant advancement in the field. In macaque monkey, observable weakness caused by an intramuscular injection of BoNT/A is detected at 33-40 U/kg, but death is caused by only slightly higher doses of 38-42 U/kg (Scott & Suzuki, 1988). This strikingly demonstrates BoNT/A's potency and narrow therapeutic window. If ChoBot's properties as demonstrated by CMAP recordings also apply to human muscle then the evidence suggests ChoBot to be a much safer therapeutic agent than BoNT/A. If the small degree of paralysis caused by saturating doses of ChoBot is found to be

tolerable clinically, then this would also allow larger amounts of ChoBot to be injected for analgesic effect, which could prove beneficial.

ChoBot was shown to be active in sensory neurons by the presence of cleaved SNAP25, both in culture and *in vivo*. This demonstrated its ability to be internalised and actively cleave its protein substrate. Although ChoBot had the least effect on muscle of all BoNTs tested, it appeared to have an improved sensory neuron targeting profile. In cultures, ChoBot was shown to be internalised into a wider population of neurons overall than BoNT/A, and was significantly increased specifically in CGRP and NF200-expressing neurons. Depolarisation-evoked CGRP release was successfully inhibited by ChoBot, demonstrating a functional effect of SNAP25 cleavage in CGRP-expressing populations. ChoBot also showed slightly enhanced uptake after *in vitro* paclitaxel exposure, suggesting a conserved mechanism of enhanced CTB binding after nerve damage reported in the literature *in vivo*.

Overall, the investigation of ChoBot shows that a ganglioside-binding botulinum toxin is able to target and cleave SNAP25 in sensory neurons, with reduced paralysis of muscle. However, when ChoBot was tested for behavioural effects in neuropathic rat models, no effect on mechanical or cold threshold was detected.

## **7.2 Limitations of the study**

Although improved sensory neuron targeting was shown in cultured DRG neurons by ChoBot compared to BoNT/A, behavioural experiments failed to show a clear analgesic effect. Although ChoBot failed to alter behavioural thresholds in the CIPN or SNI neuropathic models, this does not necessarily mean it would not be a useful therapeutic. Due to the subpopulations targeted by ChoBot, it may be the case that it would be useful for a different form of pain, such as inflammatory pain. Experiments probing the effect of ChoBot on allodynia induced by inflammatory pain models such as CFA or formalin injection, or inflammatory arthritis, may be worth performing. It is also worth bearing in mind the limitations of behavioural pain tests generally, as these only test evoked pain reflexes rather than being a measure of spontaneous pain. The development of hyperalgesia in the CIPN and SNI models was also relatively subtle in the experiments, with only a small change in mechanical and cold thresholds. Given the high variability of the behavioural data, it may be the case that this small development of hyperalgesia

is not sufficient to be able to detect any effect of ChoBot itself, so further preclinical testing using these models (for example with more biological replicates) may be of benefit.

Indeed, the preclinical testing in this thesis may not be truly applicable to the species it would be intended to be used on, having all been performed in the context of rat physiology. There are fundamental differences between the DRG of humans and rodents. Perhaps one of the most pertinent to botulinum toxin research is the differential expression of the neurofilament NF200. Both BoNT/A and ChoBot had the highest intoxication in NF200-expressing subpopulations of rat DRG neurons. 97.3% of human DRG are observed to express NF200, compared to just 61.7% of mouse DRG (Rostock et al., 2018). In humans, the expression of NF200 is not a useful marker for categorising nociceptive and non-nociceptive subpopulations. However, this difference could actually increase the efficacy of ChoBot in human sensory neurons compared to rat. The NF200-expressing subpopulation was the most highly targeted *in vitro*, and if more nociceptive neurons express NF200 in humans then ChoBot may be a more efficient analgesic than preclinical experimentation on rats would predict.

As well as the species difference, the use of dissociated primary neurons may also not be ideal. There are obvious advantages to using these neurons, primarily that they are highly physiologically relevant having been directly excised from the functioning sensory system of an adult mammal. They do not require differentiation or exogenous expression of the ion channels and proteins involved in pain signalling. They are also a heterogeneous population, which is often difficult to recapitulate with cell lines. However, it is important to remember that this population is unlikely to be perfectly representative of the DRG *in vivo*. For example, the use of NGF in culture media (as used in all the experiments in this thesis) is selective for smaller diameter, capsaicin-responsive neurons, biasing the population towards nociceptors (Winter et al., 1988).

The culture of DRG neurons also involves the microdissection of the DRG from their place *in situ*, axotomy of their peripheral and central projections, enzymatic digestion and mechanical trituration. This is a traumatic event that will undoubtedly induce a cellular response. In fact, it has been shown that DRG dissociation induces a pattern of electrical hyperexcitability similar to injury pain models that can be observed immediately after dissociation (Zheng et al., 2007). This dissociation “injury” may well confound or mask changes induced by subsequent experimental injury and is a significant problem with the use of primary culture methods. In this thesis, the

expression of the damage specific marker ATF3 was investigated in cultured DRG neurons. A surprisingly large proportion of neurons expressed ATF3, 47% and 48% at 3DIV and 7DIV respectively. This shows that even 7 days in culture isn't sufficient to overcome the neuronal stress caused by dissociation and culture conditions. Subsequently, paclitaxel *in vitro* did not induce ATF3 expression, or indeed many effects whatsoever, over control conditions. What this suggests is that the primary DRG neuron model is already significantly damaged or "neuropathic" even at baseline. As such, it may not be the best model of a naïve physiological sensory system which *in vitro* pain states can be induced within.

### **7.3 Future directions**

Cholera toxin targets GM1 specifically, but the successful action of ChoBot raises the question of whether a similar toxin could be modified further to target other gangliosides at the membrane of neurons. Although less potent than BoNT/A, ChoBot still targets the neuromuscular junction due to the expression of GM1 (Hotta et al., 2014). If a ganglioside that is specifically expressed on sensory neurons and not at the presynapse of the neuromuscular junction could be targeted instead then paralysis could potentially be avoided entirely. Unfortunately, it appears that relative ganglioside expression is very similar between human motor nerve and sensory nerve, meaning that specifically targeting sensory neurons and not muscle may not be feasible (Ogawa-Gogo & Abe, 1998). It would also require careful re-engineering of CTB, an already very complex pentameric molecule, to be able to successfully bind a specifically chosen ganglioside (Wernick et al., 2010).

A main limitation of the experiments in this thesis is the reliance on axotomised, and therefore likely injured, primary cultures of rat DRG neurons. An alternative approach could be the use of cell lines, in order to avoid axotomy and dissociation. For example, a potential alternative could be the use of differentiated human induced pluripotent stem cells (iPSCs). As well as avoiding dissociation stress, another advantage of iPSCs is that they are a human model, and can even be derived directly from patients to model disease. Many peripheral sensory neuron iPSCs are based on a differentiation protocol utilising small molecule inhibitors of developmental pathways (Chambers et al., 2012). iPSC-derived nociceptors derived from chronic pain patients show increased levels of spontaneous activity, demonstrating their applicability as a model of the human pain state (Mis et al., 2019; Namer et al., 2019). However, the iPSCs produced using this

method are specifically nociceptive in nature (expressing markers including TRPV1, peripherin and NaV1.7), rather than producing the full range of heterogeneity found in DRG *in vivo* (Middleton et al., 2021). This could limit the understanding of a novel botulinum toxin on the overall sensory system consisting of a wide variety of nociceptors and non-nociceptors.

In general, this thesis has demonstrated that a ganglioside-targeting BoNT is able to internalise into and cleave SNAP25 in sensory neurons. However, CTB has always been known to target a range of subpopulations, not specifically just nociceptive ones. The most valuable retargeted BoNT would target subpopulations known to mediate only painful sensation via a specific membrane receptor, that is not also expressed by motor neurons. Given the complex nature of gene expression in DRG neuron subpopulations, this would be a difficult task. Arguably the closest a retargeted BoNT has come is by the development of two novel toxins formed by stapling of the BoNT/A light chain and translocation domains to substance P or dermorphin (Maiarù et al., 2018). Although required to be administered centrally, these compounds were designed specifically to silence pain pathways, as both NK1R-expressing and mu opiate receptor-expressing spinal cord neurons are involved exclusively in relaying pain-mediated information. When administered to rodents these toxins induced an effective, long-lasting amelioration of neuropathic and inflammatory pain states. In a similar vein, a peripherally administered, retargeted BoNT would likely be most effective when retargeted to a pain specific receptor. For example, BoNT/A could theoretically be conjugated to ATP or CGRP. If these toxins are functional and able to be internalised into the neurons that express P2X receptors or the CGRP receptor respectively, then these could be developed as BoNTs specifically designed to target peripheral nociceptive or peripherally sensitised pathways.

Neurons are not the only cell type that are fundamentally important to pain processing. Glial cells, specifically microglia and astrocytes, are known to play a key role in the induction and maintenance of many chronic pain states (Section 1.2.1.3). Glia secrete various factors that contribute to hyperexcitability and neuroinflammation of the nociceptive connections of the spinal cord. In particular, astrocytes are known to release gliotransmitters such as glutamate and ATP by regulated exocytosis, which function as neuromodulators which enhance synaptic strength (Jourdain et al., 2007). Theoretically, if a BoNT could be produced which prevented gliotransmission then this may be able to block some of the sensitisation that is a major player in the chronification of pain states. Reports suggest that the most important SNARE protein for

exocytosis in astrocytes is SNAP23 rather than SNAP25 (Hepp et al., 1999; Schubert et al., 2011). A modified BoNT which cleaves SNAP23 rather than SNAP25 could potentially be able to block the astrocytic contribution to chronic pain if injected centrally, while sparing the neuronal signalling via SNAP25 which is crucial to the normal function of the CNS.

Overall, ChoBot shows some promise as a potential pain therapeutic, clearly being active within rodent sensory neurons *in vitro* and *in vivo*. It is less potently paralytic while demonstrating enhanced targeting properties *in vitro* when compared to the most clinically relevant BoNT, BoNT/A. However, the experiments in this thesis are limited by the methodical issues that preclinical analgesic testing commonly suffers from; namely an imperfect model cellular system, behavioural testing on rodents, and imperfect targeting of nociceptors due to the complexity and heterogeneity of DRG neurons. ChoBot also suffers from not having been designed specifically with a certain type of nociceptor or pain in mind. This makes it difficult to know in what type of chronic pain it would be useful, and how to administer it, without a barrage of preclinical testing which would potentially not translate over to human physiology. One outcome of the experiments in this thesis is the further solidification of the protein stapling technology for the formation of novel retargeted BoNTs. In the future, this method could well be used to create new BoNTs specifically designed to silence a chosen type of nociceptor involved in mediating a particular pain state.

## Appendix

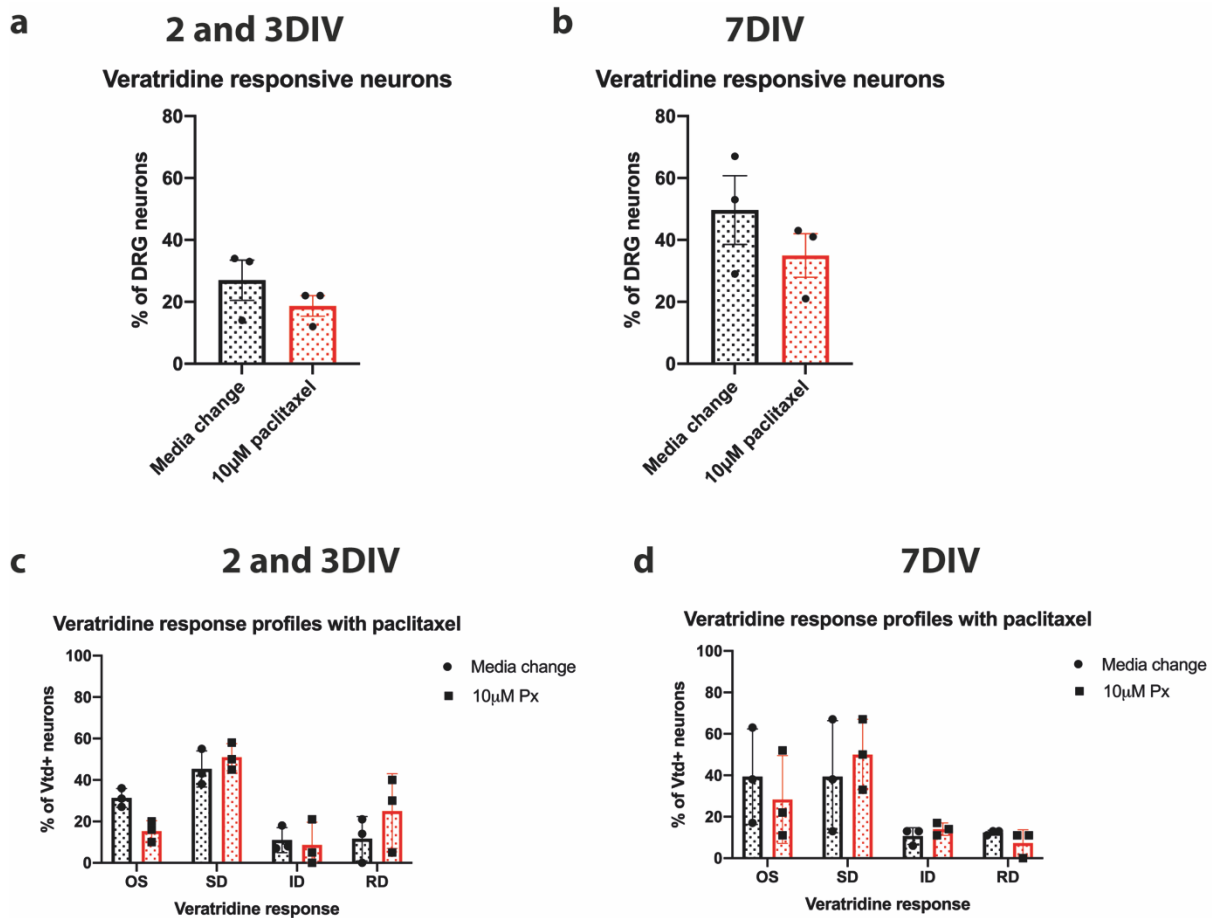


**Figure 0.1. Effect of in vitro paclitaxel exposure on veratridine response profiles in rat dorsal root ganglion (DRG) neurons. a)** DRG neurons were imaged at 2 and 3 days in vitro (DIV) after 24 hours of paclitaxel exposure. The proportion of dorsal root ganglion neurons responding to veratridine was not affected by paclitaxel. No significance of two-tailed unpaired t test. **b)** When neurons were imaged at 7DIV paclitaxel also had no effect on the proportion of neurons responding to veratridine. No significance of two-tailed unpaired t test. **c)** The veratridine responding neurons at 2 and 3 DIV were then classed into one of the 4 veratridine response profiles. Ordinary one-way ANOVA  $P=0.0002$ . Followed by Šídák's multiple comparisons test, no significance. **d)** Paclitaxel-treated and control DRG neurons at 7DIV were also classified into veratridine response profiles. Ordinary one-way ANOVA  $P=0.0302$ . Followed by Šídák's multiple comparisons test, no significance.  $N=3$  cultures for all conditions and timepoints. DIV2 and 3,  $n=279$  media change neurons,  $n=266$  paclitaxel treated neurons. DIV7,  $n=70$  media change neurons,  $n=136$  paclitaxel treated neurons. All data presented as mean  $\pm$  SEM.

## 8. Bibliography

- Adamek, P., Heles, M. & Palecek, J. (2019) 'Mechanical allodynia and enhanced responses to capsaicin are mediated by PI3K in a paclitaxel model of peripheral neuropathy', *Neuropharmacology*, 146pp. 163–174.
- Adelman, P.C., Baumbauer, K.M., Friedman, R., Shah, M., Wright, M., Young, E., Jankowski, M.P., Albers, K.M. & Koerber, H.R. (2019) 'Single-cell q-PCR derived expression profiles of identified sensory neurons', *Molecular Pain*, 15p. 1744806919884496.
- Alisky, J.M., van de Wetering, C.I. & Davidson, B.L. (2002) 'Widespread Dispersal of Cholera Toxin Subunit b to Brain and Spinal Cord Neurons Following Systemic Delivery', *Experimental Neurology*, 178(1), pp. 139–146.
- Amaya, F., Shimosato, G., Nagano, M., Ueda, M., Hashimoto, S., Tanaka, Y., Suzuki, H. & Tanaka, M. (2004) 'NGF and GDNF differentially regulate TRPV1 expression that contributes to development of inflammatory thermal hyperalgesia', *European Journal of Neuroscience*, 20(9), pp. 2303–2310.
- Amos, L.A. & Löwe, J. (1999) 'How Taxol stabilises microtubule structure', *Chemistry & Biology*, 6(3), pp. R65-69.
- Anand, P. & Bley, K. (2011) 'Topical capsaicin for pain management: therapeutic potential and mechanisms of action of the new high-concentration capsaicin 8% patch', *BJA: British Journal of Anaesthesia*, 107(4), pp. 490–502.
- Anderson, P. (2012) 'Activating Transcription Factor 3 and the Nervous System', *Frontiers in Molecular Neuroscience*, 5p. 7.
- Andreou, A.P., Leese, C., Greco, R., Demartini, C., Corrie, E., Simsek, D., Zanaboni, A., Koroleva, K., Lloyd, J.O., Lambrou, G., Doran, C., Gafurov, O., Seward, E., Giniatullin, R., Tassorelli, C. & Davletov, B. (2020) 'Double-Binding Botulinum Molecule with Reduced Muscle Paralysis: Evaluation in In Vitro and In Vivo Models of Migraine', *Neurotherapeutics*,
- Antonucci, F., Rossi, C., Gianfranceschi, L., Rossetto, O. & Caleo, M. (2008) 'Long-Distance Retrograde Effects of Botulinum Neurotoxin A', *Journal of Neuroscience*, 28(14), pp. 3689–3696.
- Arsenault, J., Ferrari, E., Niranjana, D., Cuijpers, S.A.G., Gu, C., Vallis, Y., O'Brien, J. & Davletov, B. (2013) 'Stapling of the botulinum type A protease to growth factors and neuropeptides allows selective targeting of neuroendocrine cells', *Journal of Neurochemistry*, 126(2), pp. 223–233.
- Authier, N., Gillet, J.P., Fialip, J., Eschalier, A. & Coudore, F. (2000) 'Description of a short-term Taxol-induced nociceptive neuropathy in rats', *Brain Research*, 887(2), pp. 239–249.
- Averill, S., McMahon, S.B., Clary, D.O., Reichardt, L.F. & Priestley, J.V. (1995) 'Immunocytochemical Localization of trkA Receptors in Chemically Identified Subgroups of Adult Rat Sensory Neurons', *The European journal of neuroscience*, 7(7), pp. 1484–1494.
- Bach-Rojecky, L. & Lacković, Z. (2009) 'Central origin of the antinociceptive action of botulinum toxin type A', *Pharmacology Biochemistry and Behavior*, 94(2), pp. 234–238.

- Bach-Rojecky, L., Relja, M. & Lacković, Z. (2005) 'Botulinum toxin type A in experimental neuropathic pain', *Journal of Neural Transmission (Vienna, Austria: 1996)*, 112(2), pp. 215–219.
- Bannister, K. & Dickenson, A.H. (2016) 'What do monoamines do in pain modulation?', *Current opinion in supportive and palliative care*, 10(2), pp. 143–148.
- Bear, M.F., Connors, B.W. & Paradiso, M.A. (2006) *Neuroscience: Exploring the Brain*. 3rd Revised edition. Philadelphia, PA: Jones & Bartlett Learning.
- von Berg, L., Stern, D., Pauly, D., Mahrhold, S., Weisemann, J., Jentsch, L., Hansbauer, E.-M., Müller, C., Avondet, M.A., Rummel, A., Dorner, M.B. & Dorner, B.G. (2019) 'Functional detection of botulinum neurotoxin serotypes A to F by monoclonal neoepitope-specific antibodies and suspension array technology', *Scientific Reports*, 9(1), p. 5531.
- Berge, O.-G. (2011) 'Predictive validity of behavioural animal models for chronic pain', *British Journal of Pharmacology*, 164(4), pp. 1195–1206.
- Binz, T. & Rummel, A. (2009) 'Cell entry strategy of clostridial neurotoxins', *Journal of Neurochemistry*, 109(6), pp. 1584–1595.
- Bird, G.C., Han, J.S., Fu, Y., Adwanikar, H., Willis, W.D. & Neugebauer, V. (2006) 'Pain-related synaptic plasticity in spinal dorsal horn neurons: role of CGRP', *Molecular Pain*, 2p. 31.
- Blum, T.R., Liu, H., Packer, M.S., Xiong, X., Lee, P.-G., Zhang, S., Richter, M., Minasov, G., Satchell, K.J.F., Dong, M. & Liu, D.R. (2021) 'Phage-assisted evolution of botulinum neurotoxin proteases with reprogrammed specificity', *Science*, 371(6531), pp. 803–810.
- Boehmerle, W., Huehnchen, P., Peruzzaro, S., Balkaya, M. & Endres, M. (2014) 'Electrophysiological, behavioral and histological characterization of paclitaxel, cisplatin, vincristine and bortezomib-induced neuropathy in C57Bl/6 mice', *Scientific Reports*, 4(1), p. 6370.
- Boehmerle, W., Splittgerber, U., Lazarus, M.B., McKenzie, K.M., Johnston, D.G., Austin, D.J. & Ehrlich, B.E. (2006) 'Paclitaxel induces calcium oscillations via an inositol 1,4,5-trisphosphate receptor and neuronal calcium sensor 1-dependent mechanism', *Proceedings of the National Academy of Sciences of the United States of America*, 103(48), pp. 18356–18361.
- Bonin, R.P., Bories, C. & De Koninck, Y. (2014) 'A simplified up-down method (SUDO) for measuring mechanical nociception in rodents using von Frey filaments', *Molecular Pain*, 10p. 26.
- Boyette-Davis, J., Xin, W., Zhang, H. & Dougherty, P. (2011) 'Intraepidermal nerve fiber loss corresponds to the development of Taxol-induced hyperalgesia and can be prevented by treatment with minocycline', *Pain*, 152(2), pp. 308–313.
- Bradbury, E.J., Burnstock, G. & McMahon, S.B. (1998) 'The expression of P2X3 purinoreceptors in sensory neurons: effects of axotomy and glial-derived neurotrophic factor', *Molecular and Cellular Neurosciences*, 12(4–5), pp. 256–268.
- Bradesi, S. (2010) 'Role of spinal cord glia in the central processing of peripheral pain perception', *Neurogastroenterology and Motility: The Official Journal of the European Gastrointestinal Motility Society*, 22(5), pp. 499–511.
- Bráz, J.M. & Basbaum, A.I. (2010) 'Differential ATF3 expression in dorsal root ganglion neurons reveals the profile of primary afferents engaged by diverse noxious chemical stimuli', *Pain*, 150(2), pp. 290–301.
- Brenner, D.S., Golden, J.P. & Gereau, R.W. (2012) 'A Novel Behavioral Assay for Measuring Cold Sensation in Mice', *PLoS ONE*, 7(6), .

- Breuer, B., Sperber, K., Wallenstein, S., Kiproviski, K., Calapa, A., Snow, B. & Pappagallo, M. (2006) 'Clinically significant placebo analgesic response in a pilot trial of botulinum B in patients with hand pain and carpal tunnel syndrome', *Pain Medicine (Malden, Mass.)*, 7(1), pp. 16–24.
- Broide, R.S., Rubino, J., Nicholson, G.S., Ardila, M.C., Brown, M.S., Aoki, K.R. & Francis, J. (2013) 'The rat Digit Abduction Score (DAS) assay: A physiological model for assessing botulinum neurotoxin-induced skeletal muscle paralysis', *Toxicon*, 71pp. 18–24.
- Bullens, R.W.M., O'Hanlon, G.M., Wagner, E., Molenaar, P.C., Furukawa, Keiko, Furukawa, Koichi, Plomp, J.J. & Willison, H.J. (2002) 'Complex gangliosides at the neuromuscular junction are membrane receptors for autoantibodies and botulinum neurotoxin but redundant for normal synaptic function', *The Journal of Neuroscience: The Official Journal of the Society for Neuroscience*, 22(16), pp. 6876–6884.
- Burgen, A.S.V., Dickens, F. & Zatman, L.J. (1949) 'The action of botulinum toxin on the neuromuscular junction', *The Journal of Physiology*, 109(1–2), pp. 10–24.
- Burrone, J. & Murthy, V.N. (2001) 'Synaptic plasticity: Rush hour traffic in the AMPA lanes', *Current Biology*, 11(7), pp. R274–R277.
- Camprubí-Robles, M., Planells-Cases, R. & Ferrer-Montiel, A. (2009) 'Differential contribution of SNARE-dependent exocytosis to inflammatory potentiation of TRPV1 in nociceptors', *The FASEB Journal*, 23(11), pp. 3722–3733.
- Caterina, M.J. & Julius, D. (2001) 'The vanilloid receptor: a molecular gateway to the pain pathway', *Annual Review of Neuroscience*, 24pp. 487–517.
- Caterina, M.J., Leffler, A., Malmberg, A.B., Martin, W.J., Trafton, J., Petersen-Zeit, K.R., Koltzenburg, M., Basbaum, A.I. & Julius, D. (2000) 'Impaired Nociception and Pain Sensation in Mice Lacking the Capsaicin Receptor', *Science*, 288(5464), pp. 306–313.
- Caterina, M.J., Schumacher, M.A., Tominaga, M., Rosen, T.A., Levine, J.D. & Julius, D. (1997) 'The capsaicin receptor: a heat-activated ion channel in the pain pathway', *Nature*, 389(6653), pp. 816–824.
- Chaddock, J. A., Purkiss, J.R., Duggan, M.J., Quinn, C.P., Shone, C.C. & Foster, K.A. (2000) 'A conjugate composed of nerve growth factor coupled to a non-toxic derivative of Clostridium botulinum neurotoxin type A can inhibit neurotransmitter release in vitro', *Growth Factors (Chur, Switzerland)*, 18(2), pp. 147–155.
- Chaddock, John A., Purkiss, J.R., Friis, L.M., Broadbridge, J.D., Duggan, M.J., Fooks, S.J., Shone, C.C., Quinn, C.P. & Foster, K.A. (2000) 'Inhibition of Vesicular Secretion in Both Neuronal and Nonneuronal Cells by a Retargeted Endopeptidase Derivative of Clostridium botulinum Neurotoxin Type A', *Infection and Immunity*, 68(5), pp. 2587–2593.
- Chambers, S.M., Qi, Y., Mica, Y., Lee, G., Zhang, X.-J., Niu, L., Bilsland, J., Cao, L., Stevens, E., Whiting, P., Shi, S.-H. & Studer, L. (2012) 'Combined small molecule inhibition accelerates developmental timing and converts human pluripotent stem cells into nociceptors', *Nature biotechnology*, 30(7), pp. 715–720.
- Chang, W., Berta, T., Kim, Y.H., Lee, S., Lee, S.-Y. & Ji, R.-R. (2017) 'Expression and Role of Voltage-Gated Sodium Channels in Human Dorsal Root Ganglion Neurons with Special Focus on Nav1.7, Species Differences, and Regulation by Paclitaxel', *Neuroscience Bulletin*, 34(1), pp. 4–12.

- Chaplan, S.R., Bach, F.W., Pogrel, J.W., Chung, J.M. & Yaksh, T.L. (1994) 'Quantitative assessment of tactile allodynia in the rat paw', *Journal of Neuroscience Methods*, 53(1), pp. 55–63.
- Chen, D., Frezza, M., Schmitt, S., Kanwar, J. & Dou, Q.P. (2011) 'Bortezomib as the First Proteasome Inhibitor Anticancer Drug: Current Status and Future Perspectives', *Current Cancer Drug Targets*, 11(3), pp. 239–253.
- Chen, S. & Barbieri, J.T. (2009) 'Engineering botulinum neurotoxin to extend therapeutic intervention', *Proceedings of the National Academy of Sciences*, 106(23), pp. 9180–9184.
- Chen, Y., Yang, C. & Wang, Z.J. (2011) 'Proteinase-activated receptor 2 sensitizes transient receptor potential vanilloid 1, transient receptor potential vanilloid 4, and transient receptor potential ankyrin 1 in paclitaxel-induced neuropathic pain', *Neuroscience*, 193pp. 440–451.
- Cheng, J., Deng, Y. & Zhou, J. (2021) 'Role of the Ubiquitin System in Chronic Pain', *Frontiers in Molecular Neuroscience*, 14p. 674914.
- Choksi, T., Hay, D.L., Legon, S., Poyner, D.R., Hagner, S., Bloom, S.R. & Smith, D.M. (2002) 'Comparison of the expression of calcitonin receptor-like receptor (CRLR) and receptor activity modifying proteins (RAMPs) with CGRP and adrenomedullin binding in cell lines', *British Journal of Pharmacology*, 136(5), pp. 784–792.
- Cichon, J.V., Mccaffrey, T.V., Litchy, W.J. & Knops, J.L. (1995) 'The effect of botulinum toxin type a injection on compound muscle action potential in an in vivo rat model', *The Laryngoscope*, 105(2), pp. 144–148.
- Cui, M., Khanijou, S., Rubino, J. & Aoki, K.R. (2004) 'Subcutaneous administration of botulinum toxin A reduces formalin-induced pain', *PAIN*, 107(1), pp. 125–133.
- Darby, L.M., Meng, H. & Fehrenbacher, J.C. (2017) 'Paclitaxel inhibits the activity and membrane localization of PKC $\alpha$  and PKC $\beta$ I/II to elicit a decrease in stimulated calcitonin gene-related peptide release from cultured sensory neurons', *Molecular and cellular neurosciences*, 82pp. 105–117.
- Darios, F., Niranjana, D., Ferrari, E., Zhang, F., Soloviev, M., Rummel, A., Bigalke, H., Suckling, J., Ushkaryov, Y., Naumenko, N., Shakirzyanova, A., Giniatullin, R., Maywood, E., Hastings, M., Binz, T. & Davletov, B. (2010) 'SNARE tagging allows stepwise assembly of a multimodular medicinal toxin', *Proceedings of the National Academy of Sciences of the United States of America*, 107(42), pp. 18197–18201.
- Das, G. (2017) *Basics of Pain Management*. S.I.: CBS Publishers & Distributors Pvt Ltd, India.
- Decosterd, I. & Woolf, C.J. (2000) 'Spared nerve injury: an animal model of persistent peripheral neuropathic pain', *PAIN*, 87(2), pp. 149–158.
- Doyle, T., Chen, Z., Muscoli, C., Bryant, L., Esposito, E., Cuzzocrea, S., Dagostino, C., Ryerse, J., Rausaria, S., Kamadulski, A., Neumann, W.L. & Salvemini, D. (2012) 'Targeting the Overproduction of Peroxynitrite for the Prevention and Reversal of Paclitaxel-Induced Neuropathic Pain', *The Journal of Neuroscience*, 32(18), pp. 6149–6160.
- Dubin, A.E. & Patapoutian, A. (2010) 'Nociceptors: the sensors of the pain pathway', *The Journal of Clinical Investigation*, 120(11), pp. 3760–3772.
- Duggan, M.J., Quinn, C.P., Chaddock, J.A., Purkiss, J.R., Alexander, F.C.G., Doward, S., Fooks, S.J., Friis, L.M., Hall, Y.H.J., Kirby, E.R., Leeds, N., Mouldsdales, H.J., Dickenson, A., Green, G.M., Rahman, W., Suzuki, R., Shone, C.C. & Foster, K.A. (2002) 'Inhibition of release of neurotransmitters from rat dorsal root ganglia by a novel conjugate of a Clostridium

botulinum toxin A endopeptidase fragment and Erythrina cristagalli lectin', *The Journal of Biological Chemistry*, 277(38), pp. 34846–34852.

- Duggett, N.A., Griffiths, L.A., McKenna, O.E., de Santis, V., Yongsanguanchai, N., Mokori, E.B. & Flatters, S.J.L. (2016) 'Oxidative stress in the development, maintenance and resolution of paclitaxel-induced painful neuropathy', *Neuroscience*, 333pp. 13–26.
- Durham, P.L., Cady, Ryan & Cady, Roger (2004) 'Regulation of calcitonin gene-related peptide secretion from trigeminal nerve cells by botulinum toxin type A: implications for migraine therapy', *Headache*, 44(1), pp. 35–42; discussion 42-43.
- Emery, E.C., Luiz, A.P., Sikandar, S., Magnúsdóttir, R., Dong, X. & Wood, J.N. (2016) 'In vivo characterization of distinct modality-specific subsets of somatosensory neurons using GCaMP', *Science Advances*, 2(11), p. e1600990.
- Fan, C., Chu, X., Wang, L., Shi, H. & Li, T. (2017) 'Botulinum toxin type A reduces TRPV1 expression in the dorsal root ganglion in rats with adjuvant-arthritis pain', *Toxicon*, 133(Supplement C), pp. 116–122.
- Favre-Guilmard, C., Auguet, M. & Chabrier, P.-E. (2009) 'Different antinociceptive effects of botulinum toxin type A in inflammatory and peripheral polyneuropathic rat models', *European Journal of Pharmacology*, 617(1), pp. 48–53.
- Feasby, T.E. & Brown, W.F. (1974) 'Variation of motor unit size in the human extensor digitorum brevis and thenar muscles', *Journal of Neurology, Neurosurgery, and Psychiatry*, 37(8), pp. 916–926.
- Ferrari, E., Gu, C., Niranjana, D., Restani, L., Rasetti-Escargueil, C., Obara, I., Geranton, S.M., Arsenault, J., Goetze, T.A., Harper, C.B., Nguyen, T.H., Maywood, E., O'Brien, J., Schiavo, G., Wheeler, D.W., Meunier, F.A., Hastings, M., Edwardson, J.M., Sesardic, D., et al. (2013) 'Synthetic self-assembling clostridial chimera for modulation of sensory functions', *Bioconjugate Chemistry*, 24(10), pp. 1750–1759.
- Flatters, S.J.L. & Bennett, G.J. (2006) 'Studies of peripheral sensory nerves in paclitaxel-induced painful peripheral neuropathy: Evidence for mitochondrial dysfunction', *Pain*, 122(3), pp. 245–257.
- Foran, P.G., Mohammed, N., Lisk, G.O., Nagwaney, S., Lawrence, G.W., Johnson, E., Smith, L., Aoki, K.R. & Dolly, J.O. (2003) 'Evaluation of the therapeutic usefulness of botulinum neurotoxin B, C1, E, and F compared with the long lasting type A. Basis for distinct durations of inhibition of exocytosis in central neurons', *The Journal of Biological Chemistry*, 278(2), pp. 1363–1371.
- Foster, K.A., Adams, E.J., Durose, L., Cruttwell, C.J., Marks, E., Shone, C.C., Chaddock, J.A., Cox, C.L., Heaton, C., Sutton, J.M., Wayne, J., Alexander, F.C.G. & Rogers, D.F. (2006) 'Re-engineering the target specificity of clostridial neurotoxins - a route to novel therapeutics', *Neurotoxicity Research*, 9(2), pp. 101–107.
- Freund, B. & Schwartz, M. (2003) 'Temporal relationship of muscle weakness and pain reduction in subjects treated with botulinum toxin A', *The Journal of Pain*, 4(3), pp. 159–165.
- Frey, E., Valakh, V., Karney-Grobe, S., Shi, Y., Milbrandt, J. & DiAntonio, A. (2015) 'An In Vitro Assay to Study Induction of the Regenerative State in Sensory Neurons', *Experimental neurology*, 263pp. 350–363.
- Gangadharan, V. & Kuner, R. (2013) 'Pain hypersensitivity mechanisms at a glance', *Disease Models & Mechanisms*, 6(4), pp. 889–895.

- García-Caballero, A., Gadotti, V.M., Stenkowski, P., Weiss, N., Souza, I.A., Hodgkinson, V., Bladen, C., Chen, L., Hamid, J., Pizzoccaro, A., Deage, M., François, A., Bourinet, E. & Zamponi, G.W. (2014) 'The Deubiquitinating Enzyme USP5 Modulates Neuropathic and Inflammatory Pain by Enhancing Cav3.2 Channel Activity', *Neuron*, 83(5), pp. 1144–1158.
- Gerber, S.H. & Südhof, T.C. (2002) 'Molecular Determinants of Regulated Exocytosis', *Diabetes*, 51(suppl 1), pp. S3–S11.
- Goldstein, M.E., House, S.B. & Gainer, H. (1991) 'NF-L and peripherin immunoreactivities define distinct classes of rat sensory ganglion cells', *Journal of Neuroscience Research*, 30(1), pp. 92–104.
- Gong, Y., Tagawa, Y., Lunn, M.P.T., Laroy, W., Heffer-Laue, M., Li, C.Y., Griffin, J.W., Schnaar, R.L. & Sheikh, K.A. (2002) 'Localization of major gangliosides in the PNS: implications for immune neuropathies', *Brain*, 125(11), pp. 2491–2506.
- Gornstein, E.L. & Schwarz, T.L. (2017) 'Neurotoxic mechanisms of paclitaxel are local to the distal axon and independent of transport defects', *Experimental neurology*, 288pp. 153–166.
- Gross, R.A. & Macdonald, R.L. (1987) 'Dynorphin A selectively reduces a large transient (N-type) calcium current of mouse dorsal root ganglion neurons in cell culture', *Proceedings of the National Academy of Sciences of the United States of America*, 84(15), pp. 5469–5473.
- Hackett, G., Moore, K., Burgin, D., Hornby, F., Gray, B., Elliott, M., Mir, I. & Beard, M. (2018) 'Purification and Characterization of Recombinant Botulinum Neurotoxin Serotype FA, Also Known as Serotype H', *Toxins*, 10(5), .
- Hara, T., Chiba, T., Abe, K., Makabe, A., Ikeno, S., Kawakami, K., Utsunomiya, I., Hama, T. & Taguchi, K. (2013) 'Effect of paclitaxel on transient receptor potential vanilloid 1 in rat dorsal root ganglion', *Pain*, 154(6), pp. 882–889.
- Hargreaves, K., Dubner, R., Brown, F., Flores, C. & Joris, J. (n.d.) 'A new and sensitive method for measuring thermal nociception in cutaneous hyperalgesia', *Pain*, 32(1), p. 77.
- Hayashi, T., McMahon, H., Yamasaki, S., Binz, T., Hata, Y., Südhof, T.C. & Niemann, H. (1994) 'Synaptic vesicle membrane fusion complex: action of clostridial neurotoxins on assembly.', *The EMBO Journal*, 13(21), pp. 5051–5061.
- He, Y. & Wang, Z.J. (2015) 'Nociceptor Beta II, Delta, and Epsilon Isoforms of PKC Differentially Mediate Paclitaxel-Induced Spontaneous and Evoked Pain', *The Journal of Neuroscience*, 35(11), pp. 4614–4625.
- van Hecke, O., Austin, S.K., Khan, R.A., Smith, B.H. & Torrance, N. (2014) 'Neuropathic pain in the general population: a systematic review of epidemiological studies', *Pain*, 155(4), pp. 654–662.
- Heinke, B., Gingl, E. & Sandkühler, J. (2011) 'Multiple Targets of  $\mu$ -Opioid Receptor-Mediated Presynaptic Inhibition at Primary Afferent A $\delta$ - and C-Fibers', *The Journal of Neuroscience*, 31(4), pp. 1313–1322.
- Hendrich, J., Van Minh, A.T., Hebllich, F., Nieto-Rostro, M., Watschinger, K., Striessnig, J., Wratten, J., Davies, A. & Dolphin, A.C. (2008) 'Pharmacological disruption of calcium channel trafficking by the  $\alpha 2\delta$  ligand gabapentin', *Proceedings of the National Academy of Sciences of the United States of America*, 105(9), pp. 3628–3633.
- Hepp, R., Perraut, M., Chasserot-Golaz, S., Galli, T., Aunis, D., Langley, K. & Grant, N.J. (1999) 'Cultured glial cells express the SNAP-25 analogue SNAP-23', *Glia*, 27(2), pp. 181–187.

- Hertz, D.L., Kidwell, K.M., Vangipuram, K., Li, F., Pai, M.P., Burness, M., Griggs, J.J., Schott, A.F., Poznak, C.V., Hayes, D.F., Smith, E.M.L. & Henry, N.L. (2018) 'Paclitaxel Plasma Concentration after the First Infusion Predicts Treatment-Limiting Peripheral Neuropathy', *Clinical Cancer Research*, 24(15), pp. 3602–3610.
- Hökfelt, T., Kellerth, J.O., Nilsson, G. & Pernow, B. (1975) 'Substance p: localization in the central nervous system and in some primary sensory neurons', *Science (New York, N.Y.)*, 190(4217), pp. 889–890.
- Holmgren, J., Lönnroth, I., Månsson, J. & Svennerholm, L. (1975) 'Interaction of cholera toxin and membrane GM1 ganglioside of small intestine', *Proceedings of the National Academy of Sciences of the United States of America*, 72(7), pp. 2520–2524.
- Hotta, S., Nagaoka, T., Taguchi, K., Nakatani, Y., Utsunomiya, I., Masuda, Y., Abe, K. & Yuki, N. (2014) 'Neurophysiological and immunohistochemical studies of IgG anti-GM1 monoclonal antibody on neuromuscular transmission: effects in rat neuromuscular junctions', *Neurological Sciences*, 35(2), pp. 205–213.
- Hu, K., Carroll, J., Fedorovich, S., Rickman, C., Sukhodub, A. & Davletov, B. (2002) 'Vesicular restriction of synaptobrevin suggests a role for calcium in membrane fusion', *Nature*, 415(6872), pp. 646–650.
- Huang, J., Zhang, X. & McNaughton, P.A. (2006) 'Inflammatory Pain: The Cellular Basis of Heat Hyperalgesia', *Current Neuropharmacology*, 4(3), pp. 197–206.
- Imanaka, T., Hukuda, S. & Maeda, T. (1996) 'The Role of GM1-Ganglioside in the Injured Spinal Cord of Rats: An Immunohistochemical Study Using GM1-Antisera', *Journal of Neurotrauma*, 13(3), pp. 163–170.
- Iyengar, S., Ossipov, M.H. & Johnson, K.W. (2017) 'The role of calcitonin gene-related peptide in peripheral and central pain mechanisms including migraine', *Pain*, 158(4), pp. 543–559.
- James, S.E., Burden, H., Burgess, R., Xie, Y., Yang, T., Massa, S.M., Longo, F.M. & Lu, Q. (2008) 'Anti-cancer drug induced neurotoxicity and identification of Rho pathway signaling modulators as potential neuroprotectants', *Neurotoxicology*, 29(4), pp. 605–612.
- Jamieson, S.M.F., Liu, J.J., Connor, B., Dragunow, M. & McKeage, M.J. (2007) 'Nucleolar enlargement, nuclear eccentricity and altered cell body immunostaining characteristics of large-sized sensory neurons following treatment of rats with paclitaxel', *NeuroToxicology*, 28(6), pp. 1092–1098.
- Jankovic, J. (2004) 'Botulinum toxin in clinical practice', *Journal of Neurology, Neurosurgery & Psychiatry*, 75(7), pp. 951–957.
- Jimenez-Andrade, J.M., Herrera, M.B., Ghilardi, J.R., Vardanyan, M., Melemedjian, O.K. & Mantyh, P.W. (2008) 'Vascularization of the dorsal root ganglia and peripheral nerve of the mouse: Implications for chemical-induced peripheral sensory neuropathies', *Molecular Pain*, 4p. 10.
- Joseph, J., Qu, L., Wang, S., Kim, M., Bennett, D., Ro, J., Caterina, M.J. & Chung, M.-K. (2019) 'Phosphorylation of TRPV1 S801 Contributes to Modality-Specific Hyperalgesia in Mice', *Journal of Neuroscience*, 39(50), pp. 9954–9966.
- Kidd, J.F., Pilkington, M.F., Schell, M.J., Fogarty, K.E., Skepper, J.N., Taylor, C.W. & Thorn, P. (2002) 'Paclitaxel Affects Cytosolic Calcium Signals by Opening the Mitochondrial Permeability Transition Pore \*', *Journal of Biological Chemistry*, 277(8), pp. 6504–6510.

- Kilo, S., Harding-Rose, C., Hargreaves, K.M. & Flores, C.M. (1997) 'Peripheral CGRP release as a marker for neurogenic inflammation: a model system for the study of neuropeptide secretion in rat paw skin', *Pain*, 73(2), pp. 201–207.
- Krarup, C. (1983) 'Evoked responses in normal and diseased muscle with particular reference to twitch potentiation', *Acta Neurologica Scandinavica*, 68(5), pp. 269–315.
- Kunii, M., Ohara-Imaizumi, M., Takahashi, N., Kobayashi, M., Kawakami, R., Kondoh, Y., Shimizu, T., Simizu, S., Lin, B., Nunomura, K., Aoyagi, K., Ohno, M., Ohmuraya, M., Sato, T., Yoshimura, S., Sato, K., Harada, R., Kim, Y.-J., Osada, H., et al. (2016) 'Opposing roles for SNAP23 in secretion in exocrine and endocrine pancreatic cells', *Journal of Cell Biology*, 215(1), pp. 121–138.
- Lacy, D.B., Tepp, W., Cohen, A.C., DasGupta, B.R. & Stevens, R.C. (1998) 'Crystal structure of botulinum neurotoxin type A and implications for toxicity', *Nature Structural Biology*, 5(10), pp. 898–902.
- Laedermann, C.J., Cachemaille, M., Kirschmann, G., Pertin, M., Gosselin, R.-D., Chang, I., Albesa, M., Towne, C., Schneider, B.L., Kellenberger, S., Abriel, H. & Decosterd, I. (2013) 'Dysregulation of voltage-gated sodium channels by ubiquitin ligase NEDD4-2 in neuropathic pain', *The Journal of Clinical Investigation*, 123(7), pp. 3002–3013.
- Lai, B., Agarwal, R., Nelson, L.D., Swaminathan, S. & London, E. (2010) 'Low pH-Induced Pore Formation by the T Domain of Botulinum Toxin Type A is Dependent upon NaCl Concentration', *The Journal of Membrane Biology*, 236(2), pp. 191–201.
- LaMotte, C.C., Kapadia, S.E. & Shapiro, C.M. (1991) 'Central projections of the sciatic, saphenous, median, and ulnar nerves of the rat demonstrated by transganglionic transport of cholera toxin B-subunit-HRP (B-HRP) and wheat germ agglutinin-HRP (WGA-HRP)', *The Journal of Comparative Neurology*, 311(4), pp. 546–562.
- LaPointe, N.E., Morfini, G., Brady, S.T., Feinstein, S.C., Wilson, L. & Jordan, M.A. (2013) 'Effects of eribulin, vincristine, paclitaxel and ixabepilone on fast axonal transport and kinesin-1 driven microtubule gliding: Implications for chemotherapy-induced peripheral neuropathy', *Neurotoxicology*, 37pp. 231–239.
- Latremoliere, A. & Woolf, C.J. (2009) 'Central Sensitization: A Generator of Pain Hypersensitivity by Central Neural Plasticity', *The journal of pain : official journal of the American Pain Society*, 10(9), pp. 895–926.
- Lawson, J.J., McIlwrath, S.L., Woodbury, C.J., Davis, B.M. & Koerber, H.R. (2008) 'TRPV1 unlike TRPV2 is restricted to a subset of mechanically insensitive cutaneous nociceptors responding to heat', *The Journal of Pain*, 9(4), pp. 298–308.
- Lawson, S.N., Fang, X. & Djouhri, L. (2019) 'Nociceptor subtypes and their incidence in rat lumbar dorsal root ganglia (DRGs): focussing on C-polymodal nociceptors, A $\beta$ -nociceptors, moderate pressure receptors and their receptive field depths', *Current Opinion in Physiology*, 11pp. 125–146.
- Lawson, S.N. & Waddell, P.J. (1991) 'Soma neurofilament immunoreactivity is related to cell size and fibre conduction velocity in rat primary sensory neurons.', *The Journal of Physiology*, 435(1), pp. 41–63.
- Lekan, H.A., Carlton, S.M. & Coggeshall, R.E. (1996) 'Sprouting of A beta fibers into lamina II of the rat dorsal horn in peripheral neuropathy', *Neuroscience Letters*, 208(3), pp. 147–150.

- Li, C.-L., Li, K.-C., Wu, D., Chen, Y., Luo, H., Zhao, J.-R., Wang, S.-S., Sun, M.-M., Lu, Y.-J., Zhong, Y.-Q., Hu, X.-Y., Hou, R., Zhou, B.-B., Bao, L., Xiao, H.-S. & Zhang, X. (2016) 'Somatosensory neuron types identified by high-coverage single-cell RNA-sequencing and functional heterogeneity', *Cell Research*, 26(1), pp. 83–102.
- Li, Y., Adamek, P., Zhang, Haijun, Tatsui, C.E., Rhines, L.D., Mrozkova, P., Li, Q., Kosturakis, A.K., Cassidy, R.M., Harrison, D.S., Cata, J.P., Sapire, K., Zhang, Hongmei, Kennamer-Chapman, R.M., Jawad, A.B., Ghetti, A., Yan, J., Palecek, J. & Dougherty, P.M. (2015) 'The Cancer Chemotherapeutic Paclitaxel Increases Human and Rodent Sensory Neuron Responses to TRPV1 by Activation of TLR4', *Journal of Neuroscience*, 35(39), pp. 13487–13500.
- Li, Y., North, R.Y., Rhines, L.D., Tatsui, C.E., Rao, G., Edwards, D.D., Cassidy, R.M., Harrison, D.S., Johansson, C.A., Zhang, H. & Dougherty, P.M. (2018) 'DRG Voltage-Gated Sodium Channel 1.7 Is Upregulated in Paclitaxel-Induced Neuropathy in Rats and in Humans with Neuropathic Pain', *Journal of Neuroscience*, 38(5), pp. 1124–1136.
- Liu, C.-C., Lu, N., Cui, Y., Yang, T., Zhao, Z.-Q., Xin, W.-J. & Liu, X.-G. (2010) 'Prevention of Paclitaxel-induced allodynia by Minocycline: Effect on loss of peripheral nerve fibers and infiltration of macrophages in rats', *Molecular Pain*, 6p. 76.
- Löwe, J., Li, H., Downing, K.H. & Nogales, E. (2001) 'Refined structure of  $\alpha\beta$ -tubulin at 3.5 Å resolution', *Journal of Molecular Biology*, 313(5), pp. 1045–1057.
- Lucioni, A., Bales, G.T., Lotan, T.L., McGehee, D.S., Cook, S.P. & Rapp, D.E. (2008) 'Botulinum toxin type A inhibits sensory neuropeptide release in rat bladder models of acute injury and chronic inflammation', *BJU International*, 101(3), pp. 366–370.
- Lüscher, C., Xia, H., Beattie, E.C., Carroll, R.C., Zastrow, M. von, Malenka, R.C. & Nicoll, R.A. (1999) 'Role of AMPA Receptor Cycling in Synaptic Transmission and Plasticity', *Neuron*, 24(3), pp. 649–658.
- Ma, H., Meng, J., Wang, J., Hearty, S., Dolly, J.O. & O'Kennedy, R. (2014) 'Targeted delivery of a SNARE protease to sensory neurons using a single chain antibody (scFv) against the extracellular domain of P2X(3) inhibits the release of a pain mediator', *The Biochemical Journal*, 462(2), pp. 247–256.
- Maiarù, M., Leese, C., Certo, M., Echeverria-Altuna, I., Mangione, A.S., Arsenault, J., Davletov, B. & Hunt, S.P. (2018) 'Selective neuronal silencing using synthetic botulinum molecules alleviates chronic pain in mice', *Science Translational Medicine*, 10(450), .
- Makker, P.G.S., Duffy, S.S., Lees, J.G., Perera, C.J., Tonkin, R.S., Butovsky, O., Park, S.B., Goldstein, D. & Moalem-Taylor, G. (2017) 'Characterisation of Immune and Neuroinflammatory Changes Associated with Chemotherapy-Induced Peripheral Neuropathy', *PLoS ONE*, 12(1), .
- Malek, N., Pajak, A., Kolosowska, N., Kucharczyk, M. & Starowicz, K. (2015) 'The importance of TRPV1-sensitisation factors for the development of neuropathic pain', *Molecular and Cellular Neuroscience*, 65pp. 1–10.
- Malhotra, R., Huilgol, S.C. & Selva, D. (2003) 'Botulinum Toxin and Human Serum Albumin', *Archives of Ophthalmology*, 121(11), pp. 1661–1661.
- Mangione, A.S., Obara, I., Maiarù, M., Geranton, S.M., Tassorelli, C., Ferrari, E., Leese, C., Davletov, B. & Hunt, S.P. (2016) 'Nonparalytic botulinum molecules for the control of pain', *Pain*, 157(5), pp. 1045–1055.
- Marinelli, S., Luvisetto, S., Cobianchi, S., Makuch, W., Obara, I., Mezzaroma, E., Caruso, M., Straface, E., Przewlocka, B. & Pavone, F. (2010) 'Botulinum neurotoxin type A counteracts

- neuropathic pain and facilitates functional recovery after peripheral nerve injury in animal models', *Neuroscience*, 171(1), pp. 316–328.
- Martyn, J. a. J., Fagerlund, M.J. & Eriksson, L.I. (2009) 'Basic principles of neuromuscular transmission', *Anaesthesia*, 64(s1), pp. 1–9.
- Matak, I., Bach-Rojecky, L., Filipović, B. & Lacković, Z. (2011) 'Behavioral and immunohistochemical evidence for central antinociceptive activity of botulinum toxin A', *Neuroscience*, 186pp. 201–207.
- Matak, I. & Lacković, Z. (2014) 'Botulinum toxin A, brain and pain', *Progress in Neurobiology*, 119–120pp. 39–59.
- Matak, I., Riederer, P. & Lacković, Z. (2012) 'Botulinum toxin's axonal transport from periphery to the spinal cord', *Neurochemistry International*, 61(2), pp. 236–239.
- Matak, I., Rossetto, O. & Lacković, Z. (2014) 'Botulinum toxin type A selectivity for certain types of pain is associated with capsaicin-sensitive neurons', *PAIN®*, 155(8), pp. 1516–1526.
- Matsuoka, A., Mitsuma, A., Maeda, O., Kajiyama, H., Kiyoi, H., Kodera, Y., Nagino, M., Goto, H. & Ando, Y. (2016) 'Quantitative assessment of chemotherapy-induced peripheral neurotoxicity using a point-of-care nerve conduction device', *Cancer Science*, 107(10), pp. 1453–1457.
- McCoy, E.S., Taylor-Blake, B., Street, S.E., Pribisko, A.L., Zheng, J. & Zylka, M.J. (2013) 'Peptidergic CGRP $\alpha$  primary sensory neurons encode heat and itch and tonically suppress sensitivity to cold', *Neuron*, 78(1), pp. 138–151.
- Mehmood, R.K. (2014) 'Review of Cisplatin and Oxaliplatin in Current Immunogenic and Monoclonal Antibody Treatments', *Oncology Reviews*, 8(2), .
- Mekalanos, J.J., Collier, R.J. & Romig, W.R. (1977) 'Simple method for purifying cholera toxin, the natural toxin of *Vibrio cholerae*.', *Infection and Immunity*, 16(3), pp. 789–795.
- Meng, J., Ovsepian, S.V., Wang, J., Pickering, M., Sasse, A., Aoki, K.R., Lawrence, G.W. & Dolly, J.O. (2009) 'Activation of TRPV1 Mediates Calcitonin Gene-Related Peptide Release, Which Excites Trigeminal Sensory Neurons and Is Attenuated by a Retargeted Botulinum Toxin with Anti-Nociceptive Potential', *Journal of Neuroscience*, 29(15), pp. 4981–4992.
- Meng, J., Wang, J., Lawrence, G. & Dolly, J.O. (2007) 'Synaptobrevin I mediates exocytosis of CGRP from sensory neurons and inhibition by botulinum toxins reflects their anti-nociceptive potential', *Journal of Cell Science*, 120(16), pp. 2864–2874.
- Meng, J., Wang, J., Steinhoff, M. & Dolly, J.O. (2016) 'TNF $\alpha$  induces co-trafficking of TRPV1/TRPA1 in VAMP1-containing vesicles to the plasmalemma via Munc18–1/syntaxin1/SNAP-25 mediated fusion', *Scientific Reports*, 6.
- Middleton, S.J., Barry, A.M., Comini, M., Li, Y., Ray, P.R., Shiers, S., Themistocleous, A.C., Uhelski, M.L., Yang, X., Dougherty, P.M., Price, T.J. & Bennett, D.L. (2021) 'Studying human nociceptors: from fundamentals to clinic', *Brain*, 144(5), pp. 1312–1335.
- Millan, M.J. (2002) 'Descending control of pain', *Progress in Neurobiology*, 66(6), pp. 355–474.
- Mironov, S.L., Ivannikov, M.V. & Johansson, M. (2005) '[Ca<sup>2+</sup>]<sub>i</sub> Signaling between Mitochondria and Endoplasmic Reticulum in Neurons Is Regulated by Microtubules: FROM MITOCHONDRIAL PERMEABILITY TRANSITION PORE TO Ca<sup>2+</sup>-INDUCED Ca<sup>2+</sup> RELEASE \*', *Journal of Biological Chemistry*, 280(1), pp. 715–721.

- Mis, M.A., Yang, Y., Tanaka, B.S., Gomis-Perez, C., Liu, S., Dib-Hajj, F., Adi, T., Garcia-Milian, R., Schulman, B.R., Dib-Hajj, S.D. & Waxman, S.G. (2019) 'Resilience to Pain: A Peripheral Component Identified Using Induced Pluripotent Stem Cells and Dynamic Clamp', *The Journal of Neuroscience*, 39(3), pp. 382–392.
- Mishra, S.K., Tisel, S.M., Orestes, P., Bhangoo, S.K. & Hoon, M.A. (2011) 'TRPV1-lineage neurons are required for thermal sensation', *The EMBO Journal*, 30(3), pp. 582–593.
- Miyano, K., Tang, H.-B., Nakamura, Y., Morioka, N., Inoue, A. & Nakata, Y. (2009) 'Paclitaxel and vinorelbine, evoked the release of substance P from cultured rat dorsal root ganglion cells through different PKC isoform-sensitive ion channels', *Neuropharmacology*, 57(1), pp. 25–32.
- Mocchetti, I. (2005) 'Exogenous gangliosides, neuronal plasticity and repair, and the neurotrophins', *Cellular and molecular life sciences: CMLS*, 62(19–20), pp. 2283–2294.
- Mohammed, Z.A., Kaloyanova, K. & Nassar, M.A. (2020) 'An unbiased and efficient assessment of excitability of sensory neurons for analgesic drug discovery', *Pain*, 161(5), pp. 1100–1108.
- Morenilla-Palao, C., Planells-Cases, R., García-Sanz, N. & Ferrer-Montiel, A. (2004) 'Regulated Exocytosis Contributes to Protein Kinase C Potentiation of Vanilloid Receptor Activity', *Journal of Biological Chemistry*, 279(24), pp. 25665–25672.
- Moskowitz, P.F., Smith, R., Pickett, J., Frankfurter, A. & Oblinger, M.M. (1993) 'Expression of the class III  $\beta$ -tubulin gene during axonal regeneration of rat dorsal root ganglion neurons', *Journal of Neuroscience Research*, 34(1), pp. 129–134.
- Mostafavi, H., Thiyagarajan, S., Stratton, B.S., Karatekin, E., Warner, J.M., Rothman, J.E. & O'Shaughnessy, B. (2017) 'Entropic forces drive self-organization and membrane fusion by SNARE proteins', *Proceedings of the National Academy of Sciences*, 114(21), pp. 5455–5460.
- Moudi, M., Go, R., Yien, C.Y.S. & Nazre, M. (2013) 'Vinca Alkaloids', *International Journal of Preventive Medicine*, 4(11), p. 1231.
- Nakamura-Craig, M. & Gill, B.K. (1991) 'Effect of neurokinin A, substance P and calcitonin gene related peptide in peripheral hyperalgesia in the rat paw', *Neuroscience Letters*, 124(1), pp. 49–51.
- Nakata, T. & Yorifuji, H. (1999) 'Morphological evidence of the inhibitory effect of taxol on the fast axonal transport', *Neuroscience Research*, 35(2), pp. 113–122.
- Namer, B., Schmidt, D., Eberhardt, E., Maroni, M., Dorfmeister, E., Kleggetveit, I.P., Kaluza, L., Meents, J., Gerlach, A., Lin, Z., Winterpacht, A., Dragicevic, E., Kohl, Z., Schüttler, J., Kurth, I., Warncke, T., Jorum, E., Winner, B. & Lampert, A. (2018) 'Pain relief in a neuropathy patient by lacosamide: Proof of principle of clinical translation from patient-specific iPS cell-derived nociceptors', *EBioMedicine*, 39pp. 401–408.
- NICE-The National Institute for Health and Care Excellence (2020) *BNF: British National Formulary - NICE*. [Online] [online]. Available from: <https://bnf.nice.org.uk/drug/paclitaxel.html> (Accessed 15 May 2020).
- Nigam, P.K. & Nigam, A. (2010) 'BOTULINUM TOXIN', *Indian Journal of Dermatology*, 55(1), pp. 8–14.
- Nitzan-Luques, A., Devor, M. & Tal, M. (2011) 'Genotype-selective phenotypic switch in primary afferent neurons contributes to neuropathic pain', *Pain*, 152(10), pp. 2413–2426.

- Nugent, M., Wang, J., Lawrence, G., Zurawski, T., Geoghegan, J.A. & Dolly, J.O. (2017) 'Conjugate of an IgG Binding Domain with Botulinum Neurotoxin A Lacking the Acceptor Moiety Targets Its SNARE Protease into TrkA-Expressing Cells When Coupled to Anti-TrkA IgG or Fc- $\beta$ NGF', *Bioconjugate Chemistry*, 28(6), pp. 1684–1692.
- Nugent, M., Yusef, Y.R., Meng, J., Wang, J. & Dolly, J.O. (2018) 'A SNAP-25 cleaving chimera of botulinum neurotoxin /A and /E prevents TNF $\alpha$ -induced elevation of the activities of native TRP channels on early postnatal rat dorsal root ganglion neurons', *Neuropharmacology*, 138pp. 257–266.
- Numazaki, M., Tominaga, T., Takeuchi, K., Murayama, N., Toyooka, H. & Tominaga, M. (2003) 'Structural determinant of TRPV1 desensitization interacts with calmodulin', *Proceedings of the National Academy of Sciences*, 100(13), pp. 8002–8006.
- Ogawa-Goto, K. & Abe, T. (1998) 'Gangliosides and Glycosphingolipids of Peripheral Nervous System Myelins—a Minireview', *Neurochemical Research*, 23(3), pp. 305–310.
- Oszlács, O., Jancsó, G., Kis, G., Dux, M. & Sántha, P. (2015) 'Perineural capsaicin induces the uptake and transganglionic transport of cholera toxin b subunit by nociceptive c-fiber primary afferent neurons', *Neuroscience*, 311(Supplement C), pp. 243–252.
- Palma, N.Z., da Cruz, M., Fagundes, V. & Pires, L. (2019) 'Foodborne Botulism: Neglected Diagnosis', *European Journal of Case Reports in Internal Medicine*, 6(5), .
- Park, H.J., Lee, Y., Lee, J., Park, C. & Moon, D.E. (2006) 'The effects of botulinum toxin A on mechanical and cold allodynia in a rat model of neuropathic pain', *Canadian Journal of Anaesthesia = Journal Canadien D'anesthésie*, 53(5), pp. 470–477.
- Park, J. & Park, H.J. (2017) 'Botulinum Toxin for the Treatment of Neuropathic Pain', *Toxins*, 9(9), .
- Peck, M.W., Smith, T.J., Anniballi, F., Austin, J.W., Bano, L., Bradshaw, M., Cuervo, P., Cheng, L.W., Derman, Y., Dorner, B.G., Fisher, A., Hill, K.K., Kalb, S.R., Korkeala, H., Lindström, M., Lista, F., Lúquez, C., Mazuet, C., Pirazzini, M., et al. (2017) 'Historical Perspectives and Guidelines for Botulinum Neurotoxin Subtype Nomenclature', *Toxins*, 9(1), p. 38.
- Peeraer, E., Lutsenborg, A.V., Verheyen, A., Jongh, R.D., Nuydens, R. & Meert, T.F. (2011) 'Pharmacological evaluation of rat dorsal root ganglion neurons as an in vitro model for diabetic neuropathy', *Journal of Pain Research*, 4pp. 55–65.
- Peirs, C., Williams, S.-P.G., Zhao, X., Arokiaraj, C.M., Ferreira, D.W., Noh, M., Smith, K.M., Halder, P., Corrigan, K.A., Gedeon, J.Y., Lee, S.J., Gatto, G., Chi, D., Ross, S.E., Goulding, M. & Seal, R.P. (2021) 'Mechanical Allodynia Circuitry in the Dorsal Horn Is Defined by the Nature of the Injury', *Neuron*, 109(1), pp. 73-90.e7.
- Peters, C.M., Jimenez-Andrade, J.M., Jonas, B.M., Sevcik, M.A., Koewler, N.J., Ghilardi, J.R., Wong, G.Y. & Mantyh, P.W. (2007) 'Intravenous paclitaxel administration in the rat induces a peripheral sensory neuropathy characterized by macrophage infiltration and injury to sensory neurons and their supporting cells', *Experimental Neurology*, 203(1), pp. 42–54.
- Peters, C.M., Jimenez-Andrade, J.M., Kuskowski, M.A., Ghilardi, J.R. & Mantyh, P.W. (2007) 'An evolving cellular pathology occurs in dorsal root ganglia, peripheral nerve and spinal cord following intravenous administration of paclitaxel in the rat', *Brain research*, 1168pp. 46–59.
- Pittman, S.K., Gracias, N.G., Vasko, M.R. & Fehrenbacher, J.C. (2014) 'Paclitaxel alters the evoked release of calcitonin gene-related peptide from rat sensory neurons in culture', *Experimental Neurology*, 253pp. 146–153.

- Planells-Cases, R. & Ferrer-Montiel, A. (2007) 'TRP Channel Trafficking', in Wolfgang B. Liedtke & Stefan Heller (eds.) *TRP Ion Channel Function in Sensory Transduction and Cellular Signaling Cascades*. Frontiers in Neuroscience. [Online]. Boca Raton (FL): CRC Press/Taylor & Francis.
- Pocock, G. (2013) *By Gillian Pocock Human Physiology*. 4th Edition edition. OUP Oxford.
- Poirier, M.A., Xiao, W., Macosko, J.C., Chan, C., Shin, Y.K. & Bennett, M.K. (1998) 'The synaptic SNARE complex is a parallel four-stranded helical bundle', *Nature Structural Biology*, 5(9), pp. 765–769.
- Polomano, R.C. & Farrar, J.T. (2006) 'Pain and neuropathy in cancer survivors. Surgery, radiation, and chemotherapy can cause pain; research could improve its detection and treatment', *The American Journal of Nursing*, 106(3 Suppl), pp. 39–47.
- Polomano, R.C., Mannes, A.J., Clark, U.S. & Bennett, G.J. (2001) 'A painful peripheral neuropathy in the rat produced by the chemotherapeutic drug, paclitaxel', *Pain*, 94(3), pp. 293–304.
- Popoff, M.R. & Bouvet, P. (2013) 'Genetic characteristics of toxigenic Clostridia and toxin gene evolution', *Toxicon: Official Journal of the International Society on Toxinology*, 75pp. 63–89.
- Postma, T.J., Vermorcken, J.B., Liefing, A.J., Pinedo, H.M. & Heimans, J.J. (1995) 'Paclitaxel-induced neuropathy', *Annals of Oncology: Official Journal of the European Society for Medical Oncology*, 6(5), pp. 489–494.
- Raja, S.N., Carr, D.B., Cohen, M., Finnerup, N.B., Flor, H., Gibson, S., Keefe, F.J., Mogil, J.S., Ringkamp, M., Sluka, K.A., Song, X.-J., Stevens, B., Sullivan, M.D., Tutelman, P.R., Ushida, T. & Vader, K. (2020) 'The revised International Association for the Study of Pain definition of pain: concepts, challenges, and compromises', *PAIN*, 161(9), pp. 1976–1982.
- Relja, M. & Klepac, N. (2002) 'Different Doses of Botulinum Toxin A and Pain Responsiveness in Cervical Dystonia', *Neurology*, 58(7), p. 474.
- Restani, L., Antonucci, F., Gianfranceschi, L., Rossi, C., Rossetto, O. & Caleo, M. (2011) 'Evidence for Anterograde Transport and Transcytosis of Botulinum Neurotoxin A (BoNT/A)', *Journal of Neuroscience*, 31(44), pp. 15650–15659.
- Rivero-Melián, C. & Grant, G. (1991) 'Cholera toxin horseradish peroxidase used for studying projections of some hindlimb cutaneous nerves and plantar foot afferents to the dorsal horn and Clarke's column in the rat', *Experimental Brain Research*, 84(1), .
- Rivero-Melián, C., Rosario, C. & Grant, G. (1992) 'Demonstration of transganglionically transported cholera toxin in rat spinal cord by immunofluorescence cytochemistry', *Neuroscience Letters*, 145(1), pp. 114–117.
- Robertson, B. & Grant, G. (1985) 'A comparison between wheat germ agglutinin and cholera toxin-horseradish peroxidase as anterogradely transported markers in central branches of primary sensory neurones in the rat with some observations in the cat', *Neuroscience*, 14(3), pp. 895–905.
- Robertson, B. & Grant, G. (1989) 'Immunocytochemical evidence for the localization of the GM1 ganglioside in carbonic anhydrase-containing and RT 97-immunoreactive rat primary sensory neurons', *Journal of Neurocytology*, 18(1), pp. 77–86.
- Robertson, B., Perry, M.J. & Lawson, S.N. (1991) 'Populations of rat spinal primary afferent neurons with cholera toxin binding compared with those labelled by markers for neurofilament and carbohydrate groups: a quantitative immunocytochemical study', *Journal of Neurocytology*, 20(5), pp. 387–395.

- Rossato, M.F., Rigo, F.K., Oliveira, S.M., Guerra, G.P., Silva, C.R., Cunha, T.M., Gomez, M.V., Ferreira, J. & Trevisan, G. (2018) 'Participation of transient receptor potential vanilloid 1 in paclitaxel-induced acute visceral and peripheral nociception in rodents', *European Journal of Pharmacology*, 828pp. 42–51.
- Rostock, C., Schrenk-Siemens, K., Pohle, J. & Siemens, J. (2018) 'Human vs. Mouse Nociceptors – Similarities and Differences', *Neuroscience*, 387pp. 13–27.
- Royle, S.J. & Murrell-Lagnado, R.D. (2003) 'Constitutive cycling: A general mechanism to regulate cell surface proteins', *BioEssays*, 25(1), pp. 39–46.
- Rummel, A. (2013) 'Double Receptor Anchorage of Botulinum Neurotoxins Accounts for their Exquisite Neurospecificity', in Andreas Rummel & Thomas Binz (eds.) *Botulinum Neurotoxins*. Current Topics in Microbiology and Immunology. [Online]. Berlin, Heidelberg: Springer. pp. 61–90.
- Ruscheweyh, R., Forsthuber, L., Schoffnegger, D. & Sandkühler, J. (2007) 'Modification of classical neurochemical markers in identified primary afferent neurons with A $\beta$ -, A $\delta$ -, and C-fibers after chronic constriction injury in mice', *Journal of Comparative Neurology*, 502(2), pp. 325–336.
- Sakamoto, T., Torii, Y., Takahashi, M., Ishida, S., Goto, Y., Nakano, H., Harakawa, T., Ginnaga, A., Kozaki, S. & Kaji, R. (2009) 'Quantitative determination of the biological activity of botulinum toxin type A by measuring the compound muscle action potential (CMAP) in rats', *Toxicon*, 54(6), pp. 857–861.
- Salvemini, D., Little, J.W., Doyle, T. & Neumann, W.L. (2011) 'Roles of Reactive Oxygen and Nitrogen Species in Pain', *Free radical biology & medicine*, 51(5), pp. 951–966.
- Samanta, A., Hughes, T.E.T. & Moiseenkova-Bell, V.Y. (2018) 'Transient Receptor Potential (TRP) Channels', *Sub-cellular biochemistry*, 87pp. 141–165.
- Sandkühler, J. (2009) 'Models and Mechanisms of Hyperalgesia and Allodynia', *Physiological Reviews*, 89(2), pp. 707–758.
- Sántha, P. & Jancsó, G. (2003) 'Transganglionic transport of cholera toxin by capsaicin-sensitive c-fibre afferents to the substantia gelatinosa of the spinal dorsal horn after peripheral nerve section', *Neuroscience*, 116(3), pp. 621–627.
- Sanz-Salvador, L., Andrés-Borderia, A., Ferrer-Montiel, A. & Planells-Cases, R. (2012) 'Agonist- and Ca<sup>2+</sup>-dependent Desensitization of TRPV1 Channel Targets the Receptor to Lysosomes for Degradation', *Journal of Biological Chemistry*, 287(23), pp. 19462–19471.
- Schaible, H.-G., Ebersberger, A. & Natura, G. (2011) 'Update on peripheral mechanisms of pain: beyond prostaglandins and cytokines', *Arthritis Research & Therapy*, 13(2), p. 210.
- Schiavo, G., Poulain, B., Benfenati, F., DasGupta, B.R. & Montecucco, C. (1993) 'Novel targets and catalytic activities of bacterial protein toxins', *Trends in Microbiology*, 1(5), pp. 170–174.
- Schiavo, G., Rossetto, O., Santucci, A., DasGupta, B.R. & Montecucco, C. (1992) 'Botulinum neurotoxins are zinc proteins', *The Journal of Biological Chemistry*, 267(33), pp. 23479–23483.
- Schmidt, M., Dubin, A.E., Petrus, M.J., Earley, T.J. & Patapoutian, A. (2009) 'Various signals involved in nociception regulate TRPA1 levels at the plasma membrane', *Neuron*, 64(4), pp. 498–509.
- Schubert, V., Bouvier, D. & Volterra, A. (2011) 'SNARE protein expression in synaptic terminals and astrocytes in the adult hippocampus: A comparative analysis', *Glia*, 59(10), pp. 1472–1488.

- Scott, A.B. & Suzuki, D. (1988) 'Systemic toxicity of botulinum toxin by intramuscular injection in the monkey', *Movement Disorders*, 3(4), pp. 333–335.
- Scripture, C.D., Figg, W.D. & Sparreboom, A. (2006) 'Peripheral Neuropathy Induced by Paclitaxel: Recent Insights and Future Perspectives', *Current Neuropharmacology*, 4(2), pp. 165–172.
- Seretny, M., Currie, G.L., Sena, E.S., Ramnarine, S., Grant, R., MacLeod, M.R., Colvin, L.A. & Fallon, M. (2014) 'Incidence, prevalence, and predictors of chemotherapy-induced peripheral neuropathy: A systematic review and meta-analysis', *Pain*, 155(12), pp. 2461–2470.
- Setou, M., Nakagawa, T., Seog, D.-H. & Hirokawa, N. (2000) 'Kinesin Superfamily Motor Protein KIF17 and mLin-10 in NMDA Receptor-Containing Vesicle Transport', *Science*, 288(5472), pp. 1796–1802.
- Setou, M., Seog, D.-H., Tanaka, Y., Kanai, Y., Takei, Y., Kawagishi, M. & Hirokawa, N. (2002) 'Glutamate-receptor-interacting protein GRIP1 directly steers kinesin to dendrites', *Nature*, 417(6884), pp. 83–87.
- Shehab, S.A.S., Spike, R.C. & Todd, A.J. (2003) 'Evidence against cholera toxin B subunit as a reliable tracer for sprouting of primary afferents following peripheral nerve injury', *Brain Research*, 964(2), pp. 218–227.
- Shimizu, T., Shibata, M., Toriumi, H., Iwashita, T., Funakubo, M., Sato, H., Kuroi, T., Ebine, T., Koizumi, K. & Suzuki, N. (2012) 'Reduction of TRPV1 expression in the trigeminal system by botulinum neurotoxin type-A', *Neurobiology of Disease*, 48(3), pp. 367–378.
- Sikorra, S., Litschko, C., Müller, C., Thiel, N., Galli, T., Eichner, T. & Binz, T. (2016) 'Identification and Characterization of Botulinum Neurotoxin A Substrate Binding Pockets and Their Re-Engineering for Human SNAP-23', *Journal of Molecular Biology*, 428(2, Part A), pp. 372–384.
- da Silva, L.B., Karshenas, A., Bach, F.W., Rasmussen, S., Arendt-Nielsen, L. & Gazerani, P. (2014) 'Blockade of glutamate release by botulinum neurotoxin type A in humans: A dermal microdialysis study', *Pain Research & Management : The Journal of the Canadian Pain Society*, 19(3), pp. 126–132.
- Simone, D.A., Nolano, M., Johnson, T., Wendelschafer-Crabb, G. & Kennedy, W.R. (1998) 'Intradermal Injection of Capsaicin in Humans Produces Degeneration and Subsequent Reinnervation of Epidermal Nerve Fibers: Correlation with Sensory Function', *Journal of Neuroscience*, 18(21), pp. 8947–8959.
- Sinclair, S.R., Kane, S.A., Van der Schueren, B.J., Xiao, A., Willson, K.J., Boyle, J., de Lepeleire, I., Xu, Y., Hickey, L., Denney, W.S., Li, C.-C., Palcza, J., Vanmolkot, F.H.M., Depré, M., Van Hecken, A., Murphy, M.G., Ho, T.W. & de Hoon, J.N. (2010) 'Inhibition of capsaicin-induced increase in dermal blood flow by the oral CGRP receptor antagonist, telcagepant (MK-0974)', *British Journal of Clinical Pharmacology*, 69(1), pp. 15–22.
- Sparreboom, A., Tellingen, O. van, Nooijen, W.J. & Beijnen, J.H. (1996) 'Nonlinear Pharmacokinetics of Paclitaxel in Mice Results from the Pharmaceutical Vehicle Cremophor EL', *Cancer Research*, 56(9), pp. 2112–2115.
- Staff, N.P., Fehrenbacher, J.C., Caillaud, M., Damaj, M.I., Segal, R.A. & Rieger, S. (2020) 'Pathogenesis of paclitaxel-induced peripheral neuropathy: A current review of in vitro and in vivo findings using rodent and human model systems', *Experimental neurology*, 324p. 113121.
- Stemkowski, P.L. & Smith, P.A. (2012) 'Sensory Neurons, Ion Channels, Inflammation and the Onset of Neuropathic Pain', *Canadian Journal of Neurological Sciences*, 39(4), pp. 416–435.

- Stenoien, D.L. & Brady, S.T. (1999) 'Molecular Motors: Kinesin, Dynein and Myosin', *Basic Neurochemistry: Molecular, Cellular and Medical Aspects*. 6th edition,
- Stirling, L.C., Forlani, G., Baker, M.D., Wood, J.N., Matthews, E.A., Dickenson, A.H. & Nassar, M.A. (2005) 'Nociceptor-specific gene deletion using heterozygous Nav1.8-Cre recombinase mice', *Pain*, 113(1–2), pp. 27–36.
- Stucky, C.L. & Lewin, G.R. (1999) 'Isolectin B(4)-positive and -negative nociceptors are functionally distinct', *The Journal of Neuroscience: The Official Journal of the Society for Neuroscience*, 19(15), pp. 6497–6505.
- Studer, M. & McNaughton, P.A. (2010) 'Modulation of single-channel properties of TRPV1 by phosphorylation', *The Journal of Physiology*, 588(Pt 19), pp. 3743–3756.
- Su, Y.-Y., Ye, M., Li, L., Liu, C., Pan, J., Liu, W.-W., Jiang, Y., Jiang, X.-Y., Zhang, X., Shu, Y. & Bao, L. (2013) 'KIF5B Promotes the Forward Transport and Axonal Function of the Voltage-Gated Sodium Channel Nav1.8', *Journal of Neuroscience*, 33(45), pp. 17884–17896.
- Sun, R.-Q., Lawand, N.B., Lin, Q. & Willis, W.D. (2004) 'Role of calcitonin gene-related peptide in the sensitization of dorsal horn neurons to mechanical stimulation after intradermal injection of capsaicin', *Journal of Neurophysiology*, 92(1), pp. 320–326.
- Sun, R.-Q., Lawand, N.B. & Willis, W.D. (2003) 'The role of calcitonin gene-related peptide (CGRP) in the generation and maintenance of mechanical allodynia and hyperalgesia in rats after intradermal injection of capsaicin', *Pain*, 104(1–2), pp. 201–208.
- Sun, R.-Q., Tu, Y.-J., Lawand, N.B., Yan, J.-Y., Lin, Q. & Willis, W.D. (2004) 'Calcitonin gene-related peptide receptor activation produces PKA- and PKC-dependent mechanical hyperalgesia and central sensitization', *Journal of Neurophysiology*, 92(5), pp. 2859–2866.
- Suter, M.R., Wen, Y.-R., Decosterd, I. & Ji, R.-R. (2007) 'Do glial cells control pain?', *Neuron glia biology*, 3(3), pp. 255–268.
- Swett, J.E., Torigoe, Y., Elie, V.R., Bourassa, C.M. & Miller, P.G. (1991) 'Sensory neurons of the rat sciatic nerve', *Experimental Neurology*, 114(1), pp. 82–103.
- Tang, M., Meng, J. & Wang, J. (2019) 'New Engineered-Botulinum Toxins Inhibit the Release of Pain-Related Mediators', *International Journal of Molecular Sciences*, 21(1), .
- Tasnim, A., Rammelkamp, Z., Slusher, A.B., Wozniak, K., Slusher, B.S. & Farah, M.H. (2016) 'Paclitaxel causes degeneration of both central and peripheral axon branches of dorsal root ganglia in mice', *BMC Neuroscience*, 17.
- Taylor-Clark, T.E., Udem, B.J., Macglashan, D.W., Ghatta, S., Carr, M.J. & McAlexander, M.A. (2008) 'Prostaglandin-induced activation of nociceptive neurons via direct interaction with transient receptor potential A1 (TRPA1)', *Molecular Pharmacology*, 73(2), pp. 274–281.
- Tian, Q., Hu, J., Xie, C., Mei, K., Pham, C., Mo, X., Hepp, R., Soares, S., Nothias, F., Wang, Y., Liu, Q., Cai, F., Zhong, B., Li, D. & Yao, J. (2019) 'Recovery from tachyphylaxis of TRPV1 coincides with recycling to the surface membrane', *Proceedings of the National Academy of Sciences of the United States of America*, 116(11), pp. 5170–5175.
- Todd, A.J. (2010) 'Neuronal circuitry for pain processing in the dorsal horn', *Nature reviews. Neuroscience*, 11(12), pp. 823–836.
- Toftthagen\*, C., McAllister, R.D. & Visovsky, C. (2013a) 'Peripheral Neuropathy Caused by Paclitaxel and Docetaxel: An Evaluation and Comparison of Symptoms', *Journal of the advanced practitioner in oncology*, 4(4), pp. 204–215.

- Toftthagen\*, C., McAllister, R.D. & Visovsky, C. (2013b) 'Peripheral Neuropathy Caused by Paclitaxel and Docetaxel: An Evaluation and Comparison of Symptoms', *Journal of the advanced practitioner in oncology*, 4(4), pp. 204–215.
- Tong, Y.-G., Wang, H.F., Ju, G., Grant, G., Hökfelt, T. & Zhang, X. (1999) 'Increased uptake and transport of cholera toxin B-subunit in dorsal root ganglion neurons after peripheral axotomy: Possible implications for sensory sprouting', *Journal of Comparative Neurology*, 404(2), pp. 143–158.
- Torii, Y., Goto, Y., Nakahira, S. & Ginnaga, A. (2014) 'Establishment of alternative potency test for botulinum toxin type A using compound muscle action potential (CMAP) in rats', *Toxicon*, 90pp. 97–105.
- Treede, R.D., Kenshalo, D.R., Gracely, R.H. & Jones, A.K. (1999) 'The cortical representation of pain', *Pain*, 79(2–3), pp. 105–111.
- Treede, R.D., Meyer, R.A. & Campbell, J.N. (1998) 'Myelinated mechanically insensitive afferents from monkey hairy skin: heat-response properties', *Journal of Neurophysiology*, 80(3), pp. 1082–1093.
- Treede, R.-D., Rief, W., Barke, A., Aziz, Q., Bennett, M.I., Benoliel, R., Cohen, M., Evers, S., Finnerup, N.B., First, M.B., Giamberardino, M.A., Kaasa, S., Kosek, E., Lavand'homme, P., Nicholas, M., Perrot, S., Scholz, J., Schug, S., Smith, B.H., et al. (2015) 'A classification of chronic pain for ICD-11', *Pain*, 156(6), pp. 1003–1007.
- Usoskin, D., Furlan, A., Islam, S., Abdo, H., Lönnerberg, P., Lou, D., Hjerling-Leffler, J., Haeggström, J., Kharchenko, O., Kharchenko, P.V., Linnarsson, S. & Ernfors, P. (2015) 'Unbiased classification of sensory neuron types by large-scale single-cell RNA sequencing', *Nature Neuroscience*, 18(1), pp. 145–153.
- Vandewauw, I., De Clercq, K., Mulier, M., Held, K., Pinto, S., Van Ranst, N., Segal, A., Voet, T., Vennekens, R., Zimmermann, K., Vriens, J. & Voets, T. (2018) 'A TRP channel trio mediates acute noxious heat sensing', *Nature*, 555(7698), pp. 662–666.
- Vyklický, L., Nováková-Tousová, K., Benedikt, J., Samad, A., Touska, F. & Vlachová, V. (2008) 'Calcium-dependent desensitization of vanilloid receptor TRPV1: a mechanism possibly involved in analgesia induced by topical application of capsaicin', *Physiological Research*, 57 Suppl 3pp. S59-68.
- Wang, J., Casals-Diaz, L., Zurawski, T., Meng, J., Moriarty, O., Nealon, J., Edupuganti, O.P. & Dolly, O. (2017) 'A novel therapeutic with two SNAP-25 inactivating proteases shows long-lasting anti-hyperalgesic activity in a rat model of neuropathic pain', *Neuropharmacology*, 118pp. 223–232.
- Wang, T., Molliver, D.C., Jing, X., Schwartz, E.S., Yang, F.-C., Samad, O.A., Ma, Q. & Davis, B.M. (2011) 'Phenotypic Switching of Nonpeptidergic Cutaneous Sensory Neurons following Peripheral Nerve Injury', *PLOS ONE*, 6(12), p. e28908.
- Wang, T.-H., Wang, H.-S. & Soong, Y.-K. (2000) 'Paclitaxel-induced cell death', *Cancer*, 88(11), pp. 2619–2628.
- Weaver, B.A. (2014) 'How Taxol/paclitaxel kills cancer cells', *Molecular Biology of the Cell*, 25(18), pp. 2677–2681.
- Welch, M.J., Purkiss, J.R. & Foster, K.A. (2000) 'Sensitivity of embryonic rat dorsal root ganglia neurons to Clostridium botulinum neurotoxins', *Toxicon*, 38(2), pp. 245–258.

- Wen, Y.-R., Suter, M.R., Kawasaki, Y., Huang, J., Pertin, M., Kohno, T., Berde, C.B., Decosterd, I. & Ji, R.-R. (2007) 'Nerve conduction blockade in the sciatic nerve prevents but does not reverse the activation of p38 mitogen-activated protein kinase in spinal microglia in the rat spared nerve injury model', *Anesthesiology*, 107(2), pp. 312–321.
- Wernick, N.L.B., Chinnapen, D.J.-F., Cho, J.A. & Lencer, W.I. (2010) 'Cholera Toxin: An Intracellular Journey into the Cytosol by Way of the Endoplasmic Reticulum', *Toxins*, 2(3), pp. 310–325.
- Wey, J., Tang, S. & Wu, T. (2006) 'Disulfide bond reduction corresponds to dimerization and hydrophobicity changes of Clostridium botulinum type A neurotoxin', *Acta Pharmacologica Sinica*, 27(9), pp. 1238–1246.
- Wiesenfeld-Hallin, Z., Hökfelt, T., Lundberg, J.M., Forssmann, W.G., Reinecke, M., Tschopp, F.A. & Fischer, J.A. (1984) 'Immunoreactive calcitonin gene-related peptide and substance P coexist in sensory neurons to the spinal cord and interact in spinal behavioral responses of the rat', *Neuroscience Letters*, 52(1), pp. 199–204.
- Winter, J., Forbes, C.A., Sternberg, J. & Lindsay, R.M. (1988) 'Nerve growth factor (NGF) regulates adult rat cultured dorsal root ganglion neuron responses to the excitotoxin capsaicin', *Neuron*, 1(10), pp. 973–981.
- Wood, J.N. (2007) 'Ion channels in analgesia research', *Handbook of Experimental Pharmacology*, (177), pp. 329–358.
- Woolf, C.J., Shortland, P. & Coggeshall, R.E. (1992) 'Peripheral nerve injury triggers central sprouting of myelinated afferents', *Nature*, 355(6355), pp. 75–78.
- Woolf, C.J. & Thompson, S.W.N. (1991) 'The induction and maintenance of central sensitization is dependent on N-methyl-D-aspartic acid receptor activation; implications for the treatment of post-injury pain hypersensitivity states', *Pain*, 44(3), pp. 293–299.
- Wozniak, K.M., Vornov, J.J., Wu, Y., Liu, Y., Carozzi, V.A., Rodriguez-Menendez, V., Ballarini, E., Alberti, P., Pozzi, E., Semperboni, S., Cook, B.M., Littlefield, B.A., Nomoto, K., Condon, K., Eckley, S., DesJardins, C., Wilson, L., Jordan, M.A., Feinstein, S.C., et al. (2018) 'Peripheral Neuropathy Induced by Microtubule-Targeted Chemotherapies: Insights into Acute Injury and Long-term Recovery', *Cancer Research*, 78(3), pp. 817–829.
- Wu, C., Xie, N., Lian, Y., Xu, H., Chen, C., Zheng, Y., Chen, Y. & Zhang, H. (2016) 'Central antinociceptive activity of peripherally applied botulinum toxin type A in lab rat model of trigeminal neuralgia', *SpringerPlus*, 5.
- Xiao, L., Cheng, J., Dai, J. & Zhang, D. (2011a) 'Botulinum toxin decreases hyperalgesia and inhibits P2X3 receptor over-expression in sensory neurons induced by ventral root transection in rats', *Pain Medicine (Malden, Mass.)*, 12(9), pp. 1385–1394.
- Xiao, L., Cheng, J., Dai, J. & Zhang, D. (2011b) 'Botulinum Toxin Decreases Hyperalgesia and Inhibits P2X3 Receptor Over-Expression in Sensory Neurons Induced by Ventral Root Transection in Rats', *Pain Medicine*, 12(9), pp. 1385–1394.
- Xu, M., Gu, Y., Barry, J. & Gu, C. (2010) 'Kinesin I Transports Tetramerized Kv3 Channels through the Axon Initial Segment via Direct Binding', *Journal of Neuroscience*, 30(47), pp. 15987–16001.
- Yang, H., Siddique, R., Hosmane, S., Thakor, N. & Höke, A. (2009) 'Compartmentalized microfluidic culture platform to study mechanism of paclitaxel-induced axonal degeneration', *Experimental neurology*, 218(1), pp. 124–128.

- Yao, J. & Qin, F. (2009) 'Interaction with Phosphoinositides Confers Adaptation onto the TRPV1 Pain Receptor', *PLOS Biology*, 7(2), p. e1000046.
- Yoon, C., Young Wook, Y., Heung Sik, N., Sun Ho, K. & Jin Mo, C. (1994) 'Behavioral signs of ongoing pain and cold allodynia in a rat model of neuropathic pain', *Pain*, 59(3), pp. 369–376.
- Yousuf, M.S., Noh, M.-C., Friedman, T.N., Zubkow, K., Johnson, J.C., Tenorio, G., Kurata, H.T., Smith, P.A. & Kerr, B.J. (2019) 'Sensory Neurons of the Dorsal Root Ganglia Become Hyperexcitable in a T-Cell-Mediated MOG-EAE Model of Multiple Sclerosis', *eNeuro*, 6(2), p. ENEURO.0024-19.2019.
- Yu, R.K., Tsai, Y.-T., Ariga, T. & Yanagisawa, M. (2011) 'Structures, biosynthesis, and functions of gangliosides—An overview', *Journal of oleo science*, 60(10), pp. 537–544.
- Zajączkowska, R., Kocot-Kępska, M., Leppert, W., Wrzosek, A., Mika, J. & Wordliczek, J. (2019) 'Mechanisms of Chemotherapy-Induced Peripheral Neuropathy', *International Journal of Molecular Sciences*, 20(6), .
- Zeisel, A., Hochgerner, H., Lönnerberg, P., Johnsson, A., Memic, F., van der Zwan, J., Häring, M., Braun, E., Borm, L.E., La Manno, G., Codeluppi, S., Furlan, A., Lee, K., Skene, N., Harris, K.D., Hjerling-Leffler, J., Arenas, E., Ernfors, P., Marklund, U., et al. (2018) 'Molecular Architecture of the Mouse Nervous System', *Cell*, 174(4), pp. 999-1014.e22.
- Zhang, H. & Dougherty, P.M. (2014) 'Enhanced Excitability of Primary Sensory Neurons and Altered Gene Expression of Neuronal Ion Channels in Dorsal Root Ganglion in Paclitaxel-Induced Peripheral Neuropathy', *Anesthesiology*, 120(6), pp. 1463–1475.
- Zhang, Haijun, Yoon, S.-Y., Zhang, Hongmei & Dougherty, P.M. (2012) 'Evidence that spinal astrocytes but not microglia contribute to the pathogenesis of Paclitaxel-induced painful neuropathy', *The Journal of Pain*, 13(3), pp. 293–303.
- Zhang, S., Masuyer, G., Zhang, J., Shen, Y., Lundin, D., Henriksson, L., Miyashita, S.-I., Martínez-Carranza, M., Dong, M. & Stenmark, P. (2017) 'Identification and characterization of a novel botulinum neurotoxin', *Nature Communications*, 8(1), p. 14130.
- Zhang, X., Huang, J. & McNaughton, P.A. (2005) 'NGF rapidly increases membrane expression of TRPV1 heat-gated ion channels', *The EMBO Journal*, 24(24), pp. 4211–4223.
- Zheng, J.-H., Walters, E.T. & Song, X.-J. (2007) 'Dissociation of Dorsal Root Ganglion Neurons Induces Hyperexcitability That Is Maintained by Increased Responsiveness to cAMP and cGMP', *Journal of Neurophysiology*, 97(1), pp. 15–25.
- Zhou, S., Wang, F., Hsieh, T.-C., Wu, J.M. & Wu, E. (2013) 'Thalidomide—a notorious sedative to a wonder anticancer drug', *Current Medicinal Chemistry*, 20(33), pp. 4102–4108.
- Zimmerman, A., Bai, L. & Ginty, D.D. (2014) 'The gentle touch receptors of mammalian skin', *Science*, 346(6212), pp. 950–954.